Les effets combinés de l'hydrogène et de la dilution dans un moteur à allumage commandé

Toni Tahtouh

UNIVERSITÉ D'ORLÉANS

ÉCOLE DOCTORALE SCIENCES ET TECHNOLOGIES

INSTITUT PRISME

THÈSE présentée par :

Toni TAHTOUH

soutenue le : **15 Décembre 2010**

pour obtenir le grade de : **Docteur de l'université d'Orléans**

Discipline : Mécanique et Energétique

Les effets combinés de l'hydrogène et de la dilution dans un moteur à allumage commandé

THÈSE dirigée par :

M^{me} C. MOUNAÏM-ROUSSELLE	Professeur, Université d'Orléans

RAPPORTEURS :

M Bruno RENOU	Professeur, CORIA - I.N.S.A de Rouen
M Alexander TAYLOR	Professeur, Imperial College of London

JURY :

M Thierry POINSOT	Directeur de Recherche, IMFT - CNRS Toulouse
M Bruno RENOU	Professeur, CORIA - I.N.S.A de Rouen
M Erwann SAMSON	Ingénieur de recherche, PSA Peugeot Citroën
M Benoist THIROUARD	Ingénieur de recherche, IFP Energies nouvelles
M^{me} Bianca Maria VAGLIECO	Directeur de Recherche, Istituto Motori - CNR Naples
M^{me} C. MOUNAÏM-ROUSSELLE	Professeur, Université d'Orléans
M Fabien HALTER	Maître de conférences, Université d'Orléans

Remerciements

Cette thèse, cofinancée par la région Centre et PSA Peugeot Citroën, a été réalisée au sein de l'équipe EPM de l'institut PRISME à l'université d'Orléans.

Je tiens à remercier Christine Mounaïm-Rousselle, qui a dirigé cette étude, de m'avoir accueilli au sein de son équipe, de m'avoir donné l'opportunité de réaliser ce travail de thèse et de m'avoir soutenu au cours de cette thèse.

Je tiens à exprimer ma profonde reconnaissance à Fabien Halter pour son excellent encadrement, sa disponibilité, sa confiance et son soutien. Je le remercie aussi pour les agréables moments en dehors du laboratoire (Congrès, Sport…).

Je remercie Erwann Samson pour les discussions scientifiques et pour ses précieux conseils.

Je tiens à remercier également tous les membres de jury qui ont accepté de juger ma thèse : Thierry Poinsot (président de jury), Bruno Renou, Erwann Samson, Benoist Thirouard, Bianca Maria Vaglieco, Christine Mounaïm-Rousselle et Fabien Halter. En particulier, je remercie Bruno Renou et Alexander Taylor qui m'ont fait l'honneur d'être les rapporteurs de ce travail.

Je remercie profondément tous les membres de l'équipe EPM PRISME pour le support de mon travail et pour m'avoir supporté, en particulier, je remercie Bruno Moreau pour son aide technique sur la mise en place et le bon fonctionnement des dispositifs expérimentaux. Julien Lemaire pour son support technique sur la baie d'analyse. Christian Caillol pour ses réponses, conseils et pour les moments agréables. Christian Chauveau et Mahmoud Idir d'ICARE (CNRS) pour leur aide en PIV.

Je remercie tous les doctorants collègues EPM et ESA, pour leur sympathie et bonne humeur, en particulier : Ludovic Landry pour les discussions enrichissantes, son aide et soutien scientifique et non-scientifique, pour les moments agréables passés à l'intérieur et à l'extérieur du laboratoire (même très loin du laboratoire !). Mathieu André pour son agréable amitié et son soutien dans les moments difficiles, mais surtout aussi pour les « jeudi soir ». Bénédicte Galmiche qui n'est pas encore doctorante et donc je vais l'appeler ex-future collègue!

J'exprime toute ma gratitude aux amis qui m'ont soutenu durant ces trois années de thèse, en particulier mes frères: Elie Béchara, Jean Abboud, Alain Kfoury, Nadim Melhem, Georges Zaatar et toutes les personnes que j'ai pu rencontrer durant ma thèse.

Je dédie ce travail à :

-Toute ma famille et surtout mon père, ma mère, mes deux petites sœurs car sans leur support (à tous les niveaux) et sans leur confiance je n'aurais jamais réussi à finaliser ce travail !

-Mojej Kochanej Malgosi Czerwinskiej

-Mon Liban

« Nul ne peut atteindre l'aube sans passer par le chemin de la nuit »

G. K. G.

Tables des matières

Introduction

Les études réalisées depuis plusieurs décennies par les climatologues sur les gaz et particules altérant le climat terrestre ont prouvé que certains produits chimiques en suspension peuvent piéger la lumière provenant du soleil et réchauffer le climat, alors que d'autres rafraîchissent la planète en bloquant les rayons du soleil. Les moteurs des véhicules terrestres émergent comme étant les plus gros contributeurs au réchauffement actuel de l'atmosphère à cause des émissions des polluants et des gaz à effet de serre qui favorisent le réchauffement. En effet, le secteur des transports émet 4 gaz qui contribuent directement à l'effet de serre :

-le dioxyde de carbone (CO_2)→ 31% des émissions totales,
-le protoxyde d'azote (N_2O) seulement 0.9% des émissions totales,
-les hydrofluorocarbures (HFC) → 19% des émissions totale
et le méthane (CH_4) <0.1% des émissions totales.

Le Potentiel (ou pouvoir) de Réchauffement Global (PRG) est un indicateur qui vise à regrouper l'effet additionné de toutes les substances contribuant à l'accroissement de l'effet de serre sous une seule valeur. Ce paramètre (PRG) est exprimé en « équivalent CO_2 » : l'effet de serre attribué au CO_2, par définition, est fixé à 1 et celui des autres substances relativement au CO_2. La figure 1 illustre la répartition du pourcentage de PRG, classé par secteur, en France métropolitaine pour l'année 2008 (Source CITEPA).

Le secteur du transport routier présente donc la plus importante contribution aux émissions de gaz à effet de serre (24%) du fait du CO_2 essentiellement.

En outre des gaz à effet de serre, le transport routier est le principale responsable des émissions d'oxydes d'azote (NO, NO_2) et de dioxyde de souffre (SO_2). Le monoxyde d'azote présent dans l'air inspiré peut se dissoudre dans le sang et ainsi limiter l'oxygénation des organes. De plus, l'oxyde d'azote (NO) et le dioxyde de soufre (SO_2), combinés avec de l'eau, donnent de l'acide nitrique et sulfurique menaçant la biodiversité.

Quant au dioxyde d'azote, il pénètre dans les voies respiratoires profondes, où il fragilise la muqueuse pulmonaire face aux agressions infectieuses, notamment chez les enfants.

Dans l'atmosphère, le dioxyde d'azote se transforme en acide nitrique, contribuant à l'acidification des milieux. D'autres émissions des moteurs de véhicules, tels que les hydrocarbures imbrûlés (HC) sont aussi nocifs pour l'homme et notre planète.

En conséquence, les normes anti-pollution sont de plus en plus strictes afin de lutter contre le changement climatique. Les constructeurs automobiles doivent ainsi chercher des solutions technologiques pour réduire les émissions polluantes soit au niveau de l'échappement soit au niveau de leur production à la base.

La limite maximale des émissions NO_x, par exemple, pour un véhicule à motorisation essence a été réduite de 60% pour les véhicules mis en service après 2009 par rapport à ceux mis en service après l'année 2000.

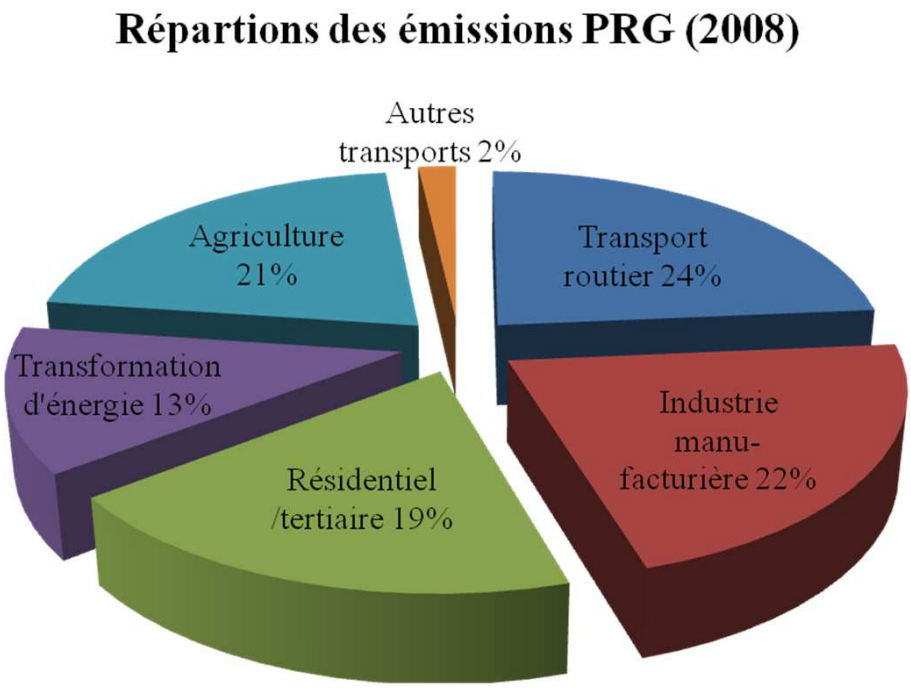

Figure 1. *Contribution des différents secteurs aux émissions de gaz à effet de serre (Source CITEPA)*

L'une des solutions est de recirculer une partie des gaz d'échappement (communément appelé EGR, comme Exhaust Gas Recirculation) à l'admission. La dilution ainsi obtenue du mélange air-carburant introduit dans la chambre de combustion permet de réduire fortement la température de combustion et, par conséquent la production de NO_x, liée au mécanisme de Zeldovich.

Cependant, dans le cas d'une dilution du mélange trop importante, la combustion est plus instable et peut ne pas s'entretenir. La vitesse de propagation de la combustion devient alors trop faible. L'une des solutions que nous avons étudié durant ce travail est la possibilité d'ajouter une faible quantité d'hydrogène afin de contrecarrer cet effet de forte dilution sur le fonctionnement des moteurs à allumage commandé.

Pour cela, notre travail s'est fait en 4 étapes principales qui forment les 4 parties de ce mémoire: une première étude bibliographique sur l'état de l'art concernant l'utilisation de l'hydrogène dans les moteurs à allumage commandé, une deuxième étude qui a consisté à la validation du potentiel de l'ajout d'hydrogène sur un moteur monocylindre, une troisième partie où des études plus fondamentales qui concernent des mesures expérimentales des vitesses de combustion laminaires, paramètre fondamental et nécessaire lorsque tout processus de combustion entre en jeu, et la dernière partie qui concerne l'étude de ces effets de l'hydrogène sur la combustion « réelle », c'est-à-dire turbulente, dans un moteur à accès optiques.

1. Etat de l'art

1.1 Propriétés de l'hydrogène

L'hydrogène se caractérise par une réactivité élevée et une vitesse de combustion jusqu'à cinq fois plus importante que celle du méthane ou de l'isooctane (tableau 1). De plus, l'hydrogène présente un domaine d'inflammabilité plus étendu que celui des autres carburants (figure 2). Grâce à ces caractéristiques, l'ajout d'une faible quantité d'hydrogène dans le mélange carburant-air-diluant permet d'augmenter les vitesses de combustion et de rendre la combustion plus stable en réduisant la durée de combustion et en diminuant les variations cycle-à-cycle.

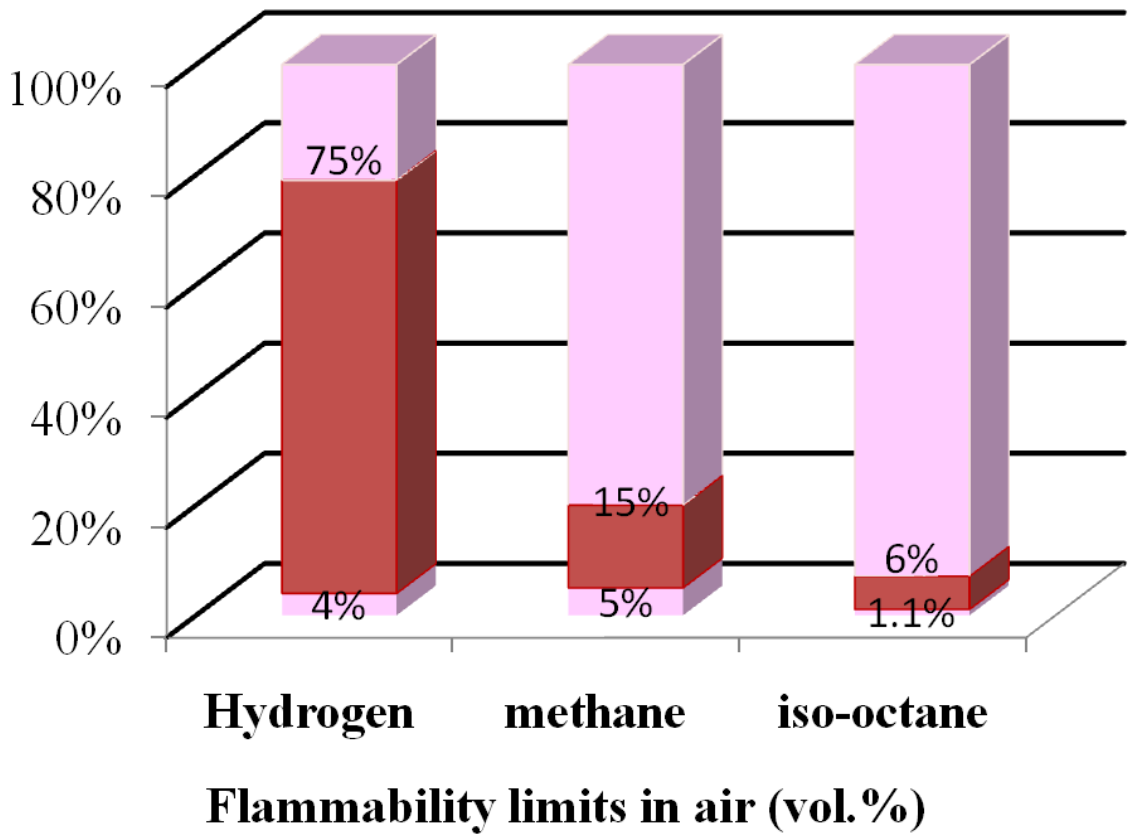

Figure 2. *Limites de flammabilité de l'hydrogène du méthane et de l'iso-octane dans l'air*

En plus de ces avantages, l'ajout d'une certaine quantité d'hydrogène permet toutefois d'améliorer la résistance du mélange carburant/air au cliquetis. Shinagawa *et al.* [1] ont étudié l'effet de l'ajout d'hydrogène dans un moteur à allumage commandé et son influence sur le cliquetis.

Ils en ont conclu que l'ajout d'hydrogène permettait de diminuer l'occurrence du cliquetis. Ceci est possible non seulement grâce à la réduction de la durée de combustion, mais aussi en défavorisant la décomposition du carburant et la production des radicaux hydroxyles. Topinka *et al.* [2] ont ajouté de l'hydrogène et du monoxyde de carbone aux carburants car le CO (RON = 106) et l'H_2 (RON >130) sont caractérisés par des indices d'octane de recherche supérieurs à ceux des carburants essences ce qui permet une meilleure résistance au cliquetis. Par exemple, en transformant 15% du carburant en CO et H_2, l'indice d'octane du mélange carburant augmente de 10. Cette augmentation défavorise l'occurrence du cliquetis en ralentissant la chimie d'auto-inflammation et en augmentant la vitesse de flamme.

Tableau 1. *Les propriétés d'hydrogène comparées à celles du méthane et de l'iso-octane dans l'air.*

P=1bar, T=300K @ Stoichiometry	Hydrogen	Methane	Isooctane
Laminar burning velocity	226 cm/s	37 cm/s	32 cm/s
Minimum ignition energy	0.02 mJ	0.29mJ	0.28mJ
Minimum quenching distance	0.6 mm	2 mm	3.5 mm
Lower heating value	120 MJ/kg	50 MJ/kg	44.3 MJ/kg
Stoichiometric air-to-fuel ratio	34.2 (kg/kg)	17.1 (kg/kg)	15 (kg/kg)
Research Octane Number (RON)	>130	120	100

1.2 Production à bord d'hydrogène

D'un point de vue technologique, l'ajout d'hydrogène dans un véhicule automobile peut se révéler compliqué pour deux raisons principales : nécessité d'équiper le véhicule avec 2 réservoirs distincts et développement d'une infrastructure pour le stockage et la distribution d'hydrogène.

L'une des alternatives intéressantes et prometteuses serait la transformation à bord du véhicule d'une quantité du carburant principal (essence, GPL, GNV) en hydrogène.

De nombreuses techniques ont été étudiées dans ce cadre, on peut citer :

- Steam Reforming Reaction (SRR)
- Water-Gas Shift Reaction (WSGR)
- Partial Oxydation (POX)
- Autothermal Reforming (ATR)
- Thermal Decomposition
- Exhaust Gas Fuel Reforming

Une revue rapide de ces différentes techniques a été effectuée par Jamal *et al.* [3] et par Tsolakis et Megaritis [4].

Cependant, la production à bord d'hydrogène à partir des hydrocarbures en utilisant ces systèmes de « reforming » présente plusieurs limitations liées à la mise en route du reformer, aux temps de réponse et à la taille requise par ce dernier.

Une solution pour remédier à ces limitations a été proposée par l'équipe de MIT : Bromberg *et al*. [5-9] ont développé un système, le Plasmatron, basé sur le principe d'une oxydation partielle du carburant par l'assistance d'un arc de type plasma. Le Plasmatron favorise la réaction exothermique qui a lieu dans des conditions carburant/air riches et qui donne comme produits de réaction le monoxyde de carbone et l'hydrogène à travers une oxydation partielle du carburant.

La figure 3 illustre cette procédure de production d'hydrogène à bord du véhicule [5].

Comme on peut le constater à partir de la figure 3, une partie du carburant (essence ou gaz naturel) et de l'air est introduite dans le Plasmatron dans des conditions de richesses élevées (supérieure au rapport stœchiométrique carburant/air) afin de n'oxyder que partiellement le carburant et ainsi produire de l'hydrogène et du monoxyde de carbone. La réaction idéale d'oxydation partielle du carburant est de la forme suivante :

$$C_m H_n + \frac{m}{2}\left(O_2 + 3.773 N_2\right) \rightarrow mCO + \frac{n}{2} H_2 + \frac{m}{2} \cdot 3.773 N_2 \quad (1)$$

Le moteur à combustion interne est utilisé comme génératrice électrique pour alimenter le Plasmatrom.

Les pertes d'énergie additionnelle dues à l'emploi de ce système sont donc principalement :

- La transformation d'une partie du travail du moteur en électricité pour l'alimentation du Plasmatrom
- Les pertes dues au dégagement d'une partie de l'énergie chimique du carburant durant son oxydation partielle dans le reformer.

Toutefois, Bromberg *et al*. [9] ont prouvé que le bilan global énergétique pouvait être positif. Ils ont ainsi donné l'exemple d'une transformation de « reforming » de 35% du carburant, ce qui permet une production d'une quantité d'hydrogène, représentant, en énergie de carburant, 13% de l'énergie totale introduite dans le moteur avec un rendement de conversion de 40%.

Le rendement global augmente donc de 2% grâce à la réduction des pertes par pompage (ouverture partielle du papillon) et à la réduction des pertes aux parois. Cette augmentation du rendement global est accompagnée d'une diminution drastique des émissions NO_x comme l'illustre la figure 4.

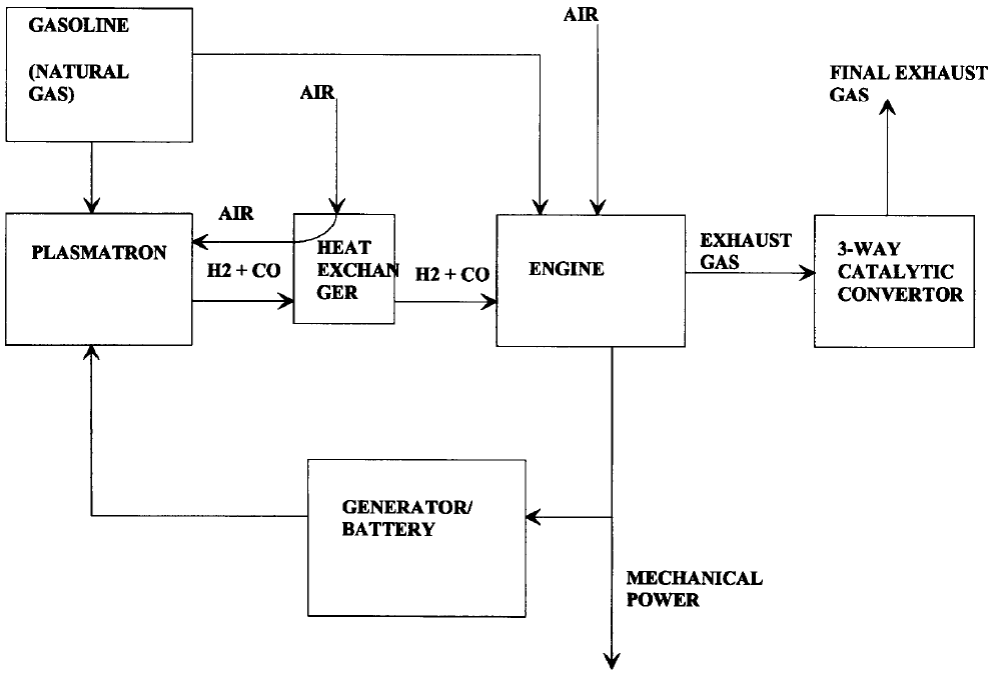

Figure 3. *Schéma du système de production d'hydrogène à bord (Plasmatron)[5]*

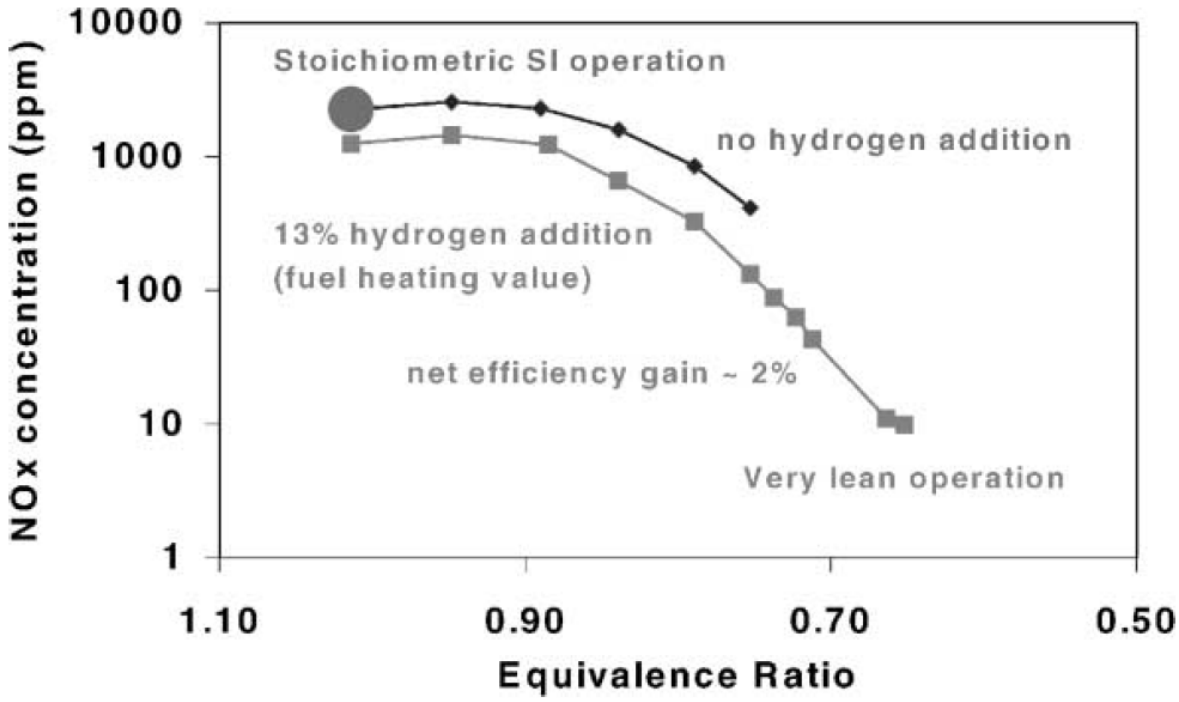

Figure 4. *Emissions de NO_x en fonction de la richesse avec ou sans ajout d'hydrogène [9].*

Le Plasmatron pourrait donc être une voie possible de la production d'hydrogène à bord du véhicule tant que les pertes énergétiques ajoutées par ce système sont compensées par un gain de rendement du à la diminution des pertes par pompage, aux parois, et finalement à une diminution de la variabilité cycle-à-cycle, avec de plus une très forte réduction des émissions polluantes [7].

Cohn *et al*. [5] ont estimé que l'augmentation du coût du véhicule causé par l'ajout de ce système de Plasmatron ne serait que de 3 à 4%.

1.3 L'ajout d'hydrogène

Tout le long de ce mémoire, l'expression « ajout d'hydrogène » signifiera la substitution d'une partie (en volume, en masse ou en énergie) du carburant principal par de l'hydrogène.

De nombreuses études numériques et expérimentales sur l'impact de l'ajout d'hydrogène dans des moteurs à allumage commandés avec comme carburant de base, le gaz naturel, l'essence ou bien le méthane sont disponibles dans la littérature [10-18]. Toutes ces études ont pour conclusions communes que l'effet de l'ajout d'hydrogène est de:

- réduire la durée de combustion
- d''augmenter l'efficacité thermique

En plus de ces résultats majeurs, on peut par exemple relever ceux d'Apostolescu et Chiriac [14] qui ont fait l'étude sur un véhicule léger alimenté principalement avec de l'essence :

- réduction de la variabilité cycle-à-cycle même avec des faibles quantités d'hydrogène (5% en masse)
- réduction des émissions HC
- augmentation des émissions NO_x dans le cas des mélanges pauvres

De même, Kahraman *et al*. [15] lors de leur étude expérimentale dans un moteur à allumage commandé (4 cylindres) alimenté par des différents mélanges de carburant CH_4-H_2 (0% H_2, 10% H_2, 20% H_2 et 30% H_2) ont relevé qu' :

- En augmentant la fraction d'hydrogène dans le carburant, le maximum de la pression cylindre se rapproche de la position du point mort haut
- Les émissions HC, CO et CO_2 sont réduites avec l'augmentation de la fraction d'hydrogène dans le carburant.

Quant à Pana *et al*. [16], lors de leur étude expérimentale et numérique, ils ont conclu que l'ajout d'hydrogène a comme impact :

- L'augmentation des émissions NO_x, due à l'augmentantation de la température de combustion. La diminution de la consommation spécifique du carburant

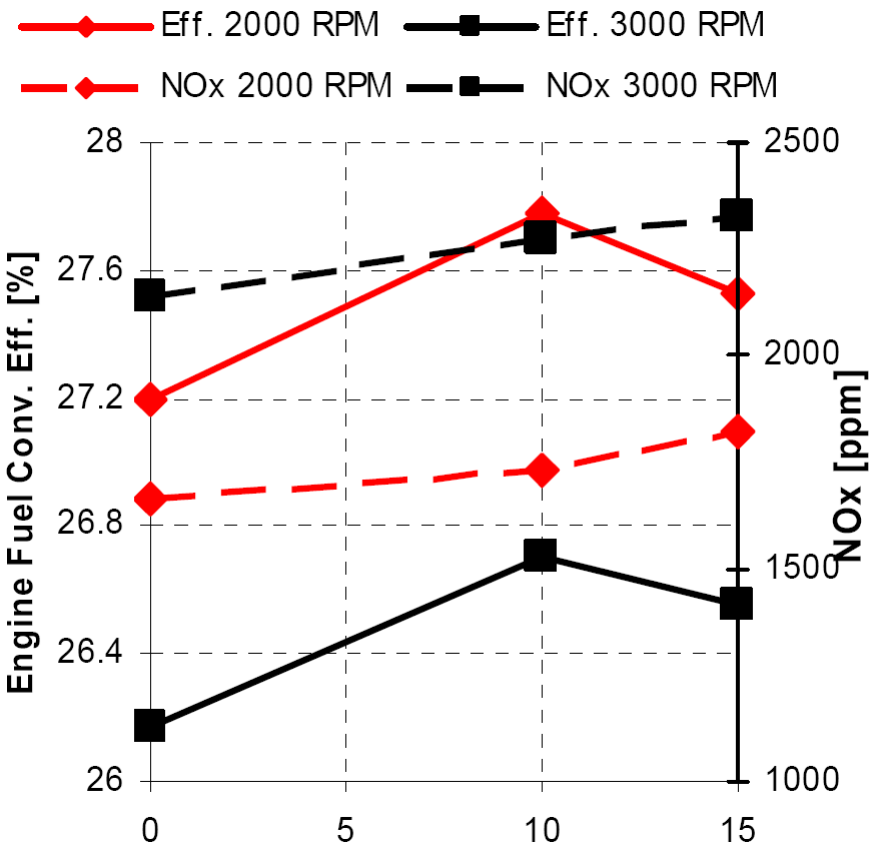

Figure 5. *Emissions de NO_x et rendement en fonction du pourcentage volumique d'hydrogène dans le gaz naturel pour deux cas moteurs [19].*

Il est intéressant de noter les résultats obtenus par Dimotoulos e*t al*. [19] sur l'effet de l'ajout d'hydrogène sur la combustion du gaz naturel (0%, 5% 10% et 15% en Volume) dans un moteur à allumage commandé (4 cylindres) Pour des quantités d'hydrogène de 15% en volume, une diminution du rendement a été observée comme l'illustre le figure 5 pour le cas de 4 bars de charges, contrairement aux études précédentes. Les auteurs justifient ce résultat en effectuant une analyse des pertes. En effet, les pertes associées à la « combustion réelle », dues à la combustion non-instantanée au point mort haut, diminuent de 3.74% à 3.12% quand la quantité d'hydrogène passe de 0% à 10%. Mais l'effet positif de l'hydrogène pour des quantités au-delà de 10% en volume devient négligeable car la durée de combustion ne diminue plus. En outre les pertes aux parois augmentent avec l'ajout d'hydrogène expliquant la diminution du rendement global en passant de 10% à 15% en hydrogène.

Cependant l'effet positif le plus intéressant est obtenu dans le cas de combustions de mélanges pauvres ou dilués qui permet une réduction des émissions NO_x tout en améliorant le rendement global.

1.4 Effets combinés de l'ajout d'hydrogène et de la dilution

L'ajout de l'EGR permet non seulement la réduction des émissions NO_x mais aussi l'amélioration du rendement global en diminuant les pertes par pompage, la réduction des pertes aux parois grâce à une diminution de la température globale dans le moteur et finalement la diminution du phénomène de dissociation des molécules (CO_2 et H_2O par exemple) qui a lieu surtout à des températures élevées.

Dimopoulos *et al*. [19] ont aussi étudié l'effet combiné de l'ajout d'hydrogène et sur la combustion du gaz naturel (0%, 5% 10% et 15% en Volume) et l'effet combiné de la dilution par l'EGR.

Ils ont ainsi constaté qu'en ajoutant de l'EGR, et pour toutes les fractions d'hydrogène dans le mélange carburant, le niveau des émissions NO_x reste inférieur à 1000 ppm. En d'autres termes, l'ajout de 15% de H_2 en volume combiné avec l'ajout de 12.5% de l'EGR en masse permet d'améliorer le rendement global de 3% et de réduire les émissions NO_x de 45% par rapport au cas référence c'est-à-dire sans dilution et sans hydrogène (niveau d'émissions supérieur à 1500 ppm). En contrepartie, les émissions d'hydrocarbures imbrûlés augmentent en mélange dilué à cause du ralentissement de la vitesse de propagation de la flamme et du coincement de la flamme aux parois. Une solution possible aussi pour remédier à cette limitation est l'ajout d'une quantité d'hydrogène plus importante (>15% en volume).

Alger *et al*. [20] ont ajouté des quantités d'hydrogène (jusqu'à 1% en volume par rapport au volume de l'air) aux conduits de l'admission d'un monocylindre fonctionnant en mélange stœchiométrique. Ils ont étudié deux charges différentes (3.1 bar et 5.5 bars en pression moyenne indiquée), deux taux de compressions (11 :1 et 14 :1) et finalement deux carburants principaux: l'essence et le gaz naturel.

Dans le cas de l'alimentation en essence, seulement 0.2% en volume d'hydrogène peut suffire en cas de forte dilution (22%-32% d'EGR) à augmenter la stabilité du moteur (covariance de la pression moyenne indiquée est inférieure à 5%). Par contre, dans le cas de l'alimentation en gaz naturel, cette stabilité du moteur ne peut être atteinte dans les mêmes conditions que si la quantité d'hydrogène atteint les 0.4%. On peut aussi noter dans cette étude que l'hydrogène permet une extension de 40%-50% des limites acceptables de dilution dans le cas de l'essence et de 20-28% dans le cas du gaz naturel.

Effet de la composition des gaz de Plasmatron à l'admission

L'utilisation d'un point de vue technologique d'un système de type Plasmatron entraîne aussi une dilution de la charge à l'admission. Tully et Heywood [21] ont ainsi étudié l'effet de la composition des gaz à l'admission (ajout d'hydrogène, d'une composition de gaz de

Plasmatron idéale et d'une composition de gaz de Plasmatron typique dans un moteur à allumage commandé alimenté en essence), comme le résume le tableau 2.

Tableau 2. *Composition des gaz de Plasmatron et rendements de conversion [21].*

	Ideal Plasmatron	Typical Plasmatron
H_2	25%	23%
CO	26%	21%
N_2	49%	52%
CO_2	0%	4%
Efficiency	85.74%	77.01%

Ils ont introduit deux rendements: le rendement indiqué et le rendement global (qui tient compte des pertes du système Plasmatron).

Ils ont aussi définit un paramètre de dilution VDP, qui tient compte à la fois de la richesse (excès d'air) et des diluants (N_2 et CO_2) présents dans le gaz du Plasmatron.

Voici leurs principales conclusions :

L'ajout de gaz de Plasmatron, qu'il soit supposé idéal ou réel permet d'améliorer le rendement indiqué. Lorsque 20% du carburant est transformé en gaz de Plasmatron (idéal), le gain en rendement global est de 12.3% en comparaison avec le cas basique (rapport stœchiométrique, sans dilution et sans gaz de Plasmatron).

Les émissions NO_x ont été réduites de 95% avec l'ajout du gaz de Plasmatron en considérant le point de fonctionnement avec le rendement maximal, grâce à l'extension des gaz de Plasmatron de la limite de dilution et donc la possibilité d'opérer avec des faibles richesses.

Pour des faibles dilutions, l'ajout des gaz de Plasmatron a permis de réduire les émissions des hydrocarbures imbrûlés. Cependant, dans les conditions de limite de dilution, ils ont constaté que ces valeurs d'émissions sont presque identiques pour tous les mélanges de carburant considérés.

L'effet de l'ajout d'hydrogène pur par rapport à celui des gaz de Plasmatron a été étudié : l'ajout des gaz de Plasmatron a un effet légèrement plus prononcé sur la combustion par rapport à l'hydrogène pur grâce à la présence du monoxyde de carbone dans les gaz de Plasmatron.

Toutefois, les pertes causées par le système de Plasmatron sont importantes et ont un impact négatif sur le rendement global comme on peut le voir sur la figure 6 (valeur plus élevèée pour l'indolène pur représentatif de l'essence).

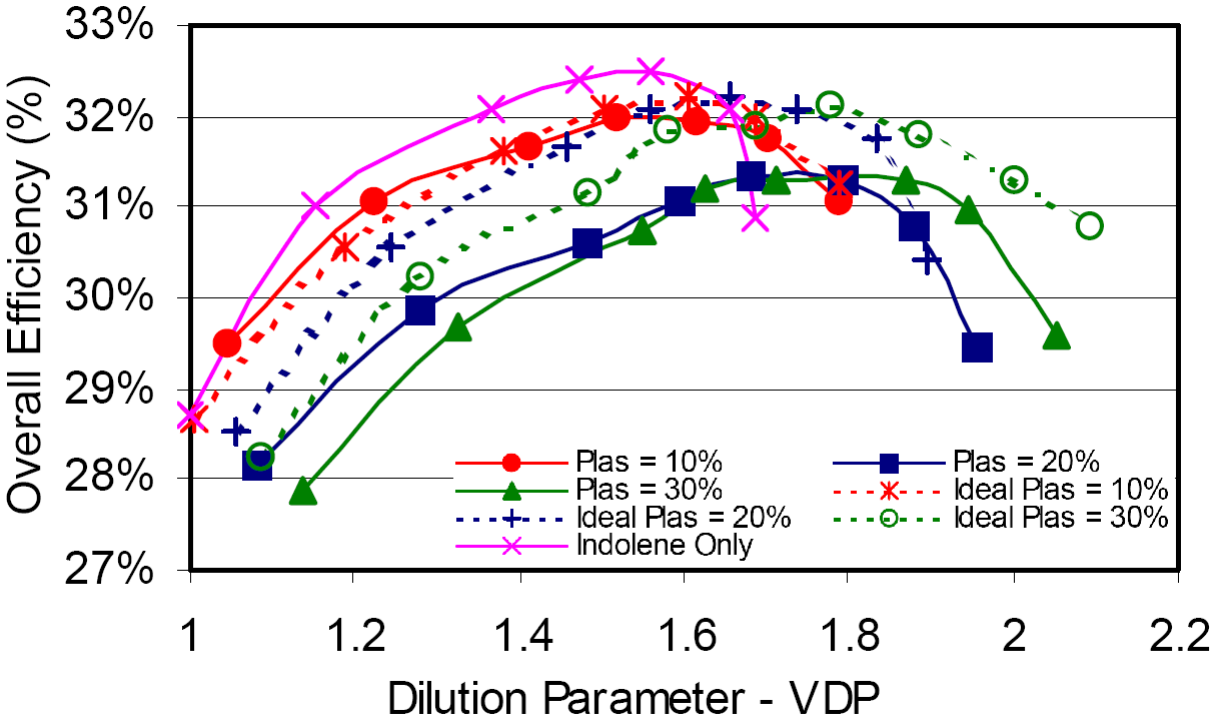

Figure 6. *Rendement global en fonction de la dilution d'après [21]*

Toutefois, les limites de dilution étant étendues par la présence de l'hydrogène, grâce à l'amélioration de la stabilité et la diminution des émissions polluantes, le rendement global peut alors être supérieur (paramètre de dilution > 1.6 par exemple ici).

D'autres auteurs [22-27]ont aussi conclu que l'effet de l'ajout d'hydrogène devient intéressant et très prononcé quand on dilue le mélange carburant-air (par exemple EGR). En particulier Hu *et al*. [22, 23] qui ont peu conclure d'après leurs travaux expérimentaux :

- L'ajout d'hydrogène permet de réduire la durée de combustion tandis que l'ajout de l'EGR a l'effet opposé sur la durée de combustion
- Les variations cycle-à-cycle diminuent avec l'ajout d'hydrogène et cet effet positif est plus prononcé dans les cas de fortes dilutionsLa pression moyenne indiquée diminue avec l'ajout de l'EGR et pour des faibles quantités d'hydrogène
- Le rendement thermique augmente avec l'ajout de l'EGR quand l'EGR est inférieur à 10%. Pour des quantités d'EGR plus importantes, le rendement thermique diminue en continuation. L'ajout d'hydrogène a l'effet opposé sur le rendement thermique, c'est-à-dire il diminue pour des faibles quantités d'hydrogène et augmente pour des fractions plus importantes d'hydrogène
- Les émissions CO, CO_2 et HC diminuent avec l'ajout d'hydrogène alors que les NO_x avec l'EGR.

Toutes ces études sur les effets combinés de l'ajout d'hydrogène et de la dilution montrent que l'on peut obtenir principalement :

1. ***Un rendement global supérieur et donc une réduction de la consommation***
2. ***Une réduction des émissions NO_x***
3. ***Une réduction des émissions HC, CO et CO_2 avec l'ajout d'hydrogène***
4. ***Une augmentation des émissions HC avec la dilution***

En outre, cette augmentation de rendement peut potentiellement compenser les pertes causées par le système de production in-situ de l'hydrogène (comme dans le cas du Plasmatron).

1.5 L'ajout d'hydrogène dans les conditions de mélanges pauvres

Une autre possibilité est la combinaison de l'ajout d'hydrogène dans des conditions de mélange pauvre. En d'autres termes c'est la dilution non plus avec de l'EGR mais avec de « l'air ».

Nombreux auteurs ont prouvé que l'ajout d'hydrogène permet une extension significative de la Lean Operating Limit (LOL, c'est-à-dire la richesse limite pour laquelle la stabilité du moteur est encore acceptable) en remplaçant une fraction du gaz naturel [27, 28] ou de l'essence [29, 30] par de l'hydrogène.

Par exemple, Hoekstra *et al*. [31] ont trouvé que 20% d'hydrogène en volume dans le carburant permet l'extension de la limite de stabilité de la richesse de 0.75 (sans hydrogène) à 0.67. En outre, l'ajout de 28% ou 36% d'hydrogène en volume à des mélanges pauvres (richesse<0.8) permet d'obtenir des valeurs d'émissions NO_x assez basses (<250ppm) avec des émissions HC modérées.

L'effet de l'ajout d'hydrogène (0,20%, 40% et 60% en volume) dans le méthane pour deux cas de régimes différents du moteur (700 et 900 tours/min), en charges partielles et pleine charge et en conditions stœchiométriques et mélanges pauvres a été étudié par Bauer et Forest [32]. Ils ont montré que :

- L'ajout de 60% d'hydrogène dans le méthane permet une extension de la limite de la combustion partielle (définie comme les conditions à partir desquelles la combustion se dégrade et les ratés d'allumages causent une réduction drastique de la puissance) de 0.58 (dcas pur méthane) à 0.34 (cas 40% méthane)
- Cependant, l'ajout d'hydrogène conduit à une réduction en puissance à cause de son faible pouvoir calorifique inférieur (en volume).
- L'ajout de 60% d'hydrogène en volume réduit les émissions CO_2 (jusqu'à 60%), CO (jusqu'à 45%) et HC (jusqu'à 60%) mais par contre, augmente les émissions NO (de ~30%)

Akansu *et al*. [33] ont aussi testé des mélanges méthane/hydrogène (0, 10%, 20% et 30% d'H_2 en volume) dans un moteur à allumage commandé (4 cylindres) en variant la richesse globale de 0.6 à 1.2. Ils en concluent que :

- Les émissions de NO_x augmentent avec l'ajout d'hydrogène. Les émissions CO et CO_2 diminuent avec l'augmentation de la fraction d'hydrogène dans le mélange carburant
- Le rendement thermique, dans le cas des mélanges pauvres, augmente avec l'ajout d'hydrogène

Les conclusions principales de l'ensemble de ces études sont donc :

1. ***Possibilité d'amélioration du rendement thermique dans les conditions de mélanges pauvres en ajoutant d'hydrogène***
2. ***Réduction des émissions NO_x en combinant les conditions de mélanges pauvres et l'ajout d'hydrogène***
3. ***Réduction des émissions HC, CO et CO_2 pour les conditions de mélanges pauvres et en ajoutant d'hydrogène***

1.6 Conclusion générale

Ces nombreuses études ont confirmé le potentiel de l'hydrogène pour moteurs à allumage commandé, c'est à dire amélioration du rendement et réduction des émissions. Toutefois, toutes ces études sont basées sur des approches globales d'analyse de performances et d'émissions polluantes. Peu d'études se sont focalisées sur l'identification précise de l'effet de l'hydrogène sur les différentes étapes du processus complexe de combustion dans les moteurs à combustion interne. On peut citer Herweg et Maly [34] qui ont développé un model 1D afin de décrire l'évolution temporelle du front de flamme dans un moteur, durant les phases initiales de développement. Meier *et al*. [35] ont utilisé une chambre à combustion avec accès optiques pour visualiser la combustion, à partir de la technique de strioscopie, aux conditions de pression et de température similaires à celles de la chambre de combustion dans un moteur à allumage commandé.

Aleiferis *et al*. [36, 37] ont mené des études expérimentale sur la phase initiale de propagation de flamme dans un moteur à allumage commandé (monocylindre à accès optiques) mais ces travaux se sont focalisés sur les conditions de mélange essence/air pauvres.

Le travail de Conte et Boulouchos [38] est une des rares études qui traite l'influence de l'ajout des gaz issus du 'reformer' dans un moteur à allumage commandé. Le suivi du développement de la combustion s'est fait grâce à des sondes d'ionisation. La vitesse de combustion laminaire aux conditions moteur augmente linéairement avec la fraction des gaz

issus du reformer, mélangée au carburant (en termes d'énergie). Mais cet effet est nettement moins prononcé sur la vitesse turbulente de combustion. Finalement dans les conditions de limite de stabilité, c'est-à-dire de grandes variations cycle-à-cycle, où le mélange est soit très pauvre soit très dilué, la combustion apparait comme indépendante de la composition du carburant.

Récemment, Fairweather *et al*. [39] ont étudié l'effet de l'ajout d'hydrogène sur la vitesse de combustion turbulente dans une enceinte. Ils ont observé que dans les conditions stœchiométriques, le rapport entre la vitesse turbulente et la vitesse laminaire de combustion ne varie pas avec l'ajout d'hydrogène pour une intensité turbulente fixée. On constate toutefois un manque d'études expérimentales concernant les effets de l'ajout d'hydrogène sur la combustion turbulente dans des conditions de mélange dilué, que ce soit dans le cas de l'essence ou de gaz naturel, que ce soit en moteurs à accès optiques. Or, la vitesse de combustion turbulente dépend principalement de la géométrie du brûleur, du nombre de Lewis du mélange, des grandeurs caractéristiques de la turbulence (intensité turbulente, échelle intégrale), de la vitesse de combustion laminaire et de l'épaisseur de la flamme [40].

Par conséquent, l'objectif global de ce travail de thèse est d'effectuer une étude détaillée de l'effet de l'ajout d'hydrogène et de la dilution sur le déroulement de la combustion dans les conditions d'un moteur à allumage commandé, alimenté soit par du méthane (représentant le GNV) ou l'isooctane (représentant l'essence).

Bien qu'il soit connu désormais que l'hydrogène réduit la durée de combustion et que la dilution augmente cette durée, affectant ainsi directement le rendement de combustion, très peu de travaux étudient en détail l'influence et le poids de chaque paramètre (structure de flamme, vitesse de combustion laminaire, intensité turbulente). C'est dans ce cadre que ce travail a donc été réalisé : répondre aux questions suivantes dans l'objectif d'apporter des éléments de compréhension sur les effets combinés de l'hydrogène et de la dilution :

- **Comment l'hydrogène et la dilution affectent le déroulement de la combustion et donc comment ils influencent la vitesse de combustion turbulente?**
- **Quel est le poids de chaque paramètre (vitesse de combustion laminaire, structure de flamme, intensité turbulente) ?**

1.7 Plan du mémoire

Le deuxième chapitre (qui est la première partie des résultats présentés) de ce mémoire présentera donc le résultat des expériences réalisées dans un moteur monocylindre à allumage commandé opaque. Le propos de cette première partie est de varier séparément plusieurs paramètres : la richesse, le taux de dilution, la fraction d'hydrogène dans le carburant et la pression d'admission, tout en fixant le travail du moteur (pression moyenne indiquée).

L'objectif est de conclure quant à l'effet de l'ajout d'hydrogène et de la dilution (à mélange stoechiométrique et pauvre) sur les performances (rendements) et d'émissions polluantes.

Les chapitres 3-7, qui forment une seconde partie de ce travail, sont consacrés à la détermination des paramètres fondamentaux de combustion laminaire, en insistant sur les méthodologies (chapitres 3 et 5) adoptées et optimisées. Nous présentons les résultats expérimentaux de vitesse de combustion laminaires et de longueurs de Markstein pour des mélanges méthane/hydrogène/di-nitrogène/air (chapitre 4) ou iso-octane/hydrogène/di-nitrogène/air (chapitre 6) avec des conditions de pression et température ambiante et à richesse 1, obtenues dans une enceinte à volume constant. De nouvelles corrélations pour l'estimation de la vitesse de combustion de ces mélanges seront aussi proposées et validées. Ces corrélations serviront à l'estimation des vitesses de combustion laminaire dans les conditions thermodynamiques rencontrées dans le moteur (pressions et températures élevées). L'objectif de ce chapitre est donc de déterminer les paramètres de combustion, qui sont primordiaux pour le développement de la combustion turbulente et qui sera étudiée dans une troisième partie.

La troisième partie (chapitres 7 et 8) expose les résultats issus d'expériences réalisées sur un moteur à allumage commandé à accès optiques via deux techniques :

- ✓ La visualisation directe du rayonnement de flamme
- ✓ La vélocimétrie par imagerie de particules et la tomographie laser par diffusion de Mie simultanées

La première technique dans le but de déterminer l'évolution du front de flamme durant les premiers instants afin de quantifier l'effet de l'ajout d'hydrogène et de la dilution sur le début de la combustion. La deuxième technique dans le but de déterminer les vitesses de combustion turbulentes de différents mélanges air/carburant considérés.

Dans ce dernier chapitre, les vitesses de combustion dans un moteur seront corrélées et expliquées en utilisant les résultats sur les propriétés laminaires issus de la seconde partie afin d'atteindre l'objectif d'étudier l'influence des paramètres laminaires et de l'intensité turbulente sur la vitesse de combustion turbulente.

1.8 Références

[1] T. Shinagawa, T. Okumura, S. Furuno, K.-O. Kim, *Effects of Hydrogen Addition to SI Engine on Knock Behavior*, SAE paper, 2004-01-1851 (2004).

[2] J. A. Topinka, M. D. Gerty, J. B. Heywood, J. C. Keck, *Knock Behavior of a Lean-Burn, H2 and CO Enhanced, SI Gasoline Engine Concept*, SAE paper, 2004-01-0975 (2004).

[3] Y. Jamal, T. Wagner, M. L. Wyszynski, *Exhaust gas reforming of gasoline at moderate temperatures*, International Journal of Hydrogen Energy, 21 (1996), pp. 507-519.

[4] A. Tsolakis, A. Megaritis, *Exhaust gas assisted reforming of rapeseed methyl ester for reduced exhaust emissions of CI engines*, Biomass and Bioenergy, 27 (2004), pp. 493-505.

[5] D. R. Cohn, A. Rabinovich, C. H. Titus, L. Bromberg, *Near-term possibilities for extremely low emission vehicles using onboard plasmatron generation of hydrogen*, International Journal of Hydrogen Energy, 22 (1997), pp. 715-723.

[6] L. Bromberg, D. R. Cohn, A. Rabinovich, N. Alexeev, *Plasma catalytic reforming of methane*, International Journal of Hydrogen Energy, 24 (1999), pp. 1131-1137.

[7] J. B. Green, N. Domingo, J. M. E. Storey, R. M. Wagner, J. S. Armfield, L. Bromberg, D. R. Cohn, A. Rabinovich, N. Alexeev, *Experimental Evaluation of SI Engine Operation Supplemented by Hydrogen Rich Gas from a Compact Plasma Boosted Reformer*, SAE Technical Paper, 2000-01-2206 (2000).

[8] L. Bromberg, D. R. Cohn, A. Rabinovich, N. Alexeev, A. Samokhin, R. Ramprasad, S. Tamhankar, *System optimization and cost analysis of plasma catalytic reforming of natural gas*, International Journal of Hydrogen Energy, 25 (2000), pp. 1157-1161.

[9] L. Bromberg, D. R. Cohn, A. Rabinovich, J. Heywood, *Emissions reductions using hydrogen from plasmatron fuel converters*, International Journal of Hydrogen Energy, 26 (2001), pp. 1115-1121.

[10] T. Suzuki, Y. Sakurai, *Effect of Hydrogen Rich Gas and Gasoline Mixed Combustion on Spark Ignition Engine*, SAE paper, 2006-01-3379 (2006).

[11] J. Wang, Z. Huang, Y. Fang, B. Liu, K. Zeng, H. Miao, D. Jiang, *Combustion behaviors of a direct-injection engine operating on various fractions of natural gas-hydrogen blends*, International Journal of Hydrogen Energy, 32 (2007), pp. 3555-3564.

[12] T. Thurnheer, P. Soltic, P. Dimopoulos Eggenschwiler, *S.I. engine fuelled with gasoline, methane and methane/hydrogen blends: Heat release and loss analysis*, International Journal of Hydrogen Energy, 34 (2009), pp. 2494-2503.

[13] B. Morrone, A. Unich, *Numerical investigation on the effects of natural gas and hydrogen blends on engine combustion*, International Journal of Hydrogen Energy, 34 (2009), pp. 4626-4634.

[14] N. Apostolescu, R. Chiriac, *A Study of Combustion of Hydrogen-Enriched Gasoline in a Spark Ignition Engine*, SAE paper, 960603 (1996).

[15] N. Kahraman, B. Çeper, S. O. Akansu, K. Aydin, *Investigation of combustion characteristics and emissions in a spark-ignition engine fuelled with natural gas-hydrogen blends*, International Journal of Hydrogen Energy, 34 (2009), pp. 1026-1034.

[16] C. Pana, N. Negurescu, M. G. Popa, A. Cernat, D. Soare, *An Investigation of the Hydrogen Addition Effects to Gasoline Fueled Spark Ignition Engine*, SAE paper, 2007-01-1468 (2007).

[17] M. A.-R. Sadiq Al-Baghdadi, H. A.-K. Shahad Al-Janabi, *Improvement of performance and reduction of pollutant emission of a four stroke spark ignition engine fueled with hydrogen-gasoline fuel mixture*, Energy Conversion and Management, 41 (2000), pp. 77-91.

[18] C. D. Rakopoulos, M. A. Scott, D. C. Kyritsis, E. G. Giakoumis, *Availability analysis of hydrogen/natural gas blends combustion in internal combustion engines*, Energy, 33 (2008), pp. 248-255.

[19] P. Dimopoulos, K. Boulouchos, C. Rechsteiner, R. H. P. Soltic, *Combustion Characteristics of Hydrogen-Natural Gas Mixtures in Passenger Car Engines*, SAE paper, 2007-24-0065 (2007).

[20] T. Alger, J. Gingrich, B. Mangold, *The Effect of Hydrogen Enrichment on EGR Tolerance in Spark Ignited Engines*, SAE paper, 2007-24-0015 (2007).

[21] E. J. Tully, J. B. Heywood, *Lean-Burn Characteristics of a Gasoline Engine Enriched with Hydrogen from a Plasmatron Fuel Reformer*, SAE paper, 2003-01-0630 (2003).

[22] E. Hu, Z. Huang, B. Liu, J. Zheng, X. Gu, B. Huang, *Experimental investigation on performance and emissions of a spark-ignition engine fuelled with natural gas-hydrogen blends combined with EGR*, International Journal of Hydrogen Energy, 34 (2009), pp. 528-539.

[23] E. Hu, Z. Huang, B. Liu, J. Zheng, X. Gu, *Experimental study on combustion characteristics of a spark-ignition engine fueled with natural gas-hydrogen blends combining with EGR*, International Journal of Hydrogen Energy, 34 (2009), pp. 1035-1044.

[24] B. Huang, E. Hu, Z. Huang, J. Zheng, B. Liu, D. Jiang, *Cycle-by-cycle variations in a spark ignition engine fueled with natural gas-hydrogen blends combined with EGR*, International Journal of Hydrogen Energy, 34 (2009), pp. 8405-8414.

[25] A. A. Quader, J. E. Kirwan, M. J. Grieve, *Engine performance and emissions near the dilute limit with hydrogen enrichment using a on-board reforming strategy*, SAE paper, 2003-01-1356 (2003).

[26] T. Allgeier, M. Klenk, T. Landenfeld, E. Conte, K. Boulouchos, J. Czerwinski, *Advanced Emission and Fuel Economy Concept Using Combined Injection of Gasoline and Hydrogen in SI-Engines*, SAE paper, 2004-01-1270 (2004).

[27] I. Saanum, M. Bysveen, P. Tunestål, B. Johansson, *Lean Burn Versus Stoichiometric Operation with EGR and 3-Way Catalyst of an Engine Fueled with Natural Gas and Hydrogen Enriched Natural Gas*, SAE paper, 2007-01-0015 (2007).

[28] M. Bysveen, *Engine characteristics of emissions and performance using mixtures of natural gas and hydrogen*, Energy, 32 (2007), pp. 482-489.

[29] T. D'Andrea, P. F. Henshaw, D. S. K. Ting, *The addition of hydrogen to a gasoline-fuelled SI engine*, International Journal of Hydrogen Energy, 29 (2004), pp. 1541-1552.

[30] C. Ji, S. Wang, *Effect of hydrogen addition on combustion and emissions performance of a spark ignition gasoline engine at lean conditions*, International Journal of Hydrogen Energy, 34 (2009), pp. 7823-7834.

[31] R. L. Hoekstra, K. Collier, N. Mulligan, L. Chew, *Experimental study of a clean burning vehicle fuel*, International Journal of Hydrogen Energy, 20 (1995), pp. 737-745.

[32] C. G. Bauer, T. W. Forest, *Effect of hydrogen addition on the performance of methane-fueled vehicles. Part I: effect on S.I. engine performance*, International Journal of Hydrogen Energy, 26 (2001), pp. 55-70.

[33] S. O. Akansu, N. Kahraman, B. Çeper, *Experimental study on a spark ignition engine fuelled by methane-hydrogen mixtures*, International Journal of Hydrogen Energy, 32 (2007), pp. 4279-4284.

[34] R. Herweg, R. R. Maly, *A Fundamental Model for Flame Kernel Formation in S. I. Engines*, SAE paper, 922243 (1992).

[35] F. Meier, J. Köhler, W. Stolz, W. H. Bloss, *Cycle-Resolved Hydrogen Flame Speed Measurements with High Speed Schlieren Technique in a Hydrogen Direct Injection SI Engine*, SAE paper, 942036 (1994).

[36] P. G. Aleiferis, A. M. K. P. Taylor, J. H. Whitelaw, K. Ishii, Y. Urata, *Cyclic Variations of Initial Flame Kernel Growth in a Honda VTEC-E Lean-Burn Spark-Ignition Engine*, SAE paper, 2000-01-1207 (2000).

[37] P. G. Aleiferis, A. M. K. P. Taylor, K. Ishii, Y. Urata, *The nature of early flame development in a lean-burn stratified-charge spark-ignition engine*, Combustion and Flame, 136 (2004), pp. 283-302.

[38] E. Conte, K. Boulouchos, *Experimental investigation into the effect of reformer gas addition on flame speed and flame front propagation in premixed, homogeneous charge gasoline engines*, Combustion and Flame, 146 (2006), pp. 329-347.

[39] M. Fairweather, M. P. Ormsby, C. G. W. Sheppard, R. Woolley, *Turbulent burning rates of methane and methane-hydrogen mixtures*, Combustion and Flame, 156 (2009), pp. 780-790.

[40] J. F. Driscoll, *Turbulent premixed combustion: Flamelet structure and its effect on turbulent burning velocities*, Progress in Energy and Combustion Science, 34 (2008), pp. 91-134.

I-Analyse des performances et des émissions de polluants

2. Combustion characteristics and emissions in a spark-ignition engine

Ce chapitre est sousmis dans la revue scientifique *International Journal of Engine Research* :

T. Tahtouh, F. Halter, E. Samson, C. Mounaïm-Rouselle, *Effects of hydrogen addition under lean and diluted conditions on combustion characteristics and emissions in a spark-ignition engine,* submitted.

2.1 Abstract

Experimental investigations on the effects of hydrogen addition to Spark- Ignition (S.I.) engines running under lean and diluted conditions are presented in this paper. Experiments were carried out in a mono-cylinder S.I. engine with different rates of nitrogen dilution (0 to 20% by volume in the total mixture) and hydrogen/iso-octane blends (from 0 to 80% by volume in the fuel). The study of the impact of hydrogen addition on combustion characteristics and emissions was performed for two different engine speeds and loads. The equivalence ratio, the rate of dilution and the intake pressure were varied either separately or simultaneously in order to maintain a constant engine load at a fixed hydrogen fraction in the fuel. The lean and dilution operating limits were also determined for all the iso-octane/hydrogen/air/nitrogen mixtures investigated and results show that these limits are extended only when the hydrogen percentage in the fuel is higher than 40% by volume. At a fixed engine load, HC and CO emissions decrease with the increase in hydrogen fraction in the intake mixture, while NO_X emissions are mainly affected by the equivalence ratio and by the amount of dilution. Pumping losses, combustion efficiency and indicated efficiency are also improved with the addition of hydrogen. High values of indicated engine efficiency with low values of HC, NO_X and CO emissions can be achieved by combining hydrogen addition with lean and/or diluted conditions.

Nomenclature:

- Cov_{imep} : coefficient of variation in net indicated mean effective pressure [%]
- $imep_g$: gross indicated mean effective pressure [kPa]
- $imep_n$: net indicated mean effective pressure [kPa]
- $pmep$: pumping mean effective pressure [kPa]
- N : engine speed [rpm]
- P_{in} : intake absolute pressure [kPa]
- X_{O_2} : mole fraction of oxygen in the total mixture [-]
- α : mole fraction of hydrogen in the iso-octane-hydrogen blend [-]
- $Perc_{\alpha total\ mixture}$: hydrogen volume percentage in the total mixture [%]
- β : mole fraction of nitrogen used for dilution in the total mixture [-]
- β_{DL} : β value for dilution operating limit [-]
- β_{air} : mole fraction of the air in excess [-]
- $\beta_{N2-excess\ air}$: mole fraction of the nitrogen contained in the air in excess [-]
- β_{tot} : equivalent dilution rate parameter [-]
- η_c : combustion efficiency [-]
- η_{i-n} : net indicated efficiency [-]
- η_{i-g} : gross indicated efficiency (not including the pumping losses) [-]
- ϕ : global equivalence ratio [-]
- ϕ_{LL} : global equivalence ratio of the lean operating limit [-]

2.2 Introduction

Due to environmental problems and increasingly drastic vehicle emissions standards, current research into Internal Combustion engines aims at reducing pollutant emissions while at the same time increasing engine efficiency.

The operation of an SI engine on lean or diluted mixtures improves thermodynamic efficiency [1, 2] and yields a reduction in CO and HC engine-out emissions [3, 4]. NO_X emissions can also be reduced as a result of decreased cylinder temperature arising from the increased dilution [1]. There are however limitations on the level of dilution and of lean mixture that can ensure the smooth running of SI engines: an increase in combustion duration, cycle-by-cycle variations, and misfire.

One approach to overcome these drawbacks by widening the lean/dilution operating range and by increasing the flame speed is the addition of a certain amount of hydrogen in the fuel. The use of hydrogen as an additive to gasoline in S.I. engines has been extensively studied [1-17].

The wide flammability range of hydrogen extends the lean combustion limits of hydrogen-gasoline mixtures, which can reduce partial burning and misfire in lean and diluted conditions. This leads to a decrease in HC [7, 8] and CO emissions [7]. The high burning velocity of hydrogen reduces the combustion duration [18], increases the thermal efficiency of the engine [1, 7-9] and reduces the coefficient of variation in indicated mean effective pressure (Cov_{imep}).

Moreover, Yüksel and Ceviz [12] concluded that the addition of hydrogen leads to a significant reduction in heat loss to the cooling water.

HC emissions, resulting from the crevice effect, are also reduced with hydrogen addition due to the short quenching distance of hydrogen: a hydrogen blend hydrocarbon flame can propagate much closer to the walls and crevices than a hydrocarbon flame.

The addition of hydrogen can also improve the Knock tendency in an SI engine since it reduces the combustion period and inhibits fuel decomposition and hydroxyl radical production [5, 6]. D'Andrea et al. [13] found that the effects of hydrogen addition on the burning duration and cycle-to-cycle variation are pronounced only under lean conditions. Moreover, in a previous experimental investigation [18] conducted in an optical spark-ignition engine, we found that the enhancement effect of hydrogen on the combustion duration is greater in the initial stages of flame kernel propagation than in the later stages and that this positive effect of hydrogen increases with the dilution rate in the mixture.

Similar conclusions on the increasingly positive effect of hydrogen addition with an increase in dilution level were underlined in [14, 15] for SI engines fuelled with different gasoline-

hydrogen mixtures and different amounts of dilution. When the net Indicated Mean Effective Pressure, $imep_n$, and the engine speeds are fixed, there are mainly three parameters that can be modified by varying the hydrogen and the dilution amounts in the mixture: the equivalence ratio, the amount of dilution and the intake pressure.

However, results that consider these variations separately (equivalence ratio, amount of dilution and intake pressure) are scarce. The aim of this study is to investigate the effect of hydrogen addition on the combustion characteristics and emissions, under lean and diluted conditions, in an SI engine fuelled with iso-octane by varying either separately or simultaneously the equivalence ratio, the amount of dilution and the intake pressure. Since the $imep_n$ reflects the engine working performance, the effects of hydrogen addition and nitrogen dilution were investigated at a fixed $imep_n$.

The lean operating limit was also determined for all the iso-octane/hydrogen/air/nitrogen mixtures investigated, at two different combined intake pressure and engine speed conditions.

2.3 Experimental setup

2.3.1 Engine

Experiments were carried out in mono-cylinder S.I. engine characterized by a four-valve pent-roof chamber, a displacement volume V_{Cyl} of $5 \cdot 10^{-4}$ m^3 and a compression ratio of 9.5. The bore, stroke and connecting rod length were respectively 88 mm, 82 mm and 137 mm. The engine was driven by an electric motor at a fixed engine speed, and equipped with an optical encoder mounted on the main shaft, giving a 0.1 Crank Angle Degree (CAD) as resolution. A conventional spark plug with an electrode space of 1mm was used. A timer card ensured synchronization of the various trigger signals and data acquisition systems. The engine sucks in the air through a thermal mass flow-meter and all other flows were evaluated from this reference flow. Hydrogen and nitrogen flows were measured by using thermal mass flow-meters with an accuracy of ±0.7% for the instantaneous flow. Before the intake pipe, all the gases passed through a plenum volume, to avoid pressure oscillations inside the intake port. To provide a premixed air-fuel mixture inside the intake pipe, the liquid fuel injection was divided into 4 small injections per cycle. The iso-octane quantity was measured by using a 0-8 kg/h Brooks Quantim (QMBM) Coriolis mass flow meter with a maximum combined standard uncertainty of ±1% for the minimum flow rate considered in the present work.

Cylinder pressure was recorded with a water-cooled AVL quartz pressure transducer connected to a charge amplifier at 0.1 CAD resolution. Before experiments, the transducer was calibrated with a Keller high pressure hydraulic calibrator.

The linearity (<±0.6%) of the transducer was verified starting from a maximum pressure of 10MPa (>maximum pressure in the engine). In this work, the absolute cylinder pressure was deduced by equalizing the in-cylinder pressure at 20 CAD after inlet valve opening timing to the intake mean absolute pressure. Thus, 100 consecutive cycles of cylinder pressure data were acquired by a PC equipped with a National Instruments acquisition board.

The exhaust emissions of NO_X, HC, CH_4, CO, CO_2, O_2 from the test engine were measured by a classical emission analyzer (from Environment S.A) with an accuracy <2% of the measured value and 1% of full scale. O_2 emissions were determined by the polarization mode dispersion measuring technique. NO_X were measured by the chemiluminescent method. CO and CO_2 were detected by the non-dispersive infrared method while HC and CH_4 emissions were determined by the heated flame ionization detector method.

2.3.2 Operating conditions and engine parameters

The criterion used in this study to determine the lean and dilution operating limits is based on the value of Cov_{imep} that should not exceed 5%.

Cov_{imep} is defined as:

$$Cov_{imep} = 100 \bullet \frac{std_{imep}}{imep_n} [\%] \quad (1)$$

where std_{imep} is the standard deviation of the net imep ($imep_n$).

The spark ignition was set at the Optimum Spark Timing (OST), which produces the maximum imep. Ji et al. [10] investigated the effect of spark timing on the performance of hydrogen-enriched gasoline in lean conditions and found that for all excess air ratios and hydrogen addition levels, Cov_{imep} attains its minimum value at the OST. The amount of hydrogen in the fuel was varied between 0% and 80% by volume and the amount of dilution in the total mixture was between 0% and 20% by volume. For all results, the parameter α is defined as the mole fraction of hydrogen in the iso-octane/hydrogen blend:

$$\alpha = \frac{X_{H_2}}{X_{C_8H_{18}} + X_{H_2}} \quad (2)$$

and the parameter of dilution, β is the mole fraction of nitrogen used for dilution in the total mixture:

$$\beta = \frac{X_{N_2-dilution}}{X_{C_8H_{18}} + X_{H_2} + X_{O_2} + X_{N_2-air} + X_{N_2-dilution}} = X_{N_2-dilution} \quad (3)$$

where $X_{C_8H_{18}}$, X_{H_2} and X_{O_2} are respectively iso-octane, hydrogen and oxygen mole fractions in the mixture, X_{N_2-air} the mole fraction of nitrogen in the air mixture ($X_{N_2-air} = 3.78 \bullet X_{O_2}$) and $X_{N_2-dilution}$ the mole fraction of nitrogen used for dilution.

The global equivalence ratio ϕ of iso-octane/hydrogen/nitrogen/air mixtures is obtained as:

$$\phi = \frac{\dot{m}_{C_8H_{18}} \bullet AF_{st-C_8H_{18}} + \dot{m}_{H_2} \bullet AF_{st-H_2}}{\dot{m}_{air}} \quad (4)$$

where $\dot{m}_{C_8H_{18}}$, $\dot{m}_{H_2}$ and $\dot{m}_{air}$ are respectively iso-octane, hydrogen and air measured mass flow rates (g/h). $AF_{st-C_8H_{18}}$ and AF_{st-H_2} are the stoichiometric air to fuel ratios of iso-octane and hydrogen respectively. The global equivalence ratio, ϕ_{ded}, was also deduced using the composition of the exhaust gases and a very good agreement with the ϕ given by the mass flow rates was found. Plotting ϕ versus the deduced equivalence ratio ϕ_{ded} and applying a simple linear least-squares fitting gives a coefficient of determination R^2 of 0.985 for all the conditions considered in the present study, i.e. 49 different conditions.

Another parameter β_{air} is introduced in order to compare the effect of nitrogen dilution and the effect of lean conditions. β_{air} is therefore the excess air mole fraction in the mixture and is defined as:

$$\beta_{air} = (1-\phi) \cdot \left(X_{O_2} + X_{N_2-air} \right) \quad (5)$$

Since:

$$\phi = \frac{\left(\frac{\dot{m}_{H_2} + \dot{m}_{C_8H_{18}}}{\dot{m}_{air}} \right)}{\left(\frac{\dot{m}_{H_2} + \dot{m}_{C_8H_{18}}}{\dot{m}_{air-stoichiometry}} \right)} = \frac{\dot{m}_{air-stoichiometry}}{\dot{m}_{air}} = \frac{\dot{V}_{air-stoichiometry}}{\dot{V}_{air}} \Rightarrow \dot{V}_{air} - \dot{V}_{air-stoichiometry} = (1-\phi) \cdot \dot{V}_{air};$$

$$\beta_{air} = \frac{\dot{V}_{air} - \dot{V}_{air-stoichiometry}}{\dot{V}_{total}} \Rightarrow \beta_{air} = (1-\phi) \cdot \frac{\dot{V}_{air}}{\dot{V}_{total}}$$

where $\dot{V}_{C_8H_{18}}$, $\dot{V}_{air}$ and $\dot{V}_{total}$ are respectively iso-octane, air and total volume flow rates (m^3/h).

The mole fraction of nitrogen contained in the air in excess $\beta_{N2-excess\,air}$, is also defined as:

$$\beta_{N2-excess\,air} = (1-\phi) \cdot \left(X_{N_2-air} \right) \quad (6)$$

The combustion efficiency η_c can be determined as [19]:

$$\eta_c = 1 - \frac{(\dot{m}_{C_8H_{18}} + \dot{m}_{H_2} + \dot{m}_{air}) \bullet \sum_i \chi_i \bullet LHV_i}{\dot{m}_{C_8H_{18}} \bullet LHV_{C_8H_{18}} + \dot{m}_{H_2} \bullet LHV_{H_2}} \quad (7)$$

where $LHV_{C_8H_{18}}$ and LHV_{H_2} are the lower heating values of iso-octane and hydrogen respectively. χ_i are the mass fractions of CO, H_2 and HC in the exhaust gases and LHV_i are the lower heating values of these species respectively.

It was assumed that the unburned hydrocarbons (HC) have the same C/H ratio and heating value as the fuel mixture.

The engine speeds, N, were 2500 and 2000 rpm. The oil and coolant temperatures were set at 80°C. The $imep_n$ was fixed at 287 ±2.5% kPa and 407 ±2.5% kPa and the corresponding reference intake pressures (absolute) P_{in} were 55 kPa and 70 kPa respectively. Thus, the effect of hydrogen blend and mixture dilution were investigated at two different operating conditions (two engine speeds and $imep_n$) in order to reach general conclusions. The different conditions investigated are summarized in Tables 1.a, 1.b, 1.c and 1.d. The hydrogen volume percentages in the total mixture $Perc_{\alpha total\,mixture} = 100\% \bullet X_{H_2}$ are also reports in Tables 1.a, 1.b, 1.c and 1.d.

The net indicated efficiency can be determined as:

$$\eta_{i-n} = \frac{imep_n \bullet V_{cyl} \bullet (N/60) \bullet (1/2)}{\dot{m}_{C_8H_{18}} \bullet LHV_{C_8H_{18}} + \dot{m}_{H_2} \bullet LHV_{H_2}} \quad (8)$$

The pumping work is the work done by the piston on the in-cylinder gases during the inlet and exhaust strokes. In the present work, the exhaust pressure (atmospheric pressure) is always higher than the intake pressure. This pumping work, calculated during the inlet and exhaust strokes, is evaluated by the pumping mean effective pressure $pmep$ (defined as a positive quantity). We defined the gross indicated mean effective pressure $imep_g$ as:

$$imep_g = imep_n + pmep \quad (9)$$

In order to exclude the effect of pumping work, the gross indicated efficiency η_{i-g} is introduced as:

$$\eta_{i-g} = \frac{(imep_g) \bullet V_{cyl} \bullet (N/60) \bullet (1/2)}{\dot{m}_{C_8H_{18}} \bullet LHV_{C_8H_{18}} + \dot{m}_{H_2} \bullet LHV_{H_2}} \quad (10)$$

Four distinct cases of operating conditions were considered in order to separate the effects of hydrogen addition, lean conditions and nitrogen dilution from the effect of pumping work, which has a strong impact on engine efficiency and varies with the intake pressure.

Table 1.a *Conditions investigated:* ***Case A***

α	β	**Equivalence ratio**	**Engine speed** [rpm]	$Imep_n$ [kPa]	P_{in} [kPa]	$Perc_{\alpha total\ mixture}$ [%]
0	0	0.7	2500	287	55	0
0.4	0	0.68	2500	287	55	0.7
0.6	0	0.68	2500	287	55	1.6
0.8	0	0.66	2500	287	55	3.6
0	0.2	0.9	2500	287	55	0
0.4	0.2	0.85	2500	287	55	0.7
0.6	0.2	0.84	2500	287	55	1.5
0.8	0.2	0.84	2500	287	55	3.7
0	0	0.7	2000	407	70	0
0.2	0	0.68	2000	407	70	0.3
0.4	0	0.68	2000	407	70	0.7
0.6	0	0.68	2000	407	70	1.6
0.8	0	0.65	2000	407	70	3.6
0	0.1	0.76	2000	407	70	0
0.2	0.1	0.75	2000	407	70	0.3
0.4	0.1	0.7	2000	407	70	0.7
0.6	0.1	0.7	2000	407	70	1.5
0.8	0.1	0.7	2000	407	70	3.5
0	0.2	0.78	2000	407	70	0
0.2	0.2	0.78	2000	407	70	0.3
0.4	0.2	0.78	2000	407	70	0.7
0.6	0.2	0.78	2000	407	70	1.4
0.8	0.2	0.78	2000	407	70	3.4

- Case A (Table 1.a): the intake pressure was maintained fixed (reference intake pressure values) and the equivalence ratio was varied to obtain the desired $imep_n$ value for different amounts of nitrogen dilution (β=0, 0.1 and 0.2) and hydrogen addition (α=0, 0.2, 0.4, 0.6 and 0.8).

Table 1.b *Conditions investigated:* ***Case B***

α	β	**Equivalence ratio**	**Engine speed** [rpm]	$Imep_n$ [kPa]	P_{in} [kPa]	$Perc_{\alpha total\ mixture}$ [%]
0.4	0.26	1	2500	287	55	0.8
0.6	0.26	1	2500	287	55	1.7
0.8	0.27	1	2500	287	55	3.9
0	0.295	1	2000	407	70	0
0.2	0.3	1	2000	407	70	0.3
0.4	0.3	1	2000	407	70	0.7
0.6	0.3	1	2000	407	70	1.6
0.8	0.3	1	2000	407	70	3.8

- Case B (Table 1.b): the intake pressure and the equivalence ratio were maintained fixed (reference intake pressure values and stoichiometric conditions) but different amounts of hydrogen were considered (α=0, 0.2, 0.4, 0.6 and 0.8), and the amount of dilution was adjusted to obtain the desired $imep_n$ value.

Table 1.c *Conditions investigated:* ***Case C***

α	β	**Equivalence ratio**	**Engine speed** [rpm]	$Imep_n$ [kPa]	P_{in} [kPa]	$Perc_{\alpha total\ mixture}$ [%]
0.4	0	0.65	2500	287	57	0.7
0.6	0	0.61	2500	287	58	1.4
0.8	0	0.54	2500	287	63	3
0.6	0.2	0.82	2500	287	56	1.5
0.8	0.2	0.7	2500	287	62	3.1
0.4	0	0.62	2000	407	73	0.7
0.6	0	0.58	2000	407	75	1.3
0.8	0	0.54	2000	407	78	3
0.4	0.1	0.67	2000	407	72	0.6
0.6	0.1	0.65	2000	407	74	1.4
0.8	0.1	0.55	2000	407	82	2.7
0.4	0.2	0.76	2000	407	72	0.6
0.6	0.2	0.73	2000	407	73	1.3
0.8	0.2	0.64	2000	407	81	2.8

- Case C (Table 1.c): the lean operating limit, ϕ_{LL}, was determined at reference intake pressures (55 kPa or 70 kPa) and for determined amounts of nitrogen dilution (β=0, 0.1 and 0.2) and hydrogen addition (α=0.4, 0.6 and 0.8). Then the equivalence ratio was fixed at the

value corresponding to the lean operating limit ϕ_{LL} found, and the intake pressure was varied to obtain the desired $imep_n$ value.

Table 1.d** Conditions investigated: **Case D

α	β	**Equivalence ratio**	**Engine speed** [rpm]	$Imep_n$ [kPa]	P_{in} [kPa]	$Perc_{\alpha total\ mixture}$ [%]
0.8	0.35	1	2500	287	60	3.5
0.4	0.31	1	2000	407	71	0.7
0.6	0.34	1	2000	407	74	1.5
0.8	0.38	1	2000	407	77	3.3

- Case D (Table 1.d): the dilution operating limit, β_{DL} , was determined at the reference intake pressure (55 kPa or 70 kPa) and with a stoichiometric equivalence ratio and for determined amounts of hydrogen addition (α=0.4, 0.6 and 0.8). The dilution amount was fixed at the value corresponding to the dilution operating limit found, β_{DL} and the intake pressure was varied to obtain the desired $imep_n$ value.

2.4 Results and discussion

2.4.1 Lean and Dilution operating limits

Lean Operating limits (L.O.L.) were determined for different amounts of hydrogen blends (α=0, 0.2, 0.4, 0.6 and 0.8) and nitrogen dilution (β=0, 0.1 and 0.2). Two couples of intake pressure and engine speed conditions were considered:

P_{in} = 70 kPa, N = 2000 rpm and P_{in} = 55 kPa, N = 2500 rpm

As shown in Figure 1.a, by increasing α from 0 to 0.8, the L.O.L decreases by 20.6% (from 0.68 to 0.54) for undiluted mixtures (β=0). Similar levels of decrease (18%-25%) in L.O.L. were also observed for the other conditions (β= 0.1 and 0.2). For small values of α (up to 0.2), no effect of hydrogen addition on the extension of L.O.L. was observed. The decrease in L.O.L. is not linear with α and is more pronounced for higher values of α, which can be explained by the non linearity between the hydrogen mole fraction (α=0.2 and α=0.8) and the hydrogen mass fraction (0.004 for α=0.2 and 0.066 for for α=0.8) or energy fraction (0.012 for α=0.2 and 0.16 for α=0.8) in the fuel mixture. It can also be seen that the L.O.L. increases with nitrogen dilution β.

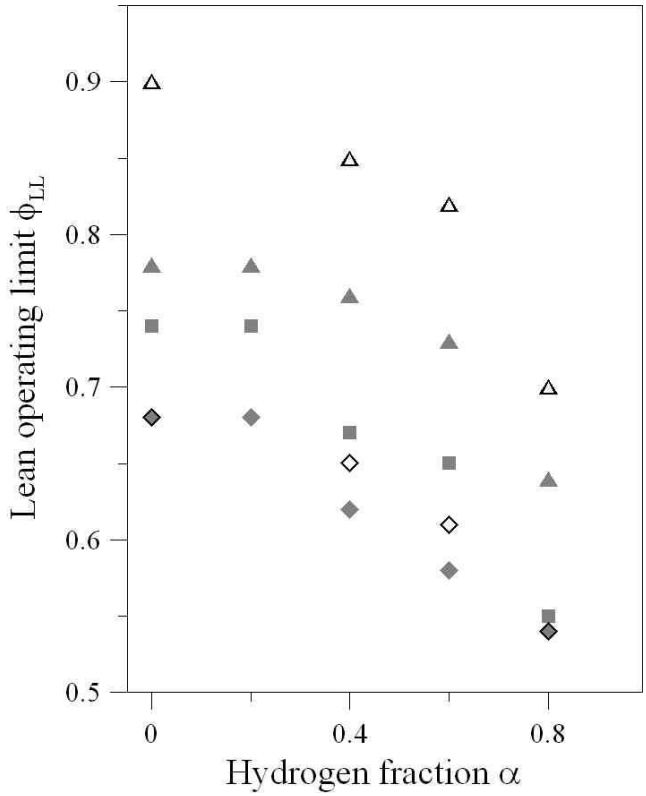

Figure 1.a *Evolution of the lean operating limit ϕ_{LL} versus hydrogen mole fraction α :*
P_{in}=55 kPa, N=2500 rpm, ◇ β =0; △ β =0.2.
P_{in}=70 kPa, N=2000 rpm, ◆ β =0; ■ β =0.1; ▲ β =0.2.

The dilution operating limit (D.O.L.) increases with hydrogen addition (Figure 1.b) and does not evolve linearly with α either. For α=0.2, the dilution tolerance is increased by 2% compared to 30% and 59% when α=0.8, for respectively P_{in} = 70 kPa, N = 2000 rpm and P_{in} = 55 kPa, N = 2500 rpm.

D'Andrea et al. [13] found that the effect of hydrogen addition for ϕ >0.85 on *imep*, burning duration and cycle-to-cycle variation is negligible when approximately 60% of hydrogen by volume was added.

Figures 2.a and 2.b compare air dilution (i.e. lean mixtures conditions) and nitrogen dilution operating limits for different hydrogen contents at fixed regimes and intake pressures. It can be observed that the air dilution allows a wider operating limit than the nitrogen dilution for all conditions. This is due to the higher oxidant concentration in the case of air dilution compared to nitrogen one.

For example, when the amount of hydrogen is equal to 0.8 (α=0.8), the maximum amount of air in excess is ~45% whereas the maximum amount of nitrogen dilution is ~35% and ~38% for respectively P_{in} = 55 kPa, N = 2500 rpm (figure 2.a) and P_{in} = 70 kPa, N = 2000 rpm (figure 2.b).

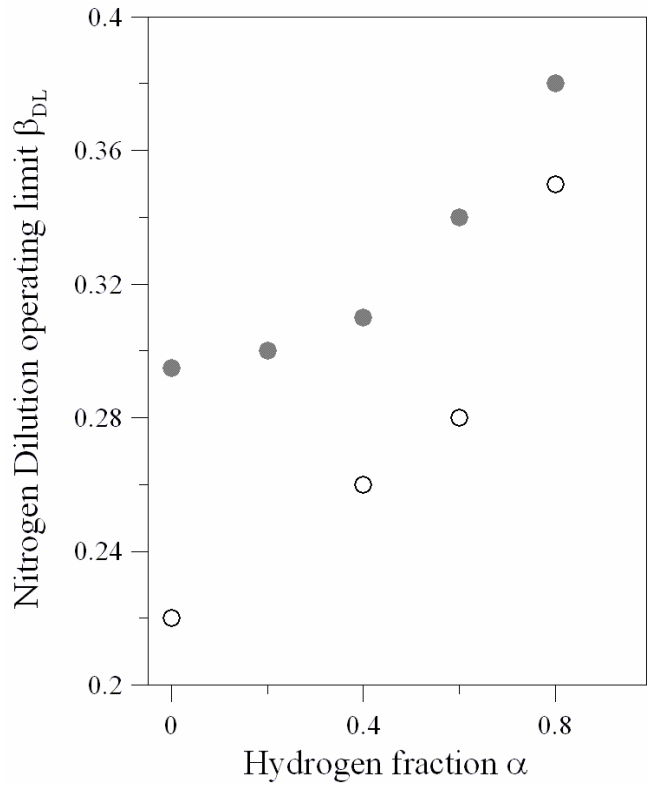

Figure 1.b *Evolution of the nitrogen dilution operating limit β_{DL} versus hydrogen mole fraction α :*
○ P_{in}=55 kPa, N=2500 rpm, ϕ =1.
● P_{in}=70 kPa, N=2000 rpm, ϕ =1.

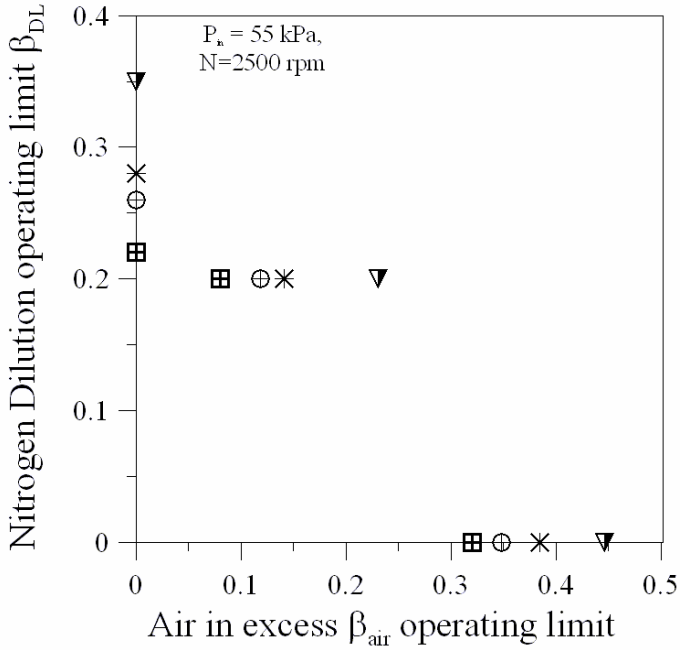

Figure 2.a *Evolution of the nitrogen dilution operating limit β_{DL} versus air addition β_{air} operating limit ($imep_n$ = 287 kPa, N = 2500 rpm):*
⊞ α =0; ⊕ α =0.4; ✳ α =0.6; ◥ α =0.8.

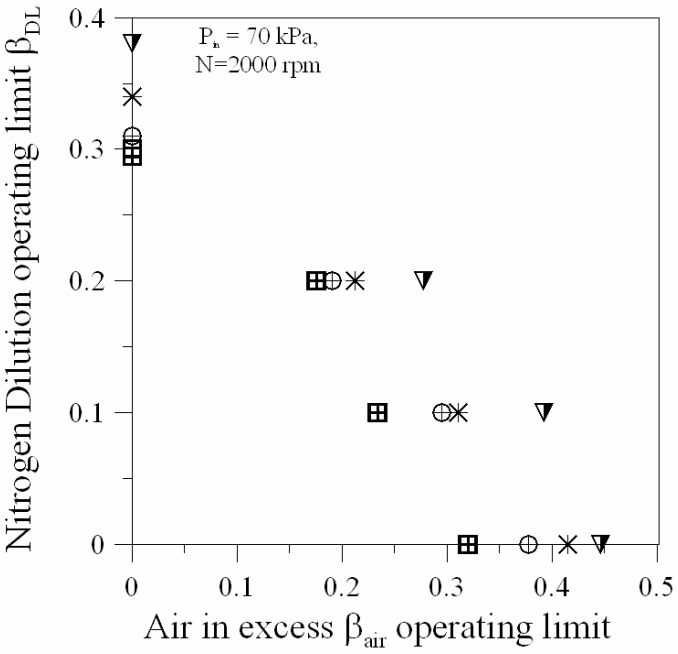

Figure 2.b *Evolution of the nitrogen dilution operating limit* β_{DL} *versus air addition* β_{air} *operating limit (*$imep_n$ *= 407 kPa,* N *= 2000 rpm):* ⊞ α *=0;* ⊕ α *=0.4;* ✳ α *=0.6;* ▽ α *=0.8.*

The main conclusion that can be drawn is that the addition of hydrogen, even with small amounts in terms of mass fraction (0.066 f or α=0.8), in the fuel mixture can widen the LOL (by ~20%) and the DOL (by 30% and 59%), results which are in good agreement with those of [9].

2.4.2 Exhaust emissions

I- HC emissions

The evolution of HC emissions versus hydrogen fraction α is presented in Figure 3.a and Figure 3.b. The impact of hydrogen addition on HC emissions is a combination of three effects:

First, the addition of hydrogen leads to an increase in the Hydrogen atoms/ Carbon atoms (H/C) ratio in the fuel and therefore reduces HC emissions. Secondly, the quenching distance of hydrogen is lower than that of iso-octane, thus the addition of hydrogen allows the flame to propagate much closer to the cylinder wall and crevices than in the case of a pure iso-octane flame (without hydrogen addition). Finally, since η_c and HC emissions are directly linked, HC emissions are lower for higher values of combustion efficiency.

HC emissions do not change for α<0.4 since the maximum difference between HC emissions corresponding to α=0 and α=0.2 (Figure 3.b) is only 2.7%. However, as this difference is comparable to the measurement accuracy, no conclusions can be drawn.

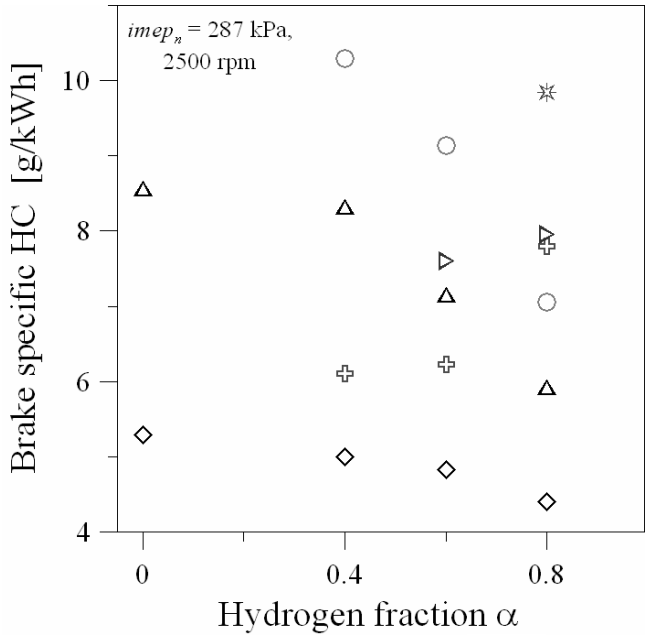

Figure 3.a *Brake specific HC versus hydrogen content α ($imep_n$ = 287 kPa, N = 2500 rpm):*
CASE C ϕ_{LL}, β =0; CASE C ϕ_{LL}, β =0.2; CASE D β_{DL}, ϕ =1;
CASE A P_{in}=55kPa, β =0; CASE A P_{in}=55kPa, β =0.2; CASE B P_{in}=55kPa, ϕ =1.

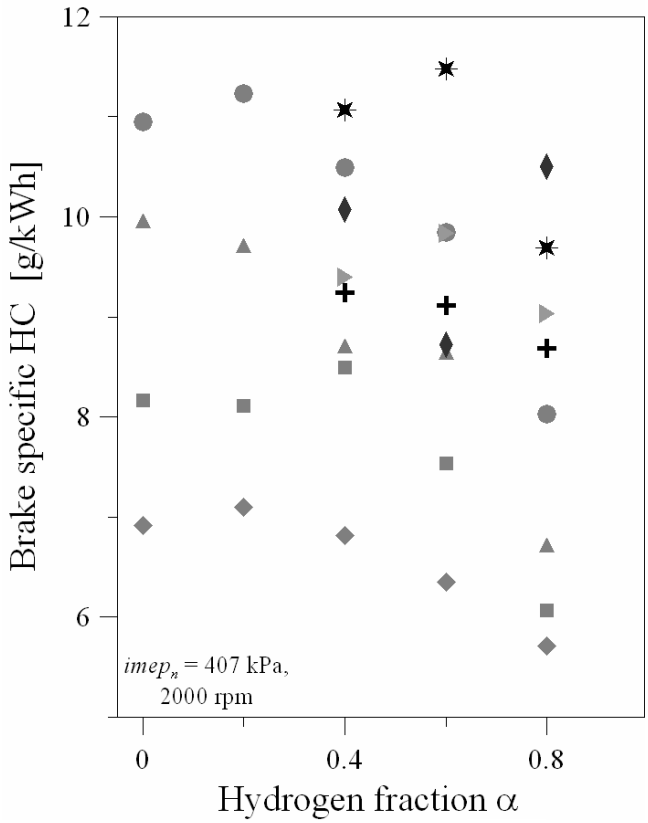

Figure 3.b *Brake specific HC versus hydrogen content α ($imep_n$ = 407 kPa, N = 2000 rpm):*
CASE C ϕ_{LL}, β =0; CASE C ϕ_{LL}, β =0.1; CASE C ϕ_{LL}, β =0.2;
CASE D β_{DL}, ϕ =1; CASE A P_{in}=70kPa, β =0; CASE A P_{in}=70kPa, β =0.1;
CASE A P_{in}=70kPa, β =0.2; CASE B P_{in}=70kPa, ϕ =1.

For α>0.4, HC emissions generally decrease with α, which is in good agreement with [20], except for Cases C with ϕ_{LL} in figure 3.a since HC emissions increase by 22% when α is increased from 0.4 to 0.8 (β=0). This can be explained by the lower burnt gas temperatures, resulting in an earlier flame quenching, and by the deterioration of the combustion quality and therefore efficiency in these conditions of lean operating range. For all other conditions with α>0.4, HC emissions decrease with α. When the hydrogen fraction α is increased from 0.4 to 0.8, the HC emissions are generally reduced by 12% to 31% in Cases A and B. This reduction is less clear in Cases C and D since we are operating in the lean or dilution operating limit, thus the deterioration of η_c and stability (Cov_{imep}) is marked and can mask the positive effect of hydrogen addition (as for example, for α<0.8 in Case C with β=0.2 and Case D in Figure 3.b).

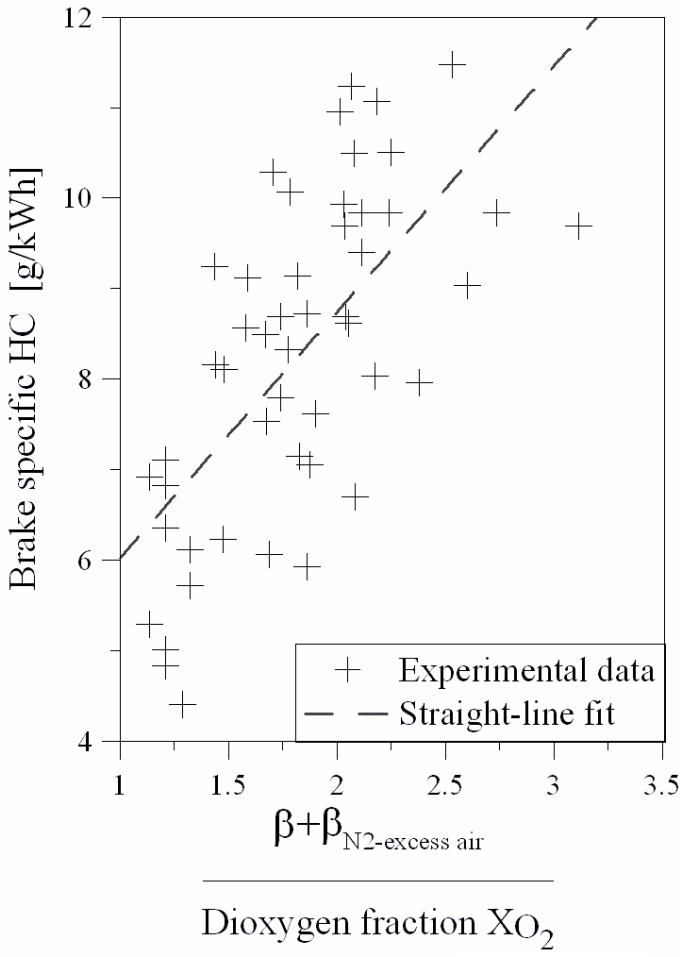

Figure 4. *Brake specific HC versus* $\frac{\beta + \beta_{N2-excess\,air}}{X_{O_2}}$

($imep_n$ *= 287 kPa,* N *= 2500 rpm and* $imep_n$ *= 407 kPa,* N *= 2000 rpm).*

Finally, it can be seen in Figures 3.a and 3.b that for the same value of α, HC emissions increase with the increase in the dilution amount β (in Case A and Case B, for the same P_{in}) and the decrease in ϕ (between Case A and Case C, for the same values of β).

When the HC emissions are plotted versus the ratio $\left(\frac{\beta+\beta_{N2-excess\,air}}{X_{O_2}}\right)$, which is the total amount of nitrogen (due to nitrogen dilution and nitrogen amount in excess air) divided by the total mole fraction of oxygen in the fresh mixture, a linear relation is found (Figure 4). This means that the nitrogen addition leads to higher values in HC emissions than the air addition (lean mixtures) for all the conditions investigated. This ratio increases with the air or nitrogen addition. However, for the same fraction of air and nitrogen addition, this ratio is higher in the case of nitrogen addition than in the case of air addition.

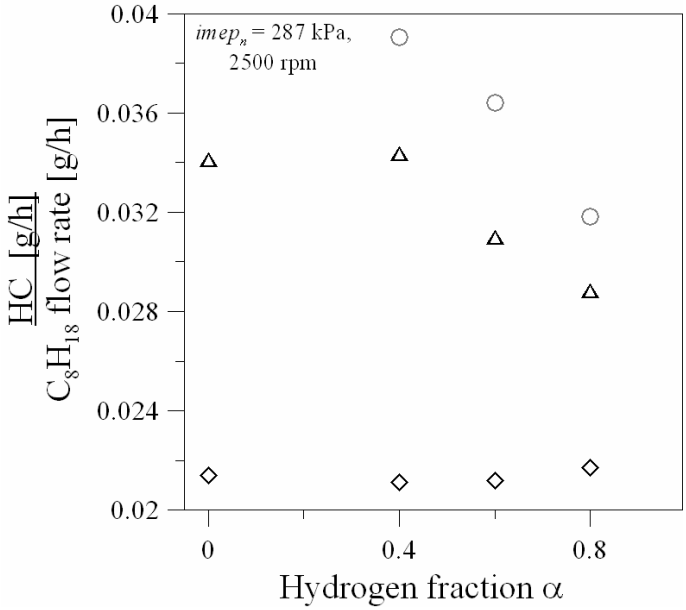

Figure 5.a *Normalized HC emissions versus hydrogen content α ($imep_n$ = 287 kPa, N = 2500 rpm): ◇ CASE A P_{in}=55kPa, β =0; △ CASE A P_{in}=55kPa, β =0.2; ○ CASE B P_{in}=55kPa, ϕ =1.*

In figures 5.a and 5.b, HC emissions were normalized by the iso-octane flow rate in order to investigate the effect of H/C ratio of the fuel mixture on the reduction of HC emissions. Cases C and D were not reported for the sake of clarity.

It can be noted that for lean mixtures, the ratio of HC emissions to the iso-octane flow rate does not change with the hydrogen addition.

The H/C ratio is therefore the main cause of HC emissions reduction.

For mixtures with nitrogen dilution, a decrease in the HC emissions is observed with the hydrogen substitution (when α is higher than 0.4). Moreover this decrease is more pronounced for mixtures characterized by higher value of β.

Thus for mixtures with nitrogen dilution, the decrease in HC emission with the hydrogen substitution is due to the combined effects cited in the beginning of the present HC emissions section: higher H/C ratio, lower quenching distance and higher combustion efficiency.

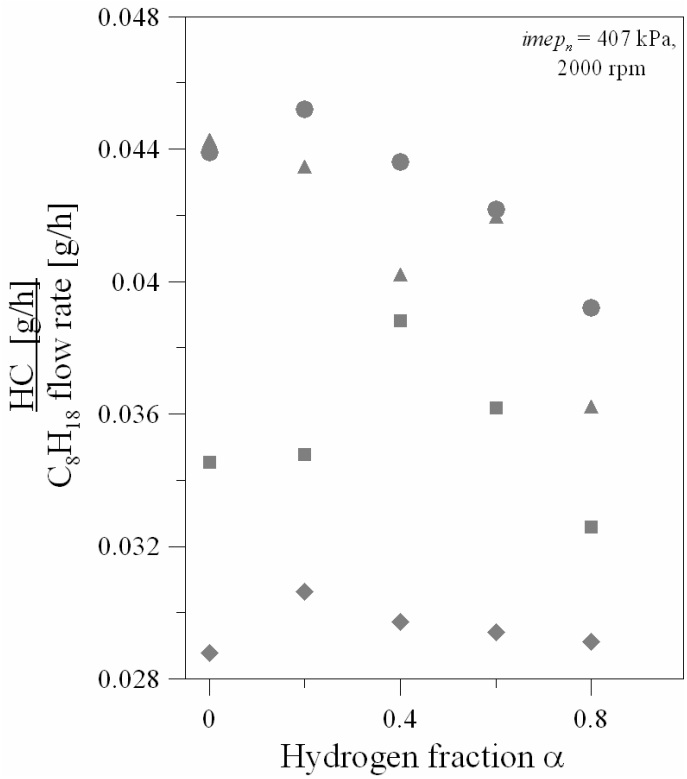

Figure 5.b *Normalized HC emissions versus hydrogen content* α *(* $imep_n$ *= 407 kPa, N = 2000 rpm):* ◆ *CASE A* P_{in}*=70kPa,* β *=0;* ■ *CASE A* P_{in}*=70kPa,* β *=0.1;* ▲ *CASE A* P_{in}*=70kPa,* β *=0.2;* ● *CASE B* P_{in}*=70kPa,* ϕ *=1.*

II- NO_X emissions

Contrary to HC emissions, results show that the addition of hydrogen does not have a pronounced effect on NO_X emissions (Figure 6.a and 6.b) for the present mixtures investigated. Thermal NO_X emissions are very sensitive to the in-cylinder temperature and the oxygen concentration in the intake mixture. Indeed, in Figure 7, one can note that NO_X emissions increase sharply with an increase of O_2 concentration for all conditions (for $imep_n$ = 287kPa and 407kPa). Furthermore, when the oxygen fraction (in volume) is less than 15%, NO_X emissions are lower than 1 g/kWh. However, only the lean operating limit conditions have different behavior due to the low burnt gases temperature inducing low thermal NO_X formation. Hydrogen addition leads to an increase in combustion temperature since the adiabatic flame temperature of hydrogen is higher than the iso-octane adiabatic temperature. However, as it extends the lean and dilution operability limits, the additional excess in air or dilution amount reduces the combustion temperature i.e. the rate of thermal NO_X formation.

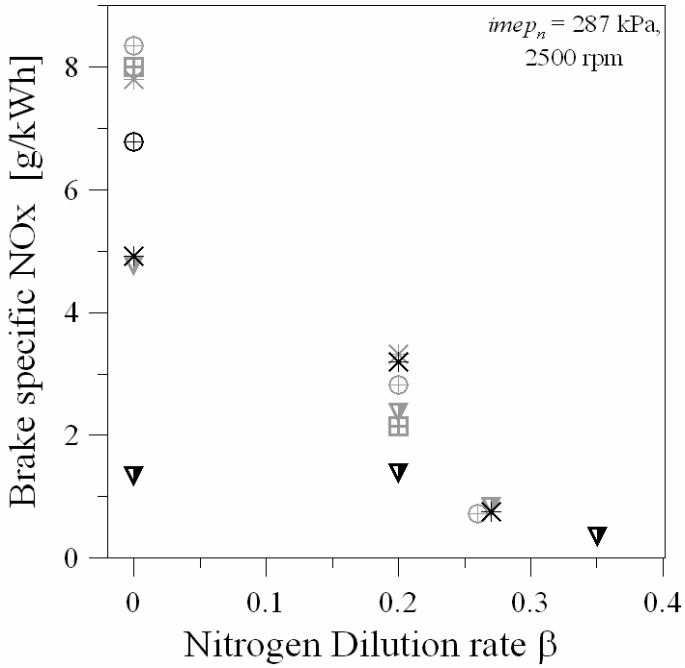

Figure 6.a *Brake specific NO_X versus nitrogen mole fraction used for the dilution β ($imep_n$ = 287 kPa, N = 2500 rpm): ⊞ α =0 CASE A and B; ⊕ α =0.4 CASE A and B; ⊕ α =0.4 CASE C and D; ✳ α =0.6 CASE A and B; ✳ α =0.6 CASE C and D; ▽ α =0.8 CASE A and B; ▼ α =0.8 CASE C and D.*

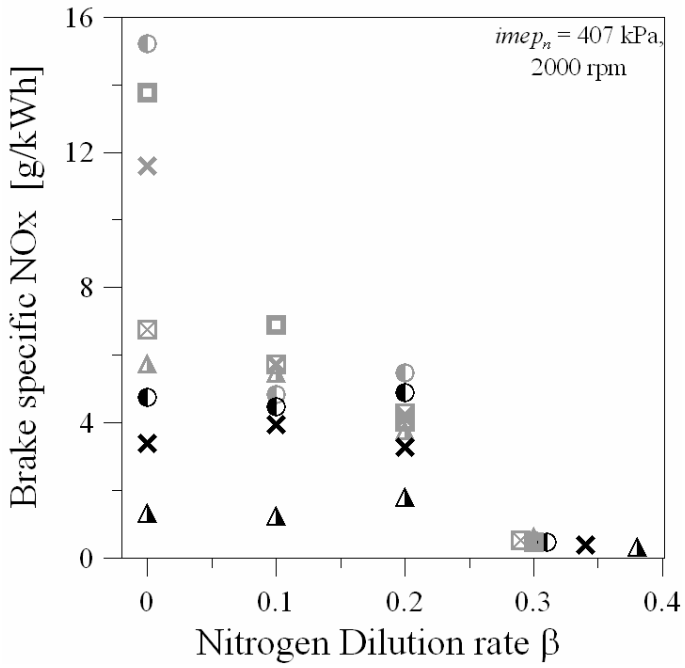

Figure 6.b *Brake specific NO_X versus nitrogen mole fraction used for the dilution β ($imep_n$ = 407 kPa, N = 2000 rpm): ☒ α =0 CASE A and B; ◻ α =0.2 CASE A and B; ◐ α =0.4 CASE A and B; ◐ α =0.4 CASE C and D; ✕ α =0.6 CASE A and B; ✕ α =0.6 CASE C and D; ◭ α =0.8 CASE A and B; ◭ α =0.8 CASE C and D.*

NO_X emissions are mainly affected by the equivalence ratio and the dilution amount: as it can be seen in Figure 6.a and 6.b, NO_X emissions decrease with an increase in β, as previously found in [1, 14]. It can also be noted that the Case C experiments present lower values of NO_X emissions for the same amount of dilution β but a smaller equivalence ratio (ϕ_{LL}) than Case A. Moreover, if only the mixtures of Case C are considered, higher amounts of hydrogen produce lower NO_X emissions since the smaller equivalence ratio (Figure 1).

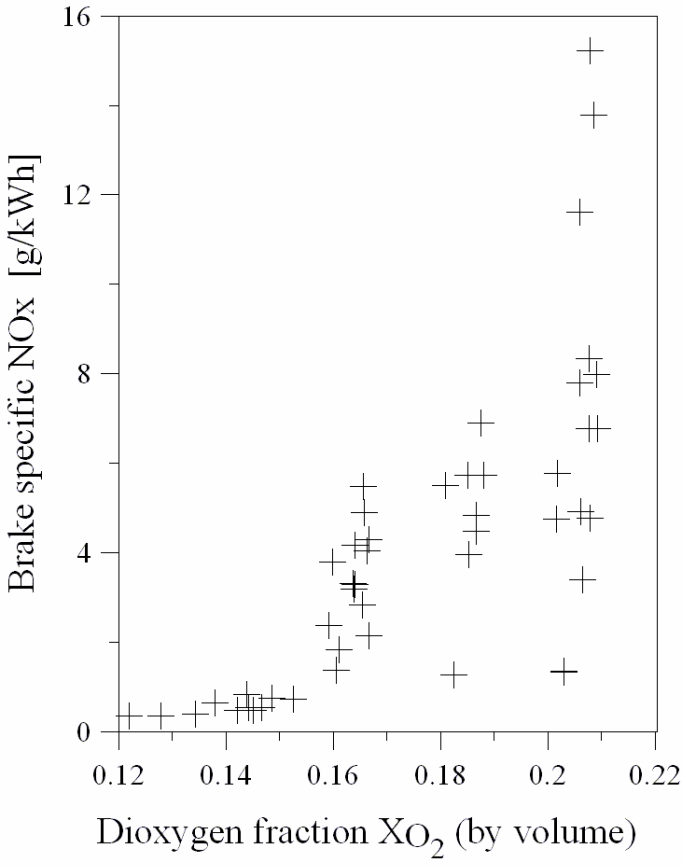

Figure 7. *Brake specific NO_X versus dioxygen mole fraction X_{O_2} ($imep_n$ = 287 kPa, N = 2500 rpm and $imep_n$ = 407 kPa, N = 2000 rpm).*

The mixtures of Case D (β_{DL} and ϕ=1) exhibit the lowest absolute values of NO_X emissions, especially the mixtures with a large amount of hydrogen which allow the use of higher rates of dilution (Figure 1.b). It can be concluded that the effect of dilution is more pronounced and has a higher reducing potential on NO_X emissions than the equivalence ratio, which is in good agreement with [14]. Moreover, in all the conditions investigated (for $imep_n$= 287kPa and 407kPa), when the nitrogen dilution percentage is higher than 25%, NO_X emissions are lower than 1 g/kWh.

These conclusions on the higher reducing effect of nitrogen addition rather than air addition on the NO_X reduction are well illustrated in Figure 8, where NO_X emissions are plotted by using logarithmic scaling versus the ratio $\frac{\beta+\beta_{N2-excess\,air}}{X_{O_2}}$.

A power law decrease in NO_X emissions is observed for all mixture with the increase in the ratio of total nitrogen fraction used.

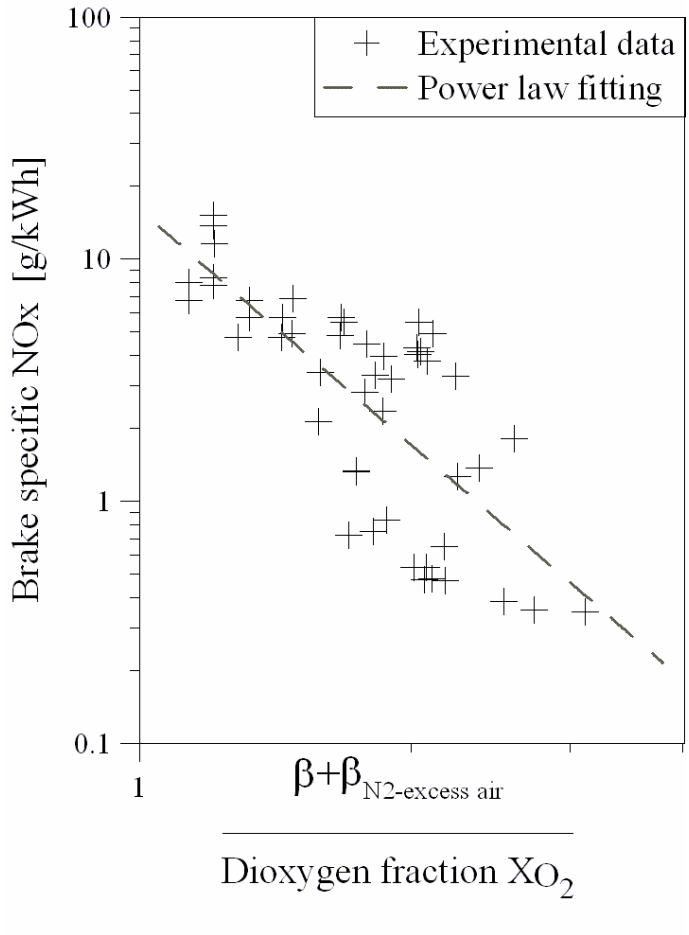

Figure 8. *Brake specific NO_X versus $\frac{\beta+\beta_{N2-excess\,air}}{X_{O_2}}$ using a logarithmic scaling*

($imep_n$ = 287 kPa, N = 2500 rpm and $imep_n$ = 407 kPa, N = 2000 rpm).

III- CO emissions

CO emissions are mainly affected by the equivalence ratio; they decrease in lean conditions due the increase in O_2 concentration which helps the oxidation of CO into CO_2. Two different ranges of values of CO emissions can be distinguished:

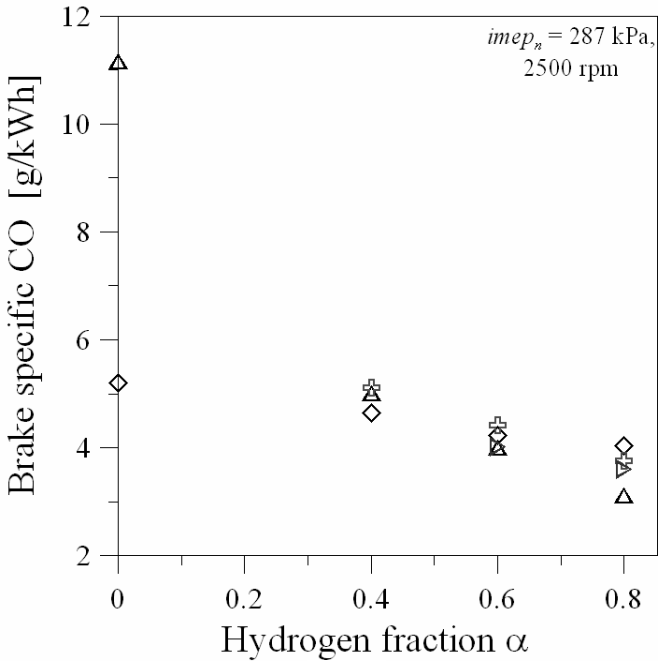

Figure 9.a *Brake specific CO versus α ($imep_n$ = 287 kPa, N = 2500 rpm, ϕ < 1):*
✣ CASE C ϕ_{LL}, β =0; ▷ CASE C ϕ_{LL}, β =0.2;
◇ CASE A P_{in}=55kPa, β =0; △ CASE A P_{in}=55kPa, β =0.2.

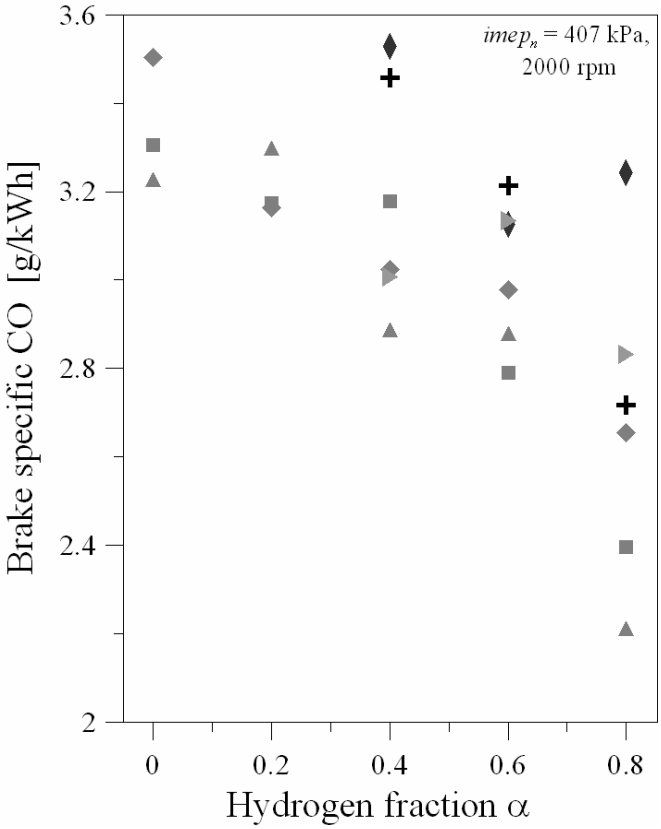

Figure 9.b *Brake specific CO versus α ($imep_n$ = 407 kPa, N = 2000 rpm, ϕ < 1):*
✚ CASE C ϕ_{LL}, β =0; ♦ CASE C ϕ_{LL}, β =0.1; ▶ CASE C ϕ_{LL}, β =0.2;
◆ CASE A P_{in}=70kPa, β =0; ■ CASE A P_{in}=70kPa, β =0.1; ▲ CASE A P_{in}=70kPa, β =0.2.

I-For Cases A and C (figures 9.a and 9.b), in lean conditions, CO emissions present low values: <11.2 g/kWh for $imep_n$=287kPa (figure 9.a) and < 3.8 g/kWh for $imep_n$=407kPa (figure 9.b). Moreover, these emissions are reduced when the hydrogen fraction in the mixture is increased due to the increase in combustion efficiency. Furthermore, as hydrogen is a carbon-free fuel, substituting a mole fraction of iso-octane by hydrogen reduces CO emissions. For Case A, the reduction in CO emissions, when α is increased from 0 to 0.8, is 22% and 72% (for $imep_n$=287kPa) and 24% and 32% (for $imep_n$=407kPa) for β = 0 and β = 0.2 respectively. CO emissions are particularly strong for the condition corresponding to α=0 in Case A with β = 0.2 compared to the other conditions in figure 9.a. This is due to the higher equivalence ratio value (0.9 with respect to ≤0.85 for the other conditions).

II-The highest values of CO emissions (>38 g/kWh) are obtained for stoichiometric conditions (Cases B and D (figure 9.c)). As expected, CO emissions also decrease with hydrogen addition even in these conditions. When α is increased from 0 to 0.8, the CO emissions are reduced by 38% for Case B ($imep_n$=407kPa).

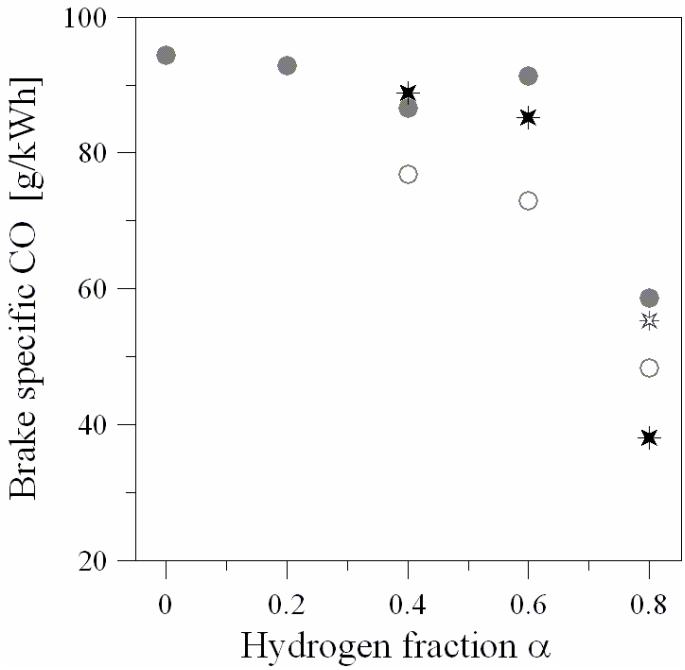

Figure 9.c *Brake specific CO versus α (ϕ = 1):*
$imep_n$ = 287 kPa, N = 2500 rpm: ✲ CASE D β_{DL}, ϕ =1; ○ CASE B P_{in}=55kPa, ϕ =1.
$imep_n$ = 407 kPa, N = 2000 rpm: ✶ CASE D β_{DL}, ϕ =1; ● CASE B P_{in}=70kPa, ϕ =1.

In Figures 10.a, 10.b and 10.c, as in the case of HC emissions, CO emissions were normalized by the iso-octane flow rate.

For lean mixtures, CO emissions decrease with the hydrogen addition only when there is nitrogen dilution. This reducing effect becomes more important for mixtures with a higher amount of nitrogen dilution β.

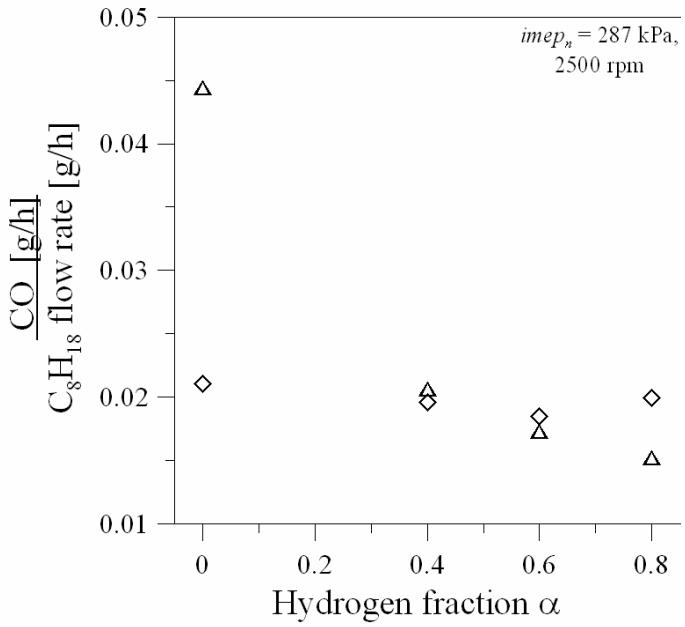

Figure 10.a *Normalized CO emissions versus α ($imep_n$ = 287 kPa, N = 2500 rpm, ϕ < 1): ◇ CASE A P_{in}=55kPa, β =0; △ CASE A P_{in}=55kPa, β =0.2.*

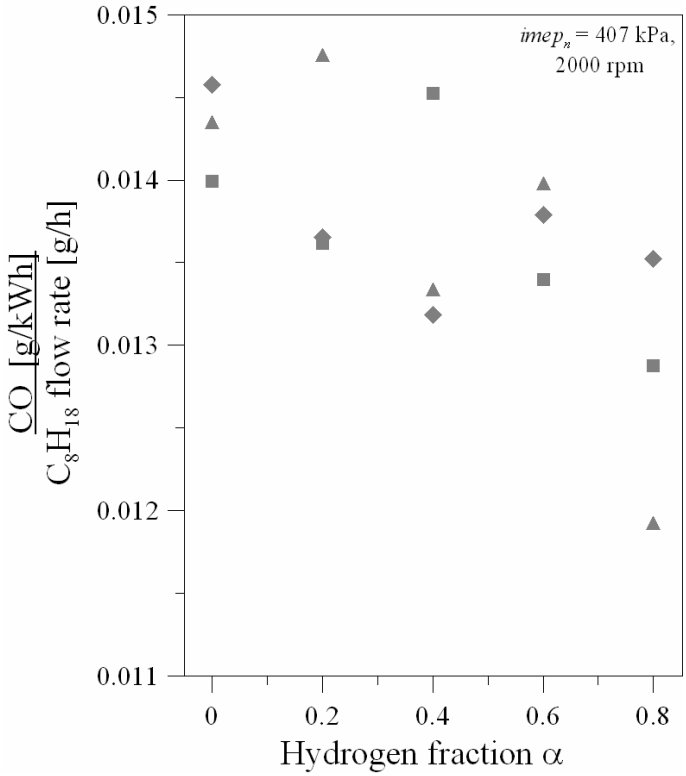

Figure 10.b *Normalized CO emissions versus α ($imep_n$ = 407 kPa, N = 2000 rpm, ϕ < 1): ◆ CASE A P_{in}=70kPa, β =0; ■ CASE A P_{in}=70kPa, β =0.1; ▲ CASE A P_{in}=70kPa, β =0.2.*

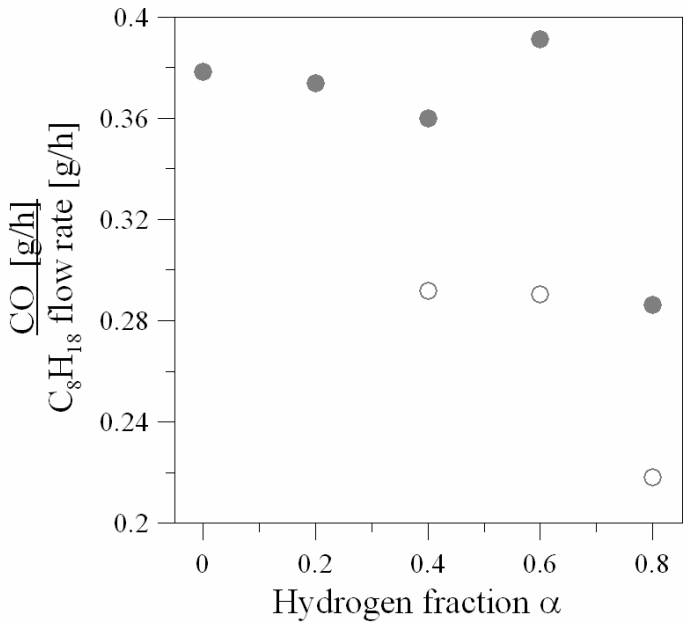

Figure 10.c *Normalized CO emissions versus α (ϕ = 1):*
$imep_n$ = 287 kPa, N = 2500 rpm: ○ CASE B P_{in}=55kPa, ϕ =1.
$imep_n$ = 407 kPa, N = 2000 rpm: ● CASE B P_{in}=70kPa, ϕ =1.

As expected, by excluding the effect of H/C ratio of the fuel mixture, the reducing effect of hydrogen substitution becomes less pronounced in Figures 10.a and 10.b than in Figures 9.a and 9.b:

Figures 10.a and 10.b for α range from 0 to 0.8, a decrease of 5% and 7% for β = 0 and 65% and 17% β = 0.2 is observed.

Figures 9.a and 9.b: when α is increased from 0 to 0.8, a decrease of 22% and 24% for β = 0 and 72% and 32% β = 0.2, respectively.

It can be concluded that for all conditions, hydrogen addition has a positive effect on CO emissions as found in other works [3, 20]. Moreover, this reducing effect of hydrogen substitution is mainly due to the decrease in the H/C ratio of the fuel mixture in the case of lean conditions without nitrogen addition.

Finally, it should be mentioned that contrary to the HC emissions case, it was not possible to found a clear relationship for all the conditions investigated between the CO emissions and the ratio of $\frac{\beta+\beta_{N2-excess\,air}}{X_{O_2}}$.

2.4.3 Combustion efficiency

Combustion efficiency reflects the degree of completeness of the combustion and directly affects the overall engine efficiency. The values of η_c are plotted versus α for $imep_n$=287kPa (2500rpm) and $imep_n$=407kPa (2000rpm) in figures 11.a and 11.b respectively. As in the CO emissions section, two ranges of η_c values can be distinguished: in the cases of lean conditions and of stoichiometric conditions. Thus, η_c has lower value at stoichiometric conditions respect to the lean conditions for the observations carried out in the HC emissions and CO emissions sections above. η_c is globally increased with the addition of hydrogen. This increase (more than 3%) is most pronounced in Cases B and D (figures 11.a and 11.b) when α is raised from 0.4 to 0.8. For Case A, an increase in η_c with α is also observed but is less significant (1%). Finally, for Case C, combustion efficiency does not seem to depend on the hydrogen fraction in the mixture. As in this case mixtures are in the lean operating limit conditions, η_c is mainly affected by the degradation of combustion stability. However, it should be mentioned that in Case C, mixtures with higher amounts of hydrogen present lower equivalence ratio values since hydrogen addition extends the lean operating limit (figure 1.a).

The conclusion is that combustion efficiency, at a fixed equivalence ratio, is improved with hydrogen addition which is in good agreement with the results presented in [9], due to the smaller quenching distance and due to higher diffusion and flame speed of hydrogen which enhance the mixing and combustion of iso-octane/air flames.

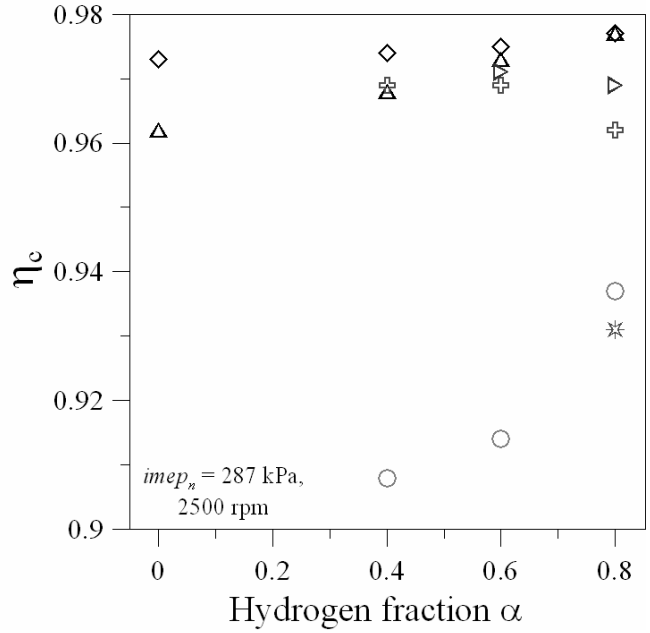

Figure 11.a *η_c versus α ($imep_n$ = 287 kPa, N = 2500 rpm):*
✚ CASE C ϕ_{LL}, β =0; ▷ CASE C ϕ_{LL}, β =0.2; ✵ CASE D β_{DL}, ϕ =1;
◇ CASE A P_{in}=55kPa, β =0; △ CASE A P_{in}=55kPa, β =0.2; ○ CASE B P_{in}=55kPa, ϕ =1.

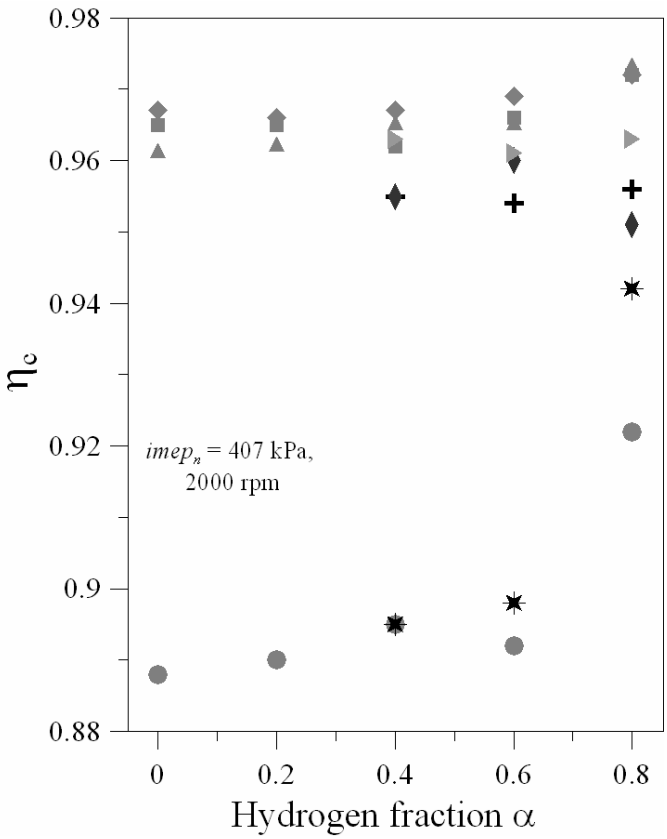

Figure 11.b *η_c versus α ($imep_n$ = 407 kPa, N = 2000 rpm):*
✚ *CASE C ϕ_{LL}, β =0;* ♦ *CASE C ϕ_{LL}, β =0.1;* ▶ *CASE C ϕ_{LL}, β =0.2;*
✷ *CASE D β_{DL}, ϕ =1;* ◆ *CASE A P_{in}=70kPa, β =0;* ■ *CASE A P_{in}=70kPa, β =0.1;*
▲ *CASE A P_{in}=70kPa, β =0.2;* ● *CASE B P_{in}=70kPa, ϕ =1.*

Another parameter was needed: β_{tot} which includes the excess in air and the nitrogen dilution effects defined as:

$$\beta_{tot} = X_{N_2-dilution} + (1-\phi)\cdot\left(X_{O_2} + X_{N_2-air}\right) = \beta + \beta_{air} \quad (11)$$

Figure 12 shows the same combustion efficiency data but plotted versus β_{tot} for all the mixtures investigated (except Cases B and D). With this total dilution rate parameter, the data present a linear decrease trend when the nitrogen dilution amount or the excess air amount increases.

Moreover, as in the case of CO emissions, the difference between the behaviour of the nitrogen dilution and the behaviour of the excess air addition was not clear for the present mixtures investigated. Thus, the main conclusion is that for these conditions (cases A and C), nitrogen addition and air addition present a similar linear decreasing effect of the combustion efficiency.

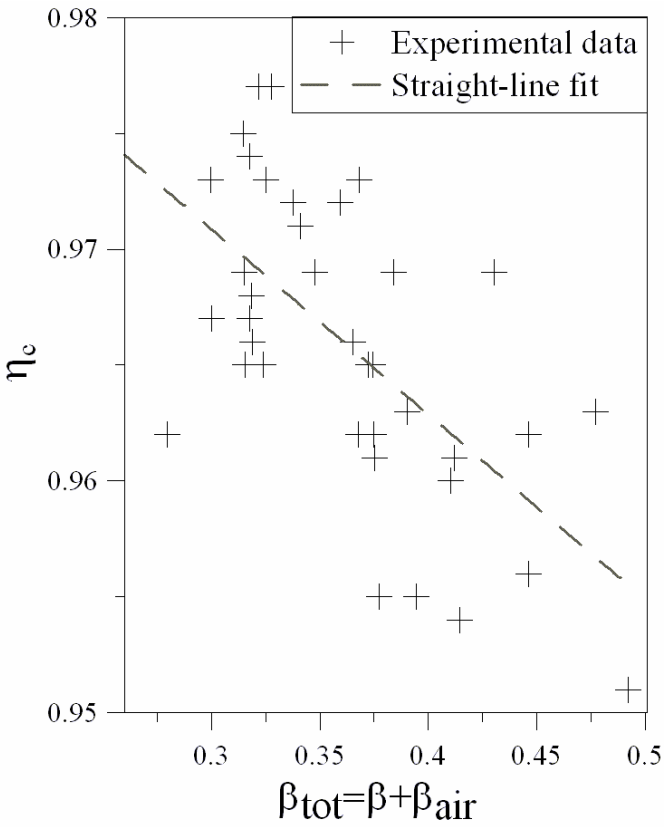

Figure 12. *η_c versus total dilution parameter $\beta_{tot} = \beta + \beta_{air}$ ($imep_n$ = 287 kPa, N = 2500 rpm and $imep_n$ = 407 kPa, N = 2000 rpm).*

2.4.4 Pumping mean effective pressure

The research engine used in this study is a naturally aspired engine so the intake pressure is lower than the exhaust pressure (atmospheric pressure). In these conditions, the work (pumping work) is done by the piston on the in-cylinder gases during the inlet and exhaust strokes. This work will decrease the total output engine work and is directly linked to the intake pressure.

In figure 13, one can note that *pmep* decreases linearly with the intake pressure, P_{in} for all conditions. Two different groups of points, characterized by a similar slope value when a linear least square fitting is applied, can be identified:

-Conditions with $imep_n$=287kPa and 2500 rpm

-Conditions with $imep_n$=407KPa and 2000 rpm

For the two conditions $imep_n$=287kPa and 2500 rpm, and $imep_n$=407KPa and 2000 rpm, when P_{in} is increased by 10kPa, *pmep* decreases by 11.5KPa. This is very important since the $imep_n$ increases by the same order of magnitude as the decrease in *pmep*.

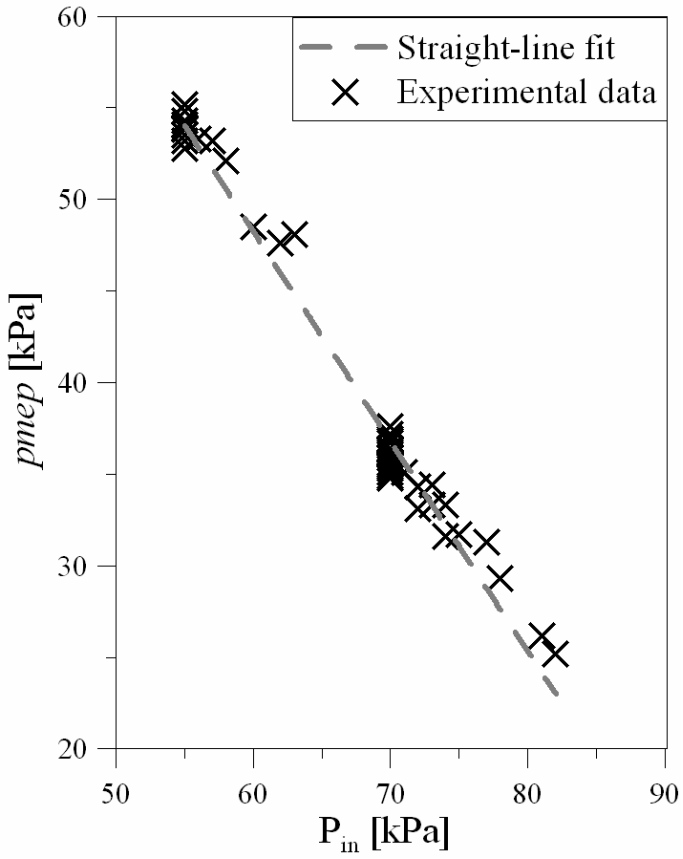

Figure 13. *pmep versus* P_{in}
($imep_n$ *= 287 kPa,* N *= 2500 rpm and* $imep_n$ *= 407 kPa,* N *= 2000 rpm).*

Hydrogen addition has, indirectly, a positive effect on pumping losses since increasing the amount of hydrogen in the mixture allows leaner and more diluted operating limits than in the case of pure iso-octane. It therefore implies lower amounts of fuel energy for the same intake pressure. Thus, to maintain a fixed work engine output, the intake pressure should be increased (in the case of leaner or more diluted mixtures) to reach the desired $imep_n$ that results in lower value of $pmep$. This is in very good agreement with the conclusions drawn in [4].

2.4.5 Indicated efficiency

I- Effects of hydrogen

Net indicated efficiency is the most significant global efficiency parameter reported in this study since all engine losses, except friction losses, are embodied in this parameter. η_{i-n} is the most appropriate global engine efficiency parameter for our study since friction losses are not the present objective. Moreover, as tests were conducted in a mono-cylinder research engine, an accurate friction investigation is not possible. The evolution of η_{i-n} versus hydrogen

fraction in the mixture is reported in figures 14.a and 14.b for $imep_n$=287kPa at 2500rpm and for $imep_n$=407kPa at 2000rpm respectively. For Case A (at a fixed intake pressure), η_{i-n} increases by amounts varying between 2.2% and 6.6% when α is increased from 0 to 0.8. The difference between the values of η_{i-n} for the conditions in Case A, at a fixed amount of hydrogen, can be attributed to heat losses and combustion efficiency. It can be seen that Cases B and D present the lowest values of η_{i-n} which can be explained by the very low values of η_c (Figures 11.a and 11.b). Moreover, η_{i-n} increases by 3% and 2.1% (Case B, at a fixed intake pressure, in Figures 14.a and 14.b respectively) and by 7.1% (Case D in Figure 14.b; 7.1% includes +~1% due to the decrease in pumping losses) when α increases from 0.4 to 0.8. At a fixed P_{in} (Case A), the highest efficiency values correspond to β=0 and to β=0.2 (figure 14.a and 14.b respectively).

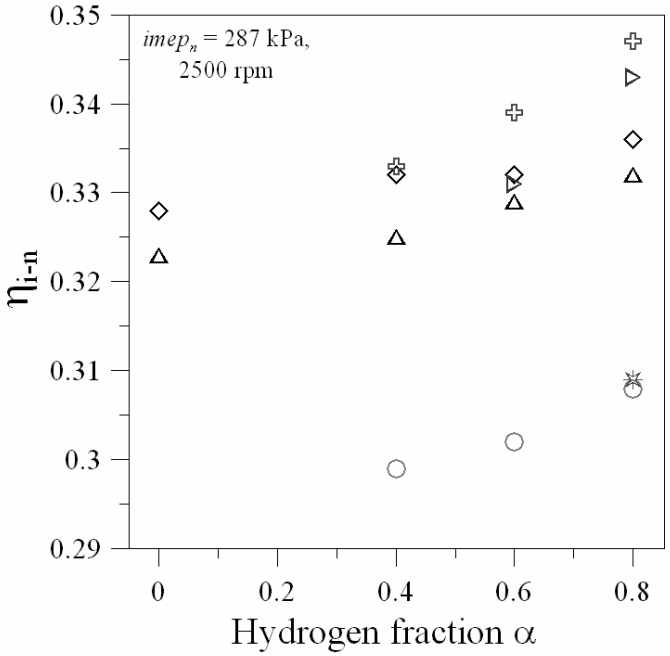

Figure 14.a *η_{i-n} versus α ($imep_n$ = 287 kPa, N = 2500 rpm):*
CASE C ϕ_{LL}, β =0; CASE C ϕ_{LL}, β =0.2; CASE D β_{DL}, ϕ =1;
CASE A P_{in}=55kPa, β =0; CASE A P_{in}=55kPa, β =0.2; CASE B P_{in}=55kPa, ϕ =1.

Case C shows the highest values of indicated efficiency due to the highest values of P_{in} and to the weight of pumping losses on the global efficiency of the engine. The experiments in Case C are also characterized by slightly lower values of η_c in comparison with Case A. Moreover, the differences in terms of η_{i-n} in Case C for α=0.8 can also be explained by the intake pressure: for β=0, P_{in} is 63kPa (Figure 14.a) and 78kPa (Figure 14.b) while for β=0.2, P_{in} is 62 kPa (Figure 14.a) and 81 kPa (Figure 14.b). The highest indicated efficiency obtained in Figure 14.a corresponds to Case C, for lean operating limit conditions and for the highest

amount of hydrogen addition. The increase in η_{i-n} is higher than 3.3% under these conditions (Case C, α=0.8 and β=0) compared to all the other conditions without hydrogen addition.

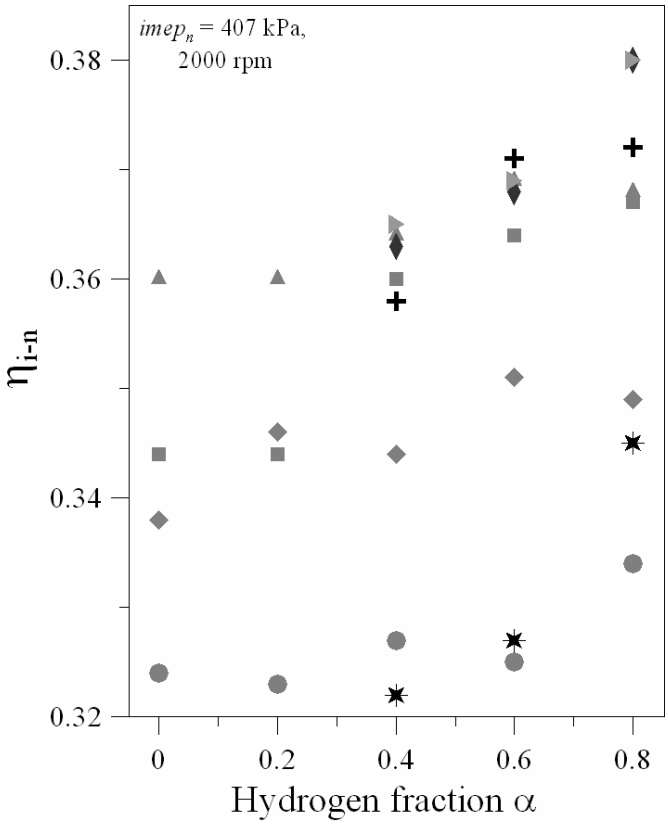

Figure 14.b *η_{i-n} versus α ($imep_n$ = 407 kPa, N = 2000 rpm):*
CASE C ϕ_{LL}, β =0; CASE C ϕ_{LL}, β =0.1; CASE C ϕ_{LL}, β =0.2;
CASE D β_{DL}, ϕ =1; CASE A P_{in}=70kPa, β =0; CASE A P_{in}=70kPa, β =0.1;
CASE A P_{in}=70kPa, β =0.2; CASE B P_{in}=70kPa, ϕ =1.

The highest value of η_{i-n} in Figure 14.b also corresponds to the highest amount of hydrogen addition combined with 10% or 20% of dilution and under lean conditions. In these conditions, the increase in η_{i-n} is higher than 5.6% with respect to all the other conditions without hydrogen addition.

Figures 15.a and 15.b exhibit the evolution of η_{i-g} versus hydrogen content in the fuel mixture. The definition of η_{i-g} is similar to that of η_{i-n} but by excluding pumping losses. Thus, Figures 14.a, 14.b and 15.a, 15.b present similar trends. The difference between η_{i-g} and η_{i-n} values is mostly pronounced at the highest amounts of hydrogen content (α=0.8) since hydrogen substitution allows more diluted and lean operating conditions than pure iso-octane mixtures.

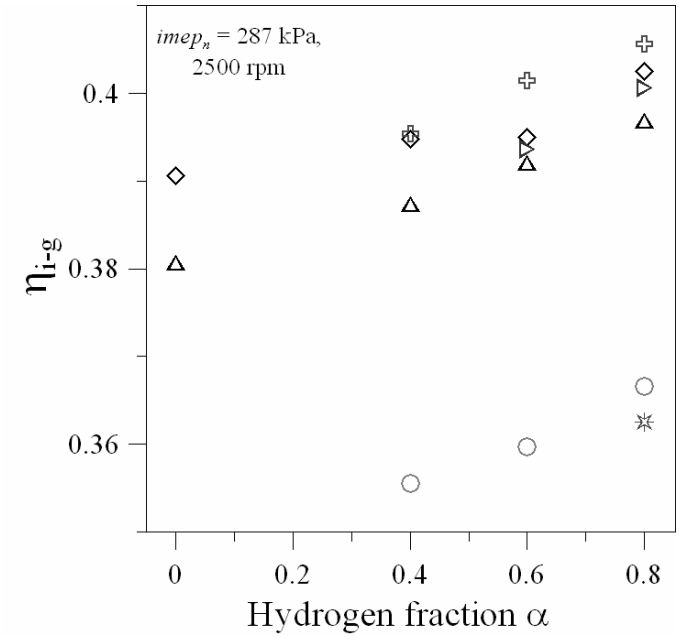

Figure 15.a η_{i-g} *versus* α *(*$imep_n$ *= 287 kPa,* N *= 2500 rpm):*
✚ *CASE C* ϕ_{LL}, β *=0;* ▷ *CASE C* ϕ_{LL}, β *=0.2;* ✵ *CASE D* β_{DL}, ϕ *=1;*
◇ *CASE A* P_{in}*=55kPa,* β *=0;* △ *CASE A* P_{in}*=55kPa,* β *=0.2;* ○ *CASE B* P_{in}*=55kPa,* ϕ *=1.*

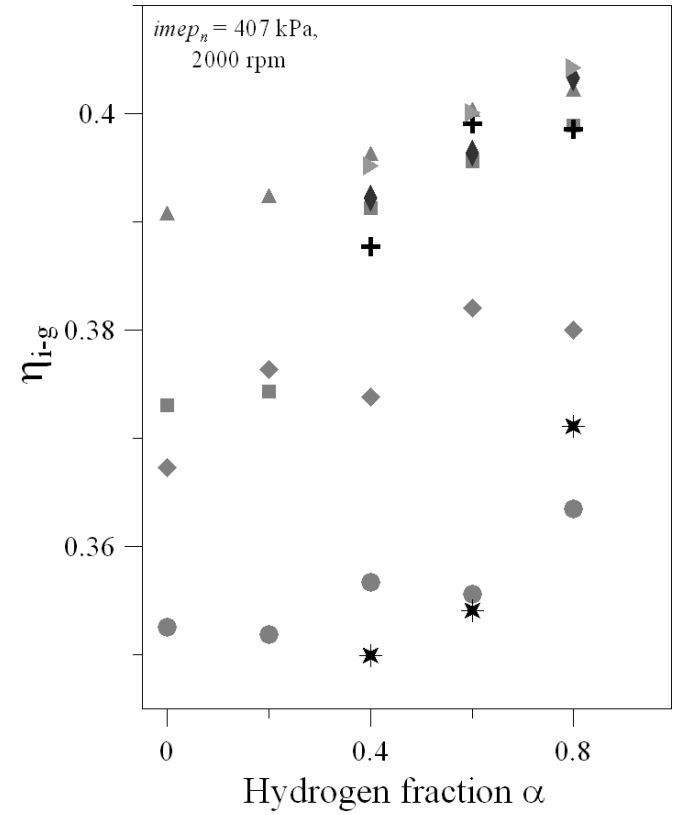

Figure 15.b η_{i-g} *versus* α *(*$imep_n$ *= 407 kPa,* N *= 2000 rpm):*
✚ *CASE C* ϕ_{LL}, β *=0;* ♦ *CASE C* ϕ_{LL}, β *=0.1;* ▶ *CASE C* ϕ_{LL}, β *=0.2;*
✶ *CASE D* β_{DL}, ϕ *=1;* ◆ *CASE A* P_{in}*=70kPa,* β *=0;* ■ *CASE A* P_{in}*=70kPa,* β *=0.1;*
▲ *CASE A* P_{in}*=70kPa,* β *=0.2;* ● *CASE B* P_{in}*=70kPa,* ϕ *=1.*

This leads, to a higher intake pressure and therefore lower pumping losses.

Hydrogen substitution presents two positive effects on the indicated efficiency:

- It reduces the pumping losses due to the extension of the lean and dilution limit since the total molar flow rate into the engine increases.

- At a fixed pumping losses, hydrogen substitution leads to a linearly increase in the indicated efficiency values.

II- Effects of dilution

As the equivalence ratio is decreased or the dilution amount is increased, the indicated efficiency increases at a fixed intake pressure. This occurs because of the lower specific heat of lean and diluted burnt gas temperature. Thus, for a given volume-expansion ratio, the burned gases expand through a larger temperature ratio prior to exhaust which leads to an increase in the expansion stroke work [1, 19].

This effect of dilution (lean or diluted mixtures) is illustrated in Figures 16.a and 16.b where η_{i-g} was plotted versus β_{tot}. It can be noted that for all conditions the trends and values are similar. In Figure 16.a, when β_{tot} is increased by 37% (form 0.28 to 0.38) η_{i-g} increases by 6% compared to the 10%, in Figure 16.b, given by an increasing of 60% in β_{tot} value (from 0.3 to 0.48). Moreover, as shown in Figures 16.a and 16.b this positive effect of dilution is not linear and decreases with the increase in β_{tot}.

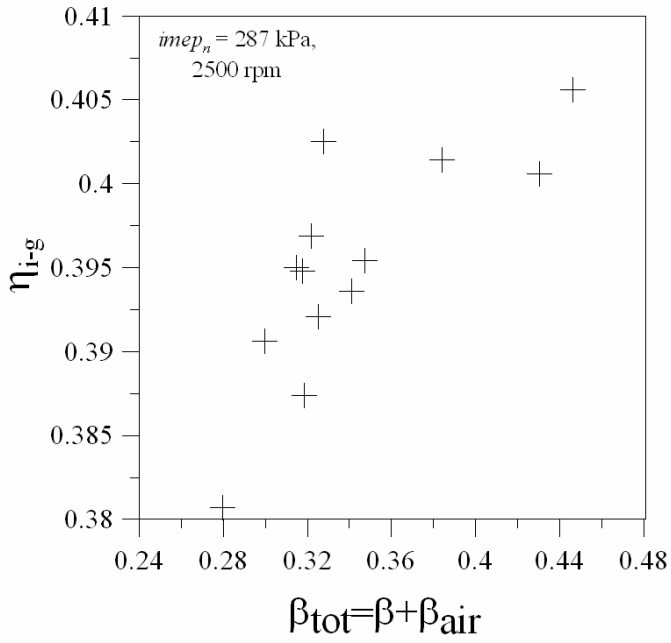

Figure 16.a *η_{i-g} versus total dilution parameter $\beta_{tot} = \beta + \beta_{air}$ ($imep_n$ = 287 kPa, N = 2500 rpm).*

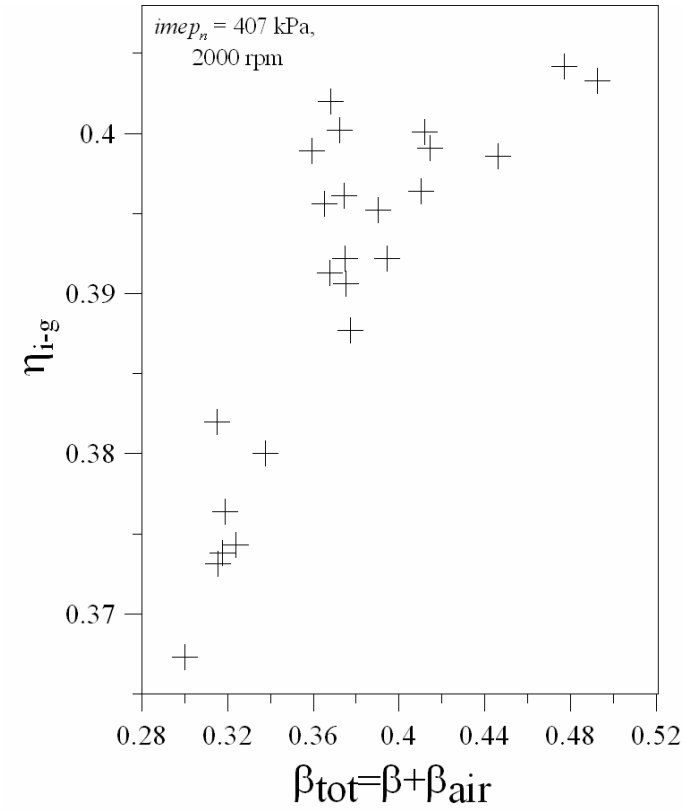

Figure 16.b *η_{i-g} versus total dilution parameter $\beta_{tot} = \beta + \beta_{air}$ ($imep_n$ = 407 kPa, N = 2000 rpm).*

2.5 Conclusion

For small amounts of hydrogen addition (<40% by volume in the fuel), the lean and dilution operating limits are the same as those of iso-octane/air mixtures. For larger values of hydrogen fractions, the lean operating limit is extended between 18% and 25% when the hydrogen percentage is increased up to 80% by volume (which corresponds to 6.6% by mass). The dilution operating limits are also extended between 30% and 59% with 80% (by volume) of hydrogen.

HC emissions are generally reduced with the increase in hydrogen fraction in the fuel mixture. This decrease is well pronounced when the hydrogen percentage in the fuel becomes higher than 40% by volume. HC emissions increase faster with the increase in nitrogen dilution than with the increases in air addition (i.e. decrease in the equivalence ratio).

NO_X emissions are mainly affected by the equivalence ratio and the dilution amount but not by the hydrogen fraction in the mixture. Moreover, the reducing effect of dilution on NO_X emission is higher than that of the equivalence ratio due to the lower oxygen concentration in the intake mixture. With hydrogen addition, very low values of NO_X emissions can be reached since hydrogen addition makes it possible to operate under a higher amount of

dilution and a lower equivalence ratio than in the case of a pure iso-octane/air mixture. For all the conditions investigated, for a nitrogen dilution percentage higher than 25%, NO_X emissions were found to be below 1g/KWh.

CO emissions decrease (between 22% and 72%) with the addition of hydrogen (80% by volume), mainly affected by the equivalence ratio. They strongly increase in the case of a stoichiometric mixture. This positive reducing effect of hydrogen addition is more pronounced for mixtures with high amounts of dilution, with high equivalence ratios and therefore for conditions with the highest values of CO emissions.

Hydrogen addition improves combustion efficiency, especially for diluted mixtures in the case of stoichiometric conditions. In this case, the increase in combustion efficiency is higher than 3%. For mixtures in lean operating conditions, combustion efficiency is mainly affected by combustion stability and not by hydrogen addition. However, at a fixed equivalence ratio, combustion efficiency increases with hydrogen addition. Combustion efficiency was also found to decrease linearly with the nitrogen or air addition.

Iso-octane/hydrogen mixtures allow more diluted and lean operating conditions than pure iso-octane mixtures. This leads, at a fixed engine work output, to a higher intake pressure and therefore lower pumping losses, since the pumping mean effective pressure was found to vary linearly with the intake pressure.

The indicated efficiency, at a fixed intake pressure, increases with the increase in hydrogen fraction in the fuel mixture and with air or nitrogen addition (i.e. lean or diluted conditions). The operating conditions which provide the highest indicated efficiency are also characterized by relatively low values of emissions: HC (7.8 g/kWh and 9 g/kWh), NO_X (1.3 g/kWh and 3.8 g/kWh) and CO (3.8 g/kWh and 3.2 g/kWh) emissions for $imep_n$=287kPa and 407kPa respectively.

High values of indicated engine efficiency and low values of HC, NO_X and CO emissions can be achieved by combining hydrogen addition (but with a hydrogen percentage greater than 40% by volume in the total volume of the iso-octane/hydrogen mixture) with lean and/or diluted air-fuel mixtures in the case of Spark Ignition engines.

2.6 References

[1] E. J. Tully and J. B. Heywood, *Lean-Burn Characteristics of a Gasoline Engine Enriched with Hydrogen from a Plasmatron Fuel Reformer*, SAE paper, 2003-01-0630 (2003).

[2] T. Suzuki and Y. Sakurai, *Effect of Hydrogen Rich Gas and Gasoline Mixed Combustion on Spark Ignition Engine*, SAE Technical Paper, 2006-01-3379 (2006).

[3] M. A.-R. Sadiq Al-Baghdadi and H. A.-K. Shahad Al-Janabi, *Improvement of performance and reduction of pollutant emission of a four stroke spark ignition engine fueled with hydrogen-gasoline fuel mixture*, Energy Conversion and Management, 41 (2000), pp. 77-91.

[4] C. Pana, N. Negurescu, M. G. Popa, A. Cernat and D. Soare, *An Investigation of the Hydrogen Addition Effects to Gasoline Fueled Spark Ignition Engine*, SAE paper, 2007-01-1468 (2007).

[5] T. Shinagawa, T. Okumura, S. Furuno and K.-O. Kim, *Effects of Hydrogen Addition to SI Engine on Knock Behavior*, SAE paper, 2004-01-1851 (2004).

[6] J. A. Topinka, M. D. Gerty, J. B. Heywood and J. C. Keck, *Knock Behavior of a Lean-Burn, H2 and CO Enhanced, SI Gasoline Engine Concept*, SAE paper, 2004-01-0975 (2004).

[7] C. Ji and S. Wang, *Combustion and emissions performance of a hybrid hydrogen-gasoline engine at idle and lean conditions*, International Journal of Hydrogen Energy, 35 (2010), pp. 346-355.

[8] N. Apostolescu and R. Chiriac, *A Study of Combustion of Hydrogen-Enriched Gasoline in a Spark Ignition Engine*, SAE paper, 960603 (1996).

[9] T. Alger, J. Gingrich and B. Mangold, *The Effect of Hydrogen Enrichment on EGR Tolerance in Spark Ignited Engines*, SAE paper, 2007-24-0015 (2007).

[10] C. Ji, S. Wang and B. Zhang, *Effect of spark timing on the performance of a hybrid hydrogen-gasoline engine at lean conditions*, International Journal of Hydrogen Energy, 35 (2010), pp. 2203-2212.

[11] M. Minutillo, *On-board fuel processor modelling for hydrogen-enriched gasoline fuelled engine*, International Journal of Hydrogen Energy, 30 (2005), pp. 1483-1490.

[12] F. Yüksel and M. A. Ceviz, *Thermal balance of a four stroke SI engine operating on hydrogen as a supplementary fuel*, Energy, 28 (2003), pp. 1069-1080.

[13] T. D'Andrea, P. F. Henshaw and D. S. K. Ting, *The addition of hydrogen to a gasoline-fuelled SI engine*, International Journal of Hydrogen Energy, 29 (2004), pp. 1541-1552.

[14] A. A. Quader, J. E. Kirwan and M. J. Grieve, *Engine performance and emissions near the dilute limit with hydrogen enrichment using a on-board reforming strategy*, SAE paper, 2003-01-1356 (2003).

[15] T. Allgeier, M. Klenk, T. Landenfeld, E. Conte, K. Boulouchos and J. Czerwinski, *Advanced Emission and Fuel Economy Concept Using Combined Injection of Gasoline and Hydrogen in SI-Engines*, SAE paper, 2004-01-1270 (2004).

[16] E. Conte and K. Boulouchos, *Experimental investigation into the effect of reformer gas addition on flame speed and flame front propagation in premixed, homogeneous charge gasoline engines*, Combustion and Flame, 146 (2006), pp. 329-347.

[17] E. Conte and K. Boulouchos, *A Quasi-Dimensional Model for Estimating the Influence of Hydrogen-Rich Gas Addition on Turbulent Flame Speed and Flame Front Propagation in IC-SI Engines*, SAE Technical Paper (2005).

[18] T. Tahtouh, F. Halter, C. Mounaïm-Rousselle and E. Samson, *Experimental investigation of the initial stages of flame propagation in a spark-ignition engine: Effects of fuel, hydrogen addition and nitrogen dilution*, SAE paper, 2010-01-1451 (2010).

[19] J. B. Heywood, *Internal Combustion Engine Fundamentals*, McGraw-Hill, 1988.

[20] C. Ji and S. Wang, *Effect of hydrogen addition on combustion and emissions performance of a spark ignition gasoline engine at lean conditions*, International Journal of Hydrogen Energy, 34 (2009), pp. 7823-7834.

II- Combustion Laminaire

Dans le chapitre précédent nous avons démontré le potentiel de l'ajout de l'hydrogène combiné à la dilution en termes d'émissions polluantes et de rendement global du moteur. Une combinaison de l'ajout de l'hydrogène et de la dilution peut donc contribuer à une réduction simultanée des émissions polluantes, spécialement les NOx thermiques, et à une diminution de la consommation spécifique du carburant.

Cependant, afin de mieux comprendre l'effet de l'hydrogène et de la dilution dans un moteur à combustion interne, il faut étudier leurs influences sur les propriétés fondamentales de la combustion. Le déroulement de combustion est déterminé principalement par la vitesse de combustion laminaire et le nombre de Lewis (rapport de diffusion thermique et de diffusion moléculaire) du mélange d'un côté et des propriétés de l'écoulement (échelle intégrale locale, intensité turbulente) d'un autre côté. Or le but de ce travail de mémoire est l'étude des effets combinés de l'hydrogène et de la dilution, qui affectent tous deux principalement les propriétés laminaires de notre mélange (vitesse de combustion laminaire et nombre de Lewis).

Dans cette deuxième partie de mémoire, la vitesse de combustion laminaire des mélanges iso-octane ou méthane avec de l'air contenant différents pourcentages d'hydrogène et de dilution sera déterminée expérimentalement. Cette vitesse de combustion laminaire est caractéristique de mélange (composition des gaz frais) pour des conditions thermodynamiques (pression et température) bien définies. Or, les conditions thermodynamiques qui peuvent être rencontrées à l'intérieur d'une chambre de combustion des moteurs sont assez particulières. En effet, même durant les phases initiales de la combustion là où le dégagement de chaleur cumulé est inférieur à 5% du dégagement de chaleur total, les températures des gaz frais (>600K) et les pressions régnantes (>10 bars) peuvent être très élevées. Obtenir expérimentalement des vitesses de combustions laminaires à ces conditions thermodynamiques n'est pas aussi simple.

Deux solutions principales se présentent pour dépasser cette difficulté :

- ✓ Faire appel à des outils numériques qui estiment à partir des mécanismes cinétiques, validés par des résultats expérimentaux obtenus dans des gammes de température et de pression bien définies, des vitesses de combustion laminaires à des conditions thermodynamiques particulières.
- ✓ Utiliser une corrélation empirique permettant d'estimer des vitesses de combustion laminaire en fonction de la température et de la pression. Ces corrélations sont aussi issues des résultats expérimentaux réalisés dans des gammes de températures et de pressions bien définies.

L'avantage de cette deuxième solution est que lorsque la corrélation est connue, l'estimation de la vitesse laminaire à une température et pression désirées est immédiate. L'objectif de cette deuxième partie de notre étude est donc d'effectuer des mesures de vitesse de combustion laminaire des mélanges carburant (iso-octane et méthane) air avec des différents niveaux de d'ajout d'hydrogène dans le carburant et de diluant, l'azote sous des conditions de pression et de température ambiantes.

Puis, à partir de ces résultats expérimentaux:

- Des corrélations, donnant la vitesse de combustion laminaire en fonction de la composition du mélange sont proposées pour des conditions de pression et de température ambiantes (chapitres 4 et 6).
- Une autre corrélation sera proposée afin d'estimer la vitesse de combustion laminaire pour différentes valeurs de température et de pression (chapitre 8).

En combinant ces deux corrélations, nous pourrons estimer la vitesse de combustion laminaire de notre mélange sous les conditions de température et de pression souhaitées. Cette étape sera réalisée dans la dernière partie de ce mémoire de thèse (partie turbulente).

Pour cela, le choix des méthodologies optimums de traitement des données (approche linéaire) pour déterminer la vitesse de combustion laminaire à taux d'étirement nul et la longueur de Markstein dans le cas d'une propagation sphérique d'une flamme prémélangée a menée à un article qui est présenté dans le chapitre 3.

La méthodologie qui a été choisie est utilisée dans le chapitre 4 pour des mélanges $CH_4/H_2/N_2$/Air. En outre, une corrélation pour l'estimation de la vitesse de combustion laminaire en fonction de la composition du mélange est proposée.

Enfin, dans le chapitre 5, une nouvelle approche non-linéaire est décrite et comparée à l'approche classique (linéaire), cela est fondamental dans le cas de l'utilisation de l'iso-octane comme carburant principal plutôt que le méthane à cause de la non-validité de certaines hypothèses de l'approximation linéaire. Cela a permis la détermination des vitesses de combustion laminaires et les longueurs de Markstein pour de mélanges $C_8H_{18}/H_2/N_2$/Air (chapitre 6).

3. Measurement of laminar burning speeds and Markstein lengths

Ce chapitre a fait l'objet d'une publication dans la revue scientifique *Combustion and Flame* :

T. Tahtouh, F. Halter, C. Mounaïm-Rouselle, *Measurement of laminar burning speeds and Markstein lengths using a novel methodology*, Combustion and Flame, 157 (2009), pp. 1825-1832.

3.1 Abstract

Three different methodologies used for the extraction of laminar information are compared and discussed. Starting from the asymptotic analysis considering a linear relation between the propagation speed and the stretch acting on the flame front, temporal radius evolutions of spherically expanding laminar flames are post-processed to obtain laminar burning velocities and Markstein lengths. The first methodology fits the temporal radius evolution with a polynomial function, while the new methodology proposed uses the exact solution of the linear relation linking the flame speed and the stretch as a fit. The last methodology consists in an analytical resolution of the problem.

To test the different methodologies, experiments have been carried out in a stainless steel combustion chamber with methane/air mixtures at atmospheric pressure and ambient temperature. The equivalence ratio was varied from 0.55 to 1.3. The classical shadowgraph technique was used to detect the reaction zone.

The new methodology has proven to be the most robust and provides the most accurate results while the polynomial methodology induces some errors due to the differentiation process. As original radii are used in the analytical methodology, it is more affected by the experimental radius determination.

Finally, laminar burning velocity and Markstein length values determined with the new methodology are compared with results reported in the literature

Nomenclature:

- K : total stretch rate [1/s]
- L_b : burned gas Markstein length [m]
- r_u : flame front radius [m]
- $r_f(t) = \frac{r_{polynomial}(t) - r_{original}(t)}{r_{polynomial}(t)} \bullet 100$: relative difference between the original and the fitted radius [%]
- u_{l0} : laminar burning velocity [m/s]
- V_S : stretched flame speed [m/s]
- V_{S0} : unstretched flame speed [m/s]
- ρ_b : density of burned gas [Kg/m^3]
- ρ_u : density of unburned mixture [Kg/m^3]

3.2 Introduction

The laminar burning speed is a fundamental parameter that characterizes both laminar and turbulent premixed combustions, within the laminar flamelet regime. Several experimental techniques can be used to determine the laminar burning speed, such as counter flow flames [1, 2], flat flames using the heat flux method [3, 4] and spherical expanding flames [5, 6]. In all these experimental methodologies, the flame front is locally affected by stretch effects. The stretch rate is a combination of two effects: the flame curvature and the strain rate. Stretch effects induce modifications on the flame front structure and propagation. The sensitivity of the flame speed to the stretch rate is characterized by the Markstein length. Investigations on the laminar burning velocity [7, 8] have exhibited the importance of local stretch on the local burning speed. Based on an asymptotic analysis, several authors [7, 9] have proposed a linear relation between the stretch rate and the flame speed. This relation is valid when the propagation phenomena are no longer affected by the initial energy deposition needed to initiate exothermic reactions. Moreover the flame thickness has to remain negligible compared to the flame radius. This linear relation has been extensively applied in outwardly propagating flames.

For spherically expanding flames, ignited from a central point, the stretch rate can be analytically derived. It is a function both of the flame front radius and of the propagation speed.

The linear extrapolation used to obtain the unstretched propagation speed is sensitive both to the quality of experiments and to the methodology used to obtain the temporal evolution of the flame front propagation speed. This determination can be done from the temporal radius evolution, either by evaluating the local gradient [5, 10-12] or by fitting the radius evolution with a polynomial function [13, 14]. In both methods, noise is introduced with the differentiation process.

The objective of the present paper is to introduce and test two different methodologies which avoid experimental noise amplification. One of these methodologies, using least squares, was initially employed by Taylor and coworkers [15, 16] . The other one consists in finding the exact solution to the differential equation obtained with asymptotic analysis. A detailed description of these different methodologies and a discussion of their sensitivity and their robustness, compared to the method using a polynomial fitting, are carried out.

As the purpose of the present study is to improve different methodologies and not to provide new laminar velocity data, it was decided to work only with methane/air mixtures under atmospheric pressure and ambient temperature. Particular attention was paid to the ignition system in order to allow a wide equivalence ratio range (ER: 0.55 – 1.3).

3.3 Experimental details

3.3.1 Combustion chamber set-up

Experiments were carried out in a cylindrical stainless steel combustion chamber with an inner volume of 24.32 litres (radius=16cm, height=30cm). Two tungsten electrodes (diameter 0.8mm), linked to a conventional capacitive discharge ignition system, are used to form the spark gap (2.8mm) at the center of this chamber. The plane of electrodes is slightly tilted with respect to the plane of visualization; this decreases the display of disturbances due to the ignition in the recorded images.

The electrodes diameter and inter-distance were chosen after several trials with different diameters (0.5, 0.8 and 1mm) and gaps (from 1 mm to 3.2 mm). A smaller electrode diameter induces fewer disturbances on the flame but leads to more problems keeping the electrodes fixed and the spark gap constant. A larger gap between electrodes provides more efficient ignition in lean conditions, but electrodes must be fairly close to create and maintain the electric arc. With the ignition system used in the present study, a flame propagation can be achieved even for very lean methane-air mixtures (E.R. = 0.52).

The volumes of methane and air are introduced into the chamber with thermal mass flow meters, connected to a computer via a RS232 serial port. Once the command to fill the combustion chamber with the needed volumes is launched, the flow meters are simultaneously opened. Before filling the chamber with the different gases, a vacuum is created in the chamber, and after introducing the different volumes of gases, the chamber is at atmospheric pressure. The pressure level is checked with a piezoelectric pressure transducer. A fan is located inside the chamber to obtain a perfectly homogenous mixture.

3.3.2 Shadowgraph set-up

Two opposite and transparent windows (diameter 10.5cm) provide optical access. A continuous Stabilite 2017 Argon ion Laser, with maximum output power of 6W, is used for the lighting. The wavelengths generated are in the range of [457.9-514.5 nm] and the beam diameter at $\frac{1}{e^2}$ is 1.4mm for this laser.

A parallel light beam is created by using two plano-convex lenses, with diameters of 15 and 70mm and focal lengths of 25 and 1000mm respectively. After passing through both lenses and the combustion chamber, the beam is displayed on a screen. The maximum beam diameter is 70mm (the diameter of the second lens). A schematic view of the whole system is presented in Figure 1.

The evolution of the flame surface is observed with a shadowgraph technique.

The shadowgraphs are recorded with a high speed CMOS APX camera operating at 8000 frames/second. The number of images considered in all experiments is therefore higher than 50.

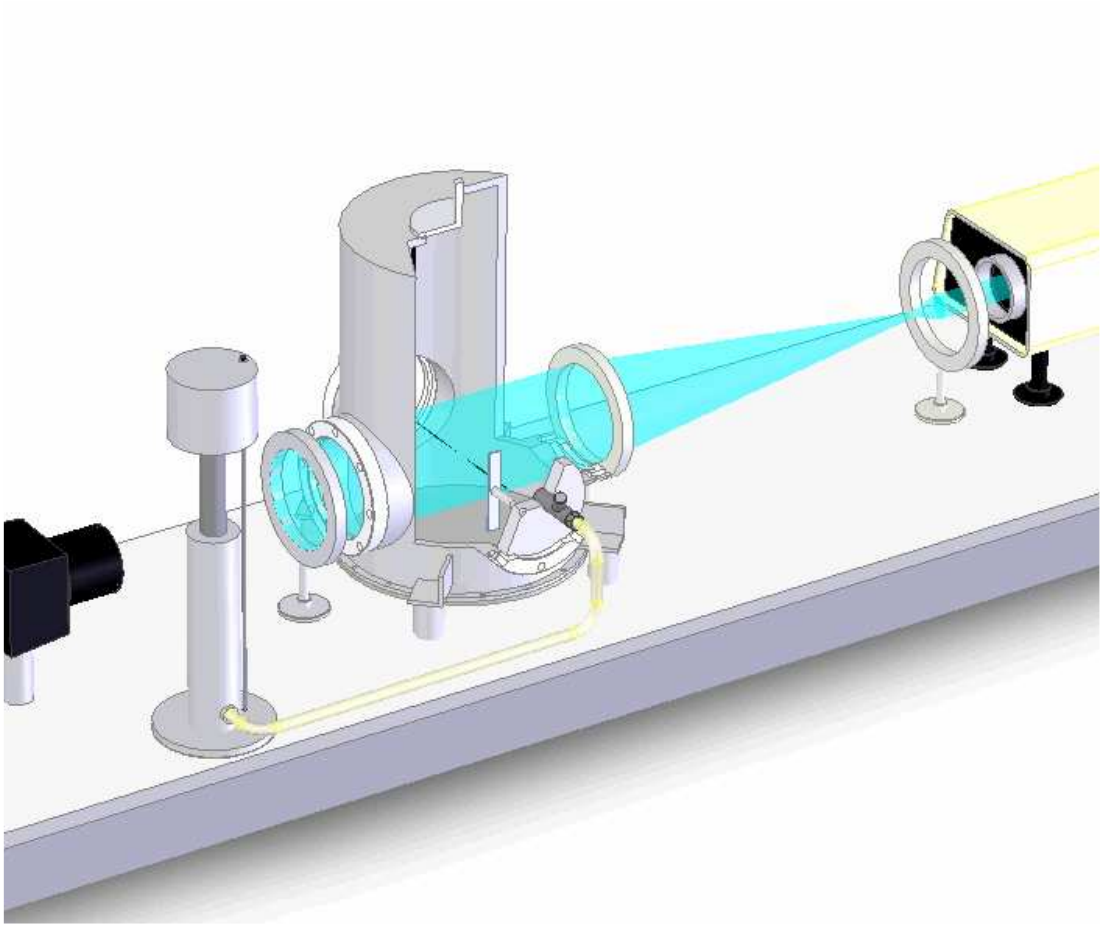

Figure 1. *Schematic view of the whole system.*

3.3.3 Experimental considerations

Bradley et al. [10] used the Schlieren technique to observe the flame front propagation. While the flame front radius determined with the Schlieren technique, r_{sch}, approximates the 450 K isotherm, Bradley et al.[9], in their computational study of spherical flame propagation, found a correlation between r_{sch} and r_u (the flame front radius corresponding to the unburned gas side) used to calculate the flame speed. However, the flame speed, i.e. the flame radius differentiation, is almost independent of the chosen isotherm [9].

Parsinejad et al [17] investigated the location of the flame edge in shadowgraph images of spherical flames. They pointed out that in the case of thin flames, the light intensity jump occurs when the normalized displacement, y/r_b, is equal to 1 and the region of reacting zone coincides with the actual edge of the flame (y is the displacement of a light ray caused by the change in refraction index through the flame and r_b the flame radius corresponding to burned gases).

For thicker flames, the location of discontinuity in the light intensity is shifted towards the unburned gases side by a distance equal to the flame front thickness. Therefore, for both cases, the luminous front distinguishable in shadowgraph images corresponds to the flame radius on the unburned gas side, r_u.

Figure 2 exhibits clearly, as predicted by the theoretical study of Parsinejad et al, an initial zone (burned gases) and a dark zone, followed by a luminous one (corresponding to the peak of light intensity). Then, the light intensity decreases and reaches a value in the zone of unburned gases close to the value of light intensity in the burned gases zone. The image quality is quite good and it can be noticed that the disturbances due to the ignition system are not discernable. Only flame radii larger than 7 mm (in order to avoid ignition disturbances [10]) and lower than 30 mm were considered (a total volume of burned gases less than 0.5% of the total volume). The total chamber pressure can therefore be considered constant.

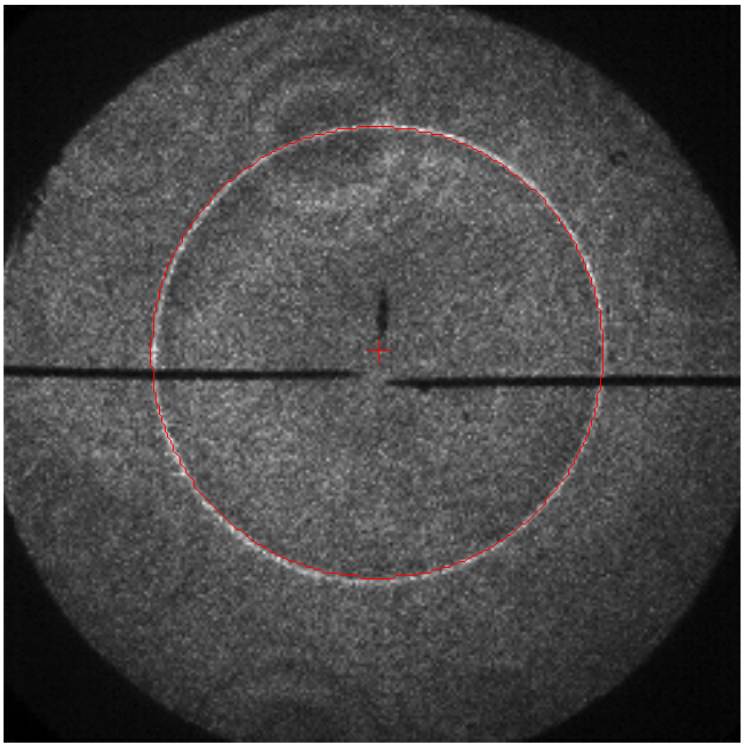

Figure 2. *Illustration of the flame front detection (E.R. = 0.6 – P=0.1 MPa – T=300K).*

The flow meter precision ($\pm 0.7\%$ on the instantaneous flow) provides a precision of $\pm 1.4\%$ on the equivalence ratios in the present experiments. The initial temperature of the combustion chamber was 300 ± 3K, implying a maximum random error of 2% on the laminar burning speed. These errors were evaluated using the correlation given by Stone and Clarke [18]. Only equivalence ratios higher than 0.6 were considered, in order to respect the range of validity of this correlation.

The initial pressure inside the combustion chamber varied between 1 and 1.03 bars. Using the same correlation [18], a maximum random error of 1.45% is obtained for the laminar burning speed.

For each equivalence ratio, experiments were performed twice and the values reported are the simple average of these two experiments.

In the present work, laminar burning velocity and Markstein Length measurements were performed for equivalence ratios from 0.55 to 1.3 and at an initial pressure of 0.1MPa and an initial temperature of 300K.

3.4 Laminar characteristics extraction

After the spark, the flame front propagates spherically as can be seen in Figure 3 for a stoichiometric mixture. The instantaneous flame front radius is obtained from image post processing after subtracting the background. The image post-processing is based on the assumption of a spherical development of the flame front. Even for the lowest equivalence ratios, the error linked to this assumption is very weak. As can be seen in Figures 2 and 3, at each temporal step, the luminous zone can be fitted by a circle. The estimate of the circle radius and centre is based on the minimization of the distance between the circle and luminous points. Thanks to the high speed image recording, the temporal evolution of the flame front can be obtained.

Figure 4 presents the temporal evolution of the flame front radius, carried out from the detection of the front flame for three different equivalence ratios (0.6, 1 and 1.3). In the case of rich mixtures, during an initial phase, the flame radius increases slowly and a faster increasing rate is observed for last stages of the flame propagation. For the stoichiometric and lean mixtures, a linear trend is observed.

During this temporal evolution, the flame front is affected by the stretch rate. The effect of stretch on premixed laminar flames has been studied in different theoretical and numerical studies [8, 19-21]. Markstein [22] was the first to suggest the existence of a linear relationship between the local burning speed and the local stretch, including strain rate and curvature effects. The relation was proposed later by Clavin [7].

$$V_S = V_{S0} - L_b \bullet K \quad (1)$$

$V_S = \frac{dr_u}{dt}$: stretched propagation flame speed

V_{S0} : unstretched propagation flame speed

L_b : Markstein length for burned gas, i.e. a measure of the flame response to the stretch

$K = \frac{1}{A} \bullet \frac{dA}{dt}$: total stretch acting on the flame, defined by the temporal rate of change of a flame surface element of area, A

In the case of a spherically outwardly expanding flame front, K can be expressed as follows:

$$K = \frac{2}{r_u} \bullet \frac{dr_u}{dt} \quad (2)$$

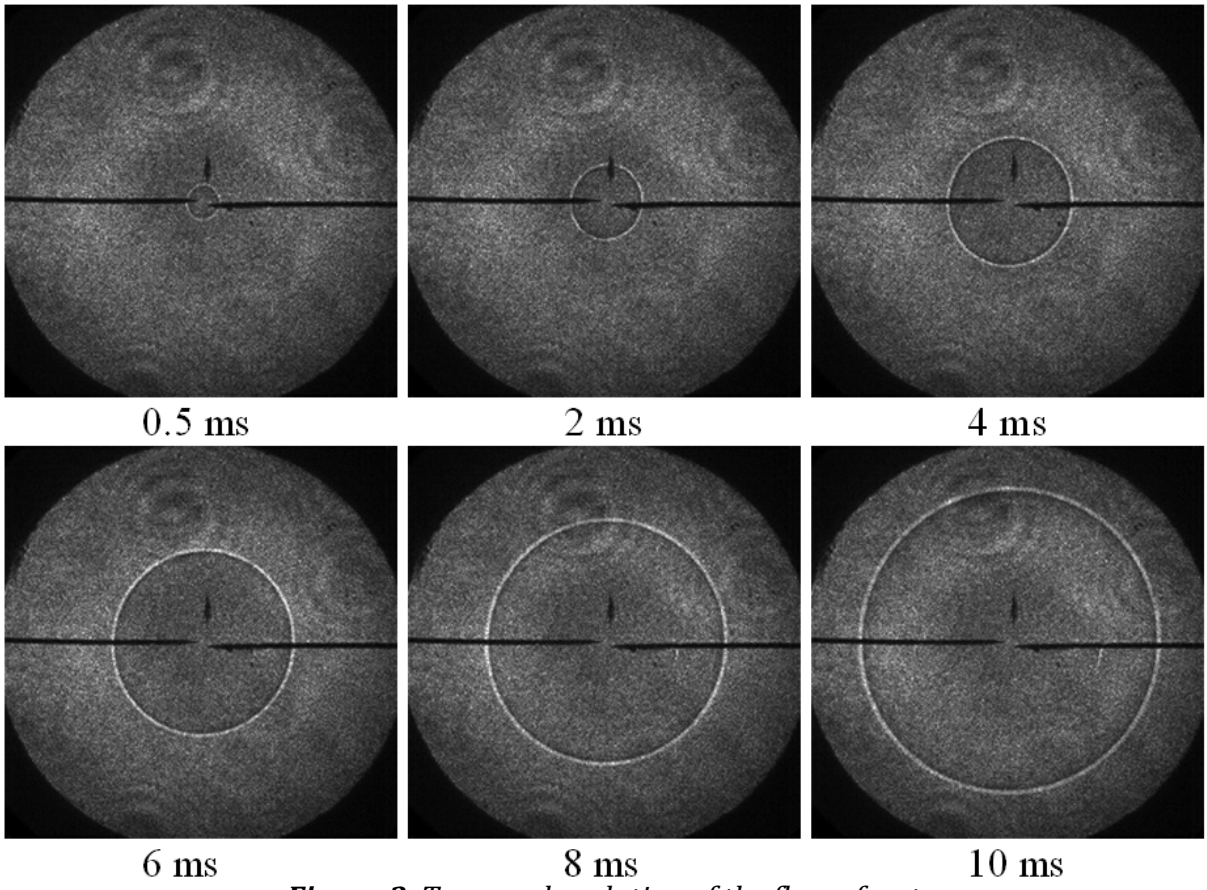

Figure 3. *Temporal evolution of the flame front*
(E.R. = 1 – P=0.1 MPa – T=300K – 8000 images/second).

For a constant pressure flame propagation, the laminar burning velocity can be deduced from the unstretched laminar flame propagation speed and the density ratio by using the following equation:

$$u_{l0} = \frac{\rho_b}{\rho_u} \bullet V_{S0}$$

ρ_b : density of burned gases; ρ_u : density of unburned gases

In spherically expanding flames, as mentioned in the previous section, the flame speed is independent of the considered isotherm and the Markstein length obtained (using Equation 1)

is always the burnt gas Markstein length. Davis et al. [23, 24] investigated the Markstein number, i.e. the Markstein length divided by the flame thickness, in counterflow premixed flames. They concluded that the Markstein number determined in the counterflow flame configuration, from the velocity and stretch measured at the cold boundary, does not represent a physico-chemical property of the mixture. Moreover, this Markstein number is more sensitive than that of the burnt gas to the location of the reference flame. It is therefore more difficult to determine accurately. They also showed that the burned gas Markstein numbers obtained with the counterflow configuration, re-normalized by the gas density ratio, are very close to the values found with spherically expanding flames. Indeed, in spherical expanding flames, the Markstein number obtained with the flame speed renormalization by the hot-to-cold gas density does not yield the Markstein length relative to cold gases.

As discussed in the introduction above, the critical point concerns the determination of the flame propagation speed. Three different methodologies are presented: the first and third ones fit the radius evolution with a function, differentiated to provide the velocity; the second provides a direct measurement of the velocity.

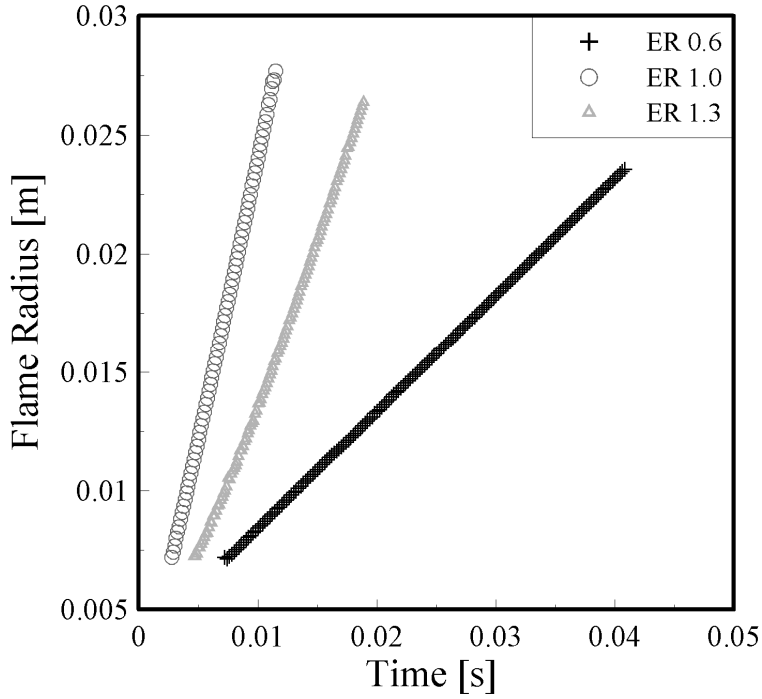

Figure 4. *Temporal evolution of the flame front radius for three different equivalence ratios, P=0.1MPa – T=300K.*

3.4.1 First methodology:

The flame propagation speed is determined after a third degree polynomial fitting of the radius, $r_{original}$ resulting from the flame front detection. A polynomial order higher than three induces more noise in the velocity and stretch evolutions. The mean relative difference between the original and the fitted radius is defined as:

$$r_f(t) = \frac{r_{polynomial}(t) - r_{original}(t)}{r_{polynomial}(t)} \bullet 100$$

Errors induced by the fitting on the radius determination are relatively small (lower than 2% for the maximum relative difference). However, the differentiation of the polynomial function can generate additional errors. Figure 5 exhibits the evolution of the flame propagation speed versus the stretch rate for three different equivalence ratios (0.6, 1.0, 1.3). The slope corresponds to the Markstein length, L_b. It can be seen that distortions occur at the beginning and at the end of these curves due to the polynomial function differentiation. Because of this noise generation, only one part of the points must be considered for the linear extrapolation as indicated in Table 1. This key part is the weak spot of this first methodology. Indeed, the determination of unstretched propagation speed and Markstein length is highly sensitive to the number of points considered. Experimental data, taken into account for the linear extrapolation, are specified in Figure 5 for the three different equivalence ratios.

3.4.2 The analytical methodology

In the present paper, the optimization process used to extract the laminar velocity information in the analytical methodology [15, 16] is the one developed by Burluka et al. [25]. This methodology, using least mean squares, requires only temporal radius evolution.

The substitution of Equation 2 into Equation 1 followed by integration yields the following equation:

$$r(t) - r(t_0) + 2 \bullet L_b \bullet \ln\left(\frac{r(t)}{r(t_0)}\right) = V_{S0} \bullet (t - t_0) \quad (3)$$

The Markstein length, L_b and the unstretched propagation speed, V_{so} are considered constant. For each time step, Equation 3 has to be verified. Then the problem consists of an optimization of the following least squares function, with L_b and V_{so} unknowns:

$$\Psi(L_b, V_{S0}) = \sum_{i=1}^{N} \left(t_i - t_0 - \frac{r_i - r_0}{V_{S0}} - 2 \bullet \frac{L_b}{V_{S0}} \bullet \ln\left(\frac{r_i}{r_0}\right) \right)^2 \quad (4)$$

where N is the number of temporal steps considered.

The values of L_b and V_{so} which minimize the previous equation are solutions of the following system:

$$\begin{cases} \dfrac{d\Psi}{dL_b} = 0 \\ \dfrac{d\Psi}{dV_{S0}} = 0 \end{cases}$$

The critical point of this methodology lies in the choice of the initial conditions (t_0 and r_0). As no differentiation process is performed, the amplification of experimental noise is avoided. The methodology is affected only by the experimental noise resulting from the flame radius extraction.

3.4.3 The new methodology

A combination of Equation 1 and Equation 2 leads to:

$$\frac{dr}{dt} = V_{S0} - 2L_b \bullet \frac{dr}{rdt} \quad (5)$$

It is clear that a polynomial function is not a solution to this equation. Therefore, the calculation of V_{S0} and L_b from polynomial fitting of a radius temporal evolution also induces additional errors. The approach of the new methodology proposed is to determine the exact solution of Equation 5, by avoiding noise generation due to the differentiation process. The function solution of Equation 5 is:

$$r(t) = 2L_b W_0(Z) \quad (6)$$

with W the Lambert function, $Z = \frac{e^{\frac{V_{S0}t + C_1}{2L_b}}}{2L_b}$ and C_1 a constant to be determined.

The Lambert function W is defined as the inverse function of $f(W) = We^W$.

By definition $\frac{dW}{dZ} = \frac{W(Z)}{Z(1+W(Z))}$ for $Z \neq \frac{-1}{e}$ and $W(Z) \neq -1$.

If L_b>0, Z>0 and consequently $W_0(Z)$ is a positive real number.

Then L_b, V_{S0} and C_1 can be found by minimizing the following equation:

$$\sum_1^N \left(r_{original}(t) - r(t)\right)^2 = \sum_1^N \left(r_{original}(t) - 2L_b W_0(Z)\right)^2 \quad (7)$$

Equation 6 can be differentiated with respect to time to obtain the stretched propagation speed and the stretch rate.

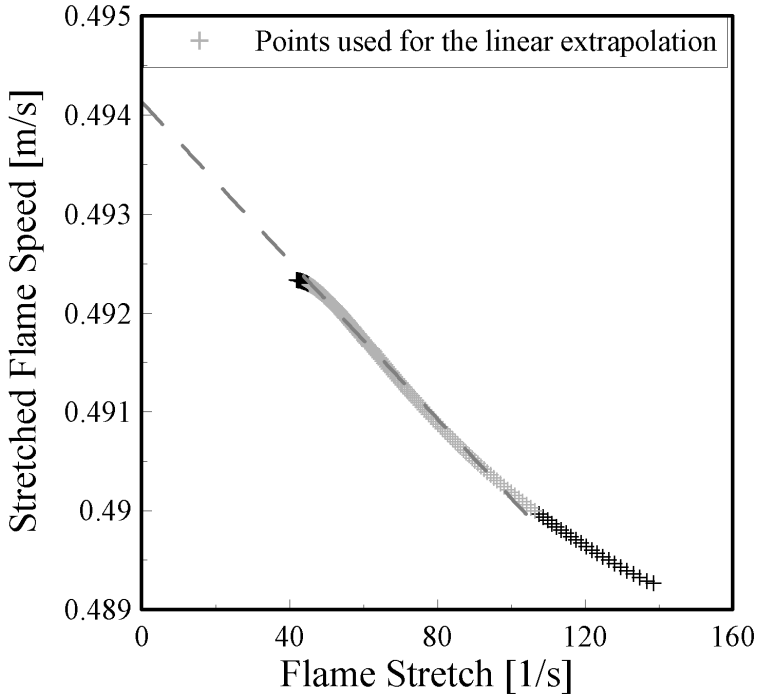

Figure 5.a *Evolution of the stretched flame speed as a function of stretch rate with the polynomial methodology. E.R.= 0.6, P=0.1 MPa – T=300K*

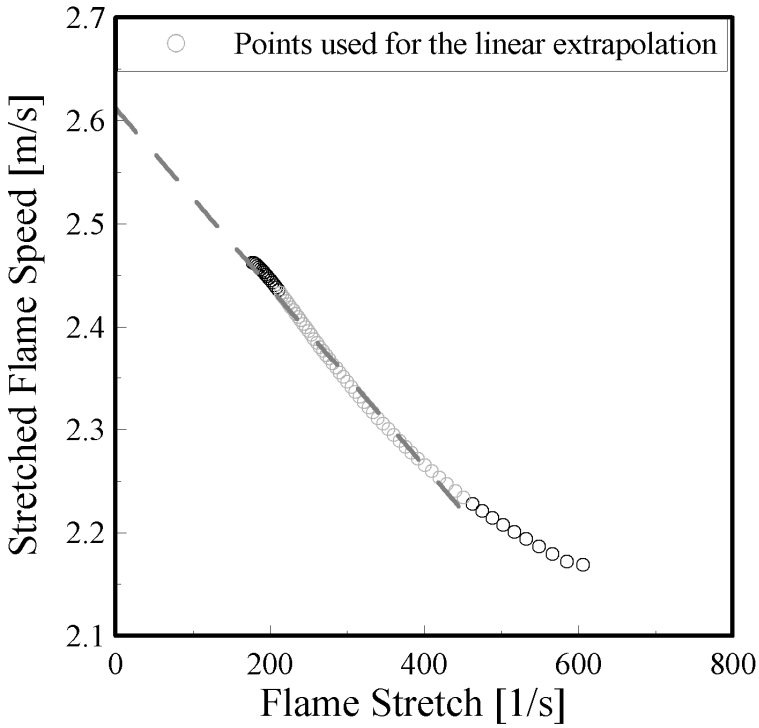

Figure 5.b *Evolution of the stretched flame speed as a function of stretch rate with the polynomial methodology. E.R.= 1, P=0.1 MPa – T=300K*

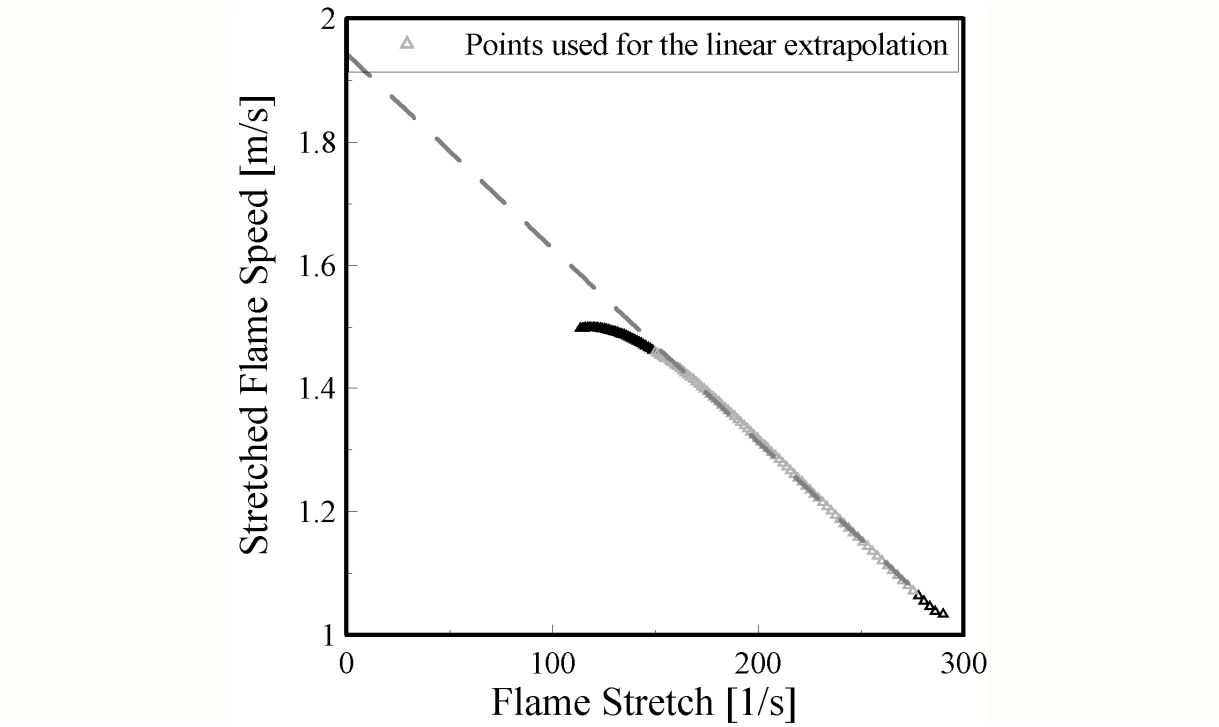

Figure 5.c *Evolution of the stretched flame speed as a function of stretch rate with the polynomial methodology. E.R.= 1.3, P=0.1 MPa – T=300K*

In the following part, the sensitivity and robustness of these three different methodologies are tested for different experimental results, performed with a set of equivalence ratios of methane-air mixtures at atmospheric pressure and ambient temperature.

3.5 Results and discussion

In a first step, a comparison, in terms of error induced by the fitting process, is performed when the polynomial and the Lambert function are used. The mean and the maximum relative difference values, r_f obtained with both methodologies and for three different equivalence ratios (0.6, 1, 1.3) are presented in Table 2. Errors induced by the fitting are small whatever the function considered.

The next step is the differentiation of the functions. Temporal evolutions of stretched propagation velocity are presented in Figure 6 for the three different equivalence ratios. In early stages of the flame propagation, the flame is affected by the spark discharge. In order to avoid these perturbations, flames with radii bigger than 7mm were taken into account in our post-processing.

The stretched flame propagation speed increases gradually with the radius, as the stretch acting on the flame front is reduced. This behaviour is characteristic of a reactive mixture with a Lewis number higher than the critical value (close to unity). Indeed, thermo-diffusive

instabilities counterbalance the destabilizing effect of hydrodynamic instabilities (for these relatively small flame radii).

At the end of the visualization process (flame radii around 3cm), the stretched flame speed tends towards an asymptotic value. Some differences in the propagation speed evolution can be observed between the two methodologies.

These differences are directly linked to the type of function used to fit the radius evolution.

Table 1. *Number of points considered and coefficient of determination for the polynomial fitting method.*

ER	Number of points used for the polynomial methodology	Coef. of determination R^2
0.6	248/296	0.991
1.0	44/70	0.993
1.3	72/114	0.999

Table 2. *Mean and maximum values of the relative difference induced by the fitting of the temporal radius evolution with the polynomial and the new methodology.*

E.R.	0.6	1	1.3
Mean value of r_f (Polynomial fitting)	0.10%	0.13%	0.24%
Maximum value of r_f (Polynomial fitting)	1.86%	0.63%	1.80%
Mean value of r_f (New methodology)	0.10%	0.13%	0.25%
Maximum value of r_f (New methodology)	1.86%	0.63%	1.82%

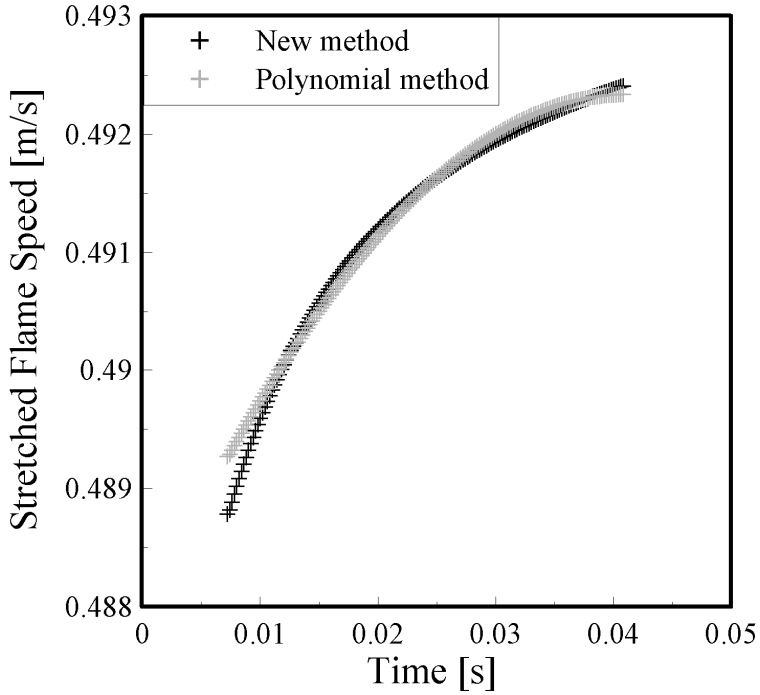

Figure 6.a *Temporal evolution of the stretched flame speed for the polynomial and the new methodology. E.R.=0.6, P=0.1MPa – T=300K*

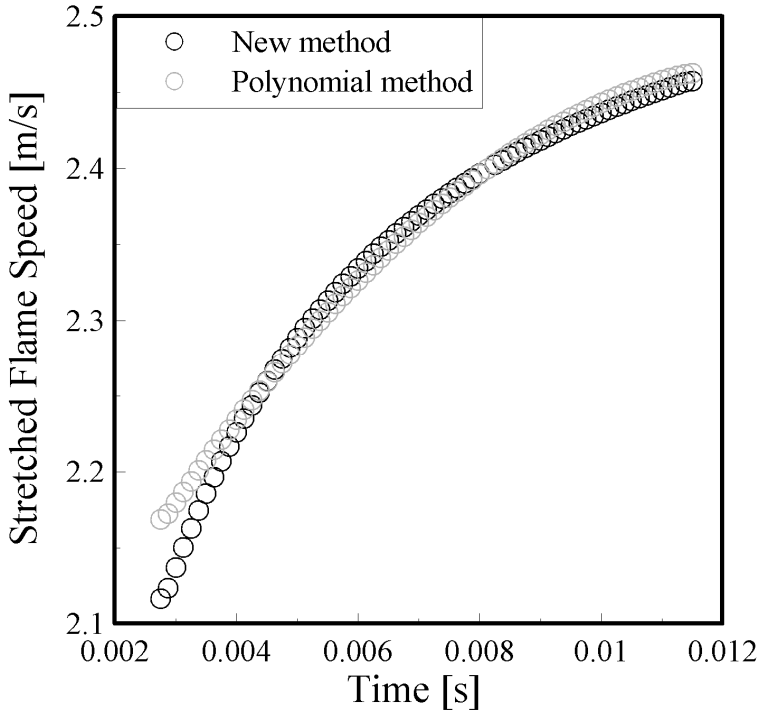

Figure 6.b *Temporal evolution of the stretched flame speed for the polynomial and the new methodology. E.R.=1, P=0.1MPa – T=300K*

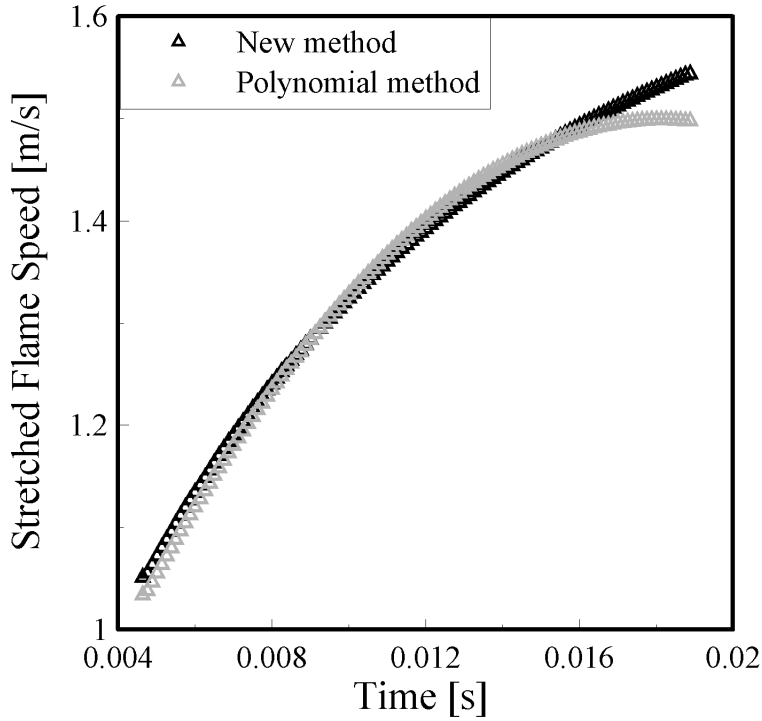

Figure 6.c *Temporal evolution of the stretched flame speed for the polynomial and the new methodology. E.R.=1.3, P=0.1MPa – T=300K*

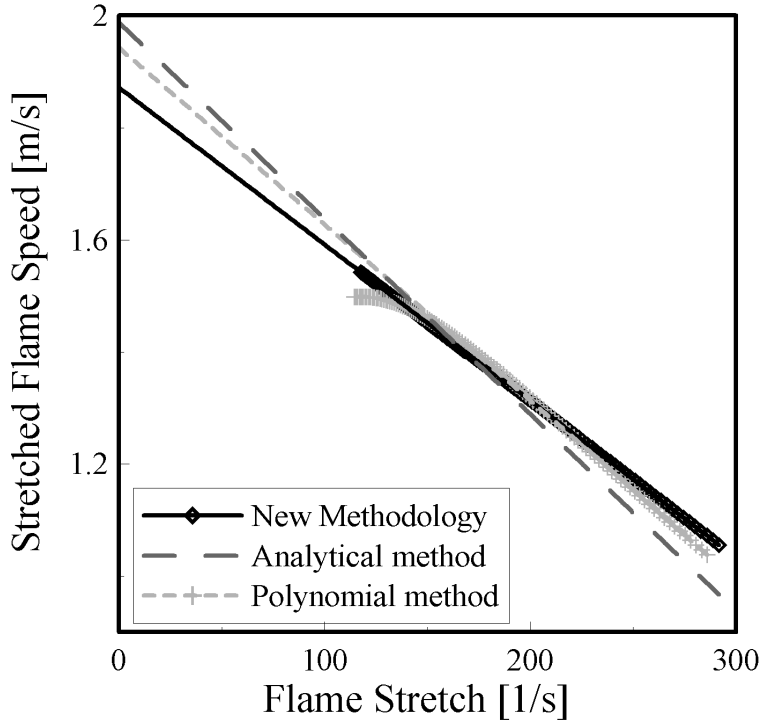

Figure 7. *Evolution of the stretched flame speed versus stretch rate for the three different methodologies (ER=1.3 - P=0.1MPa – T=300K).*

Figure 7 presents the evolutions of the flame propagation velocity versus the stretch rate for an equivalence ratio of 1.3. Using the analytical methodology leads to obtaining only two

values: the propagation speed and the Markstein Length. A dashed straight line with a slope equal to L_b and a value of velocity for zero stretch equal to V_{S0} is added to this graph. For the polynomial and the new (i.e. using the Lambert function) methodologies, the linear extrapolation is applied to obtain the non-stretched propagation speed. The values obtained are slightly different depending on the methodology used. As pointed out previously, the value obtained with the polynomial methodology is dependent on the number of points considered for the linear extrapolation. Differences observed between the new and the analytical methodology result from the fact that original radii, without any filtering, are considered for the optimization of Equation 4.

By using density ratios, estimated from adiabatic calculations, the laminar burning speeds can be determined from the unstretched flame propagation speeds. All the values of laminar burning speeds and burned gases Markstein length obtained with the different methodologies are summarised in Table 3 and presented in Figure 8. The first remark that can be made concerns the equivalence ratio of 0.55. Indeed, for this condition, only the new methodology provides a positive Markstein length value. A negative Markstein length value corresponds to a mixture with a Lewis number lower than the critical value and hence to unstable thermo-diffusive effects. As a result, the flame front, already affected by hydrodynamic instabilities, should develop cells as the combustion phenomenon is initiated. In our experiments, no cells development occurs during the flame propagation of this particular low equivalence ratio. This observation gives us more confidence in the new methodology. For all the equivalence ratios between 0.6 and 1.2, the three different methodologies give almost similar results. Subsequently, some differences appear for an equivalence ratio of 1.3. However, the linear extrapolation hypothesis, based on Equation 1, starts to become weak for these high equivalence ratio values.

It can be concluded that the polynomial methodology has little effect on the results of laminar burning velocities when the points considered for the linear extrapolation to zero stretch are not all points, but only those weakly affected by the polynomial deformation. With this methodology, part of the data (about 25%) is not used in the linear extrapolation. This methodology is highly sensitive to the choice of points for the linear extrapolation. Indeed, when all points are considered for the linear extrapolation to zero stretch rate for E.R. = 1.3, the value of laminar burning velocity changes by 11% and the value of Markstein length changes by 21%.

As the analytical methodology uses raw radius values, it is directly affected by the error induced in the flame radius determination. This noise linked to the radius determination (both experimental and numerical) becomes important when the conditions are further from stoichiometric conditions. In these cases the analytical methodology does not give accurate results. One solution could be to filter the temporal radius evolution. The most accurate values are those obtained with the new methodology.

As the temporal radius evolution is fitted with the exact solution of the differential equation (Equation 5), the differentiation process does not generate any perturbations and the errors

linked to the radius determination are lowered. Fitting with the exact solution reduces experimental noise.

Table 3. *Laminar burning speed and Markstein length values obtained with the three different methodologies, CH_4/air mixtures, P=0.1MPa – T=300K.*

	Polynomial methodology		Analytic methodology		New methodology	
ER	u_{l0} [cm/s]	L_b [mm]	u_{l0} [cm/s]	L_b [mm]	u_{l0} [cm/s]	L_b [mm]
0.55	4.91	-0.12	5.11	-0.12	5.24	0.01
0.6	8.84	0.08	8.94	0.17	8.84	0.08
0.7	17.24	0.38	17.10	0.31	17.25	0.38
0.8	24.94	0.54	25.22	0.63	25.00	0.56
0.9	31.05	0.68	31.42	0.78	31.00	0.66
1.0	35.16	0.84	35.58	0.95	35.15	0.84
1.1	36.11	1.02	36.12	1.03	35.96	0.98
1.2	32.74	1.45	32.87	1.52	32.48	1.40
1.3	26.83	4.55	26.98	3.19	24.84	3.69

In the present experiments, the flame front was perfectly spherical, mainly thanks to the quality of the ignition system (electrodes diameter and inter-distance). Moreover, the contrast presented by raw images allows an accurate determination of the flame front radius. These favorable conditions facilitate the use of the polynomial methodology and explain the low differences observed between the three different methodologies.

Furthermore, the methodologies used present different systematic and random errors.

- A random error due to the radius determination. This error is more pronounced in the analytical methodology since no radius fitting process is used. This methodology can be improved by introducing a weighting based on the errors of the circle fitting of luminous front in shadowgraphs. Another way to reduce this error is to fit the flame radius with an appropriate function.

- A random error due to the polynomial form, as the polynomial cannot be a solution for Equation 1. This error is small when the radius is fitted (as it is shown in Table 2) but it can be high when the fitted radius is differentiated. One way to reduce this error was to eliminate the data most affected by the polynomial form (Figure 5).

- For rich mixtures, the linear hypothesis becomes weak. If the flame speed-stretch linear equation is used (Equation 1), a systematic error, due to the overestimation of the calculated laminar flame speed, is induced. This error is present in all methodologies, principally in the new methodology (Table 2), because flame radii are fitted with the exact solution of the linear equation (Equation 1).

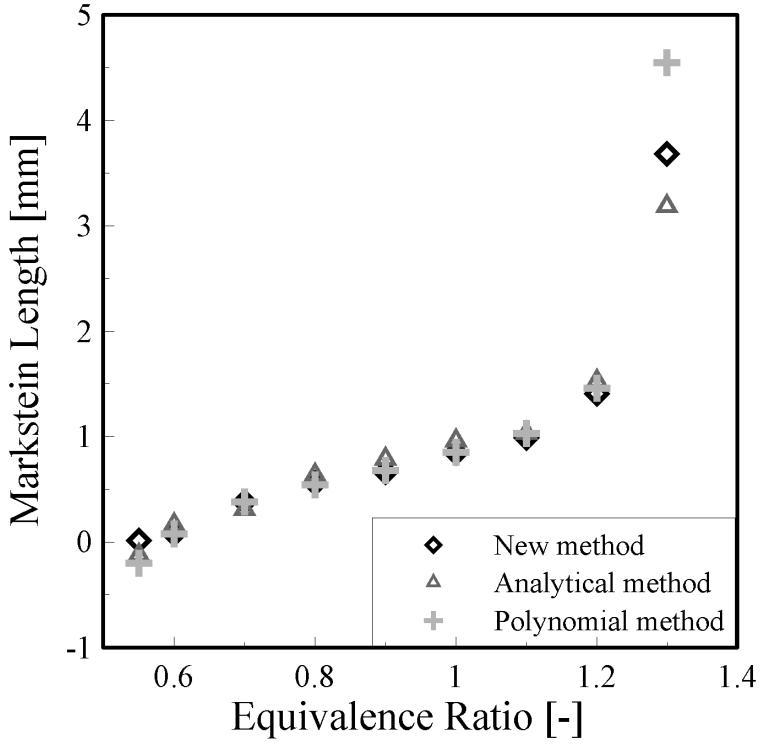

Figure 8.a *Evolution of the Markstein length as a function of the equivalence ratio for the three different methodologies (P=0.1MPa – T=300K).*

Values of V_{S0} and L_b obtained with the new methodology are compared to literature values in Figure 9. For laminar burning speeds, the comparison is performed both with experimental [5, 6, 13] and computational [9, 26] data.

Laminar burning velocities obtained with the new methodology are in good agreement with values available in the literature, whatever the equivalence ratio. A reasonable agreement is also found in Markstein lengths, even if values are more scattered. Evolutions present similar trends.

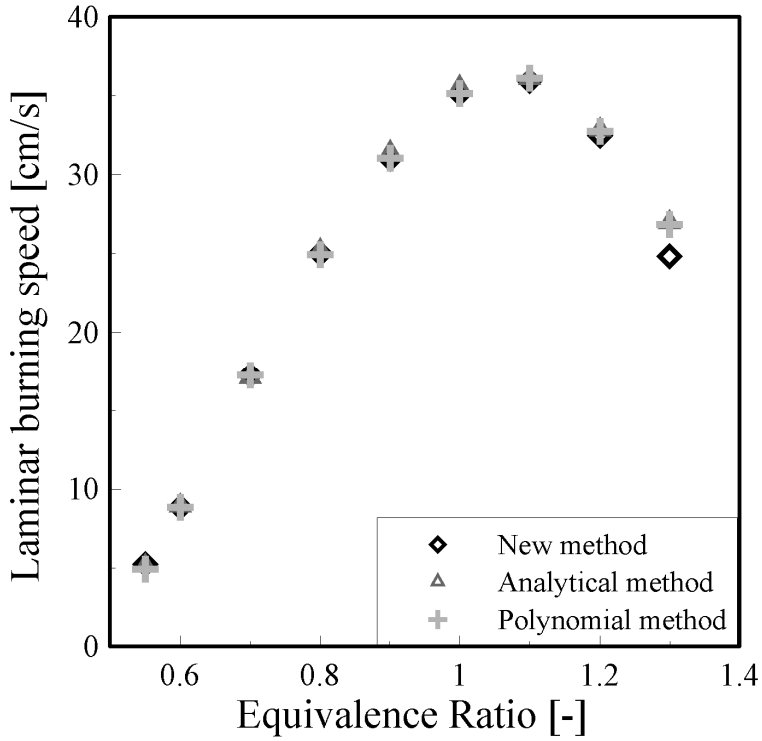

Figure 8.b *Evolution of the laminar burning velocity as a function of the equivalence ratio for the three different methodologies (P=0.1MPa – T=300K).*

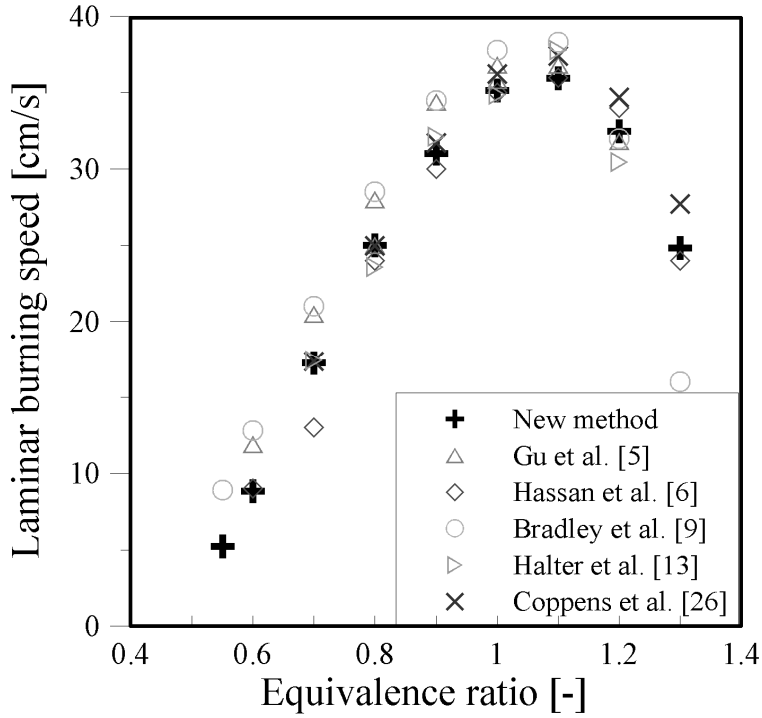

Figure 9.a. *Laminar burning velocity versus equivalence ratio (CH_4/air mixtures - P=0.1MPa – T=300K).*

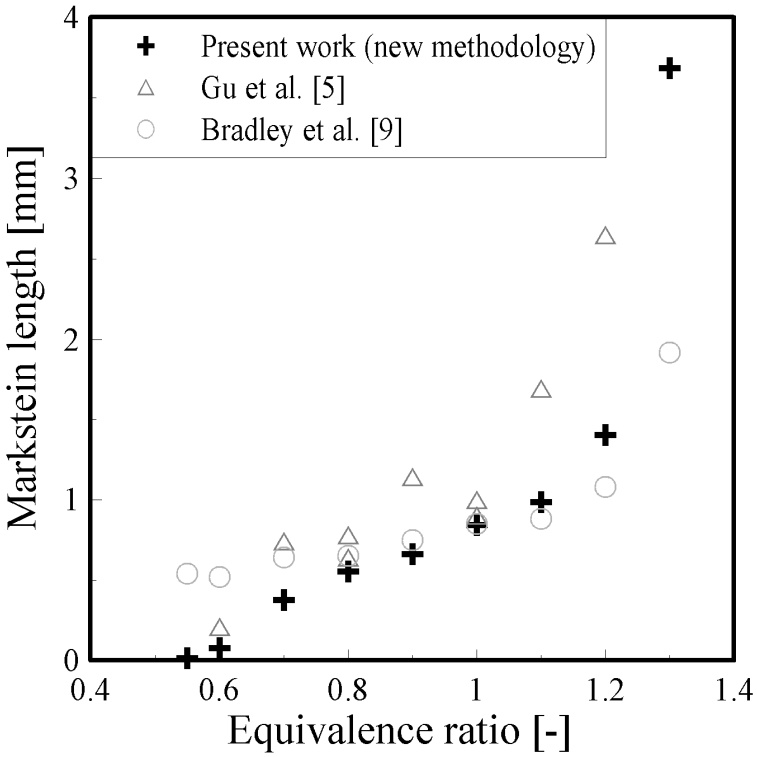

Figure 9.b *Markstein length versus equivalence ratio (CH_4/air mixtures - P=0.1MPa – T=300K).*

3.6 Conclusion

Three different methodologies used for the extraction of laminar information are compared and discussed. Starting from the asymptotic analysis considering a linear relation between the propagation speed and the stretch acting on the flame front, temporal radius evolutions of spherically expanding laminar flames are post-processed to obtain laminar burning velocities and Markstein lengths.

The first methodology, based on a polynomial fitting of the flame radii, introduces some errors related to the amplification of noise due to the differentiation process. Indeed, the function expressing the radius as a polynomial is not a solution to the linear equation linking the flame speed and the stretch. As a result, only part of the experimental points is taken into account for the linear extrapolation.

The second methodology, initially used by Taylor et al. [15, 16], which consists in an optimization problem [25], avoids the differentiation process and the errors induced. This methodology uses the raw radius values. One improvement could be to filter first the temporal radius evolution to avoid experimental scatter. The critical point of this methodology lies in the choice of the initial conditions (t_0, r_0).

A new methodology based on the resolution of Clavin's equation, linking linearly the flame speed and the stretch, is here presented. This methodology, introducing a Lambert function,

possesses several advantages compared to the other two. As the temporal radius evolution is fitted by the exact solution of the differential equation, errors induced by the radius determination are lowered. Moreover, the differentiation process, which is the weak part of the polynomial methodology, does not induce any additional perturbations.

In order to test the different methodologies, experiments were carried out with methane/air mixtures at atmospheric pressure and ambient temperature. The equivalence ratio was varied from 0.55 to 1.3. Particular attention was paid to the ignition system (both electrodes diameter and inter-distance) to improve the image quality. Moreover, the electrode plane was slightly tilted with respect to the plane of visualization to limit the influence of disturbances due to the ignition in the recorded images. The classical shadowgraph technique was used to detect the reaction zone.

Close to stoichiometric conditions, the three methodologies give similar results in terms of laminar burning velocity and Markstein length. For lean and rich mixtures, the relative difference between the results given by the different methodologies is greater. The new methodology proves to be the most robust one and provides more accurate results.

Finally, a very good agreement is obtained between values of laminar burning speed and Markstein length values determined with the new methodology and values found in the literature.

3.7 References

[1] B. H. Chao, F. N. Egolfopoulos, C. K. Law, *Structure and propagation of premixed flame in nozzle-generated counterflow*, Combustion and Flame, 109 (1997), pp. 620-638.

[2] G. S. Jackson, R. Sai, J. M. Plaia, C. M. Boggs, K. T. Kiger, *Influence of H2 on the response of lean premixed CH4 flames to high strained flows*, Combustion and Flame, 132 (2003), pp. 503-511.

[3] K. J. Bosschaart, L. P. H. de Goey, J. M. B. C. f. F. M. in collaboration with, *The laminar burning velocity of flames propagating in mixtures of hydrocarbons and air measured with the heat flux method*, Combustion and Flame, 136 (2004), pp. 261-269.

[4] A. A. Konnov, I. V. Dyakov, J. De Ruyck, *Measurement of adiabatic burning velocity in ethane-oxygen-nitrogen and in ethane-oxygen-argon mixtures*, Experimental Thermal and Fluid Science, 27 (2003), pp. 379-384.

[5] X. J. Gu, M. Z. Haq, M. Lawes, R. Woolley, *Laminar burning velocity and Markstein lengths of methane-air mixtures*, Combustion and Flame, 121 (2000), pp. 41-58.

[6] M. I. Hassan, K. T. Aung, G. M. Faeth, *Measured and predicted properties of laminar premixed methane/air flames at various pressures*, Combustion and Flame, 115 (1998), pp. 539-550.

[7] P. Clavin, *Dynamic behavior of premixed flame fronts in laminar and turbulent flows*, Progress in Energy and Combustion Science, 11 (1985), pp. 1-59.

[8] M. Matalon, B. J. Matkowsky, *Flames as gasdynamic discontinuities*, Journal of Fluid Mechanics Digital Archive, 124 (1982), pp. 239-259.

[9] D. Bradley, P. H. Gaskell, X. J. Gu, *Burning velocities, markstein lengths, and flame quenching for spherical methane-air flames: A computational study*, Combustion and Flame, 104 (1996), pp. 176-198.

[10] D. Bradley, R. A. Hicks, M. Lawes, C. G. W. Sheppard, R. Woolley, *The Measurement of Laminar Burning Velocities and Markstein Numbers for Iso-octane-Air and Iso-octane-n-Heptane-Air Mixtures at Elevated Temperatures and Pressures in an Explosion Bomb*, Combustion and Flame, 115 (1998), pp. 126-144.

[11] S. Y. Liao, D. M. Jiang, Q. Cheng, *Determination of laminar burning velocities for natural gas*, Fuel, 83 (2004), pp. 1247-1250.

[12] S. Verhelst, R. Woolley, M. Lawes, R. Sierens, *Laminar and unstable burning velocities and Markstein lengths of hydrogen-air mixtures at engine-like conditions*, Proceedings of the Combustion Institute, 30 (2005), pp. 209-216.

[13] F. Halter, C. Chauveau, N. Djebaïli-Chaumeix, I. Gökalp, *Characterization of the effects of pressure and hydrogen concentration on laminar burning velocities of methane-hydrogen-air mixtures*, Proceedings of the Combustion Institute, 30 (2005), pp. 201-208.

[14] N. Lamoureux, N. Djebaïli-Chaumeix, C. E. Paillard, *Laminar flame velocity determination for H2-air-He-CO2 mixtures using the spherical bomb method*, Experimental Thermal and Fluid Science, 27 (2003), pp. 385-393.

[15] D. R. Dowdy, D. B. Smith, S. C. Taylor, A. Williams, *The use of expanding spherical flames to determine burning velocities and stretch effects in hydrogen/air mixtures*, Symposium (International) on Combustion, 23 (1991), pp. 325-332.

[16] M. J. Brown, I. C. McLean, D. B. Smith, S. C. Taylor, *Markstein lengths of CO/H2/air flames, using expanding spherical flames*, Symposium (International) on Combustion, 26 (1996), pp. 875-881.

[17] F. Parsinejad, J. Keck, H. Metghalchi, *On the location of flame edge in Shadowgraph pictures of spherical flames: a theoretical and experimental study*, Experiments in Fluids, 43 (2007), pp. 887-894.

[18] R. Stone, A. Clarke, P. Beckwith, *Correlations for the Laminar-Burning Velocity of Methane/Diluent/Air Mixtures Obtained in Free-Fall Experiments*, Combustion and Flame, 114 (1998), pp. 546-555.

[19] S. M. Candel, T. J. Poinsot, *Flame Stretch and the Balance Equation for the Flame Area*, Combustion Science and Technology, 70 (1990), pp. 1 - 15.

[20] S. H. Chung, C. K. Law, *An invariant derivation of flame stretch*, Combustion and Flame, 55 (1984), pp. 123-125.

[21] M. Matalon, *On Flame Stretch*, Combustion Science and Technology, 31 (1983), pp. 169-181.

[22] G. H. Markstein, *Experimental and theoretical studies of flame-front stability*, Journal of the Aeronautical Sciences, 18 (1951), pp. 199-209.

[23] S. G. Davis, J. Quinard, G. Searby, *Markstein numbers in counterflow, methane- and propane- air flames: a computational study*, Combustion and Flame, 130 (2002), pp. 123-136.

[24] S. G. Davis, J. Quinard, G. Searby, *Determination of Markstein numbers in counterflow premixed flames*, Combustion and Flame, 130 (2002), pp. 112-122.

[25] A. A. Burluka, M. Fairweather, M. B. Ormsby, C. G. W. Sheppard, R. Wooley, *The laminar burning properties of premixed methane-hydrogen flames determined using a novel analysis method*, Third European Combustion Meeting (2007).

[26] F. H. V. Coppens, J. De Ruyck, A. A. Konnov, *Effects of hydrogen enrichment on adiabatic burning velocity and NO formation in methane + air flames*, Experimental Thermal and Fluid Science, 31 (2007), pp. 437-444.

4. Laminar flame characteristics of $CH_4/H_2/N_2$/air flames

Ce chapitre a fait l'objet d'une publication dans la revue scientifique *International Journal of Hydrogen Energy* :

T. Tahtouh, F. Halter, E. Samson, C. Mounaïm-Rousselle, *Effects of hydrogen addition and nitrogen dilution on the laminar flame characteristics of premixed methane-air flames*, International Journal of Hydrogen Energy, 34 (2009), pp. 8329-8338.

4.1 Abstract

The effect of hydrogen addition and nitrogen dilution on laminar flame characteristics was investigated. The spherical expanding flames technique, in a constant volume bomb, was employed to extract laminar flame characteristics. The mole fraction of hydrogen in the methane-hydrogen mixture was varied from 0 to 1 and the mole fraction of nitrogen in the total mixture (methane-hydrogen-air-diluent) from 0 to 0.35. Measurements were performed at an initial pressure of 0.1 MPa and an initial temperature of 300 K. The mixtures investigated were under stoichiometric conditions.

Based on experimental measurements, a new correlation for calculating the laminar burning velocity of methane-hydrogen-air-nitrogen mixtures is proposed. The laminar burning velocity was found to increase linearly with hydrogen mass fraction for all dilution ratios while the burned gas Markstein length decreases with the increase in hydrogen amount in the mixture except for high hydrogen mole fractions (>0.6).

Nitrogen dilution has a nonlinear reducing effect on the laminar burning velocity and an increasing effect on the burned gas Markstein length. The experimental results and the proposed correlation obtained are in good agreement with literature values.

Nomenclature:

- K : total stretch rate [1/s]
- L_b : burned gas Markstein length [m]
- r_u : flame front radius [m]
- $r_{inc} = \left(\frac{u_{l0[\alpha=i \quad \beta=j]} - u_{l0[\alpha=0 \quad \beta=j]}}{u_{l0[\alpha=0 \quad \beta=j]}} \right)$: relative variation in the laminar burning velocity [-]
- u_{l0} : laminar burning velocity [m/s]
- V_S : stretched flame speed [m/s]
- V_{S0} : unstretched flame speed [m/s]
- α : mole fraction of hydrogen in the iso-octane-hydrogen blend [-]
- β : mole fraction of nitrogen used for dilution in the total mixture [-]
- γ : hydrogen mass percentage in the methane-hydrogen blend [%]
- ρ_b : density of burned gas [Kg/m^3]
- ρ_u : density of unburned mixture [Kg/m^3]

4.2 Introduction

In recent years, the addition of hydrogen to hydrocarbon-air mixtures has received considerable attention. Firstly, and foremost, there is the introduction of hydrogen as an energy carrier to replace present-day fossil fuel energy carriers wherever possible [1, 2]. Adding hydrogen to hydrocarbon energy carriers is considered to be a viable route in enabling a transition towards a sustainable economy based on hydrogen. Secondly, the feasibility of NOx –reduction can be increased by operating at lower combustion temperatures (e.g. Exhaust Gas Recirculation which relies on fuel-air dilution). A major drawback of the latter is that the burning velocity is reduced and the flammability limit is approached so that the flame becomes less stable and more susceptible to extinction. One strategy to overcome these limitations is the addition of an amount of hydrogen because of its high laminar burning velocity, low ignition energy and wide flammability limits. These properties widen the dilution operability ranges.

Akansu et al. [3], Bauer and Forest [4] and Karim et al. [5] investigated the use of natural gas-hydrogen mixtures in Internal Combustion Engines and observed a decrease in HC, CO_2 and CO emissions when the hydrogen percentage was increased. While NOx emission values generally increase with an increase in hydrogen content, if a catalytic converter, an EGR system or a lean burn technique are used, NOx emission values can be reduced to extremely low levels. Hydrogen addition can also improve the torque and knock tendency due to the reduction of burning duration [6].

Laminar burning velocity is a fundamental parameter to characterize both laminar and turbulent premixed combustion in the case of the wrinkled thin flamelet regime. It therefore leads to a better understanding of the combustion process in combustion engines and power generation systems.

Numerical and experimental investigations on hydrogen addition [7-13] and on nitrogen dilution [14, 15] showed that the laminar burning velocity increases with increasing hydrogen fraction in the fuel blends, and that nitrogen dilution to fuel reduces the burning velocity. Yu et al. [7] found that the laminar burning velocity varies linearly with the ratio between the amount of hydrogen added to the methane-air mixture plus the amount of air needed to oxidize it totally, and the amount of methane plus the amount of air available for its oxidation (R_H). Milton and Keck [16] concluded from their results that there is no simple relation between laminar burning velocity and any of the chemical parameters such as H-atom fraction or H/C ratio.

Zhang et al. [17] investigated the effects of hydrogen fraction on laminar burning velocity, flame temperature, Markstein number and Damkholer number in the case of methane-hydrogen-air flames and obtained an increase in Damkholer number with that of the hydrogen fraction, indicating that hydrogen addition can widen the extinction limits of a natural gas-air

flame. However, there is a lack of data, especially for the combined effects of hydrogen addition and nitrogen dilution in methane-air mixtures. Recently, Miao et al. [18, 19] measured laminar burning velocities and Markstein lengths of diluted hydrogen-enriched natural gas mixtures but without suggesting any correlation.

An experimental technique to determine the laminar flame speed and the corresponding Markstein length involves spherically expanding flames [20, 21]. A well-known advantage of spherically expanding flames ignited from a central ignition point is the accurate estimates of the stretch rate [22-24]. In this work, spherical expanding flames are studied by using the shadowgraph technique (see [25] for details).

Based on asymptotic analysis [26], several authors [27-29] have proposed a linear relation between stretch rate and flame speed. The linear relation proposed by Clavin [28] is employed to extract the value of unstretched laminar flame speed and Markstein length. This paper presents new experimental results of laminar burning velocities and Markstein lengths for CH_4-H_2-N_2-air mixtures. A correlation for the laminar burning velocity as a function of the N_2 and H_2 contents is also suggested.

4.3 Experimental details

Experiments were conducted in a cylindrical stainless steel combustion chamber with an inner volume of 24.32 litres. Two tungsten electrodes (diameter 0.8mm), linked to a conventional capacitive discharge ignition system, are used to form the spark gap (2.8mm) at the center of this chamber. The plane of electrodes is slightly tilted with respect to the plane of visualization, thus decreasing the display of disturbances due to ignition in the recorded images.

The volumes of different gases are introduced into the chamber with thermal mass flowmeters, connected to a computer via a RS232 serial port. Once the command to fill the combustion chamber with the needed volumes has been launched, the flowmeters are simultaneously opened. Before filling the chamber with gases, a vacuum is created in the chamber, and after introducing the different volumes of gases, the chamber is at atmospheric pressure. The pressure level is checked with a piezoelectric pressure transducer. A fan is located inside the chamber to obtain a perfectly homogenous mixture.

Two opposed and transparent viewports (diameter 10.5cm) provide optical access. The lighting is provided by a continuous Stabilite 2017 Argon ion Laser, with maximum output power of 6W. The wavelengths generated are in the range of [457.9-514.5 nm] and the beam diameter at $\frac{1}{e^2}$ is 1.4mm for this laser. A parallel light beam is created by using two plano-convex lenses, with diameters of 15 mm and 70 mm and focal lengths of 25 mm and 1000 mm respectively. After passing through both lenses and the combustion chamber, the beam is displayed on a screen. The maximum beam diameter cannot exceed 70 mm (the diameter of the second lens). A schematic view of the whole system was given in Figure 1 (chapter 3).

The evolution of the flame surface is observed from the shadowgraph images, recorded with a high speed CMOS APX camera operating at 6000 frames/second.

In these images, the luminous front that is distinguishable corresponds to the flame radius on the unburned gases side r_u [30].

An analysis of the different errors attributable to the experimental procedure in a previous study [25] showed that the maximum uncertainty in the determination of the laminar burning velocity, linked to these errors, was less than 5%.

4.4 Properties of mixtures

In this study, measurements of laminar burning velocity and Markstein length were performed at an initial pressure of 0.1 MPa and an initial temperature of 300K. All the investigated mixtures were under stoichiometric conditions even for the hydrogen blended fuel. For each mixture, at least four experimental measurements were made and the data reported in the following are the simple average of these tests.

Table 1. *Hydrogen and diluent mole fractions of investigated mixtures.*

α / β	0	0.1	0.15	0.2	0.3	0.6	0.8	1
0	done	done	done	done	done			
0.1	done	done	done	done	done			
0.2	done	done	done	done	done			
0.3	done	done	done	done	done	done	done	done
0.35		done	done	done	done			done

For all results, parameter α is the mole fraction of hydrogen in the methane-hydrogen blend:

$$\alpha = \frac{X_{H_2}}{X_{CH_4} + X_{H_2}}$$

The parameter of dilution β is the mole fraction of nitrogen used for dilution in the total mixture:

$$\beta = \frac{X_{N_2-dilution}}{X_{CH_4} + X_{H_2} + X_{O_2} + X_{N_2-air} + X_{N_2-dilution}} = X_{N_2-dilution}$$

where X_{CH_4}, X_{H_2} and X_{O_2} are respectively methane, hydrogen and oxygen mole fractions in the mixture, X_{N_2-air} the mole fraction of nitrogen in the air mixture ($X_{N_2-air} = 3.78 \bullet X_{O_2}$) and

$X_{N_2-dilution}$ the mole fraction of nitrogen used for dilution. The different hydrogen and diluent mole fractions of all the investigated mixtures are summarized in Table 1.

4.5 Extraction of Laminar Characteristics

Under the assumption of a spherical flame front propagation, the instantaneous flame front radius is obtained from post-processing after subtracting the background. At each time step, the luminous zone is fitted by a circle. The estimate of the circle radius and centre is based on the minimization of the distance between the circle and luminous points. The image quality is quite good and it can be noticed in Figure 1 that disturbances due to the ignition system are not discernable. Bradley et al. [31] found that the flame speed becomes independent of the spark energy at a radius about 5 mm. In the present work, only flame radii larger than 7 mm were considered in order to avoid ignition disturbances and up to a value lower than 30 mm, i.e. a total volume of burned gases less than 0.5% of the total volume. The total chamber pressure can therefore be considered constant.

The temporal evolution of the flame front was obtained thanks to the high speed image recording. Figure 2 shows an example of the measured flame radius, r_u versus the time after ignition for different mixtures with different hydrogen mole fractions ($\alpha =$ 0, 0.1, 0.2 and 0.3) but at a fixed diluent mole fraction ($\beta = 0.2$).

After the spark, the flame is ignited and propagates spherically. Even for high dilution levels (Figure 1) where the flame propagation is affected by natural convection, the error induced by assuming a spherical shape for the flame front is very low. The flame growth depends on the mixture composition. It can be seen clearly in Figure 2 that the flame radius increase becomes faster for a higher hydrogen mole fraction in the mixture. For α=0 the spark energy was greater than that of α=0.1. This phenomenon is well illustrated in Figure 2. Due to the higher spark energy, in the earlier stage, when flame propagation is still affected by the spark energy, the flames corresponding to α=0 present a higher acceleration than those having α=0.1. Considering the same time reference, for a time lower than 0.016 s, the flame with α=0 exhibits a flame radius larger than that corresponding to α=0.1.

The unstretched flame speed and the Markstein length can be deduced from the temporal evolution of the flame front, as proposed by Clavin [28]:

$$V_S = V_{S0} - L_b \bullet K \quad (1)$$

V_S : the stretched propagation flame speed

$$V_S = \frac{dr_u}{dt} \quad (2)$$

V_{S0} : the unstretched propagation flame speed

L_b : the Markstein length for burned gas, a measure of the flame response to the stretch

K : the total stretch acting on the flame, defined by the temporal rate of change of a flame surface element of area, A :

$$K = \frac{1}{A} \bullet \frac{dA}{dt}.$$

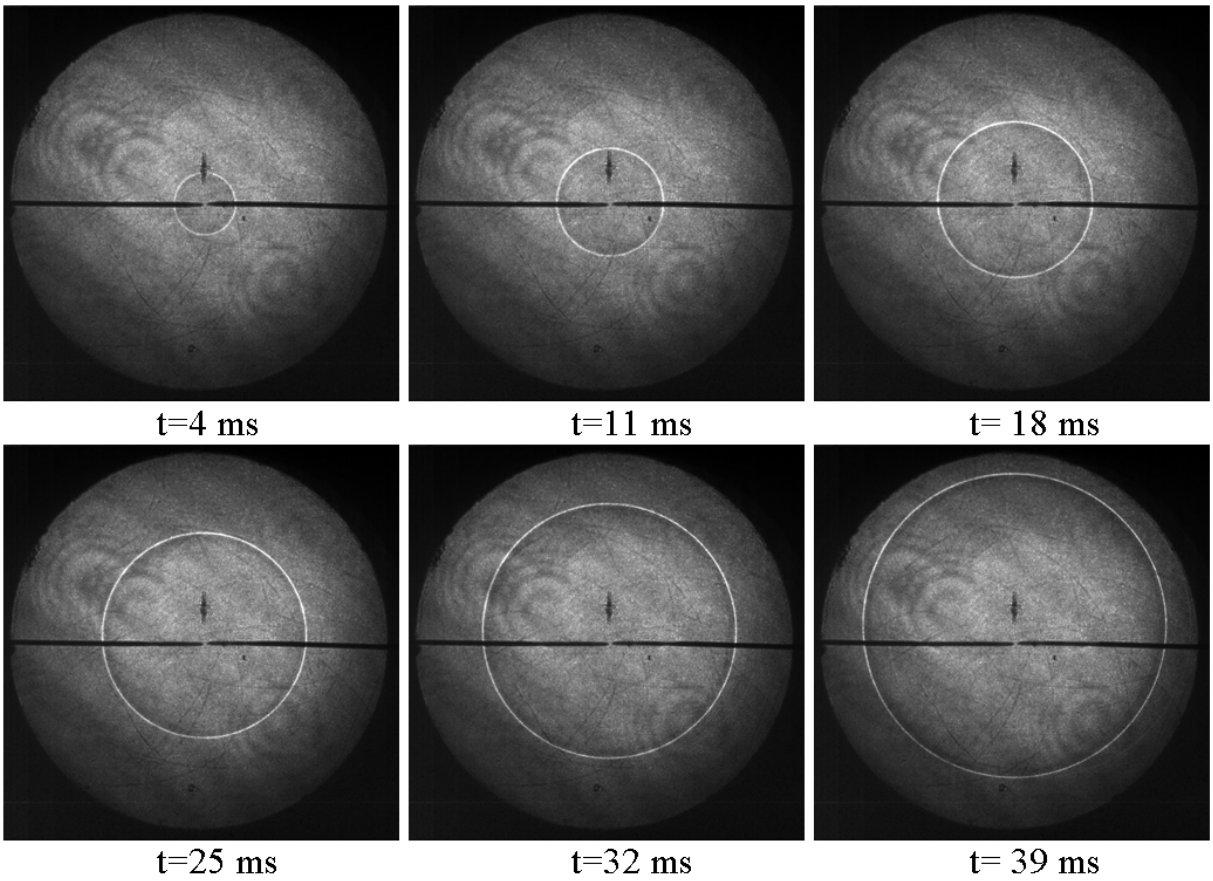

Figure 1. *Examples of flame propagation shadowgraphs (α =0.3, β =0.3, P=0.1 MPa, T=300K, 6000 images/second).*

This relation is valid when the propagation phenomena are no longer affected by the initial energy deposit needed to initiate exothermic reactions and when the value of stretched flame speed is nearly the value of the adiabatic unstretched flame speed. Moreover the flame thickness has to remain negligible compared to the flame radius (thin flames) and finally, the unburned gases must be initially at rest and have a uniform temperature and composition.

This linear relation has been extensively applied in outwardly propagating flames. In fact the stretch rate affects the laminar flame speed by two distinct contributions [32]: a curvature effect and a strain effect, with each of these being proportional to a Markstein length, namely, the curvature Markstein length and the strain Markstein length. In the case of a spherically

outwardly expanding flame front, the stretch rate K can be written as follows [33] to obtain the stretch Markstein length:

$$K = \frac{2}{r_u} \bullet \frac{dr_u}{dt} \quad (3)$$

The unstretched flame speed and the Markstein length were provided by fitting the temporal radius evolution with the exact solution to Eq. (1) [25]. This fitting eliminates the additional perturbation induced by the radius derivation process for the calculation of the stretched flame speed Eq. (2) or the total stretch rate Eq. (3). Furthermore, it reduces experimental noise.

- Positive Markstein lengths

As reported in [25] the exact solution of Eq. (1) for positive values of L_b is:

$$r(t) = 2L_b \bullet W_0\left(Z\right)$$

where W is the Lambert function and W_0 the principal branch of the Lambert function. Z is defined as:

$$Z = \frac{e^{\frac{V_{S0}t + C_1}{2L_b}}}{2L_b}$$

with C_1 a constant to be determined using initial conditions

$$\left(r\left(t_0\right) = r_0 \Rightarrow Z = r_0 \bullet \frac{e^{\frac{V_{S0} \bullet (t - t_0) + r_0}{2L_b}}}{2L_b} \right).$$

The Lambert function W is defined as the multi-value inverse function of $f(W) = We^W$.

For positive values of L_b, $Z > 0$ and therefore the principal branch $W_0(Z)$ is the only branch of W that gives real values.

- Negative Markstein lengths

For negative values of L_b, the alternate branch $W_{-1}(Z)$ should be used and the solution of Eq. (1) becomes:

$$r\left(t\right) = 2L_b \bullet W_{-1}\left(Z\right)$$

Z has the same definition as before.

L_b and V_{S0} are found by minimizing the following equation:

$$\sum_{1}^{N}\left(r_u(t)-r(t)\right)^2=\sum_{1}^{N}\left(r_u(t)-2L_b W_{-1}(Z)\right)^2$$

r_u is the raw radius resulting from the flame front detection.

For a constant pressure flame propagation, the laminar burning velocity can be deduced from the unstretched propagation flame speed and the density ratio by using the following equation**:**

$$u_{l0}=\frac{\rho_b}{\rho_u}\bullet V_{S0} \quad (4)$$

ρ_b : the density of burned gases; ρ_u : the density of unburned gases

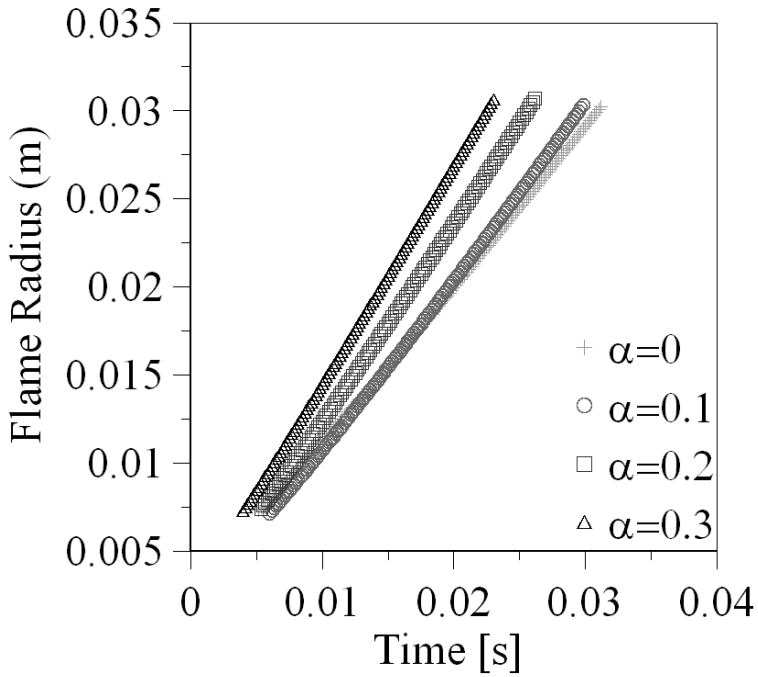

Figure 2. *Examples of temporal evolution of the flame front radius for different* α *(* β *=0.2, P=0.1 MPa, T=300K).*

A computational method using the adiabatic flame calculation with Premix [34] and based on a detailed chemical kinetic scheme (GRIMECH 3.0) [35] was used to provide the burned and the unburned gases densities, needed to extract the laminar burning velocity, and to calculate the laminar burning velocities for comparison with experimental results.

4.6 Results and discussion

4.6.1 Laminar burning velocities

Figure 3 shows the evolution of flame speed as a function of flame stretch rate for the same mixtures as presented in Figure 2. The effect of stretch on the flame speed changes with the content of hydrogen mole fraction in the mixture. The dependence of the stretched flame speed with the stretch rate decreases with the addition of hydrogen, as indicated by the change of slopes. The temporal evolution of stretched propagation speeds are illustrated in Figure 4 for four different mixtures. The symbols in this graph represent one third of the measured data since the symbol frequency was 3. The stretched flame propagation speed increases gradually with time for all the represented mixtures except for $\alpha = 0.6$, $\beta = 0.3$ where it decreases with time due to the negative value of its corresponding burnt gas Markstein length. The flame stretch decreases with radius development for all mixtures. Furthermore, in the final phase of flame propagation, the stretched flame speed tends towards an asymptotic value.

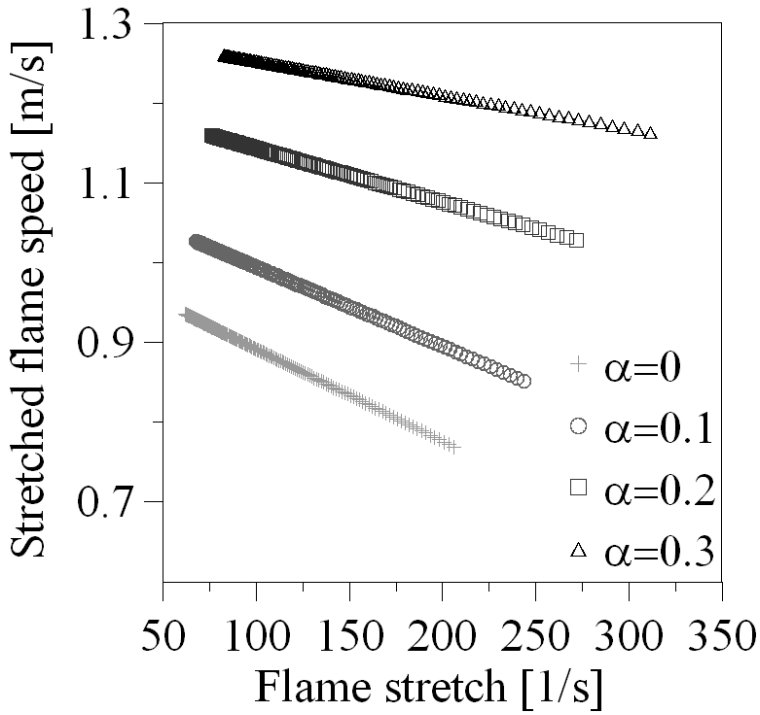

Figure 3. *Evolution of the stretched flame speed versus the flame stretch for different hydrogen contents (β =0.2, P=0.1 MPa, T=300K).*

The laminar burning velocity versus β values and for different values of α is plotted on Figure 5. For the sake of clarity, the values for mixtures with $\alpha > 0.3$ are not reported in this graph. However, they are reported in the following graphs. As Figure 5 shows, increasing the hydrogen percentage in the mixture leads to an increase in the laminar burning velocity, which is consistent with results reported in the literature [7-12]. The absolute laminar burning

velocity increase due to the addition of hydrogen decreases as the dilution with N_2 becomes higher; for example:

$u_{l0[\alpha=0,3 \quad \beta=0]} - u_{l0[\alpha=0 \quad \beta=0]} = 0.085$ m/s

while $u_{l0[\alpha=0,3 \quad \beta=0,3]} - u_{l0[\alpha=0 \quad \beta=0,3]} = 0.029$ m/s.

A relative variation in the laminar burning velocity can be calculated as:

$$r_{inc} = \left(\frac{u_{l0[\alpha=i \quad \beta=j]} - u_{l0[\alpha=0 \quad \beta=j]}}{u_{l0[\alpha=0 \quad \beta=j]}} \right)$$

where $i = 0.1$, 0.15, 0.2 and 0.3 and $j = 0$, 0.1, 0.2 and 0.3

The values of r_{inc} plotted in Figure 6, show that the relative variation, r_{inc} can be considered constant, with the same hydrogen mole fraction, for different diluent mole fractions.

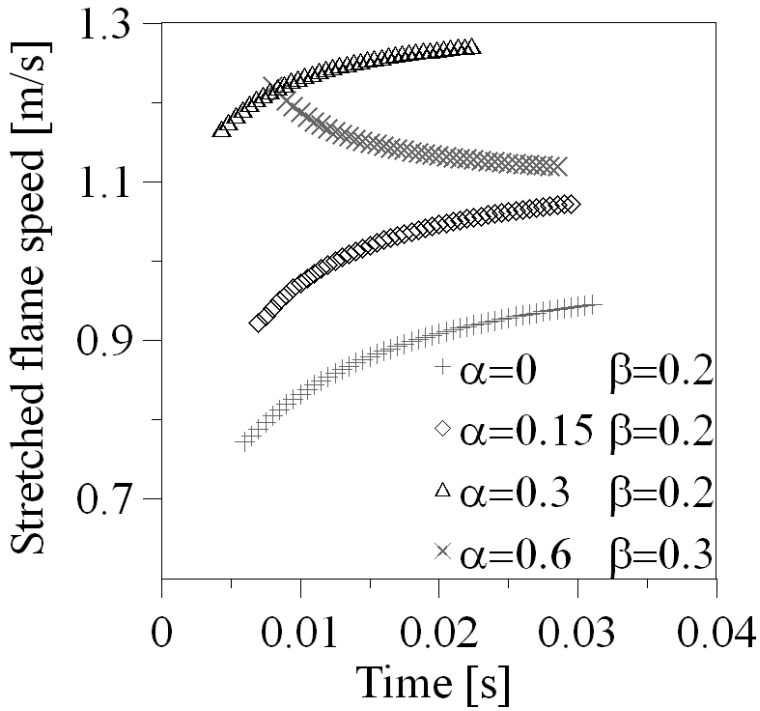

Figure 4. *Temporal evolution of the stretched flame speed for four different mixtures (symbol frequency = 3), (P=0.1 MPa, T=300K).*

From Figure 5 it can be seen that laminar burning velocity decreases as β increases. This decrease exhibits a nonlinear trend for all α, which is consistent with the work of Miao et al. [19]. The laminar burning velocities are also plotted in Figure 7 versus α for different β and for all the mixtures studied.

For low hydrogen mole fractions ($\alpha < 0.3$) the laminar burning velocity seems to increase linearly with hydrogen mole fraction, therefore when the data corresponding to $\alpha > 0.3$ are considered, it can be concluded that the hydrogen mole fraction has a nonlinear increasing effect on laminar burning velocity.

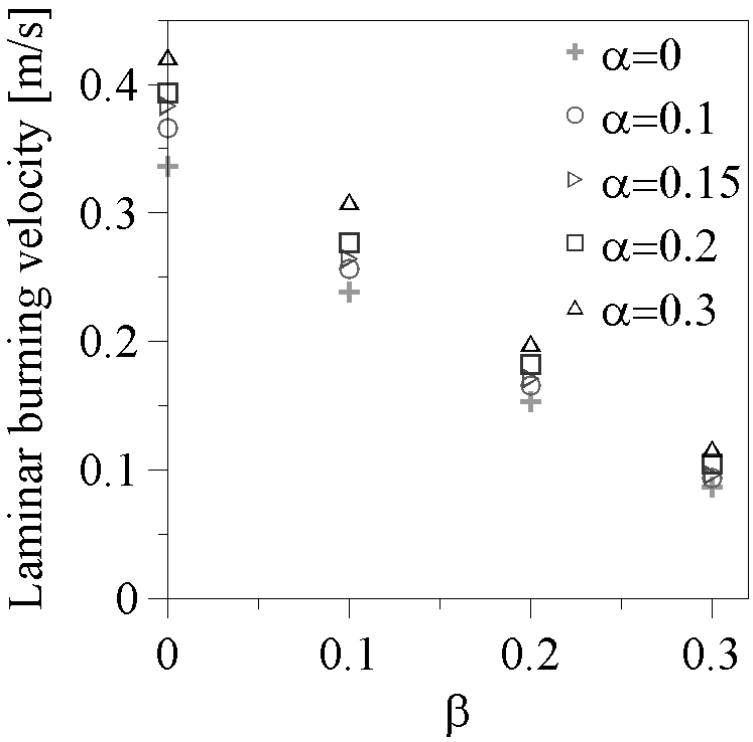

Figure 5. *Experimental laminar burning velocity versus β (P=0.1 MPa, T=300K).*

In order to present a possible correlation for the laminar burning velocity of the CH_4-H_2-N_2-air mixtures, all the results are plotted versus the hydrogen mass percentage, γ, in Figure 8. γ is defined as:

$$\gamma = 100 \bullet \frac{m_{H_2}}{m_{CH_4} + m_{H_2}} \quad (5);$$

m_{H_2} : hydrogen mass in the mixture; m_{CH_4} : methane mass in the mixture.

As can be seen in Figure 8, the laminar burning velocity evolves linearly with the hydrogen mass percentage contrary to its evolution according to the mole percentage as shown in Figure 7. Considering a linear evolution, the coefficients of determination, R^2, obtained by fitting the curves corresponding to the different β values (Figure 8) present values greater than 0.98.

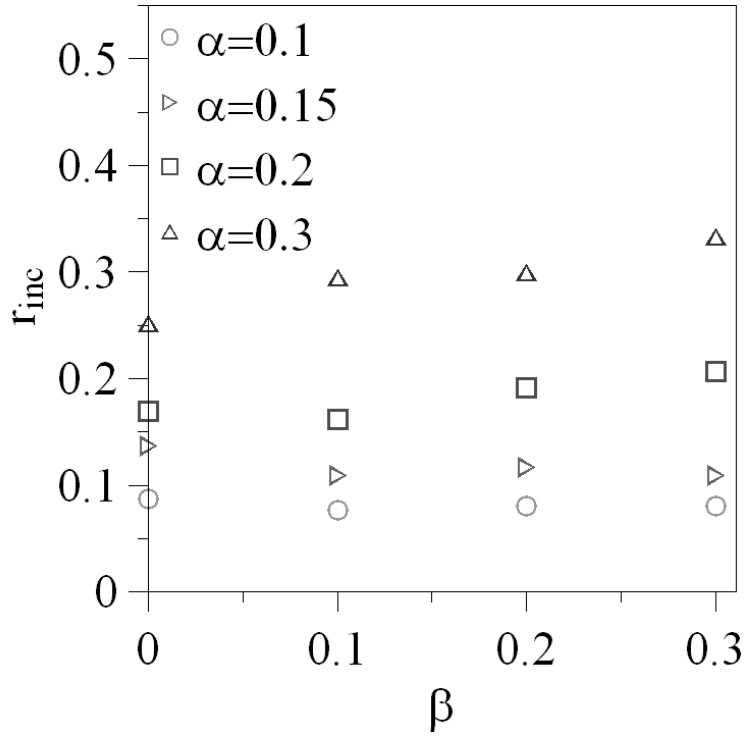

Figure 6. *r_{inc} versus β (P=0.1 MPa, T=300K).*

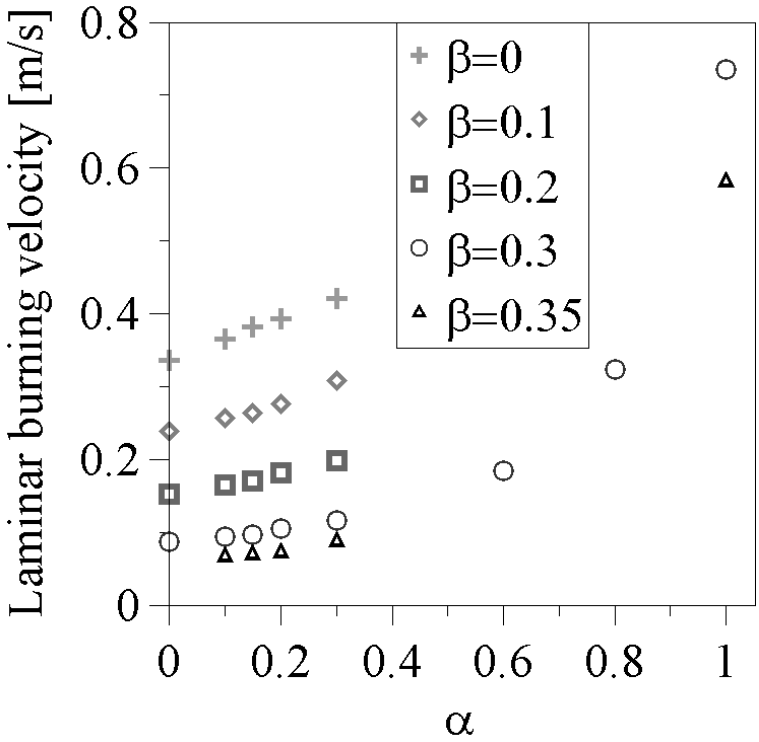

Figure 7. *Experimental laminar burning velocity versus hydrogen mole fraction, α (P=0.1 MPa, T=300K).*

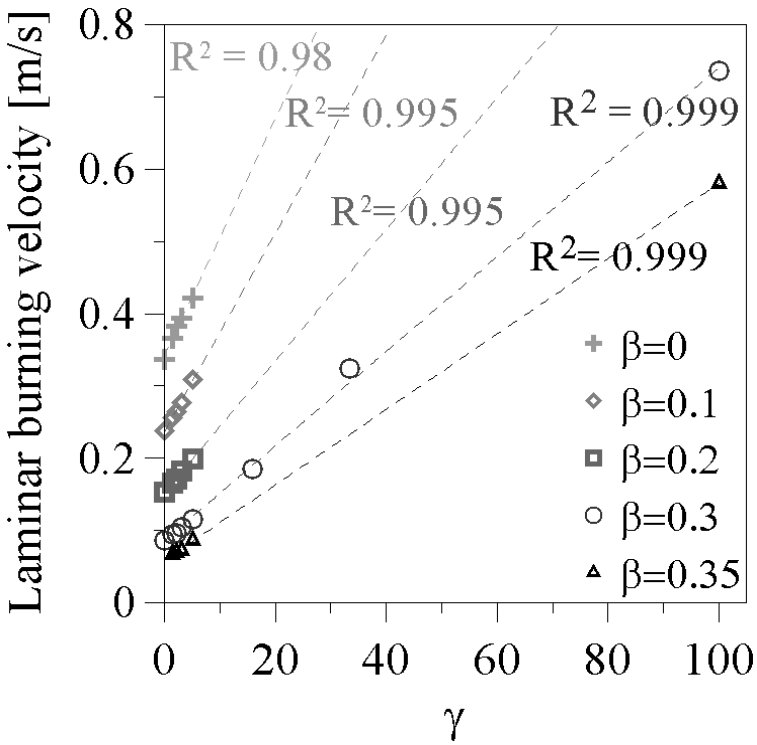

Figure 8. *Experimental laminar burning velocity versus hydrogen mass fraction, γ (P=0.1 MPa, T=300K).*

4.6.2 Correlation

Based on the linear effect of hydrogen mass percentage on the laminar burning velocity, a simple correlation can be suggested as: $u_{l0,\beta} = a_\beta * \gamma + b_\beta$, determined for each β value. This expression can be generalized:

$$u_{l0} = A(\beta) \bullet \gamma + B(\beta) \quad (6)$$

with $A(\beta)$ and $B(\beta)$ two variables function of β, the dilution rate. The slope of each straight-line fit, a_β, is plotted versus β in Figure 9. The linear constant b_β does not evolve linearly with β as can be seen in Figure 10. The best fit is obtained for a second order polynomial fit (the coefficient of determination R^2 is close to unity).

For β=0.35, as seen in Figure 10, the linear extrapolation is not representative of all the data, since the first four data β=0.35 and γ=1.377, 2.17, 3.046 and 5.11 are so distant from the last data with γ=100. To overcome this problem, a general expression of the laminar burning velocity: $u_{l0} = (a_{corr} \bullet \beta + b_{corr}) \bullet \gamma + c_{corr} \bullet \beta^2 + d_{corr} \bullet \beta + e_{corr}$ was used to achieve a better fit with experimental data. Thus, all experimental data are considered and they have the same weight in the determination of the correlation. However, it was found that the laminar burning velocity value for β=0 and γ=100 is required in the best fitting data to extend this correlation range.

Since an experimental measurement of the laminar velocity of this mixture was not planned, it was decided to use a mean value $u_{l0\alpha=1}$=2.26 m/s of some experimental and computational values available in the literature [12, 36, 37, 16, 38].

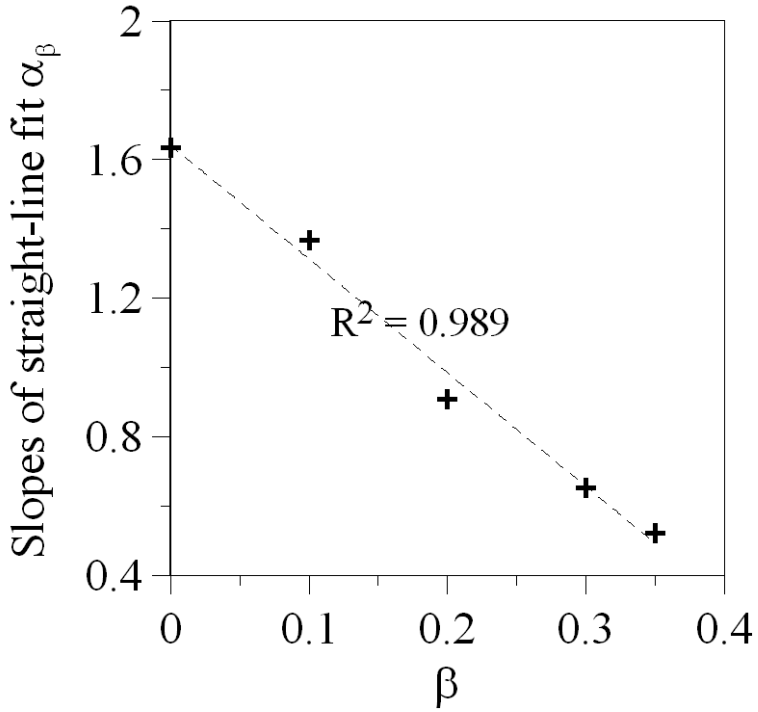

Figure 9. *Slopes a_β versus β.*

a_{corr}, b_{corr}, c_{corr}, d_{corr} and e_{corr} are the coefficients of the correlation obtained with a best fitting over 29 values; our experimental results (28 values) and the mean value $u_{l0\alpha=1}$=2.26 m/s for β=0 and γ=100. This leads to an $A(\beta) = a_{corr} \bullet \beta + b_{corr} = -3.8 \bullet \beta + 1.83$ and to $B(\beta) = c_{corr} \bullet \beta^2 + d_{corr} \bullet \beta + e_{corr} = 100.6 \bullet \beta^2 - 115.31 \bullet \beta + 33.96$.

Finally, by expressing hydrogen mass percentage γ as a function of hydrogen mole fraction α, Eq. (6) becomes:

$$u_{l0}\left[cm/s\right] = A(\beta) \bullet \left(\frac{-201.6 \bullet \alpha}{14.027 \bullet \alpha - 16.043} \right) + B(\beta) \quad (7)$$

The differences between experimental data and the present correlation (Eq. (7)) present a maximum value of 4.8 % and a mean absolute value of 1.7%.

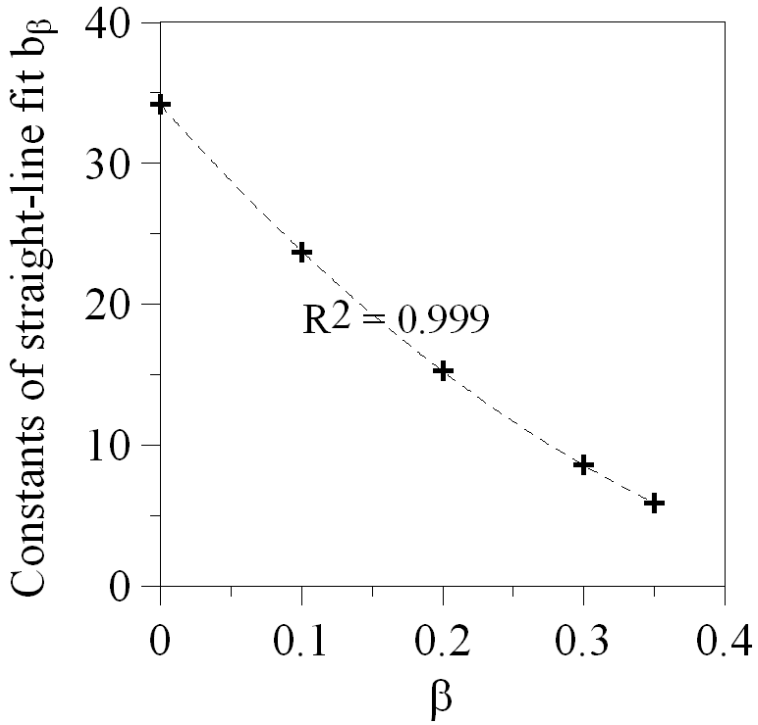

Figure 10. *Constants b_β versus β.*

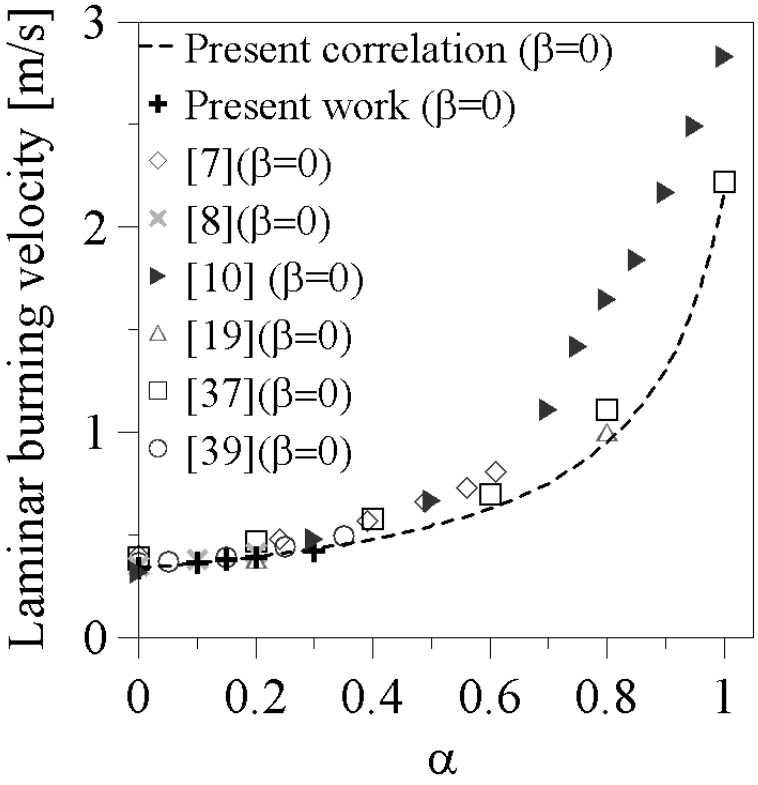

Figure 11.a *Laminar burning velocity versus hydrogen mole fraction, α (β =0).*

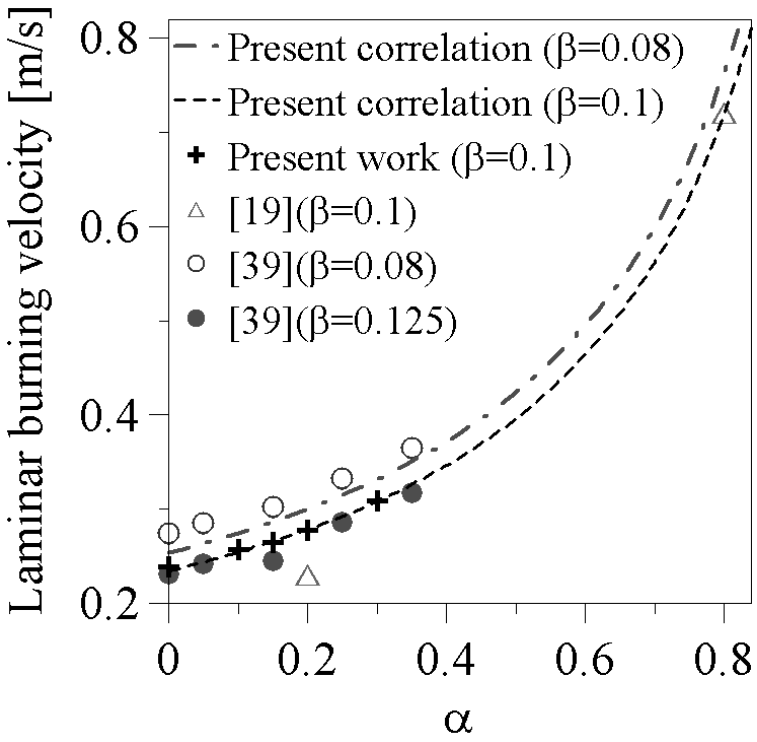

Figure 11.b *Laminar burning velocity versus hydrogen mole fraction, α ($0< \beta <0.15$).*

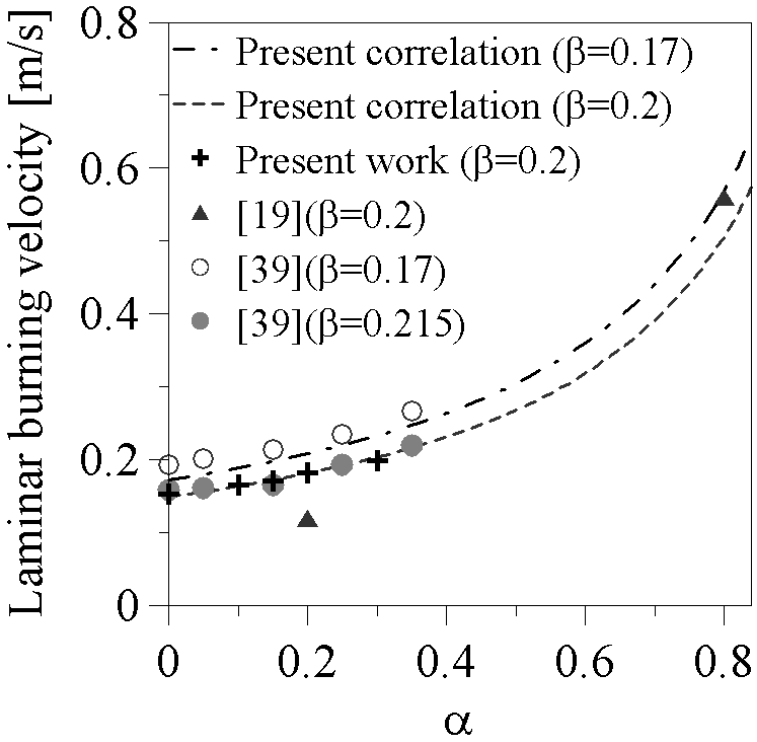

Figure 11.c *Laminar burning velocity versus hydrogen mole fraction, α ($0.15< \beta <0.215$).*

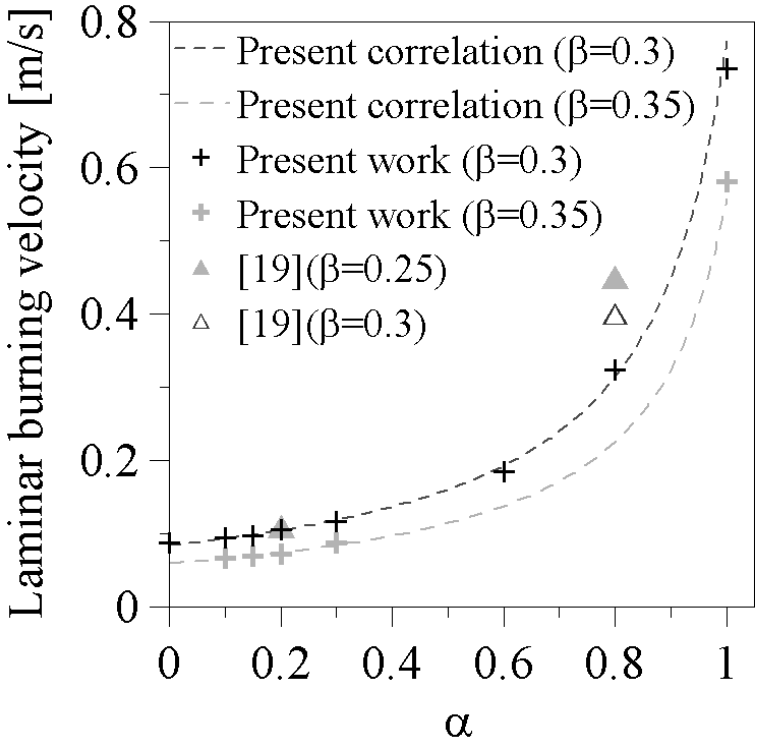

Figure 11.d *Laminar burning velocity versus hydrogen mole fraction, α (0.215< β <0.35).*

Figures 11.a, 11.b, 11.c and 11.d show comparison of the present measured laminar burning velocity values with those found in the literature (experimental values and correlations) [39, 37, 7, 8, 19, 14, 10] and with the present correlation (Eq. (7)). A very good agreement is observed between these different reported values of laminar burning velocity except with Ilbas et al. [10] when α is higher than 0.5 (β=0). However, it should be noted that in this hydrogen addition range, the values calculated by Ilbas et al. are higher than those obtained by other authors [12, 36, 37, 16, 38].

Figure 12 shows a comparison between the present correlation (Eq. (7)) and the correlations expressed in [7] and [37]. The correlation reported in [37] is in very good agreement with Eq. (7) for all hydrogen addition ranges. The correlation reported in [7] yields slightly higher values but exhibits the same trend as Eq. (7) in its range of validity. Figure 13 shows the dilution effect on the laminar burning velocity. It presents a comparison between the present correlation, the correlation given in [14] and computational values obtained using the GRI mechanism. The correlation of Stone et al. [14] exhibits good agreement with the proposed one, but its range of validity is limited to $\beta \leq$ 0.15. Thus, computational data were reported and a very good agreement is observed with Eq. (7) for the higher dilution levels. The results reported in [19] and [37] correspond to natural gas, not to methane, even though methane represents more than 96% in volumetric fraction of the natural gas considered.

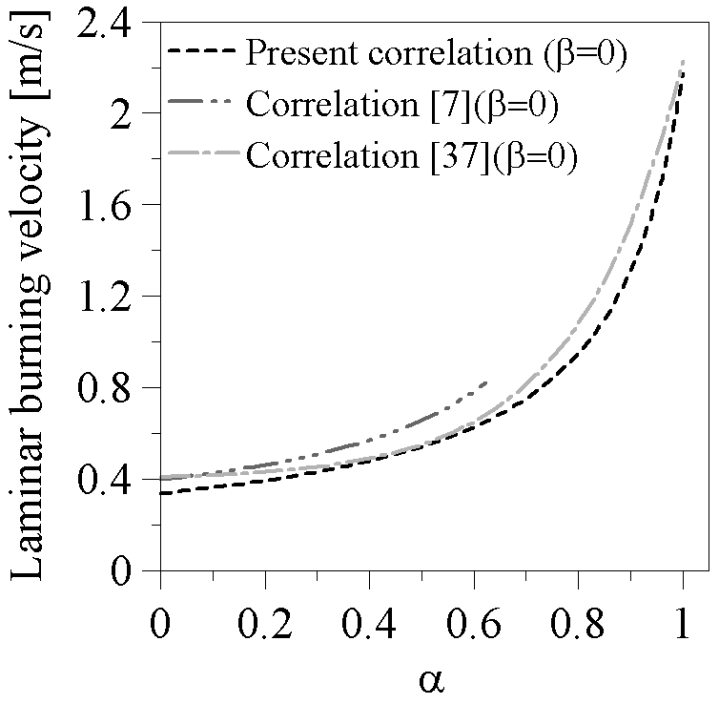

Figure 12. *Comparison between the present correlation and two others [7, 37] for $\beta = 0$ (P=0.1 MPa, T=300K).*

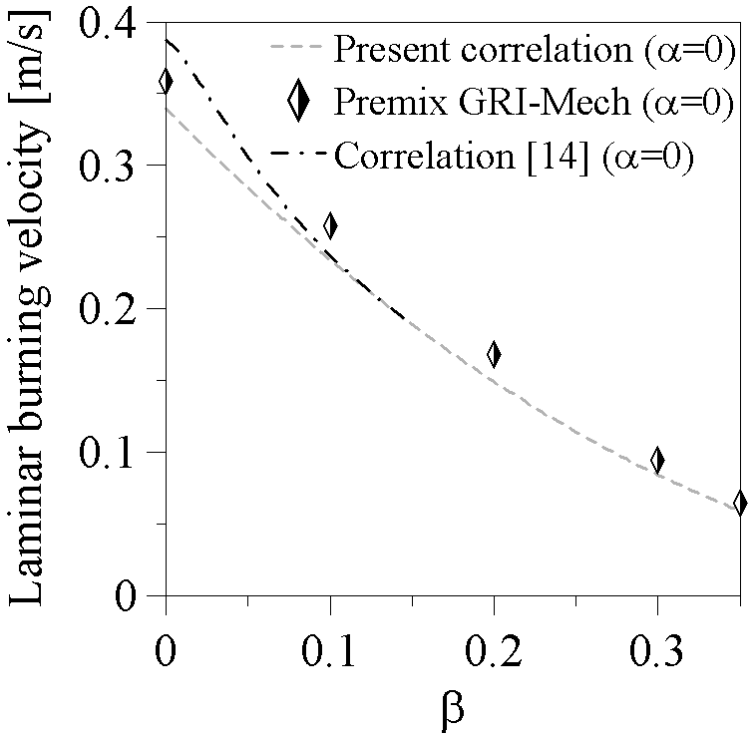

Figure 13. *Comparison between the present correlation for the laminar burning velocity versus β, the one given by Stone et al. [14] and the computational values obtained with Premix for $\alpha = 0$ (P=0.1 MPa, T=300K).*

4.6.3 Markstein length

In spherically expanding flames, the flame speed is independent of the considered isotherm [29] and the Markstein length obtained is always the burned gas Markstein length [40, 41]. The L_b, as defined in Eq. (1), is the opposite of the slope of the stretched flame speed versus stretch rate. The values of Markstein length obtained in the present work are plotted and compared to literature values in Figure 14. For mixtures with less than 30% of hydrogen in volume, the stretched flame speed increases gradually with the radius, as the stretch effect on the flame front is reduced, indicating a positive value of Markstein length. Mixtures having more than 60% of hydrogen in volume show a reduction in flame speed with a decrease in stretch rate, resulting in a negative value of the Markstein length. In fact, for $L_b > 0$, thermo-diffusive instabilities counterbalance the destabilizing effect of hydrodynamic instabilities (for these relatively small flame radii considered), while for $L_b < 0$, mixtures are diffusively unstable. For all data (except for $\alpha > 0.6$), a decrease of L_b for higher values of α is observed.

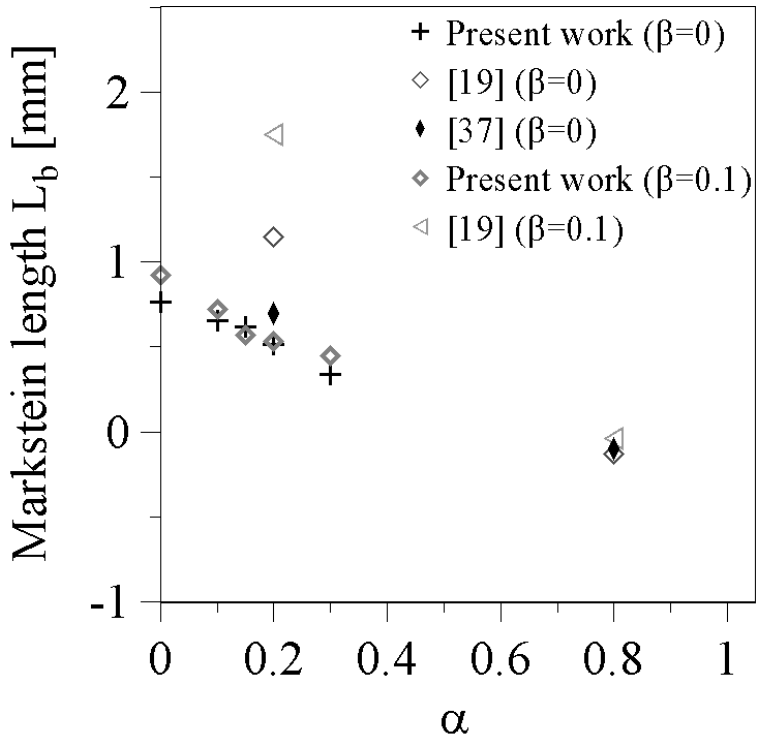

Figure 14.a *Markstein length values versus the hydrogen content α and for different dilution rates β <0.2 (P=0.1 MPa, T=300K).*

For $\alpha \leq 0.3$, hydrogen addition reduces the dependence of the flame speed versus the stretch rate. On the other hand, with higher values of α, hydrogen addition results in an increase in flame instability.

Two different effects of diluent mole fraction, depending on the hydrogen mole fraction, α, were also observed. First, an increase in the diluent mole fraction indicates a higher value of L_b for $\alpha \leq 0.3$. Then, when the diluent mole fraction becomes higher, the value of L_b decreases.

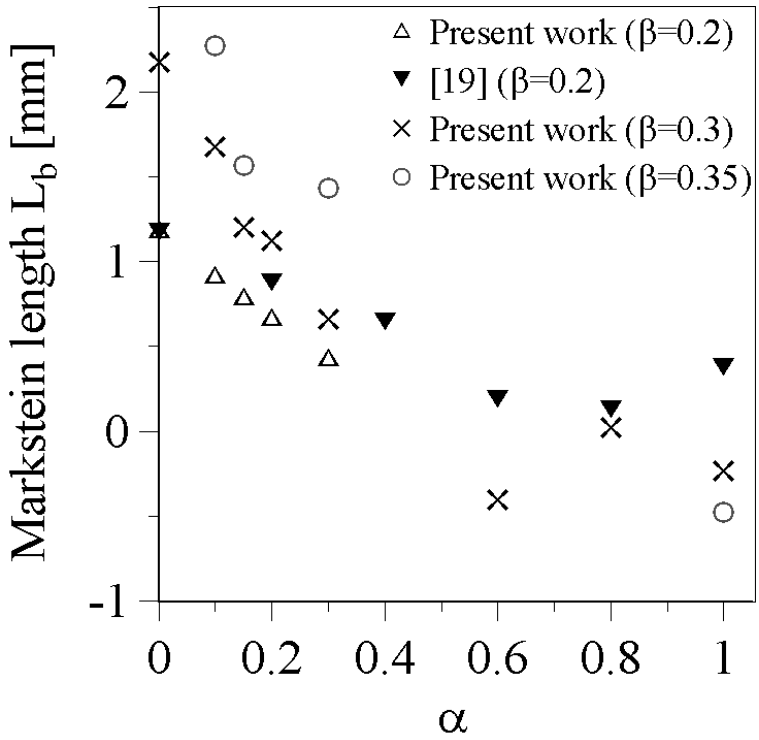

Figure 14.b *Markstein length values versus the hydrogen content α and for different dilution rates β >0.2 (P=0.1 MPa, T=300K).*

4.7 Conclusion

The combined effect, in terms of laminar flame characteristics, of hydrogen addition and nitrogen dilution in methane-air mixtures was investigated in a constant volume chamber. The laminar burning velocities and the burned gas Markstein lengths were obtained using the spherical expanding flames technique.

Based on the present experimental data, an empirical correlation is suggested to estimate the laminar burning velocity of CH_4-H_2-N_2-air mixtures under stoichiometric conditions, at 1 bar pressure and ambient temperature. This correlation was validated for a wide range of dilution levels ($0<\beta<0.35$) and for all hydrogen mole fractions ($0<\alpha<1$). A very good agreement with literature values was obtained for the suggested correlation and the present experimental results. The same good agreement was found with other correlations for methane-hydrogen-air and for methane-air-nitrogen mixtures since no general correlation was found in the literature.

The laminar flame speed increases with hydrogen addition. Moreover, for a fixed diluent fraction, the increasing effect of the hydrogen mass fraction on the laminar burning velocity was found to be linear. The relative variation in the laminar burning velocity was found to be constant, for mixtures with the same hydrogen mole fraction and with different diluent mole fractions.

Markstein length decreases with hydrogen addition, indicating a reduction in the dependence of the flame speed towards the stretch. Then, for higher hydrogen mole fractions, the mixture is diffusively unstable and a negative value of Markstein length is found. To increase the diluent mole fraction in the mixture involves a nonlinear decrease in the laminar burning velocity. Furthermore, it was found that the dilution increases the stretch effect on the flame speed which is evidenced by higher values of burned gas Markstein length.

4.8 References

[1] S. Dunn, *Hydrogen futures: toward a sustainable energy system*, International Journal of Hydrogen Energy, 27 (2002), pp. 235-264.

[2] A. E. Dahoe, V. V. Molkov, *On the development of an International Curriculum on Hydrogen Safety Engineering and its implementation into educational programmes*, International Journal of Hydrogen Energy, 32 (2007), pp. 1113-1120.

[3] S. O. Akansu, Z. Dulger, N. Kahraman, T. N. Veziroglu, *Internal combustion engines fueled by natural gas--hydrogen mixtures*, International Journal of Hydrogen Energy, 29 (2004), pp. 1527-1539.

[4] C. G. Bauer, T. W. Forest, *Effect of hydrogen addition on the performance of methane-fueled vehicles. Part I: effect on S.I. engine performance*, International Journal of Hydrogen Energy, 26 (2001), pp. 55-70.

[5] G. A. Karim, I. Wierzba, Y. Al-Alousi, *Methane-hydrogen mixtures as fuels*, International Journal of Hydrogen Energy, 21 (1996), pp. 625-631.

[6] T. Shinagawa, T. Okumura, S. Furuno, K. O. Kim, *Effects of hydrogen addition to SI engine on knock behavior*, SAE 2004-01-1851 (2004).

[7] G. Yu, C. K. Law, C. K. Wu, *Laminar flame speeds of hydrocarbon + air mixtures with hydrogen addition*, Combustion and Flame, 63 (1986), pp. 339-347.

[8] F. Halter, C. Chauveau, N. Djebaïli-Chaumeix, I. Gökalp, *Characterization of the effects of pressure and hydrogen concentration on laminar burning velocities of methane-hydrogen-air mixtures*, Proceedings of the Combustion Institute, 30 (2005), pp. 201-208.

[9] C. Mandilas, M. P. Ormsby, C. G. W. Sheppard, R. Woolley, *Effects of hydrogen addition on laminar and turbulent premixed methane and iso-octane-air flames*, Proceedings of the Combustion Institute, 31 (2007), pp. 1443-1450.

[10] M. Ilbas, A. P. Crayford, I. Yilmaz, P. J. Bowen, N. Syred, *Laminar-burning velocities of hydrogen-air and hydrogen-methane-air mixtures: An experimental study*, International Journal of Hydrogen Energy, 31 (2006), pp. 1768-1779.

[11] F. H. V. Coppens, J. De Ruyck, A. A. Konnov, *Effects of hydrogen enrichment on adiabatic burning velocity and NO formation in methane + air flames*, Experimental Thermal and Fluid Science, 31 (2007), pp. 437-444.

[12] V. Di Sarli, A. D. Benedetto, *Laminar burning velocity of hydrogen-methane/air premixed flames*, International Journal of Hydrogen Energy, 32 (2007), pp. 637-646.

[13] J. Wang, Z. Huang, C. Tang, H. Miao, X. Wang, *Numerical study of the effect of hydrogen addition on methane-air mixtures combustion*, International Journal of Hydrogen Energy, 34 (2009), pp. 1084-1096.

[14] R. Stone, A. Clarke, P. Beckwith, *Correlations for the Laminar-Burning Velocity of Methane/Diluent/Air Mixtures Obtained in Free-Fall Experiments*, Combustion and Flame, 114 (1998), pp. 546-555.

[15] C. Prathap, A. Ray, M. R. Ravi, *Investigation of nitrogen dilution effects on the laminar burning velocity and flame stability of syngas fuel at atmospheric condition*, Combustion and Flame, 155 (2008), pp. 145-160.

[16] B. E. Milton, J. C. Keck, *Laminar burning velocities in stoichiometric hydrogen and hydrogen---hydrocarbon gas mixtures*, Combustion and Flame, 58 (1984), pp. 13-22.

[17] Y. Zhang, J. Wu, S. Ishizuka, *Hydrogen addition effect on laminar burning velocity, flame temperature and flame stability of a planar and a curved CH4-H2-air premixed flame*, International Journal of Hydrogen Energy, 34 (2009), pp. 519-527.

[18] H. Miao, M. Ji, Q. Jiao, Q. Huang, Z. Huang, *Laminar burning velocity and Markstein length of nitrogen diluted natural gas/hydrogen/air mixtures at normal, reduced and elevated pressures*, International Journal of Hydrogen Energy, 34 (2009), pp. 3145-3155.

[19] H. Miao, Q. Jiao, Z. Huang, D. Jiang, *Measurement of laminar burning velocities and Markstein lengths of diluted hydrogen-enriched natural gas*, International Journal of Hydrogen Energy, 34 (2009), pp. 507-518.

[20] X. J. Gu, M. Z. Haq, M. Lawes, R. Woolley, *Laminar burning velocity and Markstein lengths of methane-air mixtures*, Combustion and Flame, 121 (2000), pp. 41-58.

[21] M. I. Hassan, K. T. Aung, G. M. Faeth, *Measured and predicted properties of laminar premixed methane/air flames at various pressures*, Combustion and Flame, 115 (1998), pp. 539-550.

[22] S. H. Chung, C. K. Law, *An invariant derivation of flame stretch*, Combustion and Flame, 55 (1984), pp. 123-125.

[23] M. Matalon, *On Flame Stretch*, Combustion Science and Technology, 31 (1983), pp. 169-181.

[24] M. Matalon, B. J. Matkowsky, *Flames as gasdynamic discontinuities*, Journal of Fluid Mechanics Digital Archive, 124 (1982), pp. 239-259.

[25] T. Tahtouh, F. Halter, C. Mounaïm-Rousselle, *Measurement of laminar burning speeds and Markstein lengths using a novel methodology*, Combustion and Flame, 156 (2009), pp. 1735-1743.

[26] W. B. Bush, F. E. Fendell, *Asymptotic Analysis of the Structure of a Steady Planar Detonation*, Combustion Science and Technology, 2 (1971), pp. 271-285.

[27] G. H. Markstein, *Experimental and theoretical studies of flame-front stability*, Journal of the Aeronautical Sciences, 18 (1951), pp. 199-209.

[28] P. Clavin, *Dynamic behavior of premixed flame fronts in laminar and turbulent flows*, Progress in Energy and Combustion Science, 11 (1985), pp. 1-59.

[29] D. Bradley, P. H. Gaskell, X. J. Gu, *Burning velocities, markstein lengths, and flame quenching for spherical methane-air flames: A computational study*, Combustion and Flame, 104 (1996), pp. 176-198.

[30] F. Parsinejad, J. Keck, H. Metghalchi, *On the location of flame edge in Shadowgraph pictures of spherical flames: a theoretical and experimental study*, Experiments in Fluids, 43 (2007), pp. 887-894.

[31] D. Bradley, R. A. Hicks, M. Lawes, C. G. W. Sheppard, R. Woolley, *The Measurement of Laminar Burning Velocities and Markstein Numbers for Iso-octane-Air and Iso-octane-n-Heptane-Air Mixtures at Elevated Temperatures and Pressures in an Explosion Bomb*, Combustion and Flame, 115 (1998), pp. 126-144.

[32] A. E. Dahoe, K. Hanjalic, B. Scarlett, *Determination of the laminar burning velocity and the Markstein length of powder-air flames*, Powder Technology, 122 (2002), pp. 222-238.

[33] C. K. Law, C. J. Sung, *Structure, aerodynamics, and geometry of premixed flamelets*, Progress in Energy and Combustion Science, 26 (2000), pp. 459-505.

[34] R. J. Kee, F. M. Rupley, J. A. Miller, *Chemkin-II: A Fortran chemical kinetics package for the analysis of gas phase chemical kinetics*, Report No. SAND89-8009B, Sandia National Laboratories (1989).

[35] G. P. Smith, D. M. Golden, M. Frenklach, N. W. Moriarty, B. Eiteneer, M. Goldenberg, C. T. Bowman, R. K. Hanson, S. Song, V. V. Lissianski,Z. Qin, http://www.me.berkeley.edu/gri_mech/

[36] A. E. Dahoe, *Laminar burning velocities of hydrogen-air mixtures from closed vessel gas explosions*, Journal of Loss Prevention in the Process Industries, 18 (2005), pp. 152-166.

[37] Z. Huang, Y. Zhang, K. Zeng, B. Liu, Q. Wang, D. Jiang, *Measurements of laminar burning velocities for natural gas-hydrogen-air mixtures*, Combustion and Flame, 146 (2006), pp. 302-311.

[38] S. Verhelst, R. Woolley, M. Lawes, R. Sierens, *Laminar and unstable burning velocities and Markstein lengths of hydrogen-air mixtures at engine-like conditions*, Proceedings of the Combustion Institute, 30 (2005), pp. 209-216.

[39] F. H. V. Coppens, J. De Ruyck, A. A. Konnov, *The effects of composition on burning velocity and nitric oxide formation in laminar premixed flames of CH4 + H2 + O2 + N2*, Combustion and Flame, 149 (2007), pp. 409-417.

[40] S. G. Davis, J. Quinard, G. Searby, *Determination of Markstein numbers in counterflow premixed flames*, Combustion and Flame, 130 (2002), pp. 112-122.

[41] S. G. Davis, J. Quinard, G. Searby, *Markstein numbers in counterflow, methane- and propane- air flames: a computational study*, Combustion and Flame, 130 (2002), pp. 123-136.

5. Nonlinear effects of stretch on the flame front propagation

Ce chapitre a fait l'objet d'une publication dans la revue scientifique *Combustion and Flame* :

F. Halter, T. Tahtouh, C. Mounaïm-Rousselle, *Nonlinear effects of stretch on the flame front propagation*, Combustion and Flame, 157 (2010), pp. 1825-1832.

5.1 Abstract

In all experimental configurations, the flame is affected by stretch (curvature and/or strain rate). To obtain the unstretched flame speed, independent of the experimental configuration, the measured flame speed needs to be corrected. Usually, a linear relationship linking the flame speed to stretch is used. However, this linear relation is the result of several assumptions, which may be uncorrected. The present study aims at evaluating the error in the laminar burning speed evaluation induced by using the traditional linear methodology. Experiments were performed in a closed vessel at atmospheric pressure for two different mixtures: methane/air and iso-octane/air. The initial temperature was respectively 300K and 400K for methane and iso-octane. Both methodologies (linear and non-linear) are applied and results in terms of laminar speed and burned gas Markstein length are compared. Methane and iso-octane were chosen because they present opposite evolutions in their Markstein length when the equivalence ratio is increased.

The error induced by the linear methodology is evaluated, taking the non-linear methodology as the reference. It is observed that the use of the linear methodology starts to induce substantial errors after an equivalence ratio of 1.1 for methane/air mixtures and before an equivalence ratio of 1 for iso-octane/air mixtures. One solution to increase the accuracy of the linear methodology for these critical cases consists in reducing the number of points used in the linear methodology by increasing the initial flame radius used.

Nomenclature:

- K : total stretch rate [1/s]
- $Ka = \frac{\delta_{L0}}{S_{L0}} k = \frac{2U}{R}$: Karlovitz number [-]
- Le : Lewis number [-]
- L_b : burned gases Markstein length [m]
- $Ma = \frac{L_b}{\delta_L^0}$: Markstein number [-]
- $R = \frac{R_f}{\delta}$: normalized flame radius [-]
- R_f : flame radius [m]
- $R_{f\_initial}$: flame radius of the first flame image used in the post-processing [m]
- $S_b = \frac{dR_f}{dt}$: flame speed with respect to the burned mixture [m/s]
- S_b^0 : unstretched laminar flame speed [m/s]
- $S_u^0 = \sigma S_b^0$: laminar burning speed with respect to the unburned mixture [m/s]
- $S_{ulinear}^0$: laminar burning speed determined with the linear formulation [m/s]
- $S_{unon-linear}^0$: laminar burning speed determined with the non-linear formulation [m/s]
- T_f : flame temperature [K]
- $U = \frac{S_b}{S_b^0}$: normalized flame speed [-]
- β : Zeldovich number [-]
- δ : flame thickness of an adiabatic planar flame [m]
- ρ_b : density of burned gas [Kg/m^3]
- ρ_u : density of unburned mixture [Kg/m^3]
- $\sigma = \frac{T_{fresh\ gases}}{T_{adiabatic}}$: expansion factor [-]
- $\Delta = \left| \frac{L_b}{R_{f\_initial}} \right|$: ratio between the burnt gases Markstein length and the flame radius [-]

5.2 Introduction

Laminar flame speed is a widely used parameter describing the propagation of a one-dimensional, planar, adiabatic, premixed flame. This response embodies fundamental information on the diffusivity, reactivity and exothermicity of a given air-fuel mixture.

Flame stretch, which measures the temporal flame surface deformation, plays an important role in the propagation, stability and structure of premixed flames. Many authors have proposed relations representing the effects of stretch on the flame propagation. Karlovitz et al. [1] proposed a direct correlation of flame speed and flame stretch. Zeldovich and Franck Kamenetskii [2] were the first to use large activation energy asymptotics to obtain a formulation of the flame speed, i.e. the rational solution of conservation equations in the limit $\vartheta \to \infty$, with $\vartheta = \frac{R}{R T_u}$, the dimensionless activation energy, E the activation energy, T_u the unburned gases temperature and R the gas constant. Eckhaus [3] proposed an equation describing the propagation speed of three-dimensional unsteady flames. Some years later, Sivashinsky [4] and Buckmaster [5] both independently derived an equation that governs the general motion of unsteady three-dimensional flames. The structure of these flames is characterized by a small flame thickness $\left(0\left(\frac{1}{\vartheta}\right)\right)$ to which all the reaction is confined. The analysis proposed by Buckmaster [5] deals with slowly varying flames. Such flames are characterized by the fact that the deformations occur on a long scale of the order of the dimensionless activation energy (ϑ). Clavin [6] and Clavin and Williams [7] derived expressions using large activation energy asymptotics for flames described by simple chemistry and Lewis number close to 1. The relation obtained had previously been proposed by Markstein [8], based on a phenomenological approach. Chung and Law [9] used another approach, integral analysis, to study stretched flames. This analysis uses multiple-species transport and chemistry and is no longer restricted to Lewis numbers close to unity. Recently, De Goey and Ten Thije Broonkkamp [10] compared the latter two theories in terms of mass burning rate. They pointed out that the large activation energy asymptotic approach affords similar results to those of integral analysis for lowest order in the Zeldovich number for flat, weakly strained flames both when density variations are neglected or included and for Lewis numbers close to unity.

The linear relation linking flame speed to stretch is commonly used to analyse experimental results. The validity of the linear relation starts to be tendentious for non-unit Lewis numbers [11], whereas the initial non-linear formulation proposed by Buckmaster [5] assumed a Lewis number far from unity. Vagelopoulos et al. [12] showed that the discrepancy between the linear and nonlinear extrapolation decreases when the Karlovitz number is small enough (0.1). Tien and Matalon [13] suggested that the linear extrapolation slightly overpredicts the flame

speed for low stretch levels. Davis and Law [14] compared results obtained with linear and non-linear extrapolations for iso-octane and n-heptane air flames and more recently, Kelley and Law [15, 16] for n-butane/air and hydrogen/air flames. They pointed out that using the linear extrapolation to determine laminar speed could induce over-predictions by substantial amounts for some conditions.

The aim of the present study is to compare results obtained with the linear and non-linear methodologies for methane/air and iso-octane/air mixtures. The validity of the linear methodology is tested for these two mixtures, and a criterion of validity is proposed.

5.3 Experimental setup

The combustion processes take place in a cylindrical stainless steel combustion chamber with an inner volume of 24.32 liters. Before filling, a vacuum is created inside the chamber. The volumes of gases are introduced into the chamber with thermal mass flow meters. Iso-octane, which is liquid at ambient pressure and temperature, is injected though a solenoid injector. The exact volume to be injected is measured with a potentiometer. The injection conditions (frequency and gate) are adjusted to finish the injection process just before the filling process of the air. The initial temperature for iso-octane/air mixtures was chosen above its boiling temperature (378 K): T_{ini}=400K. In these conditions the quantity of fuel injected is fully vaporized, whatever the equivalence ratio. The spark ignition is accomplished by two tungsten electrodes linked to a conventional discharge system. Two opposite windows (diameter 10.5 cm) provide optical access. The lighting is provided by a continuous Stabilite 2017 Argon ion Laser. The parallel light beam is created by using two plano-convex lenses. The evolution of the flame surface development is observed from shadowgraph images, recorded with a high speed CMOS-APX camera operating at 6000 frames/second. The experimental set-up is fully described in [17].

5.4 Theoretical analysis

The mathematical models presented in [18, 19] are based on the energy and species transport equations. Several hypotheses are used to obtain a formulation of the propagation speed. First, this analysis is restricted to the commonly considered density model [20], which assumes an overall one step exothermic reaction and constant values of the molecular weight, specific heat, thermal conductivity and density weighted mass diffusivity of the mixture. Moreover, the convection flux is absent from the transport equations. This assumption was validated by transient numerical simulation [18]. As a large activation energy is considered, the chemical reaction occurs only within a very thin zone of high temperature.

The flame is therefore considered to be in a quasi-steady state $\left(\frac{\partial}{\partial t}=0\right)$ and adiabatic (no heat losses). It can be noted that Chen and Ju [18] have studied the impact of heat losses. In the present study as in Chen and Ju [18], the contribution of gas expansion to convective is neglected. Lastly, our analysis is started sufficiently late so as not to take into account the initial energy deposition. The combustion process is considered isobaric. The following expressions were obtained by considering spherical expanding flames.

With all these hypotheses, the following expression, called, following Chen et al. [21, 18], the Detailed Model is obtained:

$$T_f \cdot \frac{R^{-2}e^{-UR}}{\int_R^\infty \tau^{-2}e^{-U\tau}d\tau} = \frac{1}{Le}\frac{R^{-2}e^{-ULeR}}{\int_R^\infty \tau^{-2}e^{-ULe\tau}d\tau} = \exp\left[\frac{\beta}{2}\frac{T_f-1}{\sigma+(1-\sigma)T_f}\right] \quad (1)$$

where T_f is the adiabatic flame temperature, R the normalized flame radius, U the normalized flame speed, Le the Lewis number, β the Zeldovich number and σ the expansion factor.

The different parameters (adiabatic flame temperature, Lewis number, Zeldovich number, expansion factor) can be fixed to study the evolution of the flame velocity with stretch and the sensitivity of the different parameters to this evolution can be tested. Equation 1 is unfortunately too complex to be used to extract laminar burning speed from experimental results, as too many parameters are undetermined and no algebraic solution can be expressed. A less complex formulation is required for use with experimental data. This can be achieved only by increasing the number of hypotheses.

For flames of large radius ($R=\frac{R_f}{\delta_L^0}$) the detailed model reduces to the simplified model [21]:

$$\left(U+\frac{2}{R}\right)\ln\left(U+\frac{2}{R}\right)=\frac{\beta}{R}\left(\frac{1}{Le}-1\right)-\frac{2}{R}\left(\frac{1}{Le}-1\right) \quad (2)$$

with $U=\frac{S_b}{S_b^0}$, the normalized flame speed. This formulation is similar to the one proposed by Frankel and Sivashinsky [22]. The previous expression can be simplified one step further using the two assumptions ($R\gg 1$ and $\beta\gg 2$) and :

$$U\ln U=\frac{\beta}{R}\left(\frac{1}{Le}-1\right) \quad (3)$$

The Markstein number is defined as the ratio between the Markstein length relative to the burned gas and the unstretched laminar flame thickness of an adiabatic planar flame:

$$Ma = \frac{L_b}{\delta_L^0}$$

In the present study, the Markstein length was defined as:

$$L_b = \left(\frac{\beta}{2}\right)\left(Le^{-1} - 1\right)\delta_L^0$$

The Karlovitz number is defined as [23] :

$$Ka = \frac{\delta_L^0}{S_u^0} K = \frac{2U}{\sigma R}$$

Using the previous two relations, the following expression is obtained:

$$U^2 \ln\left(U\right)^2 = -2\sigma Ka\, Ma = -\frac{2L_b K}{S_b^0} \quad (4)$$

In the limit of weakly stretched flames, the normalized flame speed is close to unity ($U = \frac{S_b}{S_b^0} = 1 + \varepsilon, \quad |\varepsilon| \ll 1$).

In this limit, and using the Taylor series ($U^2 = 1 + 0\left(U-1\right); \ln\left(U\right) = \left(U-1\right) + 0\left(U-1\right)$ the linear model initially proposed by Clavin [6] is retrieved:

$$U = 1 - \sigma Ma \cdot Ka = 1 - \frac{L_b K}{S_b^0} \quad (5)$$

In the present work, two models (Equations 4 and 5) are tested. The three models corresponding to Equations 1, 2 and 5 were numerically tested for different cases of Lewis numbers in the recent paper of Chen et al [21].

5.5 Data processing:

After the spark, the flame front propagates spherically. The instantaneous flame front radius is obtained from image post processing after subtracting the background [17]. The image post-processing is based on the assumption of a spherical development of the flame front. The propagation speed is defined as the temporal derivative of the flame radius, $S_b = \frac{dR_f}{dt}$, and is affected by the stretch rate. Stretch is defined as the temporal change of a flame surface element of area A: $K = \frac{dA}{A \cdot dt}$. In the case of a spherically outwardly expanding flame front, K

can be expressed as follows: $K = \frac{2}{R_f} \cdot \frac{dR_f}{dt}$. By taking into account a relation linking the propagation speed and the stretch rate, the unstretched propagation speed (S_b^0) can be determined. Then, for a constant pressure flame propagation, the laminar burning velocity can be deduced from the un-stretched propagation speed and the density ratio by using the following equation: $S_u^0 = \frac{\rho_b}{\rho_u} \cdot S_b^0$, with ρ_b and ρ_u respectively the density of burned and unburned gases. The densities were evaluated using the EQUIL code of the CHEMKIN package [24].

5.5.1 Non linear methodology

Equation 4 may be recast in a dimensional form:

$$\left(\frac{S_b}{S_b^0}\right)^2 \ln\left(\frac{S_b}{S_b^0}\right)^2 = -\frac{2L_bK}{S_b^0} \quad (6)$$

In this equation, the two unknowns, the unstretched propagation speed and the Markstein length, can be obtained using the flame radius and stretched propagation speed temporal evolutions. The stretched propagation speed needs to be evaluated via the derivation of the flame radius evolution, a process which can induce some uncertainties. The two unknowns are found by minimizing the following expression:

$$\sum_{i=1}^{N} \left| \left(\frac{S_b}{S_b^0}\right)^2 \ln\left(\frac{S_b}{S_b^0}\right)^2 + \frac{2L_bK}{S_b^0} \right|,$$

N corresponding to the number of time steps.

Kelley and Law [15] expressed the analytical solution, in terms of radius, of the non-linear equation, thus avoiding the derivation process needed to evaluate the stretched propagation speed. This exact solution should offer more accurate results as the optimization process is based only on the flame radius temporal evolution. However, the convergence is tricky and highly dependent on the initial conditions (initial values of propagation flame speed and Markstein length used in the optimization process).

In our experience, the best procedure is first to minimize the sum $\sum_{i=1}^{N} \left| \left(\frac{S_b}{S_b^0}\right)^2 \ln\left(\frac{S_b}{S_b^0}\right)^2 + \frac{2L_bK}{S_b^0} \right|$ and then to use the obtained output (which can be slightly erroneous due to the derivation process used to obtain the stretched propagation velocity) as the input of the methodology proposed by Kelley and Law. Differences in laminar burning speeds obtained with both resolution methodologies (minimization of the sum and that of Kelley and Law) are lower than 2% for all the mixtures studied in the present paper.

5.5.2 Linear methodology

Equation 5 may be recast in a dimensional form:

$$S_b = S_b^0 - L_b K \quad (7)$$

As reported in [17], the exact solution of this equation, in terms of flame radius, may be expressed

$$R_{th}(t) = -2L_b W(Z) \quad (8)$$

with W the Lambert function, $Z = \frac{e^{\frac{S_b^0 + C_1}{2L_b}}}{2L_b}$ and C_1 a constant to be determined.

L_b, S_b^0 and C_1 are found by minimizing the following equation:

$$\sum_1^N \left(R_f - R_{th}\right)^2$$

Full details about the resolution of the equation are reported in [17, 25].

Equation 7 may be expressed in a different form to yield the ratio $\frac{S_b}{S_b^0} \approx 1$:

$$\frac{S_b}{S_b^0} = \frac{1}{1 + \frac{2L_b}{R_f}} \quad (9)$$

Then, using a Taylor series expansion and assuming that $\frac{2L_b}{R_f} \ll 1$, the following expression is obtained :

$$\frac{S_b}{S_b^0} = 1 - \frac{2L_b}{R_f} \quad (10)$$

where $\left(\frac{-2L_b}{R_f}\right)$ can be identified as ε, the parameter introduced to define the normalized flame speed close to unity $\left(U = \frac{S_b}{S_b^0} = 1 + \varepsilon, \quad |\varepsilon| \ll 1\right)$. The ratio between the Markstein length and the initial radius considered in the post-processing seems to be a good indicator of the validity of the linear relation. A new parameter can be defined as:

$$\Delta = \left| \frac{L_b}{R_{f\_initial}} \right|$$

To compare both linear and non-linear methods, unstretched propagation flame speeds and Markstein lengths were determined for methane/air and iso-octane/air mixtures (initial pressure of 0.1 MPa for both fuels – T_{ini}=300K for methane and T_{ini} = 400 K for iso-octane), varying the equivalence ratio.

5.6 Results

5.6.1 Ignition impact

The combustion process is initiated by an energy deposit. As reported in [17], the electrodes diameter and their inter-distance was carefully chosen to minimize flame-electrodes interactions. After the spark discharge, an outward propagating shock wave is created, followed by a slower thermal wave. The flame front possesses a high propagation speed which rapidly decreases to reach the unaffected stretched propagation speed. It is important to know up to what flame radius the propagation is affected by the initial energy deposit. To focus only on the energy deposition effect, a methane/air mixture with an equivalence ratio of 0.7 is considered. As the Markstein length of this mixture is very close to zero, the propagation speed should be almost linear and independent of the stretch rate. Indeed, when the stretch rate is divided by three (350 to 125), the stretched flame speed is increased from 1.45 to 1.53, which corresponds to a variation lower than 6%. The evolution of the propagation speed of this lean mixture is plotted versus the stretch rate in Figure 1. Two distinct parts of the evolution can be observed. The first one, corresponding to high stretch rates (i.e. small flame radii) presents higher propagation speed values. For these small radii, propagation is strongly affected by the initial energy deposit. The propagation speed then decreases and starts to evolve linearly. The critical radius corresponding to this transition was found here to be 6.5 mm. One can consider that beyond this critical radius, the effect of the initial energy deposit is negligible. Certainly this critical value may be different as a function of the air-fuel mixture, but with the same order of magnitude. The value determined here is corroborated by the critical value suggested by Bradley et al. [26]. They reported that the propagation speed becomes independent of igniting energy for radii greater than 6 mm. In all our post-processing, an initial radius of 8 mm was considered.

Both methodologies (linear and non-linear) are now applied to methane/air and iso-octane/air mixtures, in order to evaluate the errors induced by the linear methodology.

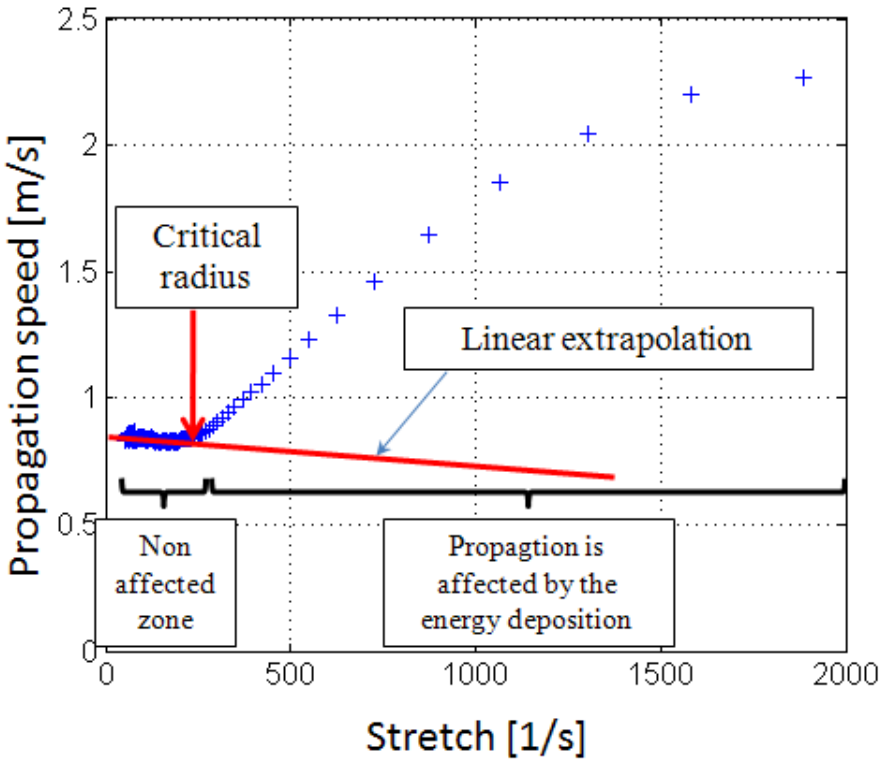

Figure 1. *Influence of the initial energy deposition on the flame front propagation (CH_4/Air – ER=0.7 – P=0.1 MPa – T=300K).*

5.6.2 Methane/air mixtures

Evolutions of the propagation speed as a function of the stretch rate are presented in Figures 2 for the whole set of equivalence ratios studied. For all the mixtures investigated, the flame is accelerated when the stretch rate decreases (i.e. when the flame radius increases). As the equivalence ratio is increased, the propagation speed is less and less linear with the stretch when the flame radius increases. In order to point out these differences in evolution, two characteristic equivalence ratios have been selected: ER=0.8 and ER=1.3.

The evolution of the propagation speed as function of the stretch rate is presented in Figures 3a and 3b for the two selected equivalence ratios (E.R.), respectively 0.8 and 1.3. On these figures, experimental data are symbolized by black crosses, the black dashed line corresponds to the propagation speed determined with the non-linear formulation and the grey dashed line, a linear evolution between the propagation speed and the stretch rate. In the case of a lean methane/air mixture, as for example here an E.R. of 0.8 (see Figure 3a), experimental results are linearly linked to the stretch rate. The initial radius considered is 8 mm as mentioned in the previous section. The linear fit performed on 55 points gives a coefficient of determination higher than 0.99. The propagation speed of the first and the last flame radii used in the processing are respectively 1.44 and 1.53 m/s. The unstretched propagation speed obtained by fitting linearly the experimental data till zero stretch is 1.60. Considering the initial flame

radius, the ratio $\frac{S_b}{S_b^0}$ is 0.9. This deviation of ten percents seems to be low enough to correctly use the linear methodology.

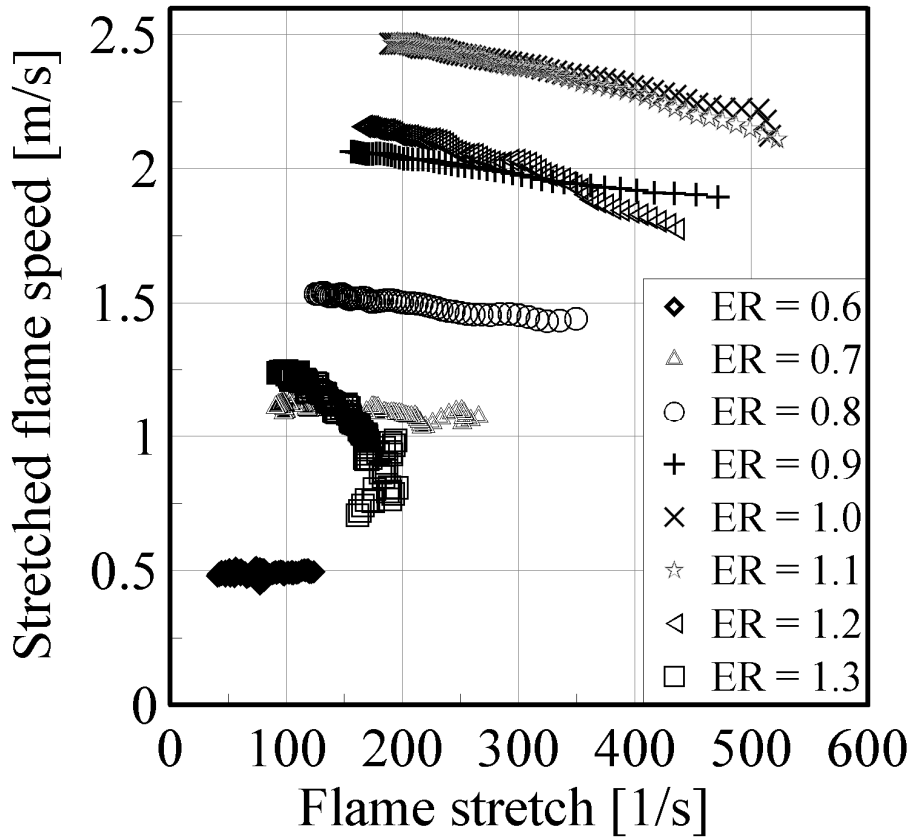

Figure 2. *Evolution of the stretched propagation speed with stretch for the different methane/air mixtures (P=0.1 MPa – T=300K).*

For a richer methane-air mixture (Figure 3b), the propagation speed exhibits a less linear evolution.

Temporal flame radius is plotted versus the total flame stretch. Initial and final flame radii of 8 mm and 27 mm are considered, which correspond to 127 successive flame images considered in the post-processing (the time step between each flame image is 1/6000 s). The propagation speed corresponding to the initial time step considered in the processing is 0.76. For this case, the unstretched propagation speed is 1.65 m/s ; the ratio $\frac{S_b}{S_b^0}$ in this case is 0.46, a value far from unity. If we refer to Equation 9, the decrease observed in the ratio $\frac{S_b}{S_b^0}$ may be due to the initial flame radius used or to the Markstein length.

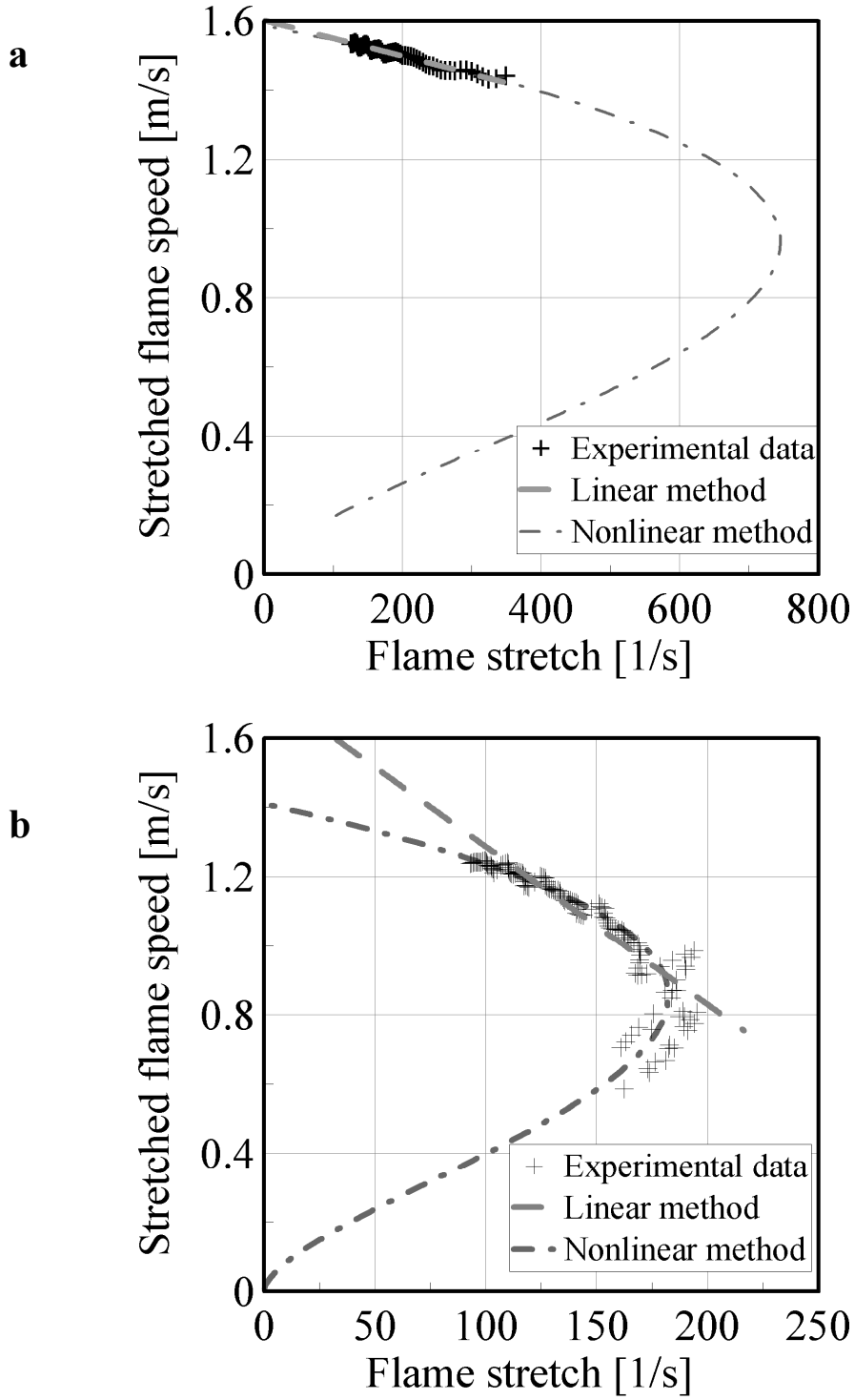

Figure 3. *Evolution of the stretched propagation speed with stretch for two equivalence ratios: ER=0.8 and ER=1.3 (CH_4/Air – P=0.1 MPa – T=300K).*

As the initial flame radius is kept constant for the whole set of mixture conditions, this decrease is directly linked to a higher value of the Markstein length, indicating that the flame front is more sensitive to stretch. In these conditions, the linear approximation is no longer valid. As a result, the Markstein length evaluated with the linear model is overestimated and therefore, the corresponding propagation speed also.

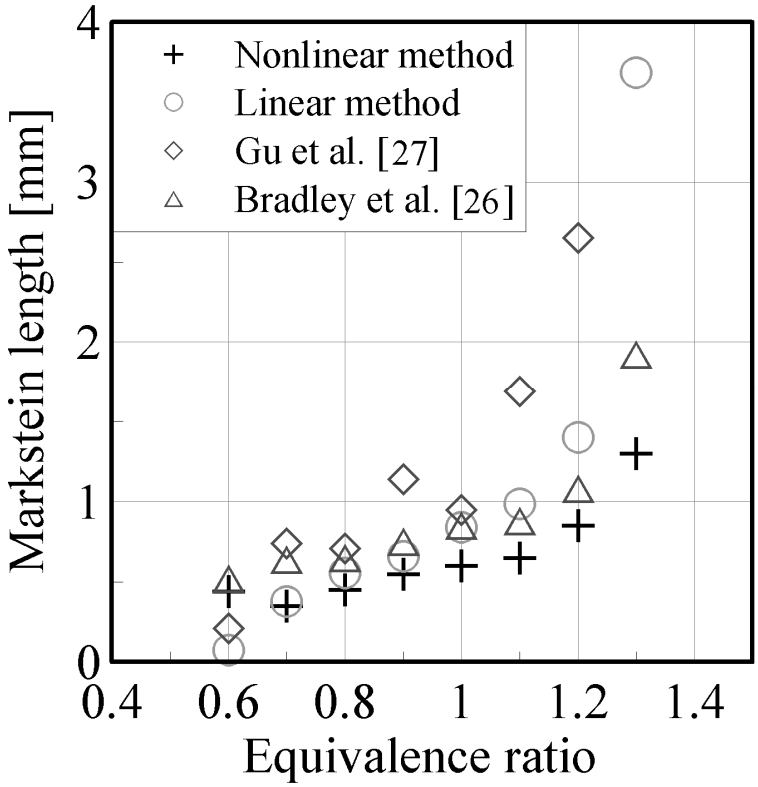

Figure 4. *Burned gas Markstein length for methane/air mixtures (P=0.1 MPa – T=300K).*

In Figure 4, the burned gases Markstein lengths, estimated from both methodologies, are presented. The observed evolution (i.e. an increase in the Markstein length when the equivalence ratio is increased) is consistent with previous results found in the literature [27, 26], deduced from the linear relation. As predicted, the linear methodology induces an overestimation of the Markstein length for rich mixtures.

This overestimation in Markstein length will result in an overestimation of the laminar burning speed. In Figure 5, values of laminar burning speed estimated with both methodologies are compared to literature values. Laminar burning speeds were estimated by dividing the unstretched propagation speed by the expansion factor. Vagelopoulos and Egolfopoulos [12] performed experiments in a counterflow burner using a direct experimental determination of unstretched laminar flame speeds. Their values are therefore representative of non stretch affected laminar burning speeds. These values are in a very good agreement with the values obtained in the present work with the nonlinear methodology. Hassan et al. [28], performed experiments in a spherical vessel. They used the linear extrapolation and their results are very similar to our results obtained using the linear methodology. It can be seen in Figure 5 that the linear methodology induces an overestimation of the burning speed for rich equivalence ratios.

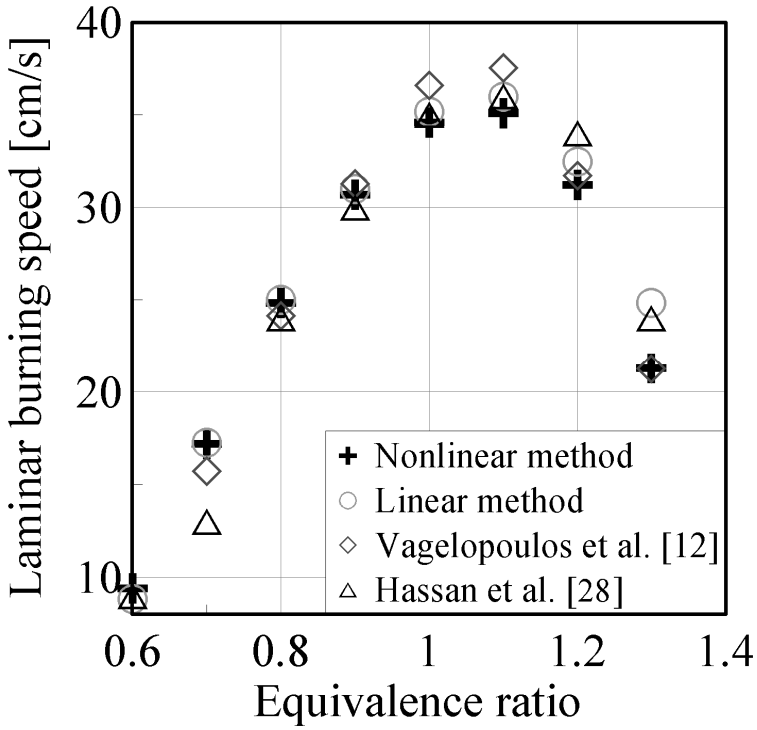

Figure 5. *Laminar flame speeds for methane/air mixtures (P=0.1 MPa – T=300K).*

Assuming the non-linear methodology as the reference, the error induced by the use of the linear methodology can be evaluated:

$$\alpha = 100 \cdot \frac{\left| S^0_{u_{linear}} - S^0_{u_{nonlinear}} \right|}{S^0_{u_{nonlinear}}}$$

This error is plotted in Figure 6 for the set of methane/air mixtures. First, the error is evaluated considering the same initial flame radius of 8 mm for all the cases. This corresponds to the diamond shaped symbols. The error increases with the equivalence ratio. It is lower than a few percent for lean mixtures and then evolves almost exponentially when the equivalence becomes richer. The use of a linear methodology, for methane/air mixtures at ambient pressure and temperature, is correct up to an equivalence ratio of 1.2 but induces substantial errors for richer mixtures. These errors are induced by the limitation of the hypothesis $\frac{S_b}{S_b^0} \approx 1$. If we refer to Equation10, the previous ratio may be related to the ratio of the Markstein length and the initial flame radius. By increasing the initial flame radius used in the processing, one can limit the divergence of $\frac{S_b}{S_b^0}$ from unity. An illustration is plotted in Figure 6, where the initial flame radius has been increased until a relative difference α lower than 2 % is obtained. For the equivalence ratio of 1.3, the relative difference, initially 21%, is reduced to 0.6 % if the initial radius considered is 20 mm.

Note that the negative effect linked to the Markstein length increase is counterbalanced and the accuracy of the linear methodology may be preserved. Of course, the number of points considered for the linear extrapolation is also reduced (44 points for a radius of 20 mm compared to 137 for 8 mm, which is still reasonable) and this could no doubt become the main limitation of the process.

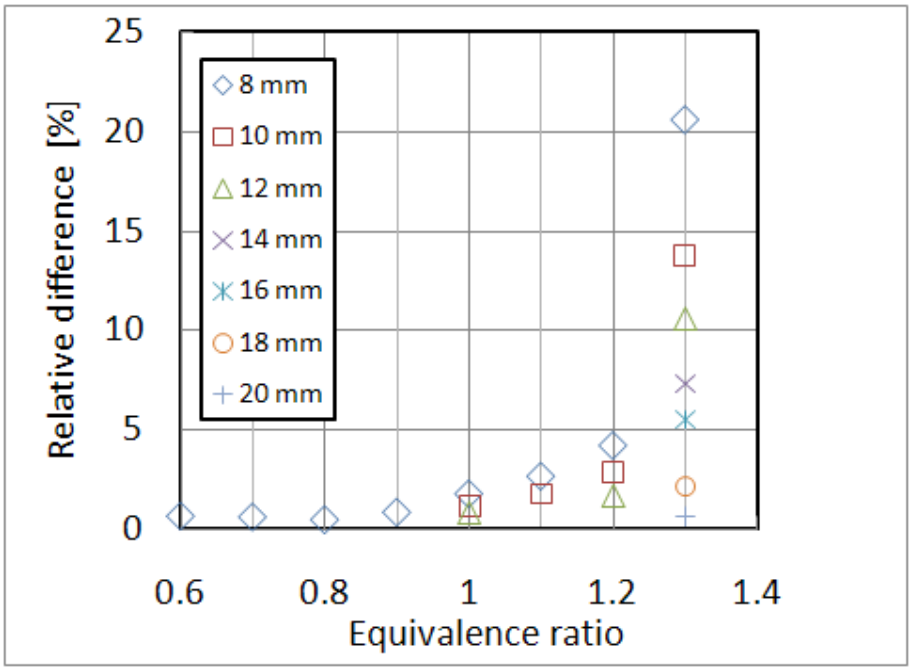

Figure 6. *Relative error* $\left(\alpha = 100 \cdot \frac{\left| S^0_{u_{linear}} - S^0_{u_{nonlinear}} \right|}{S^0_{u_{nonlinear}}} \right)$ *obtained comparing linear and non-linear methodologies. Non-linear methodology is taken as the reference. Initial flame radius is varied from 8 mm to 20 mm (methane/air – P = 0.1 MPa – 300K).*

It appears interesting to extend these conclusions to the study of another fuel, which presents a different evolution in Markstein length (decreasing with ER instead of increasing). Iso-octane, a good representative mono-molecule of gasoline in terms of octane number, was chosen.

Moreover, some experimental results can be found in the literature to compare with our results. To avoid any problems of vaporization, the initial temperature was fixed at 400K (near the Iso-octane boiling temperature of 387K).

5.6.3 Iso-octane/air mixtures

Evolutions of propagation speed with stretch for the different equivalence ratios are presented in Figure 7, where it can be seen that the higher the equivalence ratio is, the more linear the curve evolution is.

The curve corresponding to an equivalence ratio of 0.8 is largely non-linear.

The initial value of the propagation speed is 1.3 m/s; given that the unstretched propagation speed obtained by linear extrapolation is 2.2 m/s, the ratio $\frac{S_b}{S_b^0}$ is, in this case, equal to 0.6. It is interesting to note that for an equivalence ratio of 1.4, the flame acceleration is negative, corresponding to a negative value of the Markstein length. For an equivalence ratio of 1.3, the value of the propagation speed is almost constant, whatever the stretch acting on the flame front; the propagation speed is independent of the stretch (corresponding to a Markstein length equal to zero).

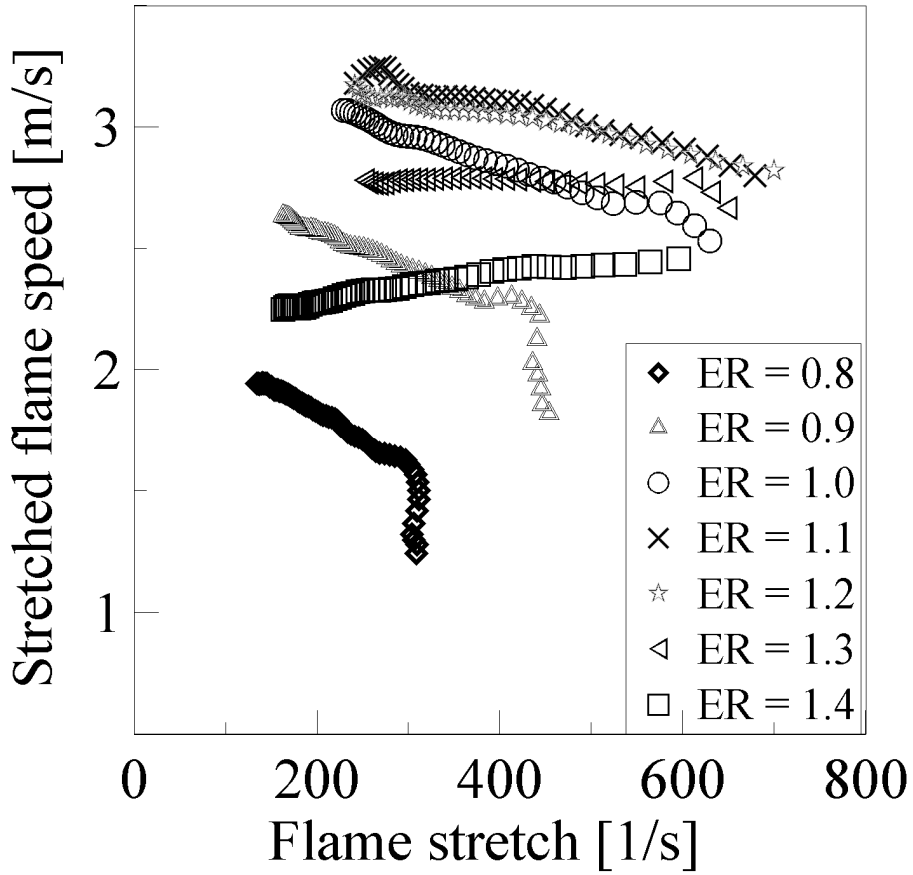

Figure 7. *Evolution of the stretched propagation speed with stretch for the different Iso-octane/air mixtures (P=0.1 MPa – T=400K).*

Markstein lengths are presented in Figure 8. A decrease is observed when the equivalence ratio is increased. Markstein lengths determined from the linear methodology and those obtained by Bradley et al. [29] (also using a linear methodology) are higher than those evaluated with the non-linear methodology in the case of lean equivalence ratios. Indeed, for an equivalence ratio of 0.8, the value obtained with the linear methodology is three times that obtained with the non-linear methodology.

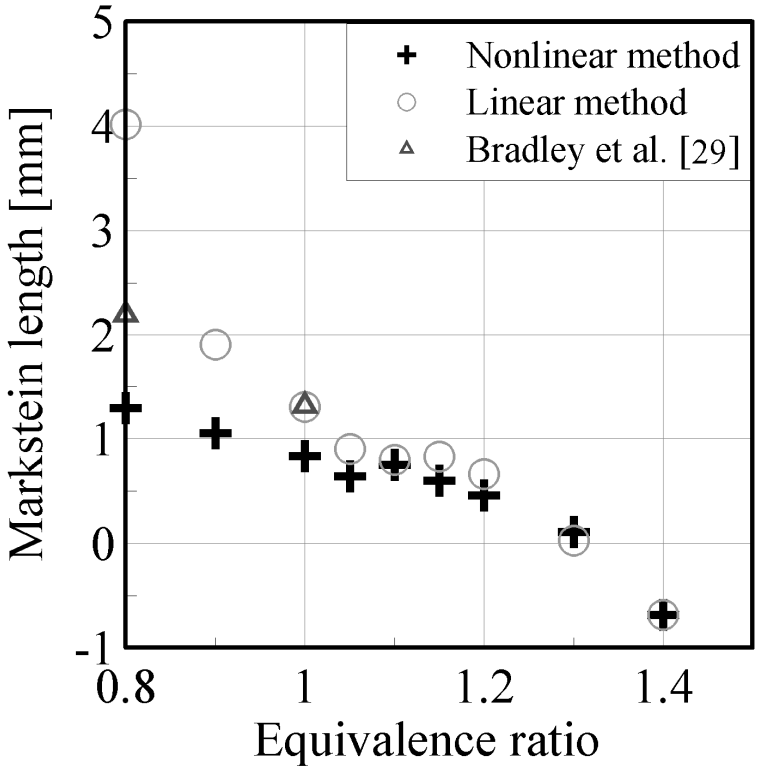

Figure 8. *Burned gas Markstein length for Iso-octane/air mixtures (0.1 MPa – 400K)*

In Figure 9, the values of laminar burning speed for iso-octane/air mixtures estimated with both methodologies are plotted and compared to values reported in the literature. Freeh et al [30] used a counterflow flame configuration, by using Particle Image Velocimetry to determine the flow field and a non linear extrapolation to remove the effects of stretch. Their non-linear methodology is based on the theoretical analysis by Tien and Matalon [13]. Tien and Matalon show that the relation between burning speed and stretch is not strictly linear. The linearity is only valid for very restricted range of low stretch values. Moreover, they show that for mixtures with a sufficiently large Lewis number, the flame speed, which first increases with increasing stretch, reaches a maximum at a moderate stretch and then decreases with stretch. Bradley et al. [29] performed their experiments in a constant volume chamber. They post-processed their extracted radii evolutions with the traditional linear methodology. For an equivalence ratio of 0.8, the value obtained by Bradley et al. [29] is close to the one found with the linear methodology.

The results obtained by Freeh et al. [30] are close to ours when the non-linear methodology is used. The laminar burning speeds obtained with the linear methodology are higher for lean equivalence ratios.

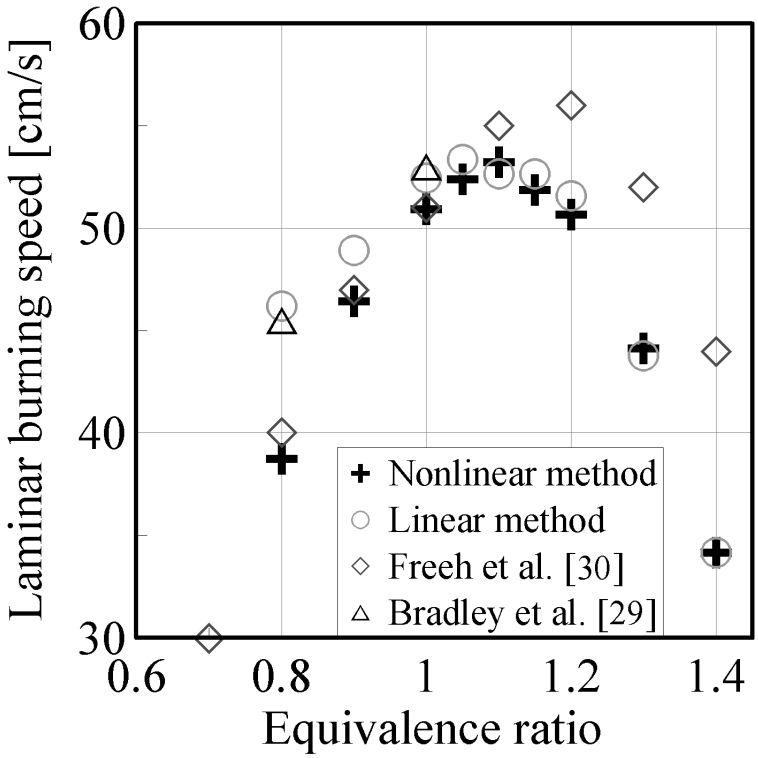

Figure 9. *Laminar flame speeds for iso-octane/air mixtures (P=0.1 MPa – T=400K).*

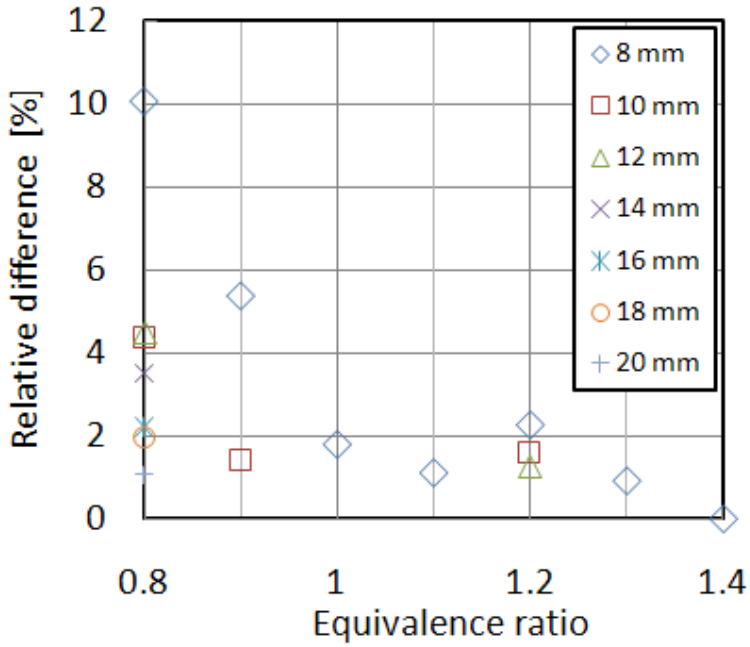

Figure 10. *Relative error* $\left(\alpha = 100 \cdot \frac{\left| S^0_{u_{linear}} - S^0_{u_{nonlinear}} \right|}{S^0_{u_{nonlinear}}} \right)$ *obtained comparing linear and non-linear methodologies. Non-linear methodology is taken as the reference. Initial flame radius is varied from 8 mm to 20 mm (Iso-octane/air – P = 0.1 MPa – 300K).*

The relative error (α) induced by using the linear methodology is evaluated and presented in Figure 10. As for methane/air, diamond shaped symbols correspond to the same initial flame radius of 8 mm. As expected by Equation 10, the relative error evolution is directly linked to the Markstein lengths evolution (when the initial flame radius is kept constant). When the initial flame radius used in the processing is increased, the error induced by the use of the linear methodology is reduced and may become negligible. For an equivalence ratio of 0.8, the initial error of 10% is reduced to 1% by considering an initial radius of 20 mm. In this case, the linear extrapolation is performed on 39 points (compared to 82 points for an initial radius of 8 mm), which remains reasonable.

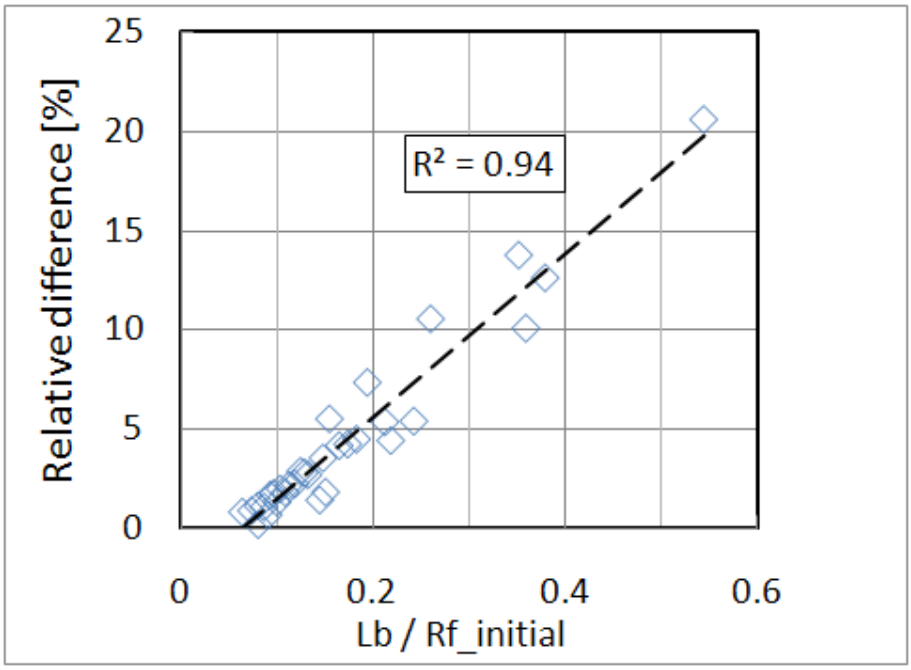

Figure 11. *Influence of the ratio* $\left(\Delta = \left|\frac{L_b}{R_{f\_initial}}\right|\right)$ *on the relative difference* (α).

It appears that the accuracy of the linear methodology is affected by an increase in the Markstein length in absolute value. According to our experimental results obtained with methane and iso-octane as fuels, when the burned gas Markstein reaches or overpasses the unity value (in mm), the use of the non-linear methodology is required. The accuracy of the linear methodology may be artificially improved by increasing the initial radius used in the data processing. Indeed, as shown in Figures 6 and 10, an error lower than two percent can be obtained by conserving a reasonable number of points used for the linear extrapolation. When the Markstein length is increased, the initial radius must also be increased to keep constant Δ, the absolute value of the ratio between the burnt gas Markstein length and the initial flame radius $\left(\Delta = \left|\frac{L_b}{R_{f\_initial}}\right|\right)$. This ratio, linked to the ratio $\frac{S_b}{S_b^0}$ via Equation 10, also seems to be correlated to α.

Figure 11 has been constructed by plotting on the same graph the different values of the ratio Δ and the corresponding values of the relative error α, varying the fuel, the equivalence ratio and for each equivalence ratio the initial radius. Although some points are scattered, a global linear trend is observed, indicative of a direct correlation. Using a linear fit on the 32 points provides a correlation coefficient of 0.94. A relative error (α) of five percent corresponds to a value of Δ equal to 0.18. This value, which is very easy to evaluate after a linear extrapolation, could be a perfect criterion of validity of the linear formulation. The only limitation could arise when too small a number of experimental points are used for this linear extrapolation.

5.7 Conclusion

In all experimental set-ups, the flame is affected by stretch (curvature and/or strain rate). To obtain a universal value of the unstretched flame speed, that is independent of the experimental configuration and characteristic of the mixture reactivity, the measured flame speed needs to be corrected. In the majority of experimental studies, a linear relationship linking the flame speed to the stretch is used. However, this linear relation is the result of several assumptions. The present study has proposed an evaluation of the error induced by using the traditional linear methodology to assess laminar burning speed. Starting from the conservation equations, the different assumptions needed to simplify the problem and to obtain a formulation of the burning speed have been recalled. The critical hypothesis $\left(\frac{S_b}{S_b^0} \approx 1\right)$ needed to validate the use of the linear methodology is tested for two different air-fuel mixtures: methane/air and iso-octane/air. Experiments were performed in a closed vessel at atmospheric pressure for different equivalence ratios. Initial temperature was 300K for methane and 400K for iso-octane. Temporal growth of the flame ball was recorded with a high speed CMOS camera. From this temporal evolution, both methodologies have been applied and results in term of laminar speed and burned gas Markstein length compared. Methane and iso-octane were chosen because of their opposite evolutions in Markstein length when the equivalence ratio is increased.

The error induced by the linear methodology is evaluated, taking the non-linear methodology as the reference $\left(\alpha = 100 \cdot \frac{\left|S^0_{u_{linear}} - S^0_{u_{nonlinear}}\right|}{S^0_{u_{nonlinear}}}\right)$. It is observed that the use of the linear methodology starts to induce substantial errors after an equivalence ratio of 1.1 for methane/air mixtures and before an equivalence ratio of 1 for iso-octane/air mixtures. These critical cases exhibit values of $\frac{S_b}{S_b^0}$ far from unity.

As this ratio is directly related to the ratio between the Markstein length and the initial flame radius used in the data processing $\left(\left|\frac{L_b}{R_{f\_initial}}\right|\right)$, one solution to increase the accuracy of the linear methodology for these critical cases consists in reducing the number of points used in the linear methodology by increasing the initial flame radius used. Indeed, by doing this, the differences between the linear and the non-linear methodology can be reduced drastically. The only limitation could concern the number of points used, which needs to be high enough. It was shown that the ratio $\frac{L_b}{R_{f\_initial}}$ is quite well correlated with the relative error α. Consequently, if a maximal relative error α of five percent is desired, the ratio $\left|\frac{L_b}{R_{f\_initial}}\right|$ should not be higher than 0.18. As the Markstein length increases, the initial radius has also to be increased in order to match this criterion.

5.8 References

[1] B. Karlovitz, D. W. Denniston Jr, D. H. Knapschaefer, F. E. Wells, *Studies on Turbulent flames: A. Flame Propagation Across velocity gradients B. turbulence Measurement in flames*, Symposium (International) on Combustion, 4 (1953), pp. 613-620.

[2] B. Zeldovich, D. Frank-Kamenetskii, *A theory of thermal flame propagation*, Acta Physicochimica URSS, 9 (1938), pp. 341–350.

[3] W. Eckhaus, *Theory of flame-front stability*, Journal of Fluid Mechanics Digital Archive, 10 (1961), pp. 80-100.

[4] G. I. Sivashinsky, *On a distorted flame front as a hydrodynamic discontinuity*, Acta Astronautica, 3 (1976), pp. 889-918.

[5] J. Buckmaster, *Slowly varying laminar flames*, Combustion and Flame, 28 (1977), pp. 225-239.

[6] P. Clavin, *Dynamic behavior of premixed flame fronts in laminar and turbulent flows*, Progress in Energy and Combustion Science, 11 (1985), pp. 1-59.

[7] P. Clavin, F. A. Williams, *Effects of molecular diffusion and of thermal expansion on the structure and dynamics of premixed flames in turbulent flows of large scale and low intensity*, Journal of Fluid Mechanics Digital Archive, 116 (1982), pp. 251-282.

[8] G. H. Markstein, *Experimental and theoretical studies of flame-front stability*, Journal of the Aeronautical Sciences, 18 (1951), pp. 199-209.

[9] S. H. Chung, C. K. Law, *An integral analysis of the structure and propagation of stretched premixed flames*, Combustion and Flame, 72 (1988), pp. 325-336.

[10] L. de Goey, J. ten Thije Boonkkamp, *Mass burning rate of premixed stretched flames: integral analysis versus large-activation-energy asymptotics*, Journal of Engineering Mathematics, 62 (2008), pp. 67-84.

[11] M. Matalon, *On Flame Stretch*, Combustion Science and Technology, 31 (1983), pp. 169-181.

[12] C. M. Vagelopoulos, F. N. Egolfopoulos, C. K. Law, *Further considerations on the determination of laminar flame speeds with the counterflow twin-flame technique*, Symposium (International) on Combustion, 25 (1994), pp. 1341-1347.

[13] J. H. Tien, M. Matalon, *On the burning velocity of stretched flames*, Combustion and Flame, 84 (1991), pp. 238-248.

[14] S. G. Davis, C. K. Law, *Laminar flame speeds and oxidation kinetics of iso-octane-air and n-heptane-air flames*, Symposium (International) on Combustion, 27 (1998), pp. 521-527.

[15] A. P. Kelley, C. K. Law, *Nonlinear effects in the experimental determination of laminar flame properties from stretched flames*, Proceeding of Eastern State Fall Technical Meeting, Chemical & Physical Processes in Combustion (2007).

[16] A. P. Kelley, C. K. Law, *Nonlinear effects in the extraction of laminar flame speeds from expanding spherical flames*, Combustion and Flame, 156 (2009), pp. 1844-1851.

[17] T. Tahtouh, F. Halter, C. Mounaïm-Rouselle, *Measurement of laminar burning speeds and Markstein lengths using a novel methodology*, Combustion and Flame, 157 (2009), pp. 1825-1832.

[18] Z. Chen, Y. Ju, *Theoretical analysis of the evolution from ignition kernel to flame ball and planar flame*, Combustion Theory and Modelling, 11 (2007), pp. 427-453.

[19] L. He, *Critical conditions for spherical flame initiation in mixtures with high Lewis numbers*, Combustion Theory and Modelling, 4 (2000), pp. 159-172.

[20] G. Joulin, P. Clavin, *Linear stability analysis of nonadiabatic flames: Diffusional-thermal model*, Combustion and Flame, 35 (1979), pp. 139-153.

[21] Z. Chen, M. P. Burke, Y. Ju, *Effects of Lewis number and ignition energy on the determination of laminar flame speed using propagating spherical flames*, Proceedings of the Combustion Institute, 32 (2009), pp. 1253-1260.

[22] M. L. Frankel, G. I. Sivashinsky, *On Quenching of Curved Flames*, Combustion Science and Technology, 40 (1984), pp. 257-268.

[23] K. K. Kuo, *Principles of combustion*, John Wiley & sons, Inc., second edition (2005).

[24] R. J. Kee, F. M. Rupley, J. A. Miller, *Chemkin-II: a Fortran chemical kinetics package for the analysis of gas phase chemical kinetics*, Report No. SAND89-8009B, Sandia National Laboratories (1989).

[25] T. Tahtouh, F. Halter, E. Samson, C. Mounaïm-Rousselle, *Effects of hydrogen addition and nitrogen dilution on the laminar flame characteristics of premixed methane-air flames*, International Journal of Hydrogen Energy, 34 (2009), pp. 8329-8338.

[26] D. Bradley, P. H. Gaskell, X. J. Gu, *Burning velocities, markstein lengths, and flame quenching for spherical methane-air flames: A computational study*, Combustion and Flame, 104 (1996), pp. 176-198.

[27] X. J. Gu, M. Z. Haq, M. Lawes, R. Woolley, *Laminar burning velocity and Markstein lengths of methane-air mixtures*, Combustion and Flame, 121 (2000), pp. 41-58.

[28] M. I. Hassan, K. T. Aung, G. M. Faeth, *Measured and predicted properties of laminar premixed methane/air flames at various pressures*, Combustion and Flame, 115 (1998), pp. 539-550.

[29] D. Bradley, R. A. Hicks, M. Lawes, C. G. W. Sheppard, R. Woolley, *The Measurement of Laminar Burning Velocities and Markstein Numbers for Iso-octane-Air and Iso-octane-n-Heptane-Air Mixtures at Elevated Temperatures and Pressures in an Explosion Bomb*, Combustion and Flame, 115 (1998), pp. 126-144.

[30] J. E. Freeh, K. Kumar, Y. Huang, C. J. Sung, *Laminar flame speeds of preheated iso-octane/air and n-decane/air flames using digital particle image velocimetry*, AIAA, 3709 (2004).

6. Laminar flame characteristics of $C_8H_{18}/H_2/N_2$/air flames

Ce chapitre a fait l'objet d'une publication dans la revue scientifique *International Journal of Hydrogen Energy* :

T. Tahtouh, F. Halter, C. Mounaïm-Rousselle, *Laminar premixed flame characteristics of hydrogen blended iso-octane-air-nitrogen mixtures*, International Journal of Hydrogen Energy, *in press* (2010).

6.1 Abstract

The combined effects of hydrogen addition and nitrogen dilution on laminar flame characteristics for iso-octane/air stoichiometric mixtures were investigated. The spherical expanding flames technique, in a constant volume bomb, was employed. The mole fraction of hydrogen in the iso-octane/hydrogen mixture was varied from 0 to 1 and the mole fraction of nitrogen in the total mixture (iso-octane/hydrogen/air/diluent) from 0 to 0.4.

Measurements were performed at an initial pressure of 0.1 MPa and an initial temperature of 300 K.

The laminar burning velocity strongly decreases with nitrogen dilution and for all dilution rates increases linearly with hydrogen mass percentage.

The burned gas Markstein length is reduced with the increase in hydrogen amount in the mixture until it reaches negative values, the opposite effect of nitrogen dilution. From these new experimental data, an experimental correlation to estimate the laminar burning velocity of iso-octane-hydrogen-air-nitrogen mixtures is proposed.

The experimental values of laminar burning velocities are found to be in very good agreement with those predicted by the high temperature mechanism developed by Jerzembeck et al. [1].

Nomenclature:

- K : Total stretch rate [1/s]
- L_b : Burned gas Markstein length [m]
- r_u : Flame front radius [m]
- u_{l0} : Laminar burning velocity [m/s]
- V_S : Stretched flame speed [m/s]
- V_{S0} : Unstretched flame speed [m/s]
- $V_{Slinear}$: Stretched flame speed given by the linear formulation [m/s]
- $V_{Snon\ linear}$: Stretched flame speed given by the non linear formulation [m/s]
- α : Mole fraction of hydrogen in the iso-octane-hydrogen blend [-]
- β : Mole fraction of nitrogen used for dilution in the total mixture [-]
- γ : Hydrogen mass percentage in the iso-octane-hydrogen blend [%]
- ρ_b : Density of burned gas [Kg/m^3]
- ρ_u : Density of unburned mixture [Kg/m^3]
- ε_{linear}: Relative difference between the experimental V_S and the calculated value $V_{Slinear}$ [-]
- $\varepsilon_{nonlinear}$: Relative difference between the experimental V_S and the calculated $V_{Snon\ linear}$ [-]

6.2 Introduction

The proposal of the future European directive will force automotive manufacturers to drastically reduce NOx. Exhaust gas recirculation (EGR) is a well-known in-cylinder method to reduce NO_x emissions, making it possible to decrease the combustion temperature. However, there are also several limitations associated with diluted combustion in the case of Spark-Ignition (S.I.) engines: the presence of diluents induces a reduction in the burning velocity and also the flammability limit. Therefore, as the flame becomes less stable and is closer to the extinction limit, one consequence is an increase in cycle to cycle variation.

One approach to overcome these drawbacks could be the addition of an amount of hydrogen to increase the engine stability since hydrogen has a high diffusion coefficient, high laminar burning velocity, low ignition energy and wide flammability limits. The use of hydrogen as an additive to gasoline in S.I. engines has been extensively studied [2-7]. These investigations showed that using hydrogen enrichment leads to a reduction in heat loss, an improvement in engine thermal efficiency, a decrease in pollutant levels (for CO_2 and HC), in flame development and propagation durations [2-7] and finally a better engine cyclic stability. In SI engines, the addition of hydrogen can also reduce the knock tendency by increasing the flame speed [8, 9].

Laminar burning velocity is an important fundamental property of an air-fuel mixture. First, experimental data of laminar burning velocity can be used to validate chemical reaction mechanisms. Secondly, it leads to a better understanding of the turbulent combustion process in the case of SI engines and power generation systems. Many authors [1, 10-14] have determined the laminar burning velocity of iso-octane/air mixtures numerically and experimentally. Mandilas et al. [15] investigated the effects of hydrogen addition on laminar and turbulent iso-octane/air flames and found that hydrogen enrichment increases the laminar burning velocity, which leads to the increase in turbulent burning rates. For iso-octane-reformer gas ($H_2/CO/N_2$)/air mixtures, the laminar flame speed was also found to be higher than that of pure iso-octane/air mixtures [16]. However there is a lack of data on the laminar flame characteristics of diluted hydrogen-enriched iso-octane/air mixtures.

In this study, new results concerning the laminar burning velocity and the burned gas Markstein length for Iso-octane/Hydrogen/Nitrogen/air mixtures are presented, determined experimentally by using the spherical expanding flames technique [12, 17-19]. A correlation for the laminar burning velocity as a function of the N_2 and H_2 contents is also suggested. This correlation is compared to simulated results obtained using two different kinetic mechanisms [1, 20].

6.3 Experimental device

The experimental set-up has been fully described previously [19, 21]. The experimental apparatus is a cylindrical stainless steel combustion chamber with an inner volume of 24.32 litres. Two tungsten electrodes, linked to a conventional capacitive discharge ignition system, are used to form the spark gap at the center of this chamber. The volumes of different gases are introduced into the chamber with thermal mass flowmeters. Iso-octane, present initially in a liquid form, is injected through a solenoid injector. The injector was heated to 400 K to ensure that the fuel was fully vaporized. Before filling the chamber with gases, a vacuum is created in the chamber. After introducing the different volumes of gases, the chamber is at atmospheric pressure and an initial temperature of 300K. The pressure level is checked with a piezoelectric pressure transducer. A fan is located inside the chamber to obtain a perfectly homogeneous mixture. Two opposed and transparent viewports provide optical access. The lighting is provided by a continuous Stabilite 2017 Argon ion Laser. A parallel light beam is created by using two plano-convex lenses. After passing through both lenses and the combustion chamber, the beam is displayed on a screen. The maximum beam diameter cannot exceed 70 mm (the diameter of the second lens). The evolution of the flame surface is observed from the shadowgraph images, recorded with a high speed CMOS APX camera operating at 6000 frames/second [19, 21].

Under the assumption of a spherical flame front propagation, the instantaneous flame front radius is obtained from post-processing after subtracting the background. At each time step, the luminous zone is fitted by a circle [19]. The flame propagation is initially affected by the spark ignition energy, resulting in an elevated flame speed. After this early stage (for flame radii larger than 7 mm) the effect of the initial energy deposit becomes negligible on the flame growth. Thus, only data corresponding to a flame radius larger than 8mm but below 30 mm were considered, i.e. a total volume of burned gases less than 0.5% of the total volume. The total chamber pressure can therefore be considered constant.

An analysis of the different errors attributable to the experimental procedure in a previous study [19] showed that the maximum uncertainty in the determination of the laminar burning velocity, linked to these errors, was less than 5%.

6.4 Properties of mixtures

In this study, measurements of laminar burning velocity and Markstein length were performed at an initial pressure of 0.1 MPa and an initial temperature of 300K. All the investigated mixtures were under stoichiometric conditions even for the hydrogen blended fuel. For each mixture, the experiment was carried out at least three times and the data reported in the following are the simple average of these tests.

Table 1. *Hydrogen and diluent mole fractions of investigated mixtures.*

α \ β	0	0.05	0.1	0.15	0.2	0.3	0.4
0	done	done	done	done	done		
0.4	done	done	done	done	done		
0.6	done	done	done	done	done		
0.8	done	done	done	done	done		
0.87					done	done	done
0.9					done	done	done
0.91					done	done	done
0.935					done	done	done
0.95					done	done	done
0.96							done
0.97							done
0.98							done
1						done	done

For all results, parameter α is defined as the mole fraction of hydrogen in the iso-octane/hydrogen blend:

$$\alpha = \frac{X_{H_2}}{X_{C_8H_{18}} + X_{H_2}} \quad (1)$$

And the parameter of dilution β, as the mole fraction of nitrogen used for dilution in the total mixture:

$$\beta = \frac{X_{N_2-dilution}}{X_{C_8H_{18}} + X_{H_2} + X_{O_2} + X_{N_2-air} + X_{N_2-dilution}} = X_{N_2-dilution} \quad (2)$$

where $X_{C_8H_{18}}$, X_{H_2} and X_{O_2} are respectively iso-octane, hydrogen and oxygen mole fractions in the mixture, X_{N_2-air} the mole fraction of nitrogen in the air mixture ($X_{N_2-air} = 3.78 \bullet X_{O_2}$) and

$X_{N_2-dilution}$ the mole fraction of nitrogen used for dilution. The different hydrogen and diluent mole fractions of all the investigated mixtures are summarized in Table 1.

6.5 Theoretical considerations

For outwardly propagating flames, the stretched flame speed V_S is derived from the flame radius r_u versus time data:

$$V_S = \frac{dr_u}{dt} \quad (3)$$

The total stretch acting on the flame, defined by the temporal rate of change of a flame surface element of area A is defined as:

$$K = \frac{1}{A} \bullet \frac{dA}{dt} \quad (4)$$

In this case (spherically outwardly propagating flames), the stretch rate K can be written as follows [22]:

$$K = \frac{2}{r_u} \bullet \frac{dr_u}{dt} \quad (5)$$

Based on asymptotic analysis [23] (large activation energy), a linear relation linking the flame stretch to the stretched flame speed is commonly used to extract the unstretched flame speed [24-26]. However, this linear relation is valid when the stretched flame speed is sufficiently close to the unstretched one. It was observed that while this assumption is coherent for methane/hydrogen/nitrogen/air mixtures under stochiometric conditions [21], it is no longer valid when methane is replaced by iso-octane. Therefore, the nonlinear expression initially proposed by Sivashinsky [27] and Buckmaster [28], and recently used in [29, 30], was employed in this study.

Considering the following nonlinear expression reported in [30] linking the stretched flame speed and the stretch rate:

$$\left(\frac{V_S}{V_{S0}}\right)^2 \bullet \ln\left(\frac{V_S}{V_{S0}}\right)^2 = -\frac{2 \bullet L_b \bullet K}{V_{S0}} \quad (6)$$

V_{S0} is the unstretched flame speed and L_b is the burned gas Markstein length.

This expression (Eq.(6)) is valid with the following assumptions:

A large activation energy.

An overall one step exothermic reaction.

Constant values of the molecular weight, specific heat, thermal conductivity and density weighted mass diffusivity of the mixture.

The convection flux is absent.

The flame is considered in quasi-steady state.

The flame thickness is negligible (thin flames) compared to the flame radius.

The combustion process is isobaric.

The unstretched flame speed and the burned gas Markstein length can be deduced by minimizing the following expression:

$$\sum_{i=1}^{N}\left|\left(\frac{V_S}{V_{S0}}\right)^2 \bullet \ln\left(\frac{V_S}{V_{S0}}\right)^2 + \frac{2 \bullet L_b \bullet K}{V_{S0}}\right| \quad (7)$$

N corresponding to the recording time step.

Then, the laminar burning velocity can be determined from the unstretched propagation flame speed and the density ratio by using the following expression:

$$u_{l0} = \frac{\rho_b}{\rho_u} \bullet V_{S0} \quad (8)$$

ρ_b : the density of burned gases; ρ_u : the density of unburned gases

These density values were obtained with a classical computational method using the adiabatic flame calculation with Premix in the Chemkin Package [31] and based on a detailed chemical kinetic scheme [20].

6.6 Validity of the methodology

In Figure 1, the experimental flame speed evolution is plotted as a function of the flame stretch for three hydrogen blended mixtures.

The dashed lines correspond to the linear extrapolation to zero stretch rate methodology and the continuous lines the non linear extrapolation (Eq. 6). It can be seen that the extrapolation from Eq. 6 is in better agreement with the experimental data than the linear one [25].

The relative difference, $\varepsilon_{\text{non linear}}$ between the experimental value V_s and the calculated values from the nonlinear methodology, $V_{s\ \text{non linear}}$, was found to be lower than $\varepsilon_{\text{linear}}$, defined as:

$$\varepsilon_{linear} = 100 \bullet \left| \frac{V_S - V_{S\,linear}}{V_S} \right| \quad (9)$$

For example, the maximum value of ε_{linear} for the mixtures with α=0.4, 0.6 and 0.8 are 4.8% 2.9% and 2% respectively, while $\varepsilon_{non\ linear}$ presents maximum values of 1.8%, 1.3% and 1.3% respectively.

As expected, the highest values of ε_{linear} were found for the smallest flame radii and highest stretch rates and $\frac{V_S}{V_{S0}}$ ratios, i.e. in the domain where the linear extrapolation is no longer valid.

The maximum value of the $\varepsilon_{non\ linear}$ is not necessarily linked to the smallest radii investigated.

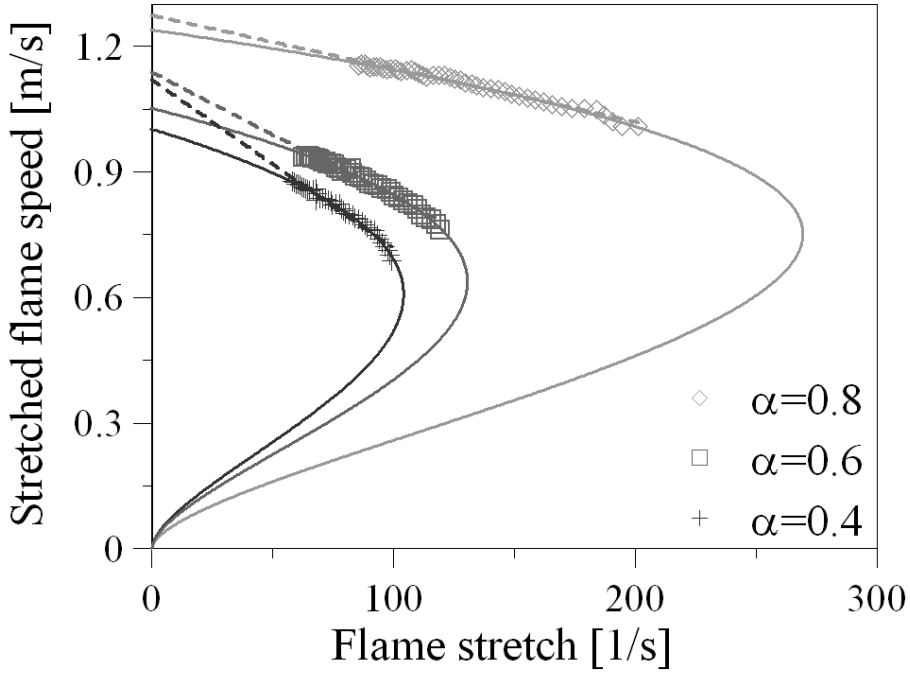

Figure 1. *Evolution of the stretched flame speed versus the flame stretch for different hydrogen contents (β =0.2, P=0.1 MPa, T=300K, stoichiometric conditions).*

6.7 Results

6.7.1 Laminar burning velocities

The values determined for stoichiometric air-iso-octane mixtures, without hydrogen addition ($\alpha = 0$) and for different mole fractions of nitrogen β are presented in Table 2. To verify the quality of our experimental set-up and of our methodology, the values are compared with results available in the literature literature [10, 11, 16, 32]: our values are lower for all dilution cases. This difference can be explained by the use of the nonlinear equation (Eq. 6).

The experimental apparatus and procedure are the same as in [32], the only difference is the extrapolation methodology used to obtain the unstretched flame speed and Markstein length.

In Figure 2.a and 2.b, the experimental values of the laminar burning velocities are plotted versus α, for different mole fractions of nitrogen β. The increase of hydrogen fraction in the mixture increases the laminar burning velocity: this effect is more pronounced with higher values of α. For example, for a 0.2 mole fraction of nitrogen, a variation of α from 0 to 0.6 involves a variation of 1.76% in the laminar burning velocity but a variation of α from 0.6 to 0.95 results in a variation of 127.4% in the laminar burning velocity. For low diluted gas fractions (β<0.2), the effect of hydrogen addition becomes more obvious when the value of α is higher than 0.6. This value, 0.6, is shifted toward the higher hydrogen fraction in the mixture when the dilution is greater. Moreover, it was found that the addition of hydrogen allows a better propagation of the flame when the mixture is strongly diluted.

Table 2. *Comparison of the laminar burning velocities of isooctane-air mixture (α=0, P=0.1 MPa, T=300K, stoichiometric conditions).*

Laminar burning velocities [m/s] for α=0					
β	**Present**	**[32]**	**[10]**	**[11]**	**[16]**
0	**0.29**	**0.33**	**0.34**	**0.32** **0.34**	**0.34**
0.05	**0.25**	**0.29**	**-**	**-**	**-**
0.1	**0.22**	**0.25**	**-**	**-**	**-**
0.15	**0.17**	**0.2**	**-**	**-**	**-**
0.2	**0.15**	**-**	**-**	**-**	**-**

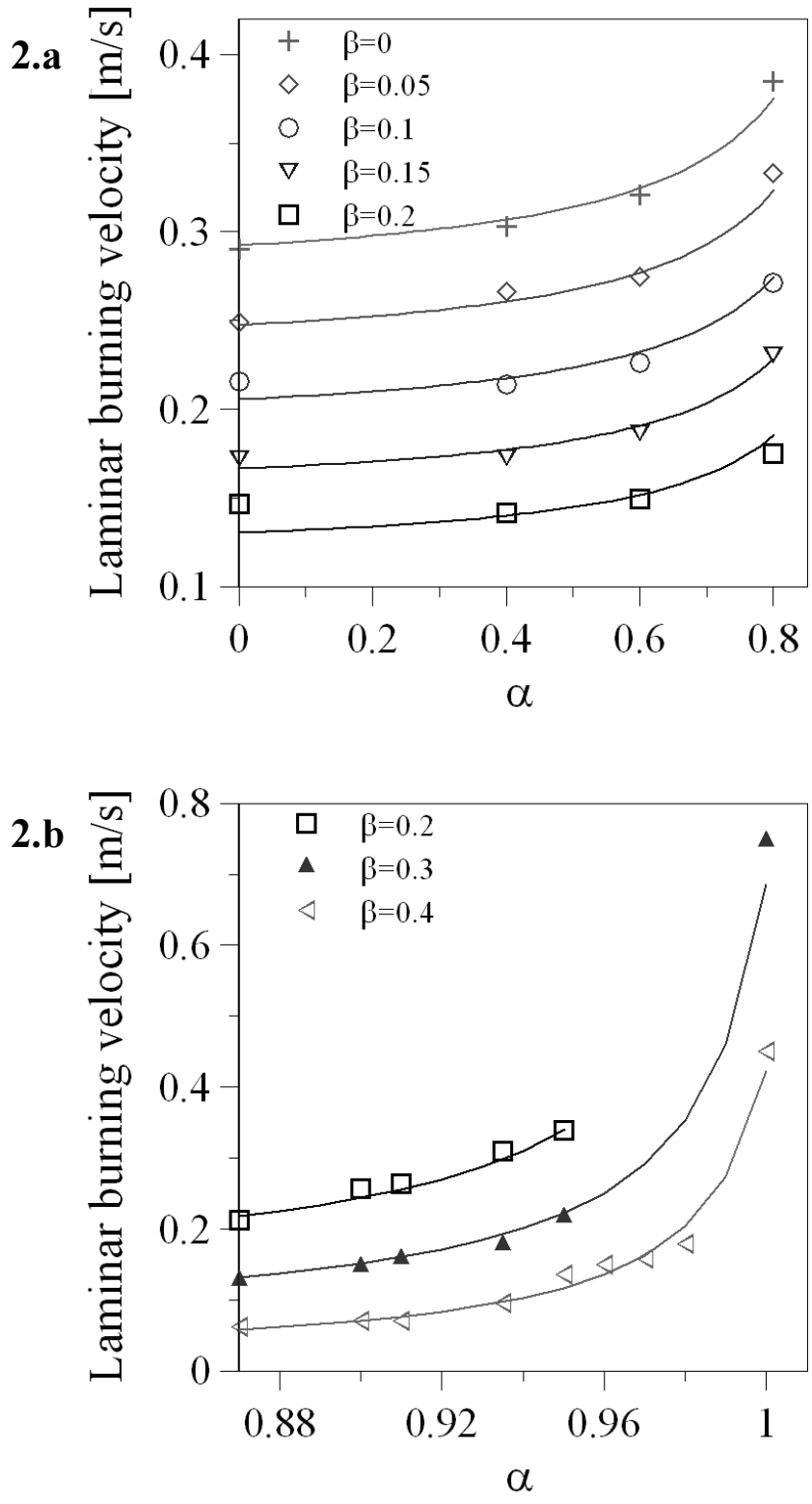

Figure 2. *Experimental laminar burning velocity versus hydrogen mole fraction α, (P=0.1 MPa, T=300K, stoichiometric conditions):* ***2.a*** *with α <0.85,* ***2.b*** *with α >0.85.*

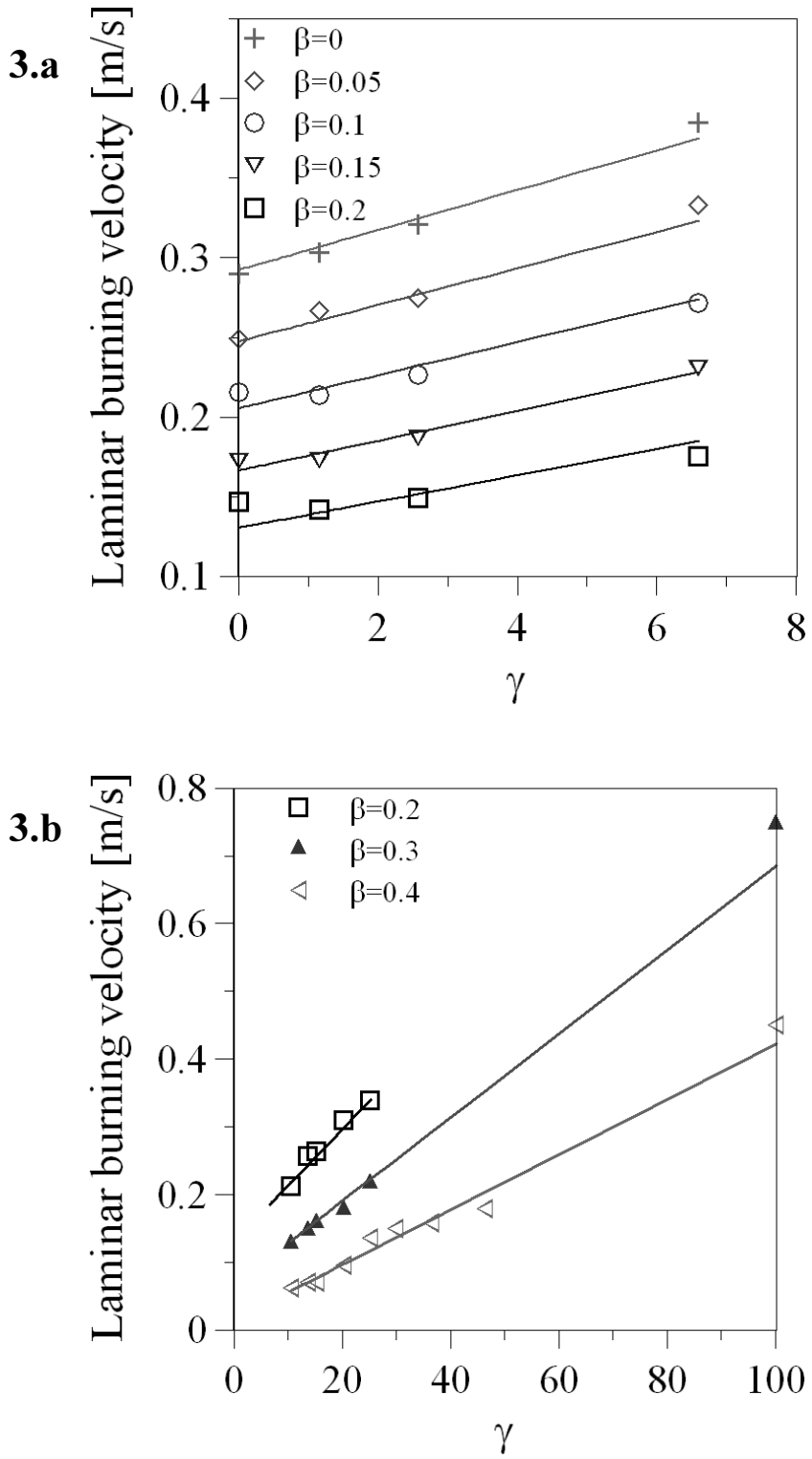

Figure 3. *Experimental laminar burning velocity versus hydrogen mass percentage γ, (P=0.1 MPa, T=300K, stoichiometric conditions):* ***3.a*** *with γ<7%,* ***3.b*** *with γ>7%.*

Up to 60% of hydrogen addition by volume in the fuel mixture, the effect on laminar burning velocity is insignificant. However, it is important to note that 60% of hydrogen addition in volume only corresponds to 2.58% in mass, which is relatively low.

This is due to the considerable difference between hydrogen and iso-octane densities. The laminar burning velocity is plotted in Figures 3a and 3b versus the hydrogen mass percentage, γ, defined as:

$$\gamma = 100 \bullet \frac{m_{H_2}}{m_{C_8H_{18}} + m_{H_2}} \quad (10)$$

m_{H_2} : hydrogen mass in the mixture; $m_{C_8H_{18}}$: iso-octane mass in the mixture.

For all the investigated mixtures, a linear evolution is obtained, similar to the trend observed in a previous study [21] in the case of methane-hydrogen-nitrogen-air mixtures.

A similar empirical correlation can therefore be suggested where the laminar burning velocity is expressed as a function of γ and β :

$$u_{l0}[cm/s] = (a_{corr} \bullet \beta + b_{corr}) \bullet \gamma + c_{corr} \bullet \beta^2 + d_{corr} \bullet \beta + e_{corr} \quad (11)$$

The coefficients obtained from the best fitting over 40 experimental values of laminar burning velocity are: a_{corr} = -2.119, b_{corr} =1.253, c_{corr} =58.798, d_{corr} =-92.676 e_{corr} =29.227.

By expressing hydrogen mass percentage γ as a function of α, Eq. (11) becomes:

$$u_{l0}[cm/s] = (a_{corr} \bullet \beta + b_{corr}) \bullet \left(\frac{-201.6 \bullet \alpha}{112.184 \bullet \alpha - 114.2} \right) + c_{corr} \bullet \beta^2 + d_{corr} \bullet \beta + e_{corr} \quad (12)$$

The maximum difference between experimental data and this empirical relationship is around 10% and the mean absolute difference for all data 3.9 %, which is of the same order as experimental error [19].

6.7.2 Laminar burning velocity simulations

Simulations of one dimensional, planar and adiabatic laminar flame propagation were performed with the CHEMKIN package [30] by using two different mechanisms for iso-octane oxidation. First, the Hasse et al. [20] mechanism, 48 reactions and 29 species, is based on the mechanism of Pitch et al. [33] but with 3 additional species (C_3H_6, N–C_3H_7, and I–C_3H_7). Secondly, Jerzembeck et al. [1] proposed a high temperature mechanism involving 99 species and 669 reactions. For all simulations, the initial flow rate of the unburned mixture was fixed at 0.04g/cm^2 and the gradient and curvature values at 0.05.

A comparison between the values obtained from the empirical correlation (Eq.12) and from the simulations with both mechanisms is shown in Figure 4.

The values given by the correlation are globally in good agreement with the simulations and exhibit a similar trend of the reducing effect of nitrogen dilution on laminar burning velocity.

One can note however that the values from the correlation (for α=0, 0.4 and 0.6 and for β= 0.05, 0.1, 0.15 and 0.2) are lower than those predicted by the Hasse et al. mechanism [20] but in a very good agreement with those predicted by the Jerzembeck et al. mechanism [1]. The maximum difference between the values obtained from the experimental correlation and from simulation with the Hasse and Jerzembeck mechanisms is respectively 19% and 6% and the average difference is 13.9% and 4.7%.

This mechanism [1] can therefore be used, in future work, to provide values of laminar burning velocity for a wide range of hydrogen addition (up to 80% by volume in the fuel mixture) and nitrogen dilution (up to 20% by volume) in iso-octane-air mixtures. However, this mechanism must be validated for higher pressures and temperatures to provide data in the case of combustion in spark ignition engines.

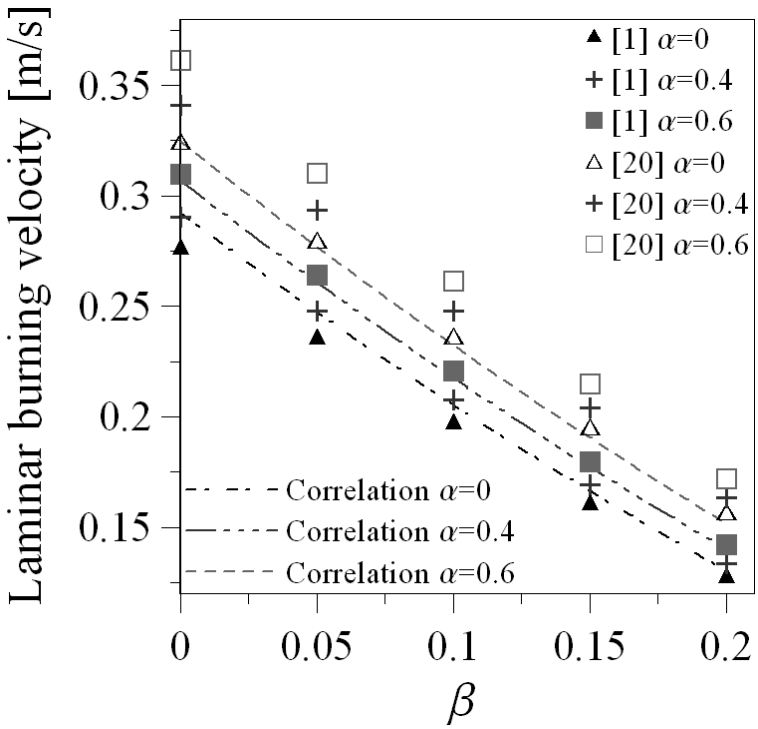

Figure 4. *Comparison of values given by the proposed correlation and the numerical simulations of laminar burning velocity versus nitrogen mole fraction β, for α = 0, α = 0.4 and α = 0.6, (P=0.1 MPa, T=300K, stoichiometric conditions).*

6.7.3 Markstein length

The sensitivity of the flame speed to the stretch rate is characterized by the Markstein length L_b. The values of burned gas Markstein length obtained in the present work are plotted versus α in Figs 5.a and 5.b. For α<0.935, L_b increases for higher amounts of dilution: the flame becomes more sensitive to the stretch rate. An opposite trend is observed when α is closer to 1. This suggests that hydrogen addition leads to a decrease in the effect of stretch rate on the flame speed as well as an increase in laminar burning speed. For α>0.935 and β=0.3 and 0.4, no regular trend can be noted since only few experimental data are available in this range

of hydrogen addition and nitrogen dilution. However for α>0.935, the mixtures investigated are characterized by a negative value of L_b since the mixtures are diffusively unstable [34].

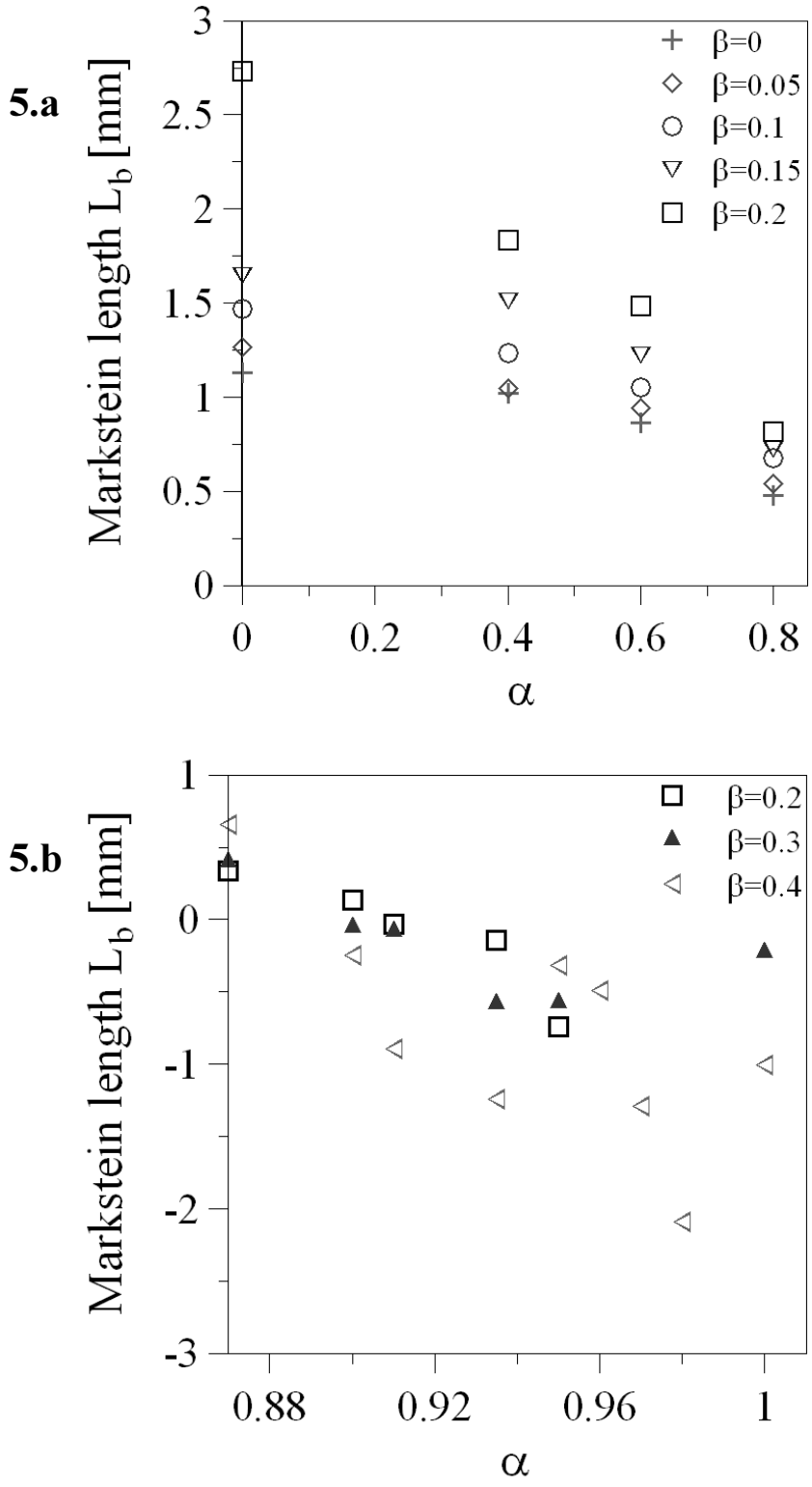

Figure 5. *Burned gas Markstein length values versus the hydrogen content α and for different dilution rates β (P=0.1 MPa, T=300K, stoichiometric conditions):* ***5.a*** *with α<0.85,* ***5.b*** *with α>0.85.*

A positive Markstein length indicates a stable flame: as the flame stretch decreases the burning velocity, any disturbances of the flame front will tend to be smoothed out. The opposite behaviour is observed for a negative Markstein length: the disturbances will thus be amplified.

Therefore the addition of hydrogen, for the investigated mixtures, induces thermo-diffusive instabilities which can be related to the high molecular diffusion coefficient of hydrogen.

6.8 Conclusion

In this work, the effects of nitrogen dilution and hydrogen enrichment of iso-octane-air mixtures on the laminar flame characteristics were studied by performing experiments in a constant volume chamber.

The laminar burning velocity increases with the addition of hydrogen. This increase was found to be linear with the hydrogen mass fraction in the mixture. Furthermore, the flame speed becomes less sensitive to the stretch rate since the burned gas Markstein length decreases. However, this increasing effect is not noticeable in the case of diluted mixtures with a lower hydrogen fraction, below 0.6. Nitrogen dilution of the mixture reduces the laminar burning velocity significantly even for small amounts of nitrogen fractions, i.e. 0.05, and increases the burned gas Markstein length.

Based on the present experimental data, an empirical correlation has been suggested to estimate the laminar burning velocity of hydrogen enriched and nitrogen diluted iso-octane/air mixtures. This correlation is valid under the present experimental conditions (atmospheric pressure, ambient temperature and stoichiometric conditions) in a wide range of dilution levels (from 0 to 0.2 mole fraction of nitrogen) and for hydrogen mole fractions less than 0.8. It is also validated for higher amounts of dilution (between 0.2 and 0.4) when molar hydrogen enrichment is more than 0.8.

Simulation values of laminar burning velocity, obtained using two different kinetic mechanisms [1, 20], were also compared to the present proposed correlation. The values of laminar burning velocity predicted by the high temperature mechanism developed by Jerzembeck et al. [1] are in very good agreement with the present correlation.

6.9 References

[1] S. Jerzembeck, N. Peters, P. Pepiot-Desjardins, H. Pitsch, *Laminar burning velocities at high pressure for primary reference fuels and gasoline: Experimental and numerical investigation*, Combustion and Flame, 156 (2009), pp. 292-301.

[2] C. Ji, S. Wang, *Effect of hydrogen addition on the idle performance of a spark ignited gasoline engine at stoichiometric condition*, International Journal of Hydrogen Energy, 34 (2009), pp. 3546-3556.

[3] C. Ji, S. Wang, *Effect of hydrogen addition on combustion and emissions performance of a spark ignition gasoline engine at lean conditions*, Int J of Hydrogen Energy, 34 (2009), pp. 7823-7834.

[4] C. Pana, N. Negurescu, M. G. Popa, A. Cernat, D. Soare, *An Investigation of the Hydrogen Addition Effects to Gasoline Fueled Spark Ignition Engine*, SAE paper, 2007-01-1468 (2007).

[5] F. Yüksel, M. A. Ceviz, *Thermal balance of a four stroke SI engine operating on hydrogen as a supplementary fuel*, Energy, 28 (2003), pp. 1069-1080.

[6] M. A.-R. Sadiq Al-Baghdadi, H. A.-K. Shahad Al-Janabi, *Improvement of performance and reduction of pollutant emission of a four stroke spark ignition engine fueled with hydrogen-gasoline fuel mixture*, Energy Conversion and Management, 41 (2000), pp. 77-91.

[7] T. D'Andrea, P. F. Henshaw, D. S. K. Ting, *The addition of hydrogen to a gasoline-fuelled SI engine*, International Journal of Hydrogen Energy, 29 (2004), pp. 1541-1552.

[8] T. Shinagawa, T. Okumura, S. Furuno, K. O. Kim, *Effects of hydrogen addition to SI engine on knock behavior*, SAE 2004-01-1851 (2004).

[9] J. A. Topinka, M. D. Gerty, J. B. Heywood, J. C. Keck, *Knock Behavior of a Lean-Burn, H2 and CO Enhanced, SI Gasoline Engine Concept*, SAE paper, 2004-01-0975 (2004).

[10] M. Metghalchi, J. C. Keck, *Burning velocities of mixtures of air with methanol, isooctane, and indolene at high pressure and temperature*, Combustion and Flame, 48 (1982), pp. 191-210.

[11] S. G. Davis, C. K. Law, *Laminar flame speeds and oxidation kinetics of iso-octane-air and n-heptane-air flames*, Symposium (International) on Combustion, 27 (1998), pp. 521-527.

[12] D. Bradley, R. A. Hicks, M. Lawes, C. G. W. Sheppard, R. Woolley, *The Measurement of Laminar Burning Velocities and Markstein Numbers for Iso-octane-Air and*

Iso-octane-n-Heptane-Air Mixtures at Elevated Temperatures and Pressures in an Explosion Bomb, Combustion and Flame, 115 (1998), pp. 126-144.

[13] A. S. Al-Shahrany, D. Bradley, M. Lawes, R. Woolley, *Measurement of unstable burning velocities of iso-octane-air mixtures at high pressure and the derivation of laminar burning velocities*, Proceedings of the Combustion Institute, 30 (2005), pp. 225-232.

[14] R. J. Johnston, J. T. Farrell, *Laminar burning velocities and Markstein lengths of aromatics at elevated temperature and pressure*, Proceedings of the Combustion Institute, 30 (2005), pp. 217-224.

[15] C. Mandilas, M. P. Ormsby, C. G. W. Sheppard, R. Woolley, *Effects of hydrogen addition on laminar and turbulent premixed methane and iso-octane-air flames*, Proceedings of the Combustion Institute, 31 (2007), pp. 1443-1450.

[16] Y. Huang, C. J. Sung, J. A. Eng, *Laminar flame speeds of primary reference fuels and reformer gas mixtures*, Combustion and Flame, 139 (2004), pp. 239-251.

[17] X. J. Gu, M. Z. Haq, M. Lawes, R. Woolley, *Laminar burning velocity and Markstein lengths of methane-air mixtures*, Combustion and Flame, 121 (2000), pp. 41-58.

[18] M. I. Hassan, K. T. Aung, G. M. Faeth, *Measured and predicted properties of laminar premixed methane/air flames at various pressures*, Combustion and Flame, 115 (1998), pp. 539-550.

[19] T. Tahtouh, F. Halter, C. Mounaïm-Rousselle, *Measurement of laminar burning speeds and Markstein lengths using a novel methodology*, Combustion and Flame, 156 (2009), pp. 1735-1743.

[20] C. Hasse, M. Bollig, N. Peters, H. A. Dwyer, *Quenching of laminar iso-octane flames at cold walls*, Combustion and Flame, 122 (2000), pp. 117-129.

[21] T. Tahtouh, F. Halter, E. Samson, C. Mounaïm-Rousselle, *Effects of hydrogen addition and nitrogen dilution on the laminar flame characteristics of premixed methane-air flames*, International Journal of Hydrogen Energy, 34 (2009), pp. 8329-8338.

[22] C. K. Law, C. J. Sung, *Structure, aerodynamics, and geometry of premixed flamelets*, Progress in Energy and Combustion Science, 26 (2000), pp. 459-505.

[23] W. B. Bush, F. E. Fendell, *Asymptotic Analysis of the Structure of a Steady Planar Detonation*, Combustion Science and Technology, 2 (1971), pp. 271-285.

[24] D. Bradley, P. H. Gaskell, X. J. Gu, *Burning velocities, markstein lengths, and flame quenching for spherical methane-air flames: A computational study*, Combustion and Flame, 104 (1996), pp. 176-198.

[25] P. Clavin, *Dynamic behavior of premixed flame fronts in laminar and turbulent flows*, Progress in Energy and Combustion Science, 11 (1985), pp. 1-59.

[26] G. H. Markstein, *Experimental and theoretical studies of flame-front stability*, Journal of the Aeronautical Sciences, 18 (1951), pp. 199-209.

[27] G. I. Sivashinsky, *Nonlinear analysis of hydrodynamic instability in laminar flames--I. Derivation of basic equations*, Acta Astronautica, 4 (1977), pp. 1177-1206.

[28] J. Buckmaster, *Slowly varying laminar flames*, Combustion and Flame, 28 (1977), pp. 225-239.

[29] A. P. Kelley, C. K. Law, *Nonlinear effects in the extraction of laminar flame speeds from expanding spherical flames*, Combustion and Flame, 156 (2009), pp. 1844-1851.

[30] F. Halter, T. Tahtouh, C. Mounaïm-Rousselle, *Nonlinear effects of stretch on the flame front propagation*, Combustion and Flame, 157 (2010), pp. 1825-1832.

[31] R. J. Kee, F. M. Rupley, J. A. Miller, *Chemkin-II: A Fortran chemical kinetics package for the analysis of gas phase chemical kinetics*, Report No. SAND89-8009B, Sandia National Laboratories (1989).

[32] F. Halter, F. Foucher, L. Landry, C. Mounaïm-Rousselle, *Effect of dilution by nitrogen and/or carbon dioxide on methane and iso-octane air flames*, Combustion Science and Technology, 181 (2009), pp. 813-827.

[33] H. Pitsch, N. Peters, K. Seshadri, *Numerical and asymptotic studies of the structure of premixed iso-octane flames*, In: Symposium (International) on Combustion, 26 (1996), pp. 763-771.

[34] D. Bradley, C. G. W. Sheppart, R. Woolley, D. A. Greenhalgh, R. D. Lockett, *The development and structure of flame instabilities and cellularity at low Markstein numbers in explosions*, Combustion and Flame, 122 (2000), pp. 195-209.

III-Combustion Turbulente

Dans la seconde partie de ce mémoire, nous avons proposé et validé des corrélations pour estimer la vitesse de combustion laminaire de notre mélange à pression atmosphérique et à température ambiante. Ces corrélations ont permis et permettent de quantifier l'effet de l'hydrogène et de la dilution sur la vitesse laminaire de combustion pour des carburants principaux, méthane et iso-octane. Cependant, la vitesse de combustion turbulente dans un moteur à allumage commandé n'est pas uniquement définie par la vitesse de combustion laminaire.

C'est pour cela que cette dernière partie de mémoire est consacrée à l'étude expérimentale de l'effet de l'hydrogène et de la dilution sur la propagation de flamme turbulente dans un moteur à allumage commandé (chapitres 7 et 8).

- ✓ Dans le chapitre 7, une première étude concerne les résultats issus des visualisations directes du rayonnement de la combustion dans un moteur à allumage commandé à accès optiques. L'objectif est de caractériser, durant la phase initiale de combustion, les effets de l'hydrogène et de la dilution sur la propagation de la flamme turbulente dans des conditions 'réelles' de fonctionnement moteur. Une très bonne corrélation entre la propagation de flamme dans un moteur et la vitesse laminaire de combustion à pression atmosphérique et température ambiante a été obtenue.

- ✓ Malgré cette bonne corrélation, cette « simple » expérience (la visualisation directe) ne permet pas la détermination de la vitesse turbulente de combustion dans un moteur en raison du manque d'informations concernant la vitesse des gaz frais. C'est pourquoi, dans le chapitre 8, la vitesse de combustion turbulente est déterminée en utilisant la vélocimétrie par imagerie de particule et la tomographie laser par diffusion de Mie avec suivi temporel.

- ✓ Au cours de ce chapitre, seront aussi proposées de nouvelles corrélations pour la vitesse de combustion laminaire des mélanges hydrocarbure/hydrogène en fonction de la température et de la pression à partir des résultats présentées dans la deuxième partie de ce travail et des données expérimentales trouvées dans la littérature. L'estimation du nombre de Lewis pour des mélanges iso-octane ou méthane/hydrogène et différents niveaux de dilution sera aussi présentée au cours de ce chapitre 8.

- ✓ Enfin, les résultats issus de ces deux différentes procédures expérimentales (a- Visualisation directe et b- la vélocimétrie par imagerie de particule et la tomographie laser) sont comparés à la fin de ce chapitre 8.

Ces différentes étapes vont finalement nous permettre de répondre aux questions introduites dans l'introduction générale « comment l'hydrogène et la dilution influence le déroulement de la combustion dans un moteur à combustion interne ? » et d'atteindre ainsi les objectifs de ce travail de mémoire.

7. Direct visualization of flame radiation

Ce chapitre a fait l'objet d'une publication pour le congrès international *Society of Automotive Engineers (SAE)*:

T. Tahtouh, F. Halter, C. MounaÏm-Rousselle,E. Samson, *Experimental Investigation of the Initial Stages of Flame Propagation in a Spark-Ignition Engine: Effects of Fuel, Hydrogen Addition and Nitrogen Dilution*, SAE Technical Paper 2010-01-1451 (2010).

7.1 Abstract

An experimental investigation was conducted in an optical mono-cylinder Spark-Ignition engine in order to explore the influence of the fuel and of the dilution rate on the initial stages of flame propagation. Images of flame radiation were acquired through the transparent piston crown with a high speed CMOS camera operating at 6000 frames/second. Experiments were performed under stoichiometric and lean conditions (0.8 of equivalence ratio), and two engine speeds (1200 rpm and 2000 rpm). The spark ignition timing was set at 30 (iso-octane) and 25 (methane) crank angle degrees before top dead center. Image acquisition was synchronized with in-cylinder pressure to allow simultaneous evaluation of the Indicated Mean Effective Pressure (IMEP) and of the heat release rate. Image post-processing was performed to obtain the temporal evolution of the projected flame area. A flame initiation criterion was defined and a flame initiation delay, based on the optical investigation, was determined for all mixtures and conditions. The effects of the fuel (pure iso-octane, methane and hydrogen blended mixtures) on the initial stages of flame propagation were studied. The effect of dilution, here simulated only by the addition of nitrogen, was also investigated. Results show that the initial flame development duration increases with the dilution rate and decreases with hydrogen addition in the air-fuel mixture. The standard deviation of the crank angle corresponding to a defined projected enflamed area (50% of the total visible area) varies with fuel composition and increases with dilution. The initial stages of flame propagation were found to correlate very well with the laminar burning velocities obtained at atmospheric pressure and ambient temperature. The positive effect of hydrogen addition is more pronounced under diluted and lean conditions compared to stoichiometric conditions. The addition of hydrogen to avoid the drawbacks of dilution by burned gases (EGR or IGR) and of lean conditions can be one solution to provide sufficiently stable combustion and therefore low thermal NOx formation in S.I. engines.

Nomenclature:

- A_f : projected flame surface [m^2]
- $A_{f\max}$: maximum luminous area [m^2]
- $A_{norm} = \frac{A_f}{A_{f\max}}$: normalized projected flame surface [-]
- CAD: crank angle degree [°]
- CA50: CAD corresponding to 50% of the cumulated heat release [°]
- E_{H_2} : hydrogen content in the fuel in term of energy percentage [%]
- IMEP: net indicated mean effective pressure [kPa]
- P_{max}: maximum in-cylinder pressure [kPa]
- S_L : laminar burning velocity at atmospheric pressure and ambient temperature [m/s]
- S_{L-ref} : S_L for the stoichiometric fuel (methane or iso-octane)-air conditions [m/s]
- α : mole fraction of hydrogen in the fuel (iso-octane or methane)-hydrogen blend [-]
- β : mole fraction of nitrogen used for dilution in the total mixture [-]
- γ: hydrogen content in the fuel in term of mass percentage [%]
- $\theta_{0.1}$: CAD corresponding to A_{norm}=0.1 [°]
- $\theta_{0.5}$: CAD corresponding to A_{norm}=0.5 [°]
- $\theta_{P\max}$: CAD corresponding to P_{max} [°]
- Δt_s : time after spark ignition [ms]
- $\phi_i = \Delta t_{s\_i} - \Delta t_{s\_ref}$: difference, at a given A_{norm}, between condition i and the reference condition [ms]
- $\Delta S_L = \left(\frac{S_L - S_{L-ref}}{S_{L-ref}} \right)$ dimensionless difference in laminar burning velocity [-]
- $\psi_i = \frac{\left[\left(\phi_i \; at \; A_{norm} = 0.5 \right) - \left(\phi_i \; at \; A_{norm} = 0.1 \right) \right] - \left[\left(\Delta t_{s-ref} \; at \; A_{norm} = 0.5 \right) - \left(\Delta t_{s-ref} \; at \; A_{norm} = 0.1 \right) \right]}{\left[\left(\Delta t_{s-ref} \; at \; A_{norm} = 0.5 \right) - \left(\Delta t_{s-ref} \; at \; A_{norm} = 0.1 \right) \right]}$: dimensionless parameter of the flame propagation [-]
- $std_{\theta_{0.5}}$: standard deviation for $\theta_{0.5}$ [°]
- std_{CA50} : standard deviations for CA50 [°]

- $Corr_{\theta 0.1-CA50}$: correlation coefficient between $\theta_{0.1}$ and CA50 [-]
- $Corr_{\theta 0.5-CA50}$: correlation coefficient between $\theta_{0.5}$ and CA50 [-]
- $Corr_{\theta 0.5-P\max}$: correlation coefficient between $\theta_{0.5}$ and P_{max} [-]
- $Corr_{\theta 0.5-\theta P\max}$: correlation coefficient between $\theta_{0.5}$ and P_{max} [-]
- $Corr_{\theta 0.5-IMEP}$: correlation coefficient between $\theta_{0.5}$ and IMEP [-]
- $Cum_{\theta_{0.5}}$: cumulated heat release at $\theta_{0.5}$ [%]

7.2 Introduction

Over the last few years, automotive manufacturers have focused on reducing pollutant emissions and on increasing engine efficiency. Optimization of the intake air-fuel mixture composition is one way to achieve these objectives especially in the case of Spark-Ignition (S.I.) engines. Natural gas can also be an attractive alternative fuel and has been widely studied as engine fuel. By operating with a diluted mixture, i.e by recirculating the exhaust gases or increasing the residual gases by changing the valve phasing, NOx emission is reduced due to the lower combustion temperatures. There are however limitations on the level of dilution and of lean mixture that can ensure the smooth running of SI engines, whatever the fuel considered here, i.e gasoline or natural gas, since diluting the fuel-air mixture or operating with a lean mixture induces an increase in combustion duration and in cyclic variations which impair engine performance. Hydrogen has a wide flammability range, a low ignition energy, high auto ignition temperature and a high laminar burning velocity. Thanks to these properties, adding an amount of hydrogen to the fuel can extend the dilution and the lean engine operability limits, which is beneficial in reducing both emission levels and fuel consumption. Hydrogen addition can also improve the knock tendency in SI engines since it reduces the combustion period and inhibits fuel decomposition and hydroxyl radical production [1, 2].

7.2.1 Hydrogen addition

Numerical and experimental studies on the impact of hydrogen addition on SI engines fuelled by natural gas, methane or gasoline can be found in the literature [3-11]. The main results obtained are a reduction in combustion duration and an increase in the thermal efficiency. Apostolescu and Chiriac [7] studied the effect of hydrogen addition in a passenger car engine fuelled with gasoline. Kahraman et al. [8] conducted experiments in a four-cylinder S.I. engine to study the effect of hydrogen addition to methane (0%H_2, 10 %H_2, 20%H_2 and 30%H_2 by volume) on the engine's performance, emission, cylinder pressure and brake thermal efficiency. The cycle-by-cycle variation, HC emissions and the burning stages durations are decreased with the addition of hydrogen while thermal efficiency is increased ([7], [8]). Pana et al. [9], from results obtained with modelling and experimental investigations carried out on a single cylinder SI engine, concluded that the addition of hydrogen increases the thermal efficiency, the NOx emission level, and the IMEP. The Brake Specific Fuel Consumption and the temporal duration of the initial and main phases of combustion are reduced when hydrogen is added.

7.2.2 Hydrogen addition combined to EGR

Dimopoulos et al. [12] investigated the H_2-Natural Gas blend combustion with and without EGR in an S.I. engine. Without EGR, the efficiency increases by approx. 2% when the H_2

content is 10% by volume. However, the engine-out NOx emissions also increase. An opposite trend is observed for engine-out CO and THC with an increasing hydrogen fraction in the fuel mixture. Less spark timing advance was required for optimal efficiency since the hydrogen component in the fuel accelerates combustion. By combining H_2-Natural Gas blends and EGR, higher efficiencies with early spark timing with also very low engine-out NOx can be reached. Alger et al. [13] investigated the effect of H_2 addition on EGR tolerance in a single-cylinder engine with two different compression ratio and load settings. They used both natural gas and gasoline as main fuels. They pointed out that a small amount of hydrogen is required to stabilize the engine at its EGR limit, defined as 5% of IMEP variations. At this EGR limit, the engine becomes stable at 0.2% H_2 by volume of the fresh air in the case of gasoline, compared to the 0.4% of H_2 needed for natural gas. Tully and Heywood [14] found that for low dilution levels, the addition of hydrogen has a small reducing effect on the 0%-10% and 10%-90% combustion durations. This positive effect becomes more and more pronounced with the increase in dilution level. They also showed that hydrogen can extend the lean combustion limit since combustion deterioration occurs at a significantly higher dilution level when hydrogen is added. Similar conclusions on the increasingly positive effect of hydrogen addition with an increase in dilution level were reached in [15-20] in SI engines fuelled with different fractions of natural gas/gasoline-hydrogen mixtures and using different rates of EGR. Hu et al. [15, 16] deduced that the brake mean effective pressure decreases with an increase in the EGR rate and at small amounts of hydrogen addition (<20% in the fuel volume) but that it increases with a further increase in the hydrogen fraction. In the case of a high EGR rate (>10%), effective thermal efficiency increases while HC, CO and CO2 emissions decrease with the increase in hydrogen fraction. Finally they observed that the reducing effect of hydrogen on the combustion duration is more pronounced on the flame development duration (the interval from ignition start to the crank angle degree CAD at which 10% mass fraction burned is reached).

7.2.3 Hydrogen addition in lean-burn conditions

Bauer and Forest [21] tested a one-cylinder S.I. engine with mixtures of hydrogen in methane of 0, 20, 40 and 60% by volume. They found that when 60% of hydrogen in the mixture is used, the partial burn limit decreases from 0.58 for pure methane to 0.34. Akansu et al. [22] experimented mixtures of 0, 10, 20 and 30% of hydrogen by volume in methane in a four-cylinder SI engine and observed an increase in NO emission values with the increase in hydrogen percentage in the mixture. However, in the case of lean burn (equivalence ratio E.R.<0.75) the NO values obtained are low and the brake thermal efficiency values increase with the increase in the hydrogen fraction. Hoekstra et al. [23] investigated the lean limit of natural gas in a SI engine with hydrogen addition. They found that 28% and 36 % of hydrogen in volume yields very low NOx levels at a 0.625 Equivalence Ratio (E.R.). Moreover, the lean operating limit was significantly extended by increasing the hydrogen amounts in the case of natural gas as fuel [20, 24] or gasoline [25, 26].

All these studies are based on the assessment of global performance and pollutant emissions. Only a few studies have focused on the initial stages of flame propagation, such as Herweg and Maly [27] who developed a 1D model for flame kernel formation in S.I. engines. Conte and Boulouchos [28] carried out experiments by using an optical spark plug and ion sensors to study the flame propagation of gasoline mixtures enriched with reformer gas. Experiments on optical engines were also done by Meier et al. [29] and Rosati and Aleiferis [30] in a hydrogen direct injection SI engine. Aleiferis et al. [31, 32] investigated the early flame development in a single-cylinder engine equipped with an optical access and fuelled with gasoline in lean-burn conditions. However, there is a lack of optical experimental investigations on the effect of hydrogen addition on diluted or lean conditions in a S.I. engine fuelled with methane or iso-octane.

The objective of this study is to provide new data on the initial stages of flame propagation in a S.I. engine fuelled mainly with iso-octane or methane and operating in diluted (with nitrogen) or lean conditions with different hydrogen fractions in the fuel.

7.3 Experimental details

7.3.1 Optical Engine

The 'transparent' mono-cylinder S.I. engine used to perform the experiments has a four-valve pent-roof chamber with a displacement volume of 500 cm3 and a compression ratio of 9.5 [33]. The bore, stroke and connecting rod length are respectively 88 mm, 82 mm and 137 mm. To provide optical access inside the combustion chamber, the piston is elongated and equipped with a quartz window (diameter 66 mm). The cylinder head is bored and has two lateral windows. The optical access engine is driven by an electric motor at a fixed regime. A schematic view of the set-up is presented in Figure 1. The engine is equipped with an optical encoder mounted on the main shaft, giving 0.1 Crank Angle Degree (CAD) resolution. A conventional spark plug with an electrode' spacing of 1mm was used. The engine is fired every sixth cycle to avoid residual gases and keep the equivalence ratio inside the cylinder constant. A timer card ensures synchronization of the various trigger signals to images and data acquisition systems. The engine sucks the air through a thermal mass flow-meter and all other flows are evaluated from this reference flow. Methane, hydrogen and nitrogen flows are measured using thermal mass flow-meters with an accuracy of ±0.7% for the instantaneous flow. Before the intake pipe, all gases pass through a plenum, to avoid pressure oscillations inside the intake port. To have a premixed mixture in the intake pipe, 4 injections per cycle were done in the case of iso-octane as fuel. The iso-octane quantity was measured by using a 0-5 kg/h Bronkhorst Coriolis mass flow meter with an accuracy of ±0.1% of full scale plus ±0.2% of flow rate.

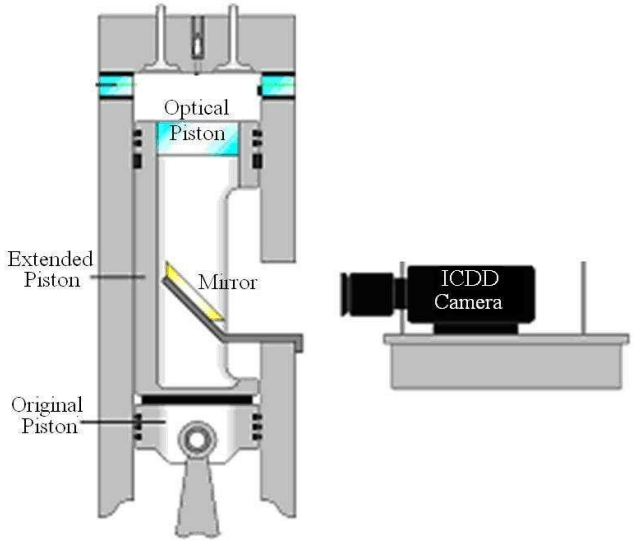

Figure 1. *Schematic view of the set-up.*

Cylinder pressure was recorded with a water-cooled AVL quartz pressure traducer connected to a charge amplifier at 0.1 CAD resolution. Before experiments, the traducer was calibrated with a Keller high pressure hydraulic calibrator. The linearity (<±0.6%) of the traducer was verified starting from a maximum pressure of 10MPa (>maximum pressure in the engine). In this work, the absolute cylinder pressure was deduced by equalizing the in-cylinder pressure at 20 CAD after inlet valve opening timing to the intake mean absolute pressure. Thus, 100 consecutive ‘’fired’’ cycles of cylinder pressure data are acquired by a PC equipped with National Instruments acquisition board.

7.3.2 High speed image acquisition

Images of flame radiation were acquired through a 45°mirror mounted in the piston extension and with an APX-i2 intensified camera coupled with a 85 mm, f/1.4 Nikon lens. The frame resolution was 512x512 pixels² at 6000 frames per second. The magnification ratio was 0.159 mm/pixel. The gain was fixed at 3.7 V, with a gate width of a few micro-seconds, which is a compromise between radiation intensity and noise amplification. The initial combustion stage (from the spark to the maximum optical area) capture varies between 15 and 30 images depending on considered conditions (Equivalence Ratio, mixture composition and engine regime). The projected flame area, A_f was determined by using post-processing in Matlab after binarization and thresholding. Images including at least one pixel having 1 as a value (which corresponds to the luminous flame zone) and characterized by a distant ≥200 pixel (the radius of the quartz window is 208 pixels which corresponds to 33mm) from the image center (the center of the quartz window) were not considered (image processing criterion). Thus the maximum luminous area $A_{f\max}$ in this study was 3165 mm2.

7.3.3 Operating conditions

The engine regimes were 1200 and 2000 rpm. The oil and coolant temperatures are set at 80°C. The intake pressure was set at 0.1MPa. The spark ignition was set at 30 CAD Before Top Dead Center (BTDC) for iso-octane mixtures and 25 CAD BTDC for methane mixtures in order to compare the initial stages of flame propagation at the same in-cylinder pressure and temperature values. The amount of hydrogen in the fuel was 0%, 20%, 40% and 60% by volume and the amount of dilution in the total mixture was 0% and 20% by volume. Both stoichiometric and lean conditions (E.R. = 0.8) were investigated. The different mixtures investigated are summarized in Tables 1.a, 1.b, 1.c and 1.d. Hydrogen contents in the fuel in term of mass percentage γ and energy percentage E_{H_2} are also reported in Tables 1.a, 1.b, 1.c and 1.d. For all results, the parameter α is defined as the mole fraction of hydrogen in the fuel (iso-octane or methane)-hydrogen blend:

$$\alpha = \frac{X_{H_2}}{X_{C_xH_y} + X_{H_2}} \quad (1)$$

And the parameter of dilution β is the mole fraction of nitrogen used for dilution in the total mixture:

$$\beta = \frac{X_{N_2-dilution}}{X_{CxHy} + X_{H_2} + X_{O_2} + X_{N_2-air} + X_{N_2-dilution}} = X_{N_2-dilution} \quad (2)$$

Where $X_{C_xH_y}$, X_{H_2} and X_{O_2} are respectively iso-octane or methane, hydrogen and dioxygen mole fractions in the mixture, X_{N_2-air} the mole fraction of nitrogen in the air mixture ($X_{N_2-air} = 3.78 \bullet X_{O_2}$) and $X_{N_2-dilution}$ the mole fraction of nitrogen used for dilution.

7.4 Results and discussion

7.4.1 Correlations

The frame acquisition rate, 6000 frames/second, induces 1 image every 1.2 CAD and 2° CA at respectively 1200 and 2000 rpm. Examples of the flame evolution are given in Figure 2.a for the C_8H_{18}-air mixture (Condition 4) and Figure 2.b for the C_8H_{18}-H_2-air-N_2 mixture (Condition 11) at stoichiometry. Δt_s is the time after spark ignition.

The flame propagation velocity is higher for the Condition 4 mixture than for Condition 11. The projected flame surface A_f was normalized with respect $A_{f\max}$:

$$A_{norm} = \frac{A_f}{A_{f\,\max}} \quad (3)$$

The evolution of A_{norm} versus the CAD was fitted with a fourth degree polynomial in order to obtain, for a fixed A_{norm}, the corresponding CAD or Δt_s. The CAD corresponding to a defined value of A_{norm}, for example 0.1 and 0.5, respectively called $\theta_{0.1}$ and $\theta_{0.5}$, was plotted versus the CA50 (corresponding to 50% of the accumulated heat release) in order to verify the image quality, the correct post-processing and the validity of the 2-D flame projected approach.

An example for CH_4-air-N_2 (condition 17) is shown in Figure 3. In this case, $\theta_{0.5}$ corresponds to 6% of total heat release, while for $\theta_{0.1}$ the cumulated heat release was <1% of the total heat release. In Figure 3, the CAD = 0 corresponds to the Top Dead Center position. High correlation coefficients were found for all values of A_{norm}, thus confirming that in S.I. engines, the combustion development depends strongly on the initial stages of flame propagation.

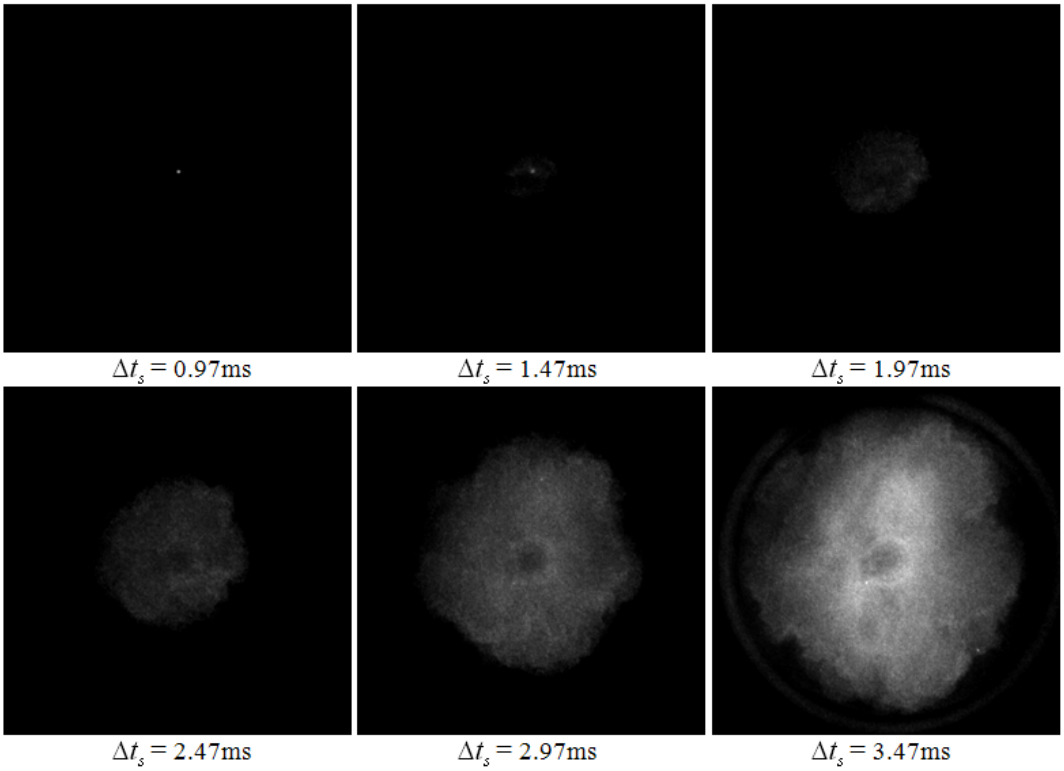

Figure 2.a *Flame evolution (condition 4).*

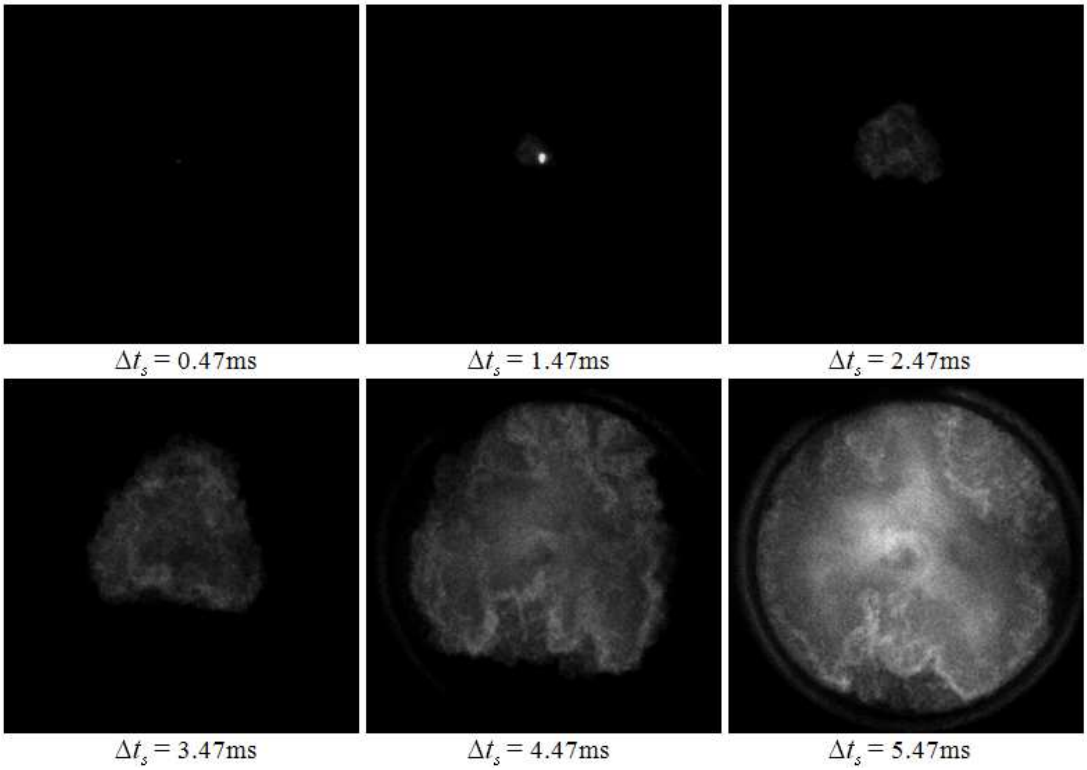

Figure 2.b *Flame evolution (condition 11).*

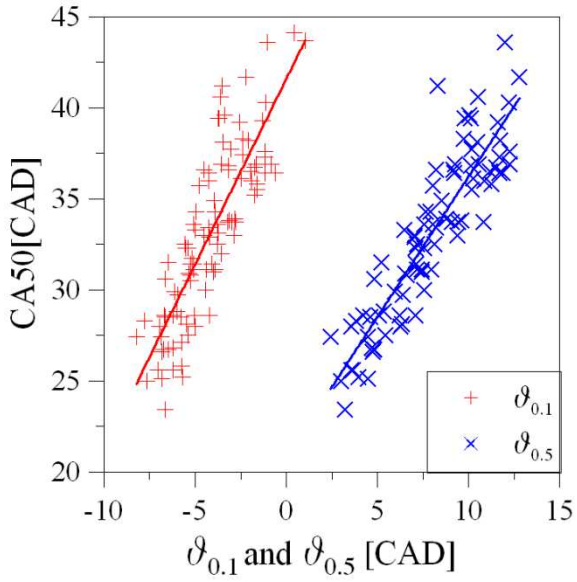

Figure 3. *$\theta_{0.1}$ and $\theta_{0.5}$ versus the CA50 (condition 17).*

The correlation coefficients between $\theta_{0.1}$, $\theta_{0.5}$ and CA50 ($Corr_{\theta 0.1-CA50}$ and $Corr_{\theta 0.5-CA50}$) are reported in Tables 1.a, 1.b, 1.c and 1.d for all cases. As expected, these correlation coefficients were found to be higher when the defined A_{norm} is 0.5 rather than 0.1 and were not dependent on the mixture composition, thus no effect of hydrogen addition or nitrogen dilution was observed.

In this study, the minimum of the equivalent flame radius r_f, determined by assuming a spherical shape was 10 mm (A_{norm} = 0.1). As Herweg and Maly [27], Natarajan et al. [34] and Bradley et al. [35] indicated, no influence of the spark on the flame growth can be considered: this is confirmed by the strong correlation found between $\theta_{0.1}$ and CA50. The CAD corresponding to the defined value of A_{norm}, from 0.1 to 0.9, i.e. θ_i (i = 0.1…0.9) were found to correlate well with the maximum of the cylinder pressure, $P_{\max}$ and the CAD corresponding to this maximum, for all investigated conditions (Tables 1.a, 1.b, 1.c and 1.d). The mean value of the correlation coefficients, called $Corr_{\theta 0.5-P\max}$ and $Corr_{\theta 0.5-\theta P\max}$, are respectively 0.86 and 0.88 except for four investigated conditions. For the stoichiometric mixtures, i.e. Conditions 3, 17 and 23, $Corr_{\theta 0.5-\theta P\max}$ has negative values, and, for condition 5, a low positive value, 0.225. These different values are linked to the spark ignition timing.

The correlation coefficients $Corr_{\theta 0.5-IMEP}$ between $\theta_{0.5}$ and the IMEP present both negative and positive values. These values with the corresponding percentage of cumulated heat release of $\theta_{0.5}$ ($Cum_{\theta_{0.5}}$) are reported in Tables 1.a, 1.b, 1.c and 1.d. It can be seen that all conditions with nitrogen dilution or lean mixtures and without hydrogen addition are characterized by negative values of $Corr_{\theta 0.5-IMEP}$. This behavior is expected, since for these conditions, the burning velocities are lower than for the other conditions while the spark ignition timing is the same. Finally, ignition occurs close to the spark timing, giving the maximum brake torque for conditions with low absolute values of $Corr_{\theta 0.5-IMEP}$ (conditions 2 and 15). This fact reflects the stability of the IMEP since a small fluctuation in the initial stage of flame propagation does not strongly affect IMEP values. Aleiferis et al. [31] did not find a correlation between CAD5 and IMEP for stoichiometric C_8H_{18}-air conditions in a stratified-charge SI engine for two spark advances. However, they found a strong correlation between CAD5 (corresponding to 5% of the accumulated heat release) and IMEP, characterized by a negative value of the correlation coefficient, for lean C_8H_{18}-air conditions.

7.4.2 Flame evolution

A criterion of the beginning of flame propagation was chosen at A_{norm} = 0.1 because the flame is no longer affected by the ignition energy and for all investigated conditions, till A_{norm} ~ 0.2, a small heat release was observed (<1%). The maximum value of A_{norm} considered in the following is A_{norm} = 0.6 since it is reached in all conditions and is sufficient for our purposes, since this work focuses on the initial stages of flame propagation. As can be seen in Tables 1.a, 1.b, 1.c and 1.d, the value A_{norm} = 0.5 corresponds to a percentage of the cumulated heat release higher than 5% in all investigated conditions. In this study the reported data are averaged data on 100 cycles for each condition.

I. C_8H_{18}-H_2-air-N_2 mixtures, E.R.= 1 at 2000 RPM (conditions 1- 3)

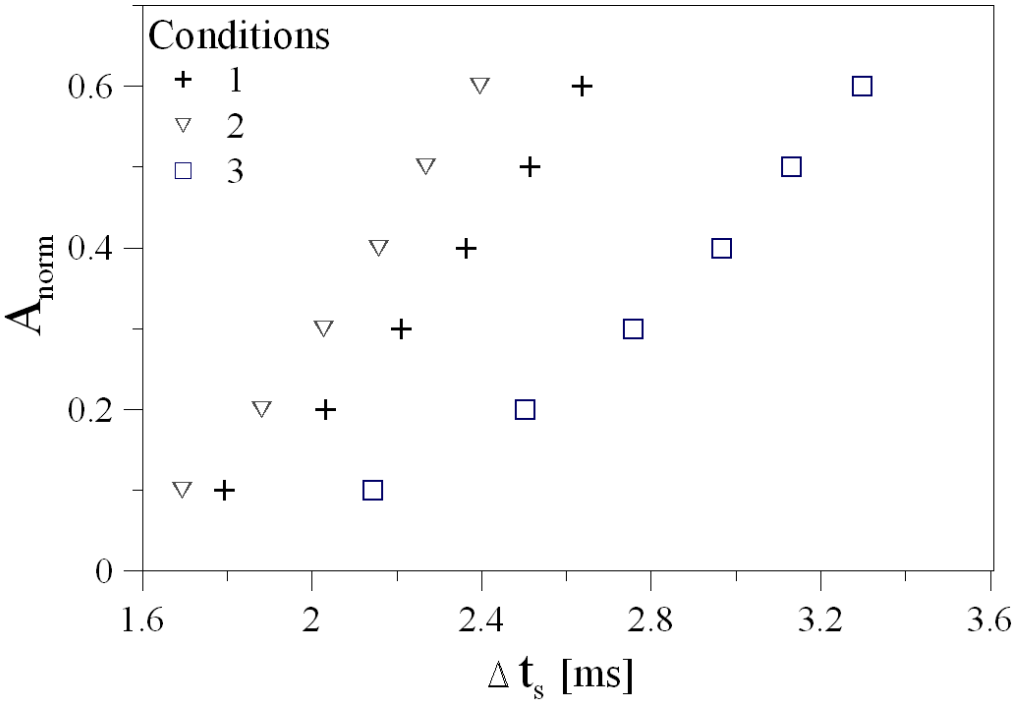

Figure 4.a *Temporal evolution of* A_{norm} *(conditions 1-3).*

Figure 4.a presents the temporal evolution of A_{norm} for C_8H_{18}-H_2-air-N_2 mixtures, E.R. = 1 at 2000 rpm. The flame reaches A_{norm} = 0.1 after 1.79 ms, 1.69 ms and 2.14 ms for conditions 1, 2 and 3 respectively. The effect of hydrogen addition is evident from the beginning: its accelerating effect increases with the flame growth. Nitrogen dilution has the opposite effect on the flame growth. The difference ϕ_i, at a given A_{norm} is defined as:

$$\phi_i\,[ms] = \Delta t_{s\_i} - \Delta t_{s\_ref} \quad (4)$$

Where i refers to the number of the condition (referred in Tables 1.a, 1.b, 1.c and 1.d) and ref, the reference conditions, (condition 1 in this section). ϕ_2 and ϕ_3, plotted versus A_{norm} in Figure 4.b present an opposite trend. However, the effect of 20% of nitrogen dilution is more pronounced than the effect of 60% of hydrogen addition in the fuel. At A_{norm} = 0.5 for example, flame propagation in the reference Condition is 9.7% slower than that in Condition 2, and 24.5% faster than that in Condition 3. Moreover, this difference in terms of time of flame propagation becomes 13.1% slower (than condition 2) and 48.9% faster (than condition 3) at CA50.

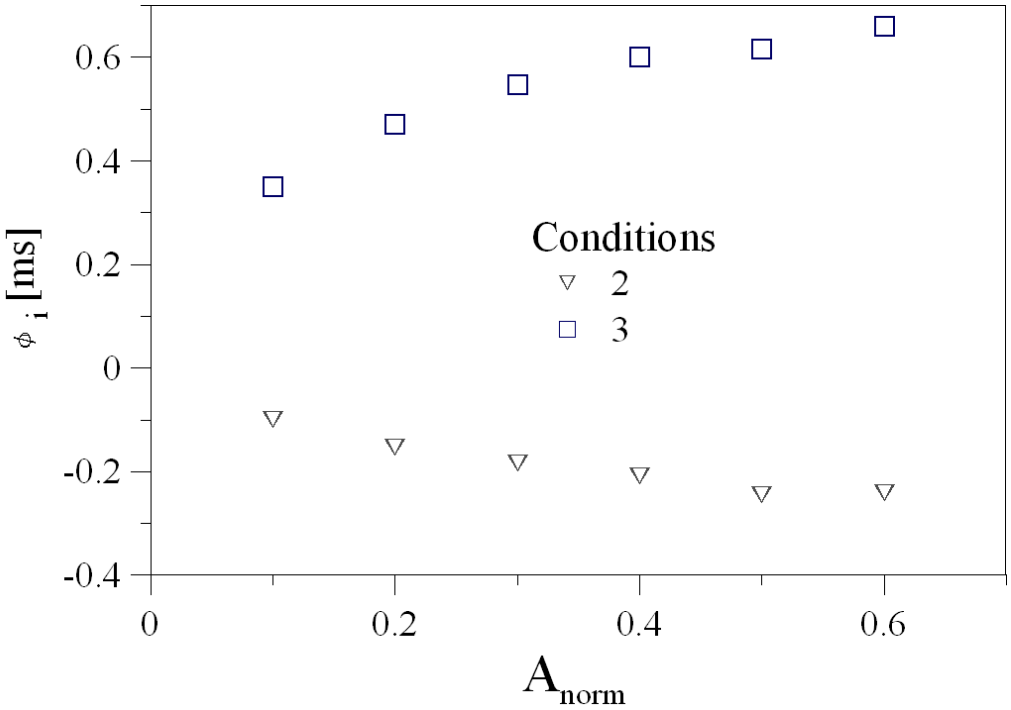

Figure 4.b *ϕ_i versus A_{norm} (conditions 1-3).*

Table 1.a *Investigated conditions (2000 rpm, E.R.=1)*

Mixture	C_8H_{18}-air	C_8H_{18}-H_2-air	C_8H_{18}-H_2-air-N_2
Condition	1	2	3
E.R.	1	1	1
α	0	0.6	0.6
β	0	0	0.2
γ [%]	0	2.6	2.6
E_{H_2} [%]	0	6.7	6.7
$Corr_{\theta 0.1-CA50}$	0.88	0.72	0.86
$Corr_{\theta 0.5-CA50}$	0.92	0.84	0.93
$Corr_{\theta 0.5-IMEP}$	-0.31	0.03	-0.85
$Cum_{\theta 0.5}$ [%]	10.7	12.8	6.3
$Corr_{\theta 0.5-P\max}$	-0.86	-0.76	-0.93
$Corr_{\theta 0.5-\theta P\max}$	0.91	0.79	-0.37

The enhancement effect of hydrogen on the combustion rate is therefore greater in the initial stages of flame propagation than in the later stages, whereas the effect of dilution remains high in later stages.

II. C_8H_{18}-H_2-air-N_2 mixtures, E.R.= 1 at 1200 RPM (conditions 4-11)

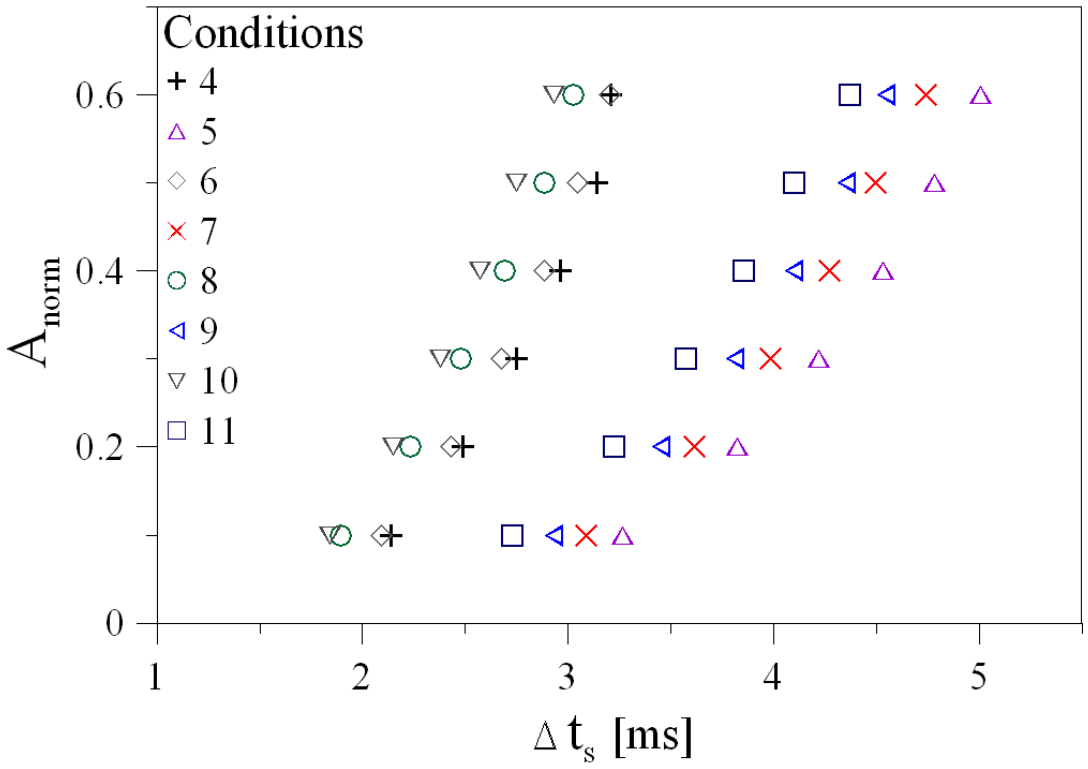

Figure 5.a *Temporal evolution of* A_{norm} *(conditions 4-11).*

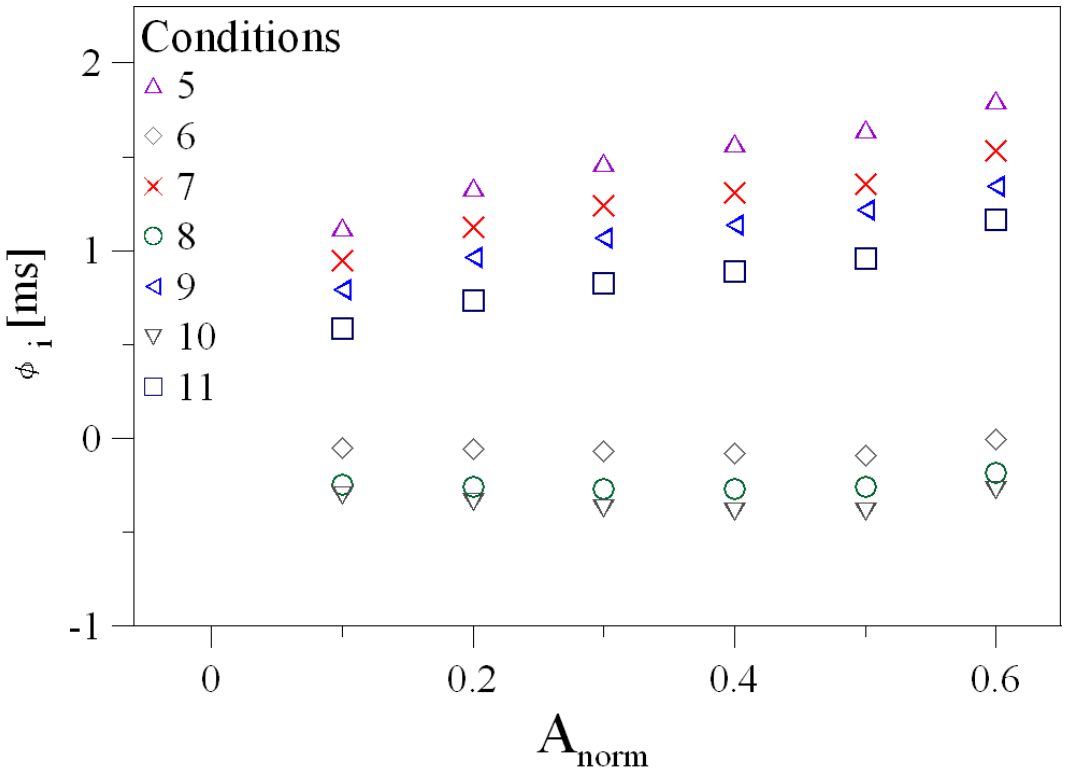

Figure 5.b ϕ_i *versus* A_{norm} *(conditions 4-11).*

Similar to Figure 4.a and Figure 4.b, the temporal evolution of A_{norm} and the evolution of ϕ_i versus A_{norm}, are plotted in Figure 5.a and Figure 5.b respectively. The reference for the calculation of ϕ_i in this section was Condition 4 (C_8H_{18}- air).

A clear difference between the conditions with and without dilution is observed. For A_{norm} = 0.5, ϕ_5 = 1.64 ms, ϕ_{10} = -0.39 ms and ϕ_{11} = 0.96 ms inducing a relative difference in percentage of respectively 52.4%, -12.45% and 30.6% with respect to the reference case (condition 4).

These relative differences become 73.32%, -12.1% and 42.1% respectively at CA50. Coherent conclusions are reached in this case for all conditions: the accelerating effect of hydrogen is mainly during the initial stage while dilution has a more prolonged decelerating effect. In addition, the accelerating effect of hydrogen, at late stages, increases with the dilution amount.

Table 1.b *Investigated conditions (1200 rpm, E.R.=1)*

Mixture	C_8H_{18}-air	C_8H_{18}-N_2-air	C_8H_{18}-H_2-air	C_8H_{18}-H_2-air-N_2	C_8H_{18}-H_2-air	C_8H_{18}-H_2-air-N_2	C_8H_{18}-H_2-air	C_8H_{18}-H_2-air-N_2
Condition	4	5	6	7	8	9	10	11
E.R.	1	1	1	1	1	1	1	1
α	0	0	0.2	0.2	0.4	0.4	0.6	0.6
β	0	0.2	0	0.2	0	0.2	0	0.2
γ [%]	0	0	0.4	0.4	1.2	1.2	2.6	2.6
E_{H_2} [%]	0	0	1.2	1.2	3.1	3.1	6.7	6.7
$Corr_{\theta 0.1-CA50}$	0.87	0.89	0.9	0.87	0.85	0.88	0.88	0.89
$Corr_{\theta 0.5-CA50}$	0.93	0.92	0.96	0.94	0.94	0.92	0.93	0.96
$Corr_{\theta 0.5-IMEP}$	0.75	-0.85	0.65	-0.81	0.82	-0.73	0.69	-0.54
$Cum_{\theta 0.5}$ [%]	7.6	6.1	7.1	6.3	6.8	5.6	6.7	6.7
$Corr_{\theta 0.5-P\max}$	-0.81	-0.91	-0.81	-0.92	-0.87	-0.91	-0.76	-0.94
$Corr_{\theta 0.5-\theta P\max}$	0.9	0.22	0.88	0.85	0.9	0.91	0.88	0.96

III. C_8H_{18}-H_2-air-N_2 mixtures, E.R.= 0.8 at 1200 RPM (conditions 12-15)

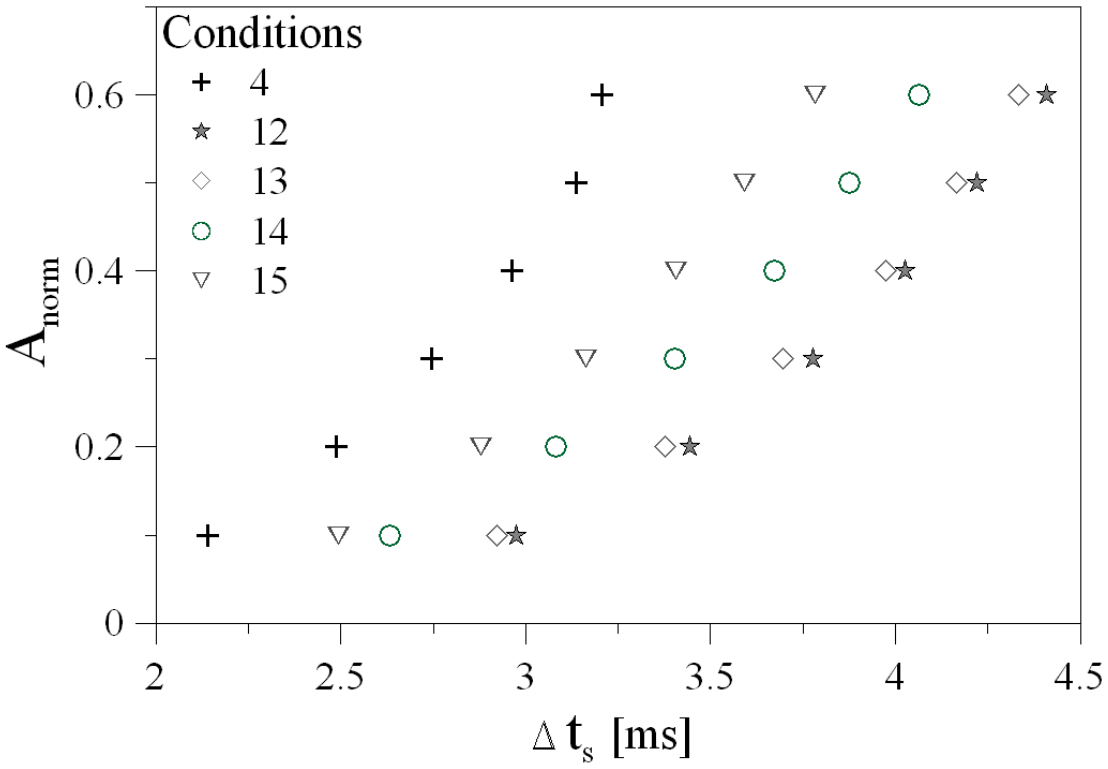

Figure 6.a *Temporal evolution of* A_{norm} *(conditions 12-15).*

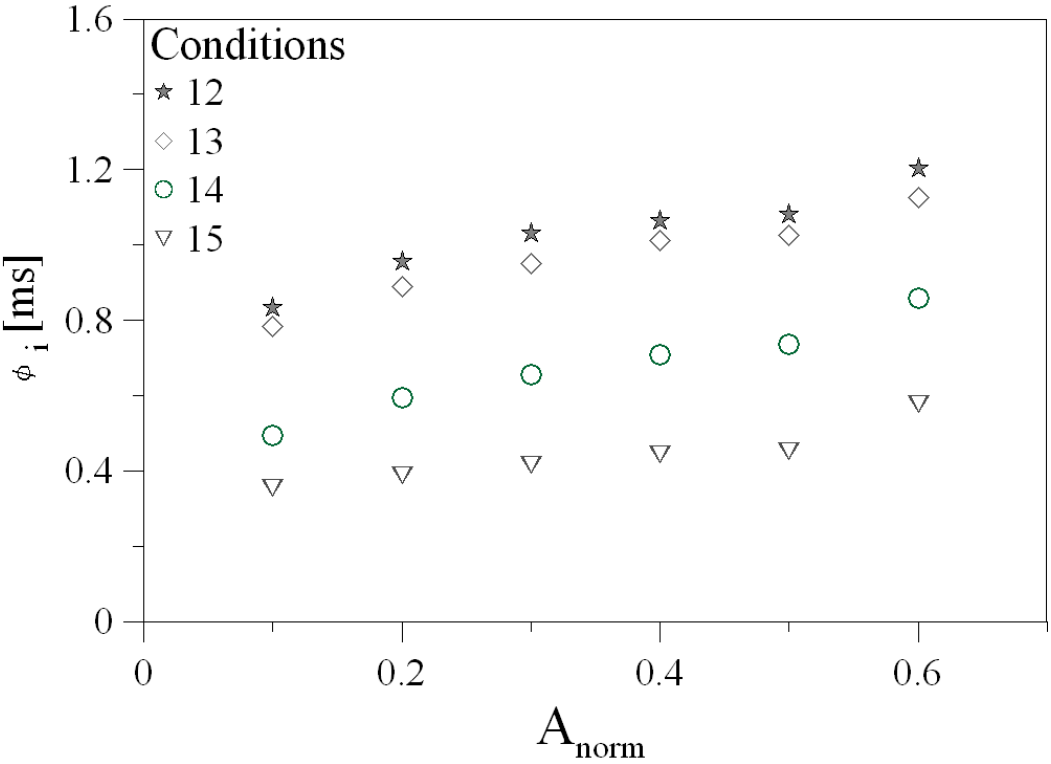

Figure 6.b ϕ_i *versus* A_{norm} *(conditions 12-15).*

The reference condition used to estimate ϕ_i is Condition 4 in this section. For A_{norm} = 0.5, the relative difference is 34.5% and 14.4% for conditions 12 and 15 respectively. Thus, Figure 6.a and Figure 6.b present the temporal evolutions of A_{norm} and the evolution of ϕ_i versus A_{norm} for these conditions. At 1200 rpm, the effect of 20% of nitrogen dilution is greater than the effect of lean combustion (E.R. = 0.8) on the initial stages of flame propagation. Furthermore the accelerating effect of hydrogen is more pronounced than in the case of dilution at later stages (CA50) since the relative differences become 27.14% and only 2.19% for conditions 12 and 15 respectively, at CA50. Thus for lean conditions, the accelerating effect of hydrogen increases during combustion and proved to be very marked in the late stages of combustion (CA50).

Table 1.c *Investigated conditions (1200 rpm, E.R.=0.8)*

Mixture	C_8H_{18}-air	C_8H_{18}-N_2-air	C_8H_{18}-H_2-air	C_8H_{18}-H_2-air-N_2
Condition	12	13	14	15
E.R.	0.8	0.8	0.8	0.8
α	0	0.2	0.4	0.6
β	0	0	0	0
γ[%]	0	0.4	1.2	2.6
E_{H_2} [%]	0	1.2	3.1	6.7
$Corr_{\theta 0.1-CA50}$	0.86	0.89	0.89	0.89
$Corr_{\theta 0.5-CA50}$	0.94	0.91	0.96	0.94
$Corr_{\theta 0.5-IMEP}$	-0.55	-0.38	-0.5	0.19
$Cum_{\theta 0.5}$ [%]	6.2	6.3	6.3	7.5
$Corr_{\theta 0.5-P\max}$	-0.91	-0.87	-0.92	-0.88
$Corr_{\theta 0.5-\theta P\max}$	0.9	0.9	0.95	0.93

IV. CH_4-H_2-air-N_2 mixtures, E.R.= 1 at 1200 RPM (conditions 16-23)

In this section, the reference condition is Condition 16. Unlike the conditions considered in section II, conditions with dilution and hydrogen addition are close to the reference conditions (16) when the temporal evolution of A_{norm} is plotted (Figure 7.a). This can be explained by the fact that in the case of methane as the main fuel, the same percentage of hydrogen addition by volume is more important in terms of mass or energy than in the case of iso-octane as reported in Tables 1.a, 1.b, 1.c and 1.d. As shown in Figure 7.b, for a small amount of hydrogen (20%) and without dilution (Condition 18), the effect of hydrogen in terms of ϕ_{18} is almost constant in the initial stages of flame propagation.

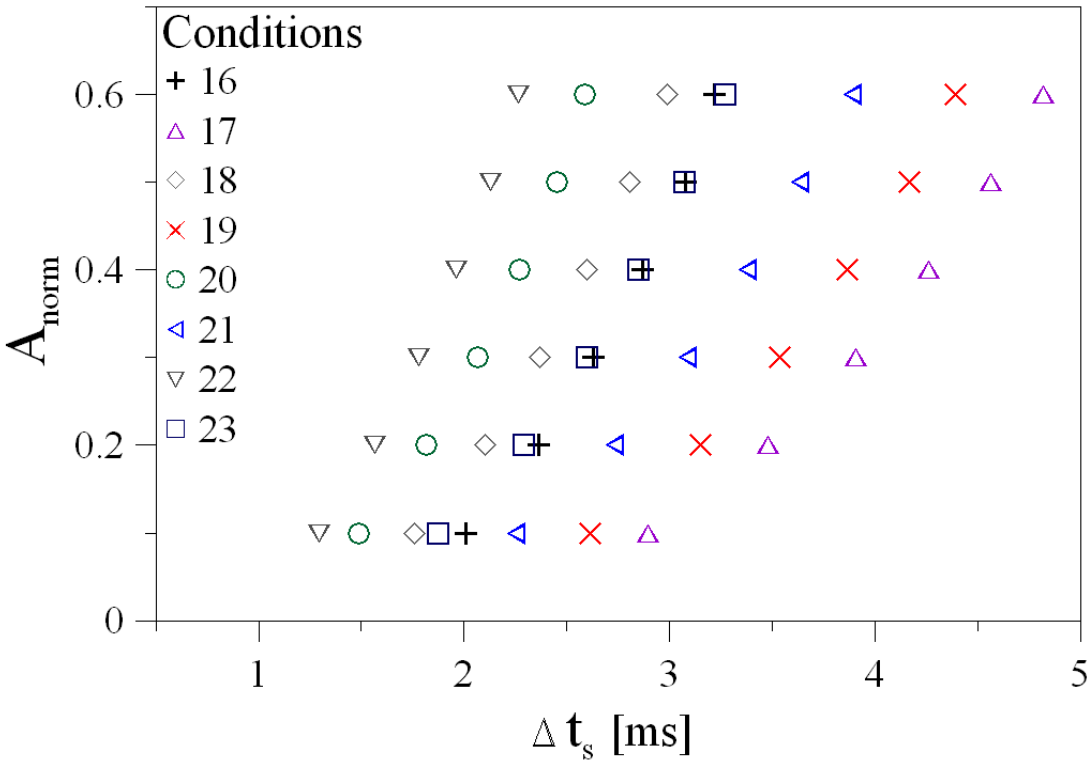

Figure 7.a *Temporal evolution of* A_{norm} *(conditions 16-23).*

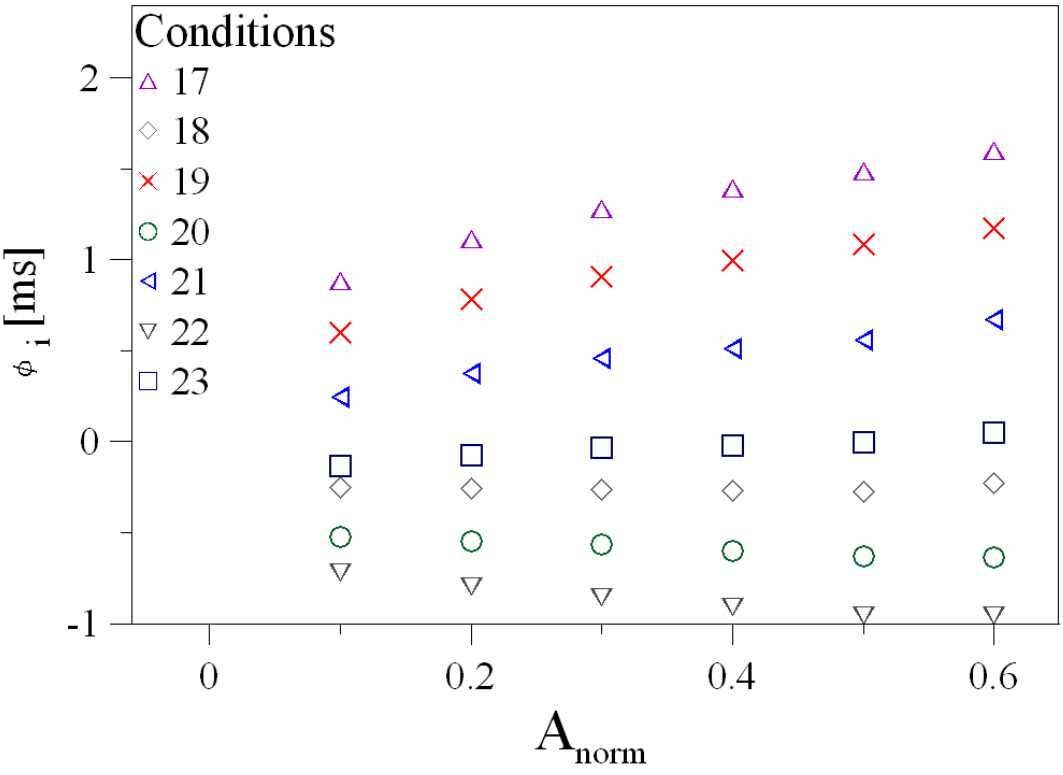

Figure 7.b ϕ_i *versus* A_{norm} *(conditions 16-23).*

Thus, even when methane is used as the main fuel, the accelerating effect of hydrogen is almost on the initial stages when there is no dilution and increases in the later stages for conditions with dilution. For example considering Condition 22, the relative difference is -30.95% for A_{norm} = 0.5 and becomes -34.2% for CA50, while the effect of dilution remains important even in late stages of flame propagation (CA50).

It is very interesting to consider the behaviour of Condition 23 since the graph of these conditions (with 60% of hydrogen in the fuel mixture and 20% of nitrogen dilution) is superposed to the graph corresponding to the reference conditions, i.e, without dilution and hydrogen addition. Thus 60% of hydrogen addition is needed to compensate for the effect of 20% of nitrogen dilution, which is in very good agreement with the laminar burning velocity results [36] since 60% of hydrogen addition was needed in the case of 20% of nitrogen dilution to obtain the same burning velocity (32cm/s) as in the case of methane-air mixture without dilution (33.96cm/s).

Table 1.d *Investigated conditions (1200 rpm, E.R.=1)*

Mixture	CH_4-air	CH_4-N_2-air	CH_4-H_2-air	CH_4-H_2-air-N_2	CH_4-H_2-air	CH_4-H_2-air-N_2	CH_4-H_2-air	CH_4-H_2-air-N_2
Condition	16	17	18	19	20	21	22	23
E.R.	1	1	1	1	1	1	1	1
α	0	0	0.2	0.2	0.4	0.4	0.6	0.6
β	0	0.2	0	0.2	0	0.2	0	0.2
γ [%]	0	0	3	3	7.7	7.7	15.9	15.9
E_{H_2} [%]	0	0	7	7	17	17	31	31
$Corr_{\theta 0.1-CA50}$	0.83	0.84	0.85	0.86	0.8	0.84	0.65	0.78
$Corr_{\theta 0.5-CA50}$	0.91	0.9	0.93	0.95	0.88	0.95	0.82	0.9
$Corr_{\theta 0.5-IMEP}$	0.63	-0.87	0.87	-0.9	0.8	-0.69	0.7	0.56
$Cum_{\theta 0.5}$ [%]	8.7	6	9.1	6.7	8.2	6.9	9.6	7.6
$Corr_{\theta 0.5-P\max}$	-0.82	-0.94	-0.87	-0.93	-0.77	-0.94	-0.64	-0.86
$Corr_{\theta 0.5-\theta P\max}$	0.89	-0.78	0.91	-0.54	0.85	0.82	0.77	0.87

The main conclusion concerning flame evolution is that the positive (enhancement) effect of hydrogen becomes more noticeable and stronger under lean and diluted conditions, which is in very good agreement with the conclusions obtained in [14-22]. Furthermore, it was found that for mixtures with stoichiometric conditions, the effect of hydrogen on the flame development is more pronounced in the initial stages than in the late stages of combustion (CA50), which is consistent with the results reported in [5, 16].

7.4.3 Correlation between Flame evolution and laminar burning velocity

I. Methane as main fuel

S_L is the laminar burning velocity at atmospheric pressure and ambient temperature for the mixture conditions 16-23. S_{L-ref} is the S_L for the stoichiometric methane-air conditions. The values of S_L are given by a correlation based on experimental results presented in a recent study [36]. A dimensionless difference ΔS_L is defined as:

$$\Delta S_L = \left(\frac{S_L - S_{L-ref}}{S_{L-ref}} \right) \quad (5)$$

Another dimensionless parameter ψ_i is also defined as:

$$\psi_i = \frac{\left[\left(\phi_i \; at \; A_{norm} = 0.5 \right) - \left(\phi_i \; at \; A_{norm} = 0.1 \right) \right] - \left[\left(\Delta t_{s-ref} \; at \; A_{norm} = 0.5 \right) - \left(\Delta t_{s-ref} \; at \; A_{norm} = 0.1 \right) \right]}{\left[\left(\Delta t_{s-ref} \; at \; A_{norm} = 0.5 \right) - \left(\Delta t_{s-ref} \; at \; A_{norm} = 0.1 \right) \right]} \quad (6)$$

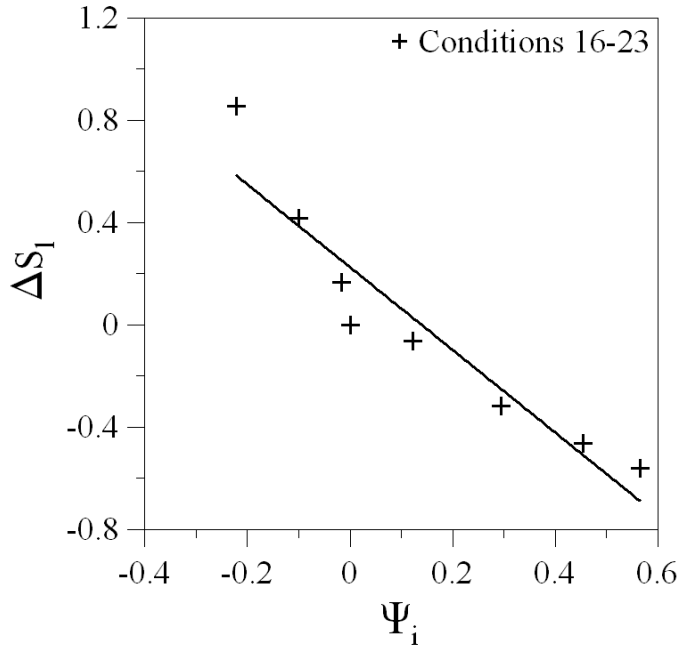

Figure 8. *Ψ_i versus ΔS_L (main fuel: methane).*

In Figure 8, ψ_i was plotted versus ΔS_L: a very good correlation is found (correlation coefficient = -0.95). Thus the point made above, concerning the coherence between the initial stages of flame propagation in S.I. engines and the laminar burning velocity data for Conditions 16 and 23, is valid for all conditions. It is clear that during the combustion

development inside the SI engine, the pressure and temperature values are not atmospheric conditions. However, as the spark ignition timing was the same for all conditions (16-23) and only the initial stages of flame propagation are considered, the pressure and temperature ranges are the same for all conditions. Moreover if we consider that the laminar burning velocity varies with pressure and temperature in the same way for all mixtures (conditions 16-23), this strong correlation found between laminar burning velocities at atmospheric conditions and the initial stages of flame propagation in the engine can be explained. The initial stages of flame propagation (considering the same range of thermodynamic conditions) are therefore directly correlated with the mixture composition.

II. Iso-octane as main fuel

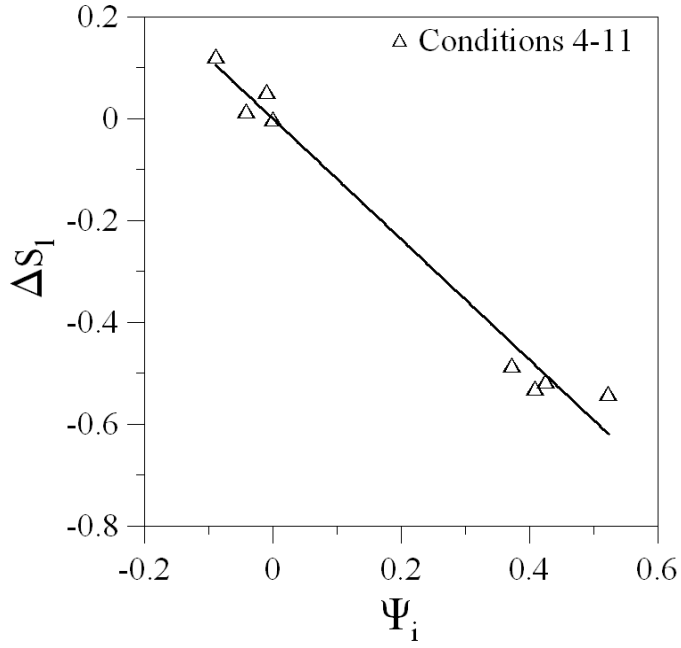

Figure 9. *Ψ_i versus ΔS_L (main fuel: iso-octane).*

Similar to the methane case, ΔS_L for C_8H_{18} mixtures (Conditions 4-11) and ψ_i (with Condition 4 as the reference) were calculated. The laminar burning velocities for these mixtures resulted from the adiabatic flame calculation with Premix [37] and based on the high temperature mechanism proposed by Jerzembeck et al. [38].

A very high correlation coefficient (-0.99) was also found, as shown in Figure 9. This high correlation coefficient value does not necessarily imply a better correlation than in the case of conditions with methane as the main fuel since the points representing the conditions (5, 7, 9 and 11) with dilution are distant from the points representing conditions without dilution (4, 6, 8 and 10). Thus no accurate conclusions can be drawn in this section.

7.4.4 Standard deviations

The standard deviations for $\theta_{0.5}$ $\left(std_{\theta_{0.5}}\right)$ and CA50 $\left(std_{CA50}\right)$ as a function of α, the volume amount of hydrogen are plotted in figure 10.a, 10.b and 10.c for conditions 4-11, 12-15 and 16-23 respectively.

For Conditions 4-11, $std_{\theta_{0.5}}$ is not affected by hydrogen addition while std_{CA50} decreases for higher fractions of hydrogen. This decrease is more noticeable for conditions with dilution: for example, with $\alpha = 0.6$ and $\beta = 0$, it decreases by 23% compared to 29% for diluted conditions ($\beta = 0.2$).

For lean conditions (Figure 10.b), $std_{\theta_{0.5}}$ is not affected by hydrogen addition while std_{CA50} decreases (by 20% with 60% of hydrogen addition) with the amount of hydrogen in the mixture.

For conditions with methane as the main fuel, the standard deviation is not influenced by hydrogen for small values of α (0.2) except, the std_{CA50} of Condition 19 with dilution since a small decrease (7% with respect to Condition 17) is observed.

For all other conditions, with $\alpha = 0.4$ and 0.6, a decrease in the standard deviation value is observed. In this case also, the decrease is greater for conditions with dilution (decreasing by 64% for std_{CA50} and by 41% for $std_{\theta_{0.5}}$ between Conditions 17 and 23) than for conditions without (decreasing by 46% and 35% for std_{CA50} and $std_{\theta_{0.5}}$ respectively when Condition 16 is compared to Condition 22).

It can be seen that Conditions 16 and 23 are characterized by highly similar values of standard deviations. Thus, adding 60% of hydrogen to the diluted conditions induces the same value of the standard deviation as that of the reference conditions without hydrogen and dilution (Condition 16).

This conclusion is coherent with those deduced in previous sections. Moreover, the general conclusion of this section is that the standard deviation increases with nitrogen dilution and the decreasing effect of hydrogen has a larger impact on later stages in combustion (CA50) than on the initial stages of flame propagation ($\theta_{0.5}$).

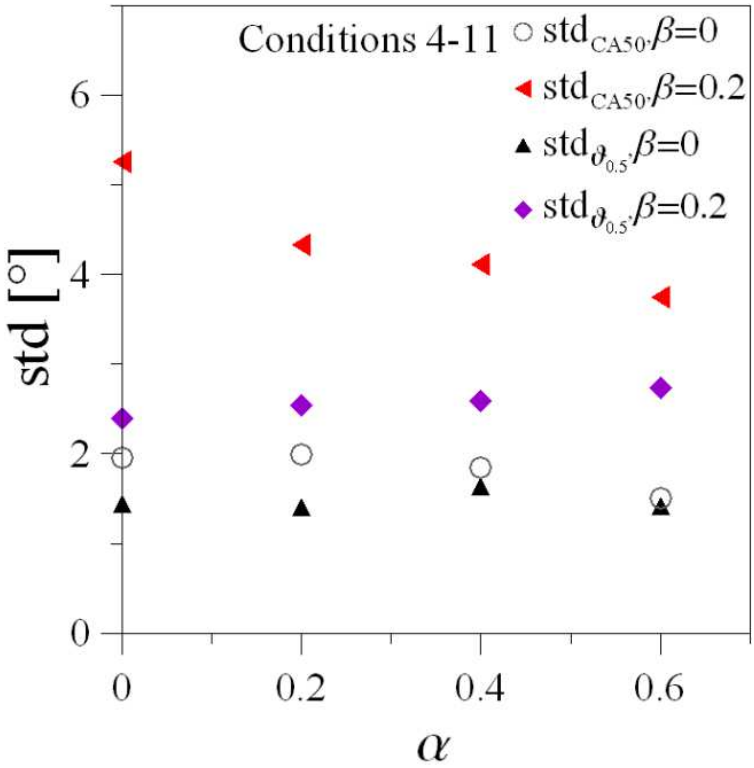

Figure 10.a *$std_{\theta_{0.5}}$ and std_{CA50} as a function of α (conditions 4-11).*

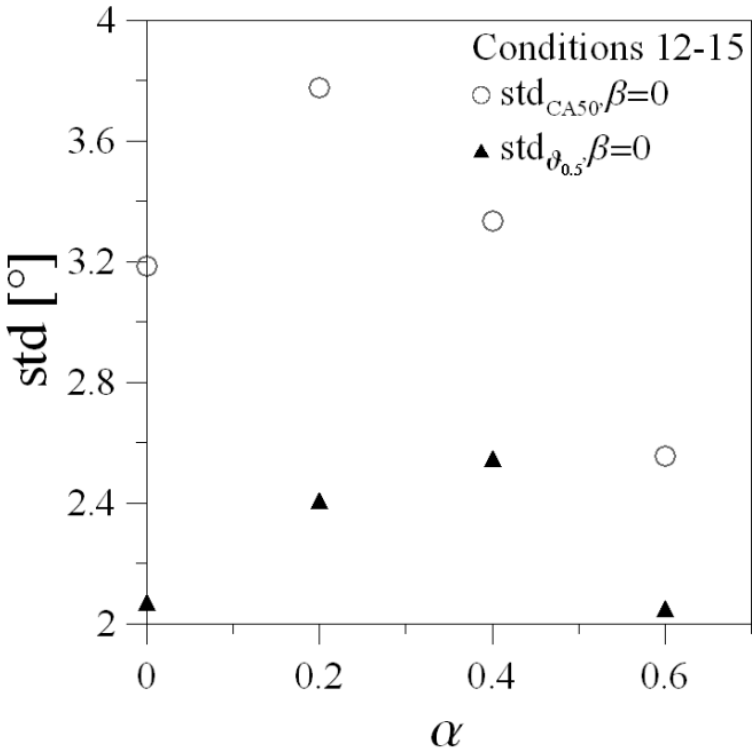

Figure 10.b *$std_{\theta_{0.5}}$ and std_{CA50} as a function of α (conditions 12-15).*

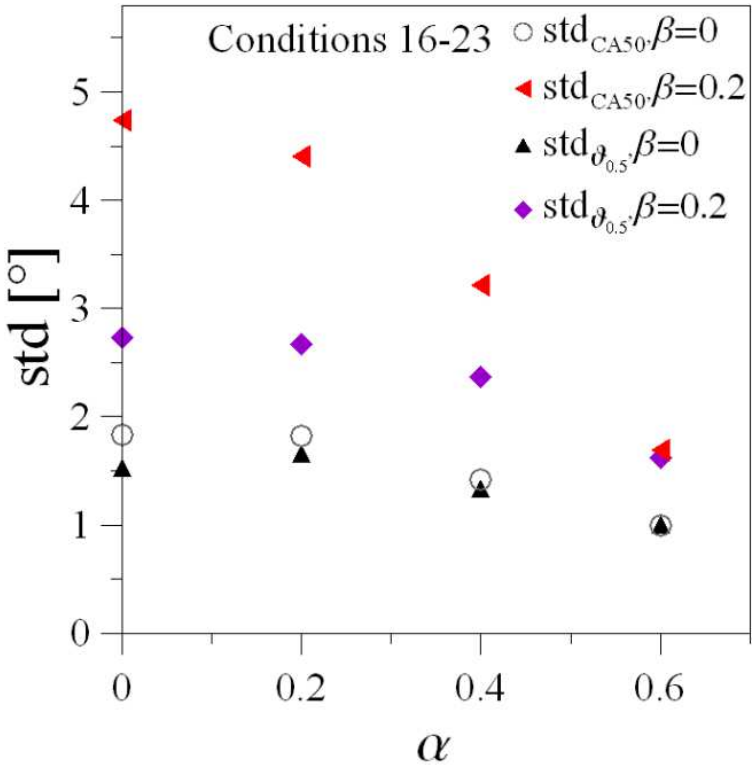

Figure 10.c *$std_{\theta_{0.5}}$ and std_{CA50} as a function of α (conditions 16-23).*

7.5 Conclusions

The initial flame stages in an optical SI engine were studied by using high speed image recording. The projected flame areas were deduced from the images acquired through the piston crown. The effects of hydrogen addition and nitrogen dilution on the methane-air and iso-octane-air mixtures under lean and stoichiometric conditions were investigated. The results obtained are summarized as follows:

- ✓ The CAD corresponding to a fixed value of projected flame area was found to correlate well with the CA50 calculated from in-cylinder pressure data. Thus in SI engines, the overall combustion depends strongly on the initial stages of flame propagation (when cumulated heat release is below 10%).
- ✓ The enhancement effect of hydrogen on the combustion duration is greater in the initial stages of flame propagation than in the later stages (CA50), while dilution has a more prolonged decelerating effect. Moreover, this positive effect of hydrogen, at late stages (CA50) increases with the dilution rate in the mixture.
- ✓ For lean conditions, the accelerating effect of hydrogen increases during combustion and becomes more pronounced during late stages of combustion (CA50).

- ✓ 60% of hydrogen addition in volume to the methane was needed to compensate the effect of 20% of nitrogen dilution in the initial stages in engine combustion (in terms of combustion duration and standard deviations), which is in very good agreement with the laminar burning velocity results since the same percentage of hydrogen addition was needed in the case of 20% of nitrogen dilution to obtain the same burning velocity as in the case of methane-air mixture without dilution.
- ✓ The initial stages of flame propagation were found to correlate well with the laminar burning velocity obtained at atmospheric pressure and ambient temperature. Thus, considering the same range of pressure and temperature, the initial stages of combustion in the S.I. engine are directly correlated with the mixture composition.
- ✓ The standard deviation increases with nitrogen dilution and the decreasing effect of hydrogen is more pronounced in diluted conditions and has, moreover, a greater impact on later stages in combustion (CA50) than on the initial stages of flame propagation.

7.6 References

[1] T. Shinagawa, T. Okumura, S. Furuno, K.-O. Kim, *Effects of Hydrogen Addition to SI Engine on Knock Behavior*, SAE paper, 2004-01-1851 (2004).

[2] J. A. Topinka, M. D. Gerty, J. B. Heywood, J. C. Keck, *Knock Behavior of a Lean-Burn, H2 and CO Enhanced, SI Gasoline Engine Concept*, SAE paper, 2004-01-0975 (2004).

[3] T. Suzuki, Y. Sakurai, *Effect of Hydrogen Rich Gas and Gasoline Mixed Combustion on Spark Ignition Engine*, SAE paper, 2006-01-3379 (2006).

[4] J. Wang, Z. Huang, Y. Fang, B. Liu, K. Zeng, H. Miao, D. Jiang, *Combustion behaviors of a direct-injection engine operating on various fractions of natural gas-hydrogen blends*, International Journal of Hydrogen Energy, 32 (2007), pp. 3555-3564.

[5] T. Thurnheer, P. Soltic, P. Dimopoulos Eggenschwiler, *S.I. engine fuelled with gasoline, methane and methane/hydrogen blends: Heat release and loss analysis*, International Journal of Hydrogen Energy, 34 (2009), pp. 2494-2503.

[6] B. Morrone, A. Unich, *Numerical investigation on the effects of natural gas and hydrogen blends on engine combustion*, International Journal of Hydrogen Energy, 34 (2009), pp. 4626-4634.

[7] N. Apostolescu, R. Chiriac, *A Study of Combustion of Hydrogen-Enriched Gasoline in a Spark Ignition Engine*, SAE paper, 960603 (1996).

[8] N. Kahraman, B. Çeper, S. O. Akansu, K. Aydin, *Investigation of combustion characteristics and emissions in a spark-ignition engine fuelled with natural gas-hydrogen blends*, International Journal of Hydrogen Energy, 34 (2009), pp. 1026-1034.

[9] C. Pana, N. Negurescu, M. G. Popa, A. Cernat, D. Soare, *An Investigation of the Hydrogen Addition Effects to Gasoline Fueled Spark Ignition Engine*, SAE paper, 2007-01-1468 (2007).

[10] M. A.-R. Sadiq Al-Baghdadi, H. A.-K. Shahad Al-Janabi, *Improvement of performance and reduction of pollutant emission of a four stroke spark ignition engine fueled with hydrogen-gasoline fuel mixture*, Energy Conversion and Management, 41 (2000), pp. 77-91.

[11] C. D. Rakopoulos, M. A. Scott, D. C. Kyritsis, E. G. Giakoumis, *Availability analysis of hydrogen/natural gas blends combustion in internal combustion engines*, Energy, 33 (2008), pp. 248-255.

[12] P. Dimopoulos, K. Boulouchos, C. Rechsteiner, R. H. P. Soltic, *Combustion Characteristics of Hydrogen-Natural Gas Mixtures in Passenger Car Engines*, SAE paper, 2007-24-0065 (2007).

[13] T. Alger, J. Gingrich, B. Mangold, *The Effect of Hydrogen Enrichment on EGR Tolerance in Spark Ignited Engines*, SAE paper, 2007-24-0015 (2007).

[14] E. J. Tully, J. B. Heywood, *Lean-Burn Characteristics of a Gasoline Engine Enriched with Hydrogen from a Plasmatron Fuel Reformer*, SAE paper, 2003-01-0630 (2003).

[15] E. Hu, Z. Huang, B. Liu, J. Zheng, X. Gu, B. Huang, *Experimental investigation on performance and emissions of a spark-ignition engine fuelled with natural gas-hydrogen blends combined with EGR*, International Journal of Hydrogen Energy, 34 (2009), pp. 528-539.

[16] E. Hu, Z. Huang, B. Liu, J. Zheng, X. Gu, *Experimental study on combustion characteristics of a spark-ignition engine fueled with natural gas-hydrogen blends combining with EGR*, International Journal of Hydrogen Energy, 34 (2009), pp. 1035-1044.

[17] B. Huang, E. Hu, Z. Huang, J. Zheng, B. Liu, D. Jiang, *Cycle-by-cycle variations in a spark ignition engine fueled with natural gas-hydrogen blends combined with EGR*, International Journal of Hydrogen Energy, 34 (2009), pp. 8405-8414.

[18] A. A. Quader, J. E. Kirwan, M. J. Grieve, *Engine performance and emissions near the dilute limit with hydrogen enrichment using a on-board reforming strategy*, SAE paper, 2003-01-1356 (2003).

[19] T. Allgeier, M. Klenk, T. Landenfeld, E. Conte, K. Boulouchos, J. Czerwinski, *Advanced Emission and Fuel Economy Concept Using Combined Injection of Gasoline and Hydrogen in SI-Engines*, SAE paper, 2004-01-1270 (2004).

[20] I. Saanum, M. Bysveen, P. Tunestål, B. Johansson, *Lean Burn Versus Stoichiometric Operation with EGR and 3-Way Catalyst of an Engine Fueled with Natural Gas and Hydrogen Enriched Natural Gas*, SAE paper, 2007-01-0015 (2007).

[21] C. G. Bauer, T. W. Forest, *Effect of hydrogen addition on the performance of methane-fueled vehicles. Part I: effect on S.I. engine performance*, International Journal of Hydrogen Energy, 26 (2001), pp. 55-70.

[22] S. O. Akansu, N. Kahraman, B. Çeper, *Experimental study on a spark ignition engine fuelled by methane-hydrogen mixtures*, International Journal of Hydrogen Energy, 32 (2007), pp. 4279-4284.

[23] R. L. Hoekstra, K. Collier, N. Mulligan, L. Chew, *Experimental study of a clean burning vehicle fuel*, International Journal of Hydrogen Energy, 20 (1995), pp. 737-745.

[24] M. Bysveen, *Engine characteristics of emissions and performance using mixtures of natural gas and hydrogen*, Energy, 32 (2007), pp. 482-489.

[25] T. D'Andrea, P. F. Henshaw, D. S. K. Ting, *The addition of hydrogen to a gasoline-fuelled SI engine*, International Journal of Hydrogen Energy, 29 (2004), pp. 1541-1552.

[26] C. Ji, S. Wang, *Effect of hydrogen addition on combustion and emissions performance of a spark ignition gasoline engine at lean conditions*, International Journal of Hydrogen Energy, 34 (2009), pp. 7823-7834.

[27] R. Herweg, R. R. Maly, *A Fundamental Model for Flame Kernel Formation in S. I. Engines*, SAE paper, 922243 (1992).

[28] E. Conte, K. Boulouchos, *Experimental investigation into the effect of reformer gas addition on flame speed and flame front propagation in premixed, homogeneous charge gasoline engines*, Combustion and Flame, 146 (2006), pp. 329-347.

[29] F. Meier, J. Köhler, W. Stolz, W. H. Bloss, *Cycle-Resolved Hydrogen Flame Speed Measurements with High Speed Schlieren Technique in a Hydrogen Direct Injection SI Engine*, SAE paper, 942036 (1994).

[30] M. F. Rosati, P. G. Aleiferis, *Hydrogen SI and HCCI Combustion in a Direct-Injection Optical Engine*, SAE paper, 2009-01-1921 (2009).

[31] P. G. Aleiferis, A. M. K. P. Taylor, K. Ishii,Y. Urata, *The nature of early flame development in a lean-burn stratified-charge spark-ignition engine*, Combustion and Flame, 136 (2004), pp. 283-302.

[32] P. G. Aleiferis, A. M. K. P. Taylor, J. H. Whitelaw, K. Ishii, Y. Urata, *Cyclic Variations of Initial Flame Kernel Growth in a Honda VTEC-E Lean-Burn Spark-Ignition Engine*, SAE paper, 2000-01-1207 (2000).

[33] O. Pajot, *Etude expérimentale de l'influence de l'aérodynamique sur le comportement et la structure du front de flamme dans les conditions d'un moteur à allumage commandé*, *PhD Thesis, University of Orleans*, 2000.

[34] V. K. Natarajan, V. Sick, D. L. Reuss, G. Silvas, *Effect of Spark-Ignition on Combustion Periods during Spark-Assisted Compression Ignition*, Taylor & Francis, 2009, pp. 1187 - 1206.

[35] D. Bradley, R. A. Hicks, M. Lawes, C. G. W. Sheppard, R. Woolley, *The Measurement of Laminar Burning Velocities and Markstein Numbers for Iso-octane-Air and Iso-octane-n-Heptane-Air Mixtures at Elevated Temperatures and Pressures in an Explosion Bomb*, Combustion and Flame, 115 (1998), pp. 126-144.

[36] T. Tahtouh, F. Halter, E. Samson, C. Mounaïm-Rousselle, *Effects of hydrogen addition and nitrogen dilution on the laminar flame characteristics of premixed methane-air flames*, International Journal of Hydrogen Energy, 34 (2009), pp. 8329-8338.

[37] R. J. Kee, F. M. Rupley, J. A. Miller, *Chemkin-II: A Fortran chemical kinetics package for the analysis of gas phase chemical kinetics*, Report No. SAND89-8009B, Sandia National Laboratories (1989).

[38] S. Jerzembeck, N. Peters, P. Pepiot-Desjardins, H. Pitsch, *Laminar burning velocities at high pressure for primary reference fuels and gasoline: Experimental and numerical investigation*, Combustion and Flame, 156 (2009), pp. 292-301.

8. Turbulent burning velocity in a spark ignition engine

8.1 Abstract

The values of turbulent burning velocities determined experimentally by using planar laser tomography and Particle Image Velocimetry techniques in an optical spark ignition engine are presented in this paper. The images were acquired through a 45° mirror mounted in the piston extension and with an APX-RS high speed camera operating at 12 000 frames/second. Experiments were carried out under stoichiometric conditions and with different amounts of nitrogen dilution (0 to 20% by volume in the total mixture) and hydrogen blends in methane or iso-octane (from 0 to 60% by volume in the fuel). The spark ignition timing was set at 30 (iso-octane) and 25 (methane) crank angle degrees before top dead center. Image post-processing was optimized to obtain the local displacement speed of the flame front. The increasing effect of hydrogen substitution on the turbulent burning velocity is in agreement with the laminar burning velocity trends. These laminar burning velocities for mixtures fueled with hydrocarbon/hydrogen at high pressures and temperatures were determined from new correlations also proposed in this paper and based on literature experimental data. A correlation between the turbulent burning velocity and the laminar burning velocity is also presented. Results show that the bi-fuel Lewis number calculated for hydrocarbon/hydrogen mixtures at engine conditions are almost constant for the conditions investigated. Finally, it was found that the laminar burning velocity, rather than the Lewis number, is the dominant parameter governing the turbulent burning velocity for all the S.I. engine conditions investigated.

Nomenclature

- A_F : flame area [m^2]
- a_t : temperature power exponent [-]
- a_p : pressure power exponent [-]
- c_p : specific heat of unburned gas [$J.Kg^{-1}.K^{-1}$]
- D_{ij} : molecular diffusivity [m^2/s]
- D_{th} : thermal diffusivity [m^2/s]
- E : energy percentage in the fuel mixture [%]
- $<h>_{Pdf}$: mean curvature [mm^{-1}]
- L_b : Markstein length [mm]
- Le : Lewis number [-]
- $Le_{Bi-fuel}$: bi-fuel Lewis number [-]
- P_0 : reference pressure [bar]
- q : non-dimensional heat release [-]
- q' : turbulence intensity [m/s]
- R_{AF} : equivalent flame radius [m]
- S_{AF} : mean flame growth speed [m/s]
- S_t : turbulent burning velocity [m/s]
- S_l : laminar burning velocity [m/s]
- S_{l0} : laminar burning velocity at atmospheric pressure and ambient temperature [m/s]
- T_0 : reference temperature [K]
- T_b^0 : adiabatic flame temperature [K]
- T_u : unburned gas temperature [K]
- x : mole fraction [-]
- x_m : mass fraction [-]
- α : mole fraction of hydrogen in the hydrocarbon-hydrogen blend [-]
- β : mole fraction of nitrogen used for dilution in the total mixture [-]

- γ : mass percentage in the fuel mixture [%]
- $\Delta\delta_{thick}$: artificial flame thickness [pixels]
- ϕ : global equivalence ratio [-]
- λ : thermal conductivity [$W.m^{-1}.K^{-1}$]
- ρ_u : unburned gas density [Kg/m^3]
- ρ_b : burned gas density [Kg/m^3]

8.2 Introduction

Over the past few years, automotive manufacturers have focused on reducing of pollutant emissions and increasing engine efficiency. Varying the intake mixture composition (i.e. fuel composition, equivalence ratio and dilution level) is one way to achieve these objectives, especially in the case of Spark-Ignition (SI) engines. By operating with a diluted mixture, i.e, by recirculating the exhaust gases or increasing the residual gases by changing the valve phasing, NOx emissions are reduced due to lower combustion temperatures. There are however limitations on the level of dilution and of lean operating range that can ensure the smooth running of SI engines, since, whatever the fuel considered i.e gasoline or natural gas, diluting the fuel-air mixture or operating with a lean mixture induces an increase in combustion duration and also in cyclic variations which impair engine performance. Thanks to its properties, i.e. wide flammability range, low ignition energy, high auto ignition temperature and high laminar burning velocity, hydrogen added to the fuel can extend the dilution and the lean engine operating limits. Hydrogen addition can also improve the knock resistance in SI engines since it reduces the combustion period and inhibits fuel decomposition and hydroxyl radical production [1, 2].

Several numerical and experimental studies on the impact of hydrogen addition in SI engines fuelled by natural gas, methane or gasoline can be found in the literature [3-11]. The main results concern reduction in combustion duration and increase in thermal efficiency.

Dimopoulos et al.[12] investigated H_2-Natural Gas blend combustion with and without EGR in an SI engine. Without EGR, the efficiency increases by approx. 2% when the H_2 content is 10% by volume. However, the engine-out NOx emissions increase whereas the opposite trend is observed for engine-out CO and THC. Less spark timing advance was required for optimal efficiency since the hydrogen component in the fuel accelerates combustion. By combining H_2-Natural Gas blends and EGR, higher efficiencies with early spark timing with also very low engine-out NOx can be reached. Alger et al. [13] investigated the effect of H_2 addition on EGR tolerance in a single-cylinder engine with two different compression ratios and load settings, using both natural gas and gasoline as the main fuels. Their results showed that only a small amount of hydrogen is required to stabilize the engine at its EGR limit. Tully and Heywood [14] found that for low dilution levels, the addition of hydrogen has a small reducing effect on the 0%-10% and 10%-90% combustion durations. This positive effect becomes more and more pronounced with the increase in dilution level. Similar conclusions on the increasingly positive effect of hydrogen addition with an increase in dilution level were reached in [15-20] in SI engines fuelled with different fractions of natural gas/gasoline-hydrogen mixtures and using different rates of EGR.

All the above studies are based on the assessment of global performance and pollutant emissions. Only a few studies have focused on the initial stages of flame propagation, such as

Herweg and Maly [21] who developed a 1D model for flame kernel formation in SI engines. Conte and Boulouchos [22] carried out experiments by using an optical spark plug and ion sensors to study the flame propagation of gasoline mixtures enriched with reformer gas. Experiments on optical engines were also done by Meier et al. [23] and Rosati and Aleiferis [24] in a hydrogen direct injection SI engine. Aleiferis et al. [25, 26] investigated the early flame development in a single-cylinder engine equipped with optical access and fuelled with gasoline in lean-burn conditions. However, there is a lack of optical experimental investigations on the effect of hydrogen addition on diluted conditions in an SI engine fuelled with methane or iso-octane. Recently, Fairweather et al. [27] investigated the effect of hydrogen addition on turbulent burning rates in a fan stirred bomb and observed that, at stoichiometric conditions, the ratio of the turbulent velocity to the laminar velocity did not change with the addition of hydrogen at a given turbulence intensity. However, no values are available in the literature for the turbulent burning velocities of hydrocarbon/hydrogen fuels in SI engines.

The objective of this study is to investigate the effect of hydrogen substitution and nitrogen dilution on the turbulent burning velocity in an optical SI engine fuelled with iso-octane or methane under stoichiometric conditions.

8.3 Experimental details

8.3.1 Optical SI engine

The 'transparent' mono-cylinder SI engine used to perform the experiments has a four-valve pent-roof chamber with a displacement volume of 500 cm^3 and a compression ratio of 9.5. The bore, stroke and connecting rod lengths are respectively 88 mm, 82 mm and 137 mm. To provide optical access inside the combustion chamber, the piston is elongated and equipped with a quartz window (diameter 66 mm). The cylinder head is bored and has two lateral windows. The optical access engine is driven by an electric motor at a fixed regime. A schematic view of the set-up is presented in Figure 1.

The engine is equipped with an optical encoder mounted on the main shaft, giving a 0.1 Crank Angle Degree (CAD) resolution. Cylinder pressure was recorded with a water-cooled AVL quartz pressure trasducer connected to a charge amplifier at a 0.1 CAD resolution. Before experiments, the trasducer was calibrated with a Keller high pressure hydraulic calibrator. The linearity ($\leq \pm 0.6\%$) of the trasducer was verified starting from a maximum pressure of 10MPa (> maximum pressure in the engine).

In this work, the absolute cylinder pressure was deduced by equalizing the in-cylinder pressure at 20 CAD after inlet valve opening timing to the intake mean absolute pressure. 100 consecutive 'fired' cycles of cylinder pressure data were acquired by a PC equipped with National Instruments acquisition board.

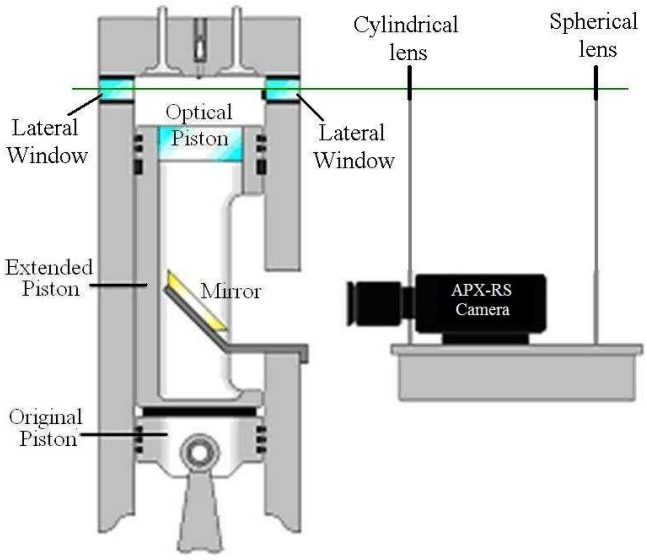

Figure 1. *Schematic view of the set-up.*

The engine sucks the air through a thermal mass flow-meter and all other flows were evaluated from this reference flow. Methane, hydrogen and nitrogen flows were measured by using thermal mass flow-meters with an accuracy of ±0.7% for the instantaneous flow. Before the intake pipe, all the gases pass through a plenum volume, to avoid pressure oscillations inside the intake port. To ensure good preparation of the air-fuel mixture in the intake pipe, 4 injections per cycle were done in the case of iso-octane as fuel. The iso-octane quantity was measured by using a 0-5 kg/h Bronkhorst Coriolis mass flow meter with an accuracy of ±0.1% of full scale plus ±0.2% of flow rate.

A conventional spark plug with an electrode spacing of 1mm was used. The engine was fired every sixth cycle to avoid residual gases and to keep the equivalence ratio inside the cylinder constant.

For all experiments, the engine regime was fixed at 1200 rpm, the oil and coolant temperatures at 80°C and the intake pressure at 0.1MPa.

Heat release rate estimate:

The heat release rate was therefore estimated from the in-cylinder pressure trace:

$$\frac{dQ_{hr}}{d\theta} = \frac{\gamma_{hr}}{\gamma_{hr}-1} p \frac{dV}{d\theta} + \frac{1}{\gamma_{hr}-1} V \frac{dp}{d\theta} + \frac{dQ_{ht}}{d\theta} \quad (1)$$

where θ is the crank angle, p the in-cylinder pressure, V the in-cylinder volume and γ_{hr} the specific heat ratio.

$\frac{dQ_{ht}}{d\theta}$ is the convective heat-transfer rate to the combustion chamber walls, estimated from the relation :

$$\frac{dQ_{ht}}{d\theta} = Ah_c(T - T_W) \quad (2)$$

with A the chamber surface area, T the mean gas temperature, T_w the mean wall temperature, and h_c the heat-transfer coefficient. This coefficient was estimated by using the correlation given by Woschni [28].

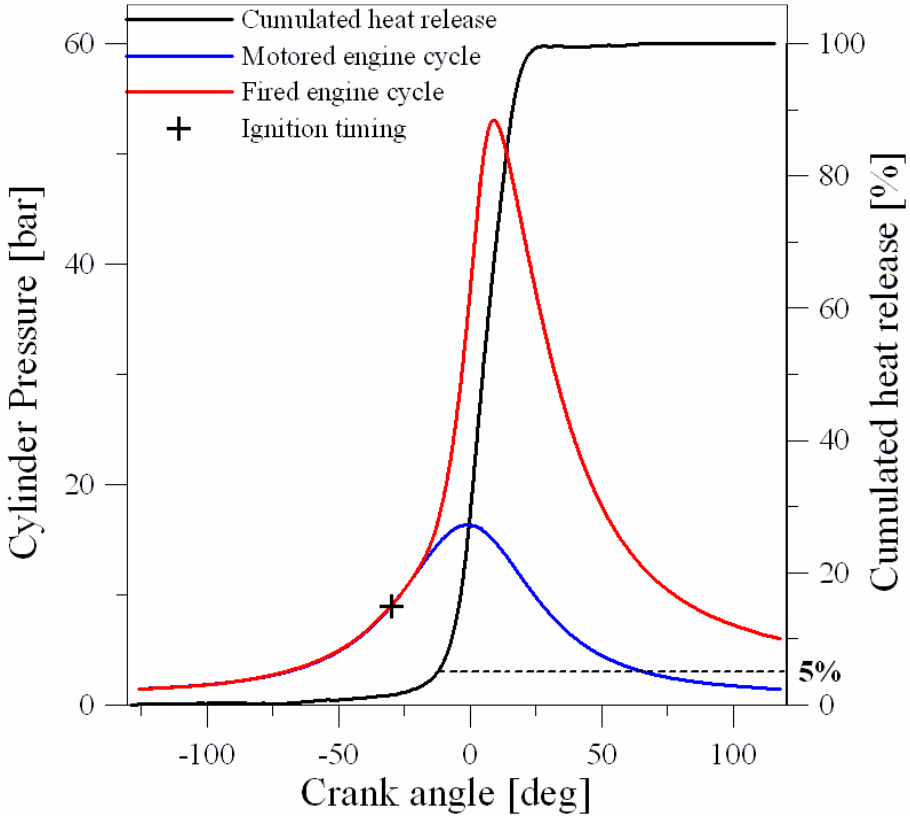

Figure 2. *Cumulated heat release (%), and Cylinder pressure for motored and fired engine versus crank angle. Ignition timing 30° BTDC.*

Figure 2 shows an example of a cumulated heat release (in percentage) for an iso-octane/air stoichiometric mixture versus CAD. The in-cylinder pressures versus CAD in the case of motored cycles (non-fired condition) and fired ones are also reported in Figure 2.

8.3.2 Operating conditions

In order to compare the initial stages of flame propagation at the same in-cylinder pressure and temperature values, the spark ignition was set at 30 CAD BTDC (Before Top Dead Center) for iso-octane mixtures and 25 CAD BTDC for methane mixtures.

The amount of hydrogen in the fuel was varied from 0% to 60% by volume and the amount of dilution in the total mixture was varied from 0% to 20% by volume. All mixtures were under stoichiometric conditions. The different mixtures investigated and the hydrogen contents in the fuel in terms of mass percentage γ and energy percentage E_{H_2} are summarized in Table

1. The pressure and temperature ranges of the unburned gases, in the investigated range of 0 to 5% of cumulated heat release, are also reported in Table 1.

Table 1. *Investigated conditions*

N°	Mixture	Temperature Range [K]	Pressure Range [bar]	α	β	γ %	E_{H_2} %
1	CH_4-air (E.R.=1)	700-778	13.6-17.4	0	0	0	0
2	CH_4-air -N2 (E.R.=1)	685-731	15.1-18	0	0.2	0	0
3	CH_4- H_2-air (E.R.=1)	729-829	13.5-17.4	0.4	0	7.7	17
4	CH_4- H_2-air- N_2 (E.R.=1)	725-768	15.9-17.9	0.4	0.2	7.7	17
5	CH_4- H_2-air- N_2 (E.R.=1)	739-793	14.2-17	0.6	0.2	15.9	31
6	C_8H_{18}-air (E.R.=1)	596-694	12-16.9	0	0	0	0
7	C_8H_{18}-air-N_2 (E.R.=1)	623-677	13.4-17.6	0	0.2	0	0
8	C_8H_{18}-H_2-air (E.R.=1)	612-709	11.3-16	0.6	0	2.6	6.7
9	C_8H_{18}-H_2-air-N_2 (E.R.=1)	616-693	12.1-16	0.6	0.05	2.6	6.7
10	C_8H_{18}-H_2-air-N_2 (E.R.=1)	632-685	13.2-17	0.6	0.2	2.6	6.7

In this study, the parameter α is defined as the mole fraction of hydrogen in the fuel (iso-octane or methane):

$$\alpha = \frac{X_{H_2}}{X_{C_xH_y} + X_{H_2}} \quad (3)$$

The dilution parameter β corresponds to the mole fraction of nitrogen used for dilution in the total mixture:

$$\beta = \frac{X_{N_2-dilution}}{X_{CxHy} + X_{H_2} + X_{O_2} + X_{N_2-air} + X_{N_2-dilution}} = X_{N_2-dilution} \quad (4)$$

where $X_{C_xH_y}$, X_{H_2} and X_{O_2} are respectively iso-octane or methane, hydrogen and di-oxygen mole fractions in the mixture, X_{N_2-air} is the mole fraction of nitrogen in the air mixture ($X_{N_2-air} = 3.78 \bullet X_{O_2}$) and $X_{N_2-dilution}$ is the mole fraction of nitrogen used for dilution.

The global equivalence ratio ϕ is defined as:

$$\phi = \frac{\dot{m}_{CxHy} \bullet AF_{st-CxHy} + \dot{m}_{H_2} \bullet AF_{st-H_2}}{\dot{m}_{air}} \quad (5)$$

where $\dot{m}_{CxHy}$, $\dot{m}_{H_2}$ and $\dot{m}_{air}$ are respectively hydrocarbon, hydrogen, and air measured mass flow rates (g/h). $AF_{st-CxHy}$ and AF_{st-H_2} are the stoichiometric air to fuel ratios of the considered hydrocarbon and hydrogen respectively.

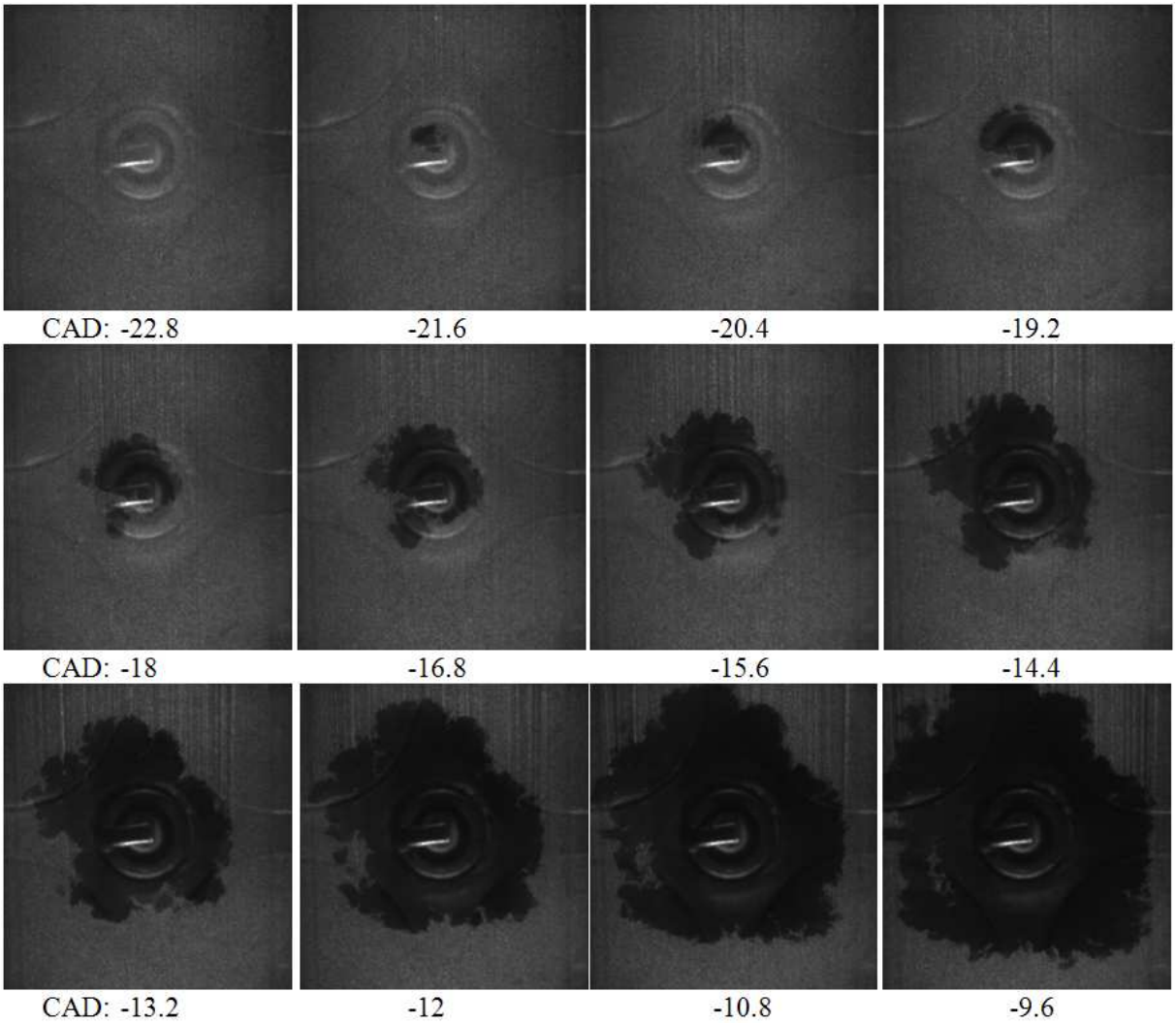

Figure 3. *Examples of flame evolution for C_8H_{18}-air flames (condition 6 in Table 1).*

8.3.3 Optical Technique

The turbulent burning velocity in the optical SI engine for different mixtures was determined by using simultaneously Mie scattering planar laser tomography and Particle Image Velocimetry (PIV) [29-33].

A Darwin 527 Nd-YLF double pulsed laser, operating at 6000Hz, combined with a 750 mm spherical lens and a 50.9 mm cylindrical lens, formed a thin sheet (~0.4mm of thickness) at 527 nm. Through the lateral windows, this thin sheet illuminated the silicon oil droplets introduced into the engine by using the seeding system described in [34]. Consequently, the observed isotherm, which corresponds to the evaporation temperature of the silicon oil particles (~500K), enables the flame front boundary to be determined.

The laser pulse separation between head 1 and head 2 was fixed at 25µs, a value needed to ensure sufficient droplet displacement in the laser sheet plane and to avoid large displacement perpendicular to this laser sheet.

The double exposure particle images were acquired through a 45° mirror mounted in the piston extension and by an APX-RS (Photron) High Speed camera coupled with a 90 mm, f/2.5 Tamron lens. The frame resolution was 512x384 pixels² at 12000 frames per second (1 couple of images every 1.2 CAD considering a regime of 1200 rpm). The magnification ratio was 0.105 mm/pixel.

A TSI system ensured synchronization of the various trigger signals to the image, laser and data acquisition systems. Examples of flame evolution are given in Figure 3 for a C_8H_{18}/air mixture (Case 6, Table 1) between 22.8 CAD BTDC and 9.6 CAD BTDC.

8.3.4 Image Analysis

The images were processed to provide both the flame front structure and the flow field characteristics.

I- Flow field analysis:

TSI Insight 3G software was used to characterize the flow field. The interrogation spots used in the PIV post-processing were fixed at 32x32 pixels² with an overlap of 50%. Two criteria were used to validate the vector map: a 1.2 signal-to-noise level and 15m/s for the maximum flow field velocity value. Spurious vectors were extrapolated by a simple local average of the validated vectors in their vicinity. In this study, aerodynamic fields and instantaneous flame front displacement were provided simultaneously.

An example of average velocity field (average on 100 cycles) without combustion is shown in Figure 4 at 14.4 CAD BTDC.

When combustion occurs, unburned gases located in the vicinity of the flame front are accelerated due to the expansion of the burnt gases. This acceleration depends on the local flame front displacement velocity and orientation. This phenomenon is presented in Figures 5.a and 5.b for an iso-octane/air mixture (Case 6, Table 1) at 14.4 CAD BTDC. For the sake of the clarity, the unburned gas velocity values (Figure 5.a) and orientation (Figure 5.b) are presented in two separate figures. It is well established that flow field cycle-to-cycle fluctuations, at the same crank angle, can be high [31, 35-38]. Nevertheless, it can be noted that the ratio of the maximum value of unburned gas velocity in Figure 5.a to that in Figure 4 (~4.6) is close to the unburned to burned gas density ratio (which is ~4.2 for this condition).

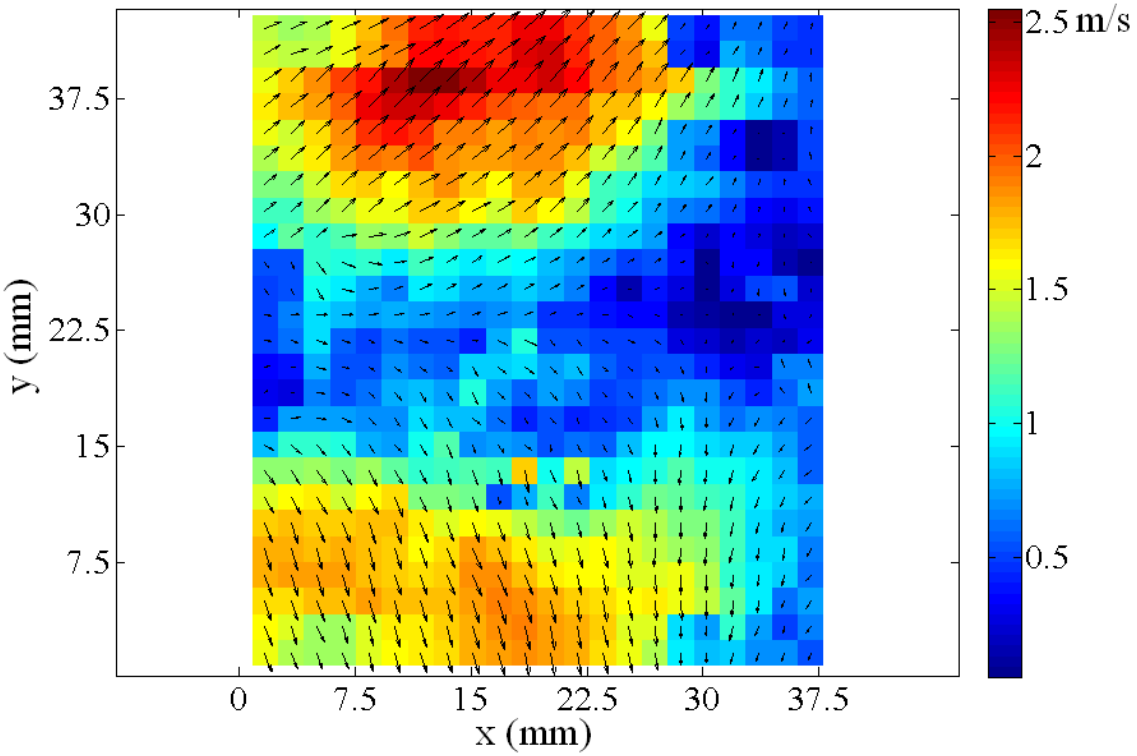

Figure 4. *Example of mean velocity field (average of 100 cycles) without combustion at 14.4 CAD BTDC.*

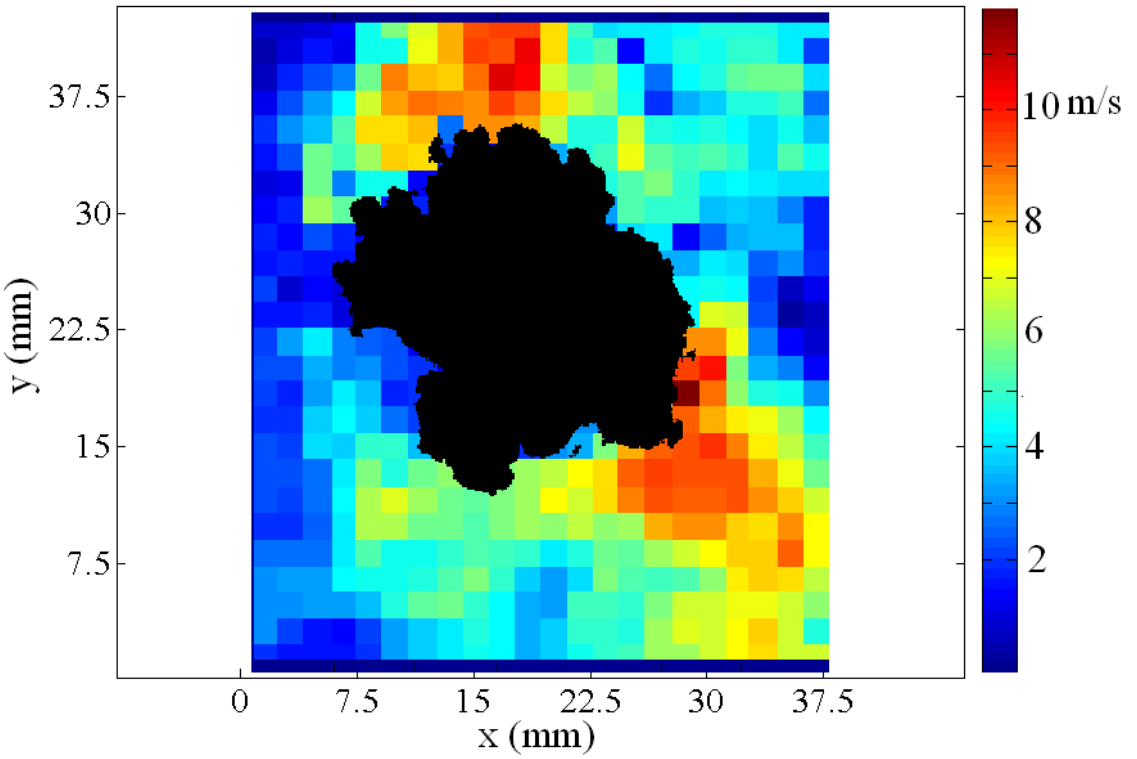

Figure 5.a *Unburned gas velocity values for C_8H_{18}-air flames at 14.4 CAD BTDC.*

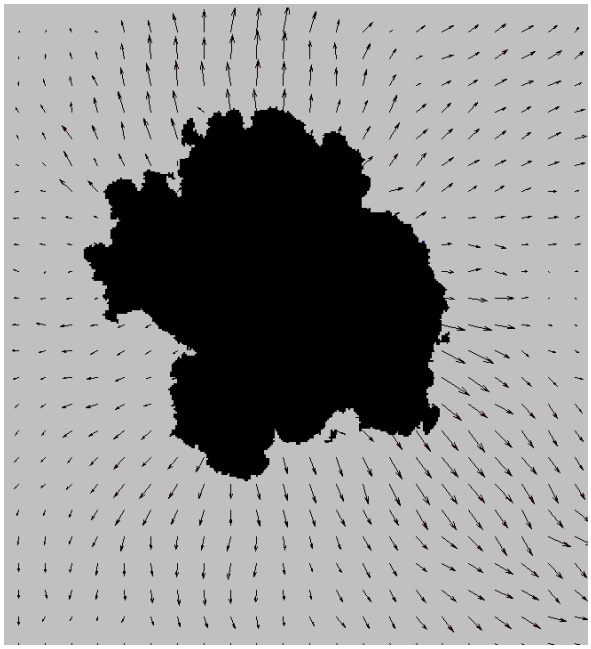

Figure 5.b *Unburned gas velocity orientations for C_8H_{18}-air flames at 14.4 CAD BTDC.*

In a previous study [39], it was found that the turbulence intensity does not vary when the intake pressure is changed and remains almost constant between 30 CAD BTDC (Before Top Dead Center) and the TDC (Top Dead Center). Consequently, the turbulence intensity q' =1.08 m/s in this work was not measured directly, but was estimated using the results reported in [40] and by assuming that the turbulence intensity is proportional to the engine speed [38, 41].

II- Flame front analysis:

a- From the Mie scattering images, the flame front was defined as the limit between the bright area, corresponding to the fresh gases, and the dark area, corresponding to the burned gases, as can be seen in Figure 3. The contours of turbulent flames were determined by post-processing the PIV images in Matlab. Subtraction of the background was first applied to eliminate noise. These images were then filtered in order to correct the non-uniformity of the laser sheet and the flame contours were extracted after binarization and thresholding steps. Finally, these detected contours were smoothed by applying a low-pass filter to remove noise from the digitizing steps.

This low-pass filter was chosen in order to obtain maximum curvature values comparable to 1/(laser sheet thickness).

b- Another image analysis technique was used to provide turbulent flame velocity data. As in S.I. engines, cycle-to-cycle fluctuations sharply affect the location of the instantaneous flame front, another approach, similar to the thickened flame model used in large eddy simulations [42-44] wass used here to filter the instantaneous contour.

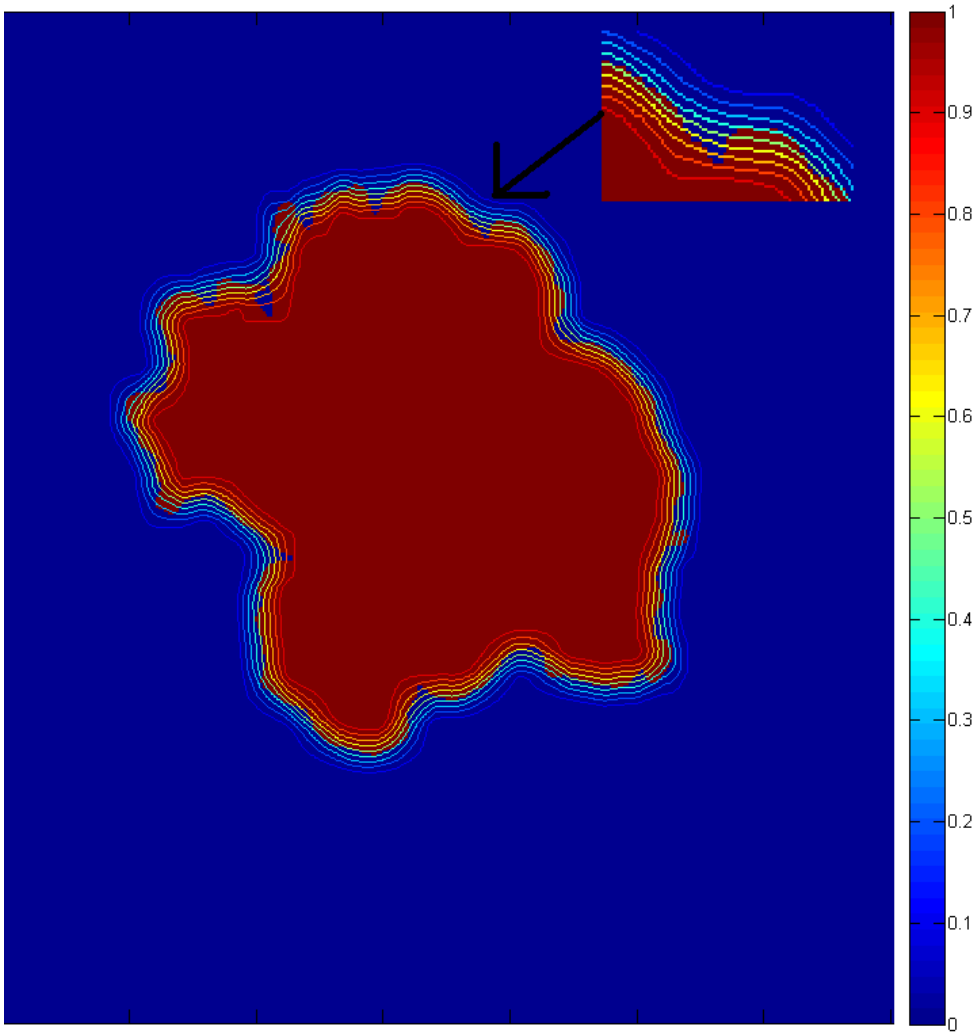

Figure 6. *Thickened flame contours.*

Since this approach artificially increases the flame thickness, the smoothed contour was thickened by $\Delta\delta_{thick}$ =21 pixels (~2.2mm) which is of the same order of magnitude as the integral scale length in this SI engine [40]. Iso-contours were obtained by moving a square matrix (dimension $\Delta\delta_{thick}$ x $\Delta\delta_{thick}$) on the binary image.

A value, on a new image, was attributed to the pixel having the same coordinates as the center of this matrix. This pixel value is the average value of the matrix.

Since the maximum pixel value in the binary image is 1, the maximum new attributed value can be equal to 1 when all the elements of this matrix are equal to 1 which corresponds to the burnt gas zone. The minimum new attributed value is 0, when all the elements of the matrix are equal to 0 which corresponds to the fresh gas zone. Iso-contours were defined, on this new image, between both burnt and unburned zones as a continuity of pixels having the same value (from 0.1-0.9). An example of this new resulting image superimposed on the binary one is shown in Figure 6. The iso-contour characterized by a pixel value of 0.5 is therefore the 'new' filtered contour, called $\hat{c}$.

8.4. Laminar flame characteristics

According to the turbulent diagrams [45] used to classify turbulent combustion regimes, the combustion process in SI engines occurs mainly in the flamelet regime. In this regime, the interfaces separating the unburned reactants from the burned products (flamelets) are assumed to have the same local structure as flickered laminar flames, thus confining the heat release to these thin interfaces.

Consequently, the analysis of turbulent burning velocity requires laminar information at engine conditions. The first part of this section is therefore devoted to obtaining a global correlation in order to evaluate the laminar burning speeds of diluted methane or iso-octane hydrogen / air mixtures at engine conditions.

As the flame development is affected by thermo-diffusive instabilities, hydrodynamic instabilities and turbulence, the Lewis number values of the mixtures are also estimated here, to evaluate the thermo-diffusive effect.

8.4.1 Laminar burning velocities

There is a lack of experimental values of laminar burning velocities at engine conditions especially for diluted mixtures and mixtures containing added hydrogen.

The laminar burning velocity values can be mainly estimated by using two methods.

The first one is based on kinetic reaction modeling by using a detailed kinetic mechanism. The second one consists in using empirical correlations which link the laminar burning velocity to pressure and temperature. In this study, the second method was chosen due to its reduced computational cost.

Laminar burning velocity pressure and temperature dependencies are commonly expressed by using a simple power law as defined by Metghalchi et al. [46]:

$$S_l = S_{l0} \bullet \left(\frac{T_u}{T_0} \right)^{a_t} \bullet \left(\frac{P}{P_0} \right)^{a_p} \quad (6)$$

with S_{l0} the burning velocity at the reference conditions, T_0 and P_0 (T_0= 300K and P_0=1 bar in the present study), T_u and P the unburned gases temperature and pressure, and a_t and a_p, two constants.

In the present study, the effect of hydrogen substitution and nitrogen dilution are embodied only in the S_{l0} formulation.

In previous studies [47, 48], the laminar burning velocity was found to correlate linearly with the mass fraction of hydrogen in the fuel mixture. It can be expressed as follows:

For methane/hydrogen/nitrogen/air mixtures:

$$S_{l0-CH_4}[cm/s] = (a_{corr} \bullet \beta + b_{corr}) \bullet \left(\frac{-201.6 \bullet \alpha}{14.027 \bullet \alpha - 16.043} \right) + c_{corr} \bullet \beta^2 + d_{corr} \bullet \beta + e_{corr} \quad (7)$$

with a_{corr} = -3.8, b_{corr} =1.83, c_{corr} =100.6, d_{corr} =-115.31 e_{corr} =33.96.

For iso-octane/hydrogen/nitrogen/air mixtures:

$$S_{l0-C_8H_{18}}[cm/s] = (a_{corr} \bullet \beta + b_{corr}) \bullet \left(\frac{-201.6 \bullet \alpha}{112.184 \bullet \alpha - 114.2} \right) + c_{corr} \bullet \beta^2 + d_{corr} \bullet \beta + e_{corr} \quad (8)$$

with a_{corr} = -2.119, b_{corr} =1.253, c_{corr} =58.798, d_{corr} =-92.676 e_{corr} =29.227.

The constants a_t and a_p were considered not to be affected when part of the main fuel (methane or iso-octane) was replaced by hydrogen. This simplification is justified by the fact that only relatively small amounts of hydrogen blends, in terms of mass, were considered here ($\leq$ 2.6% or $\leq$ 15.9% in iso-octane or methane respectively).

From this assumption, the values of these constants were evaluated by fitting numerous recently published experimental results (94 experimental values considered for methane [49-57] and 36 for iso-octane [52, 58-60]). Finally, the values were:

In the case of methane: a_{t_CH4} =1.9528 and a_{p_CH4} =-0.3981

In the case of iso-octane: a_{t_C8H18} =1.8917 and a_{p_C8H18} =-0.2251

From these values and the experimental correlation of S_{l0} (embodying the hydrogen and dilution effects), laminar burning speeds at engine conditions can be evaluated, in the range of 1-20 bars / 298-550K for methane and 1-25 bars / 298-450K for iso-octane.

The mean and maximum differences obtained between the present correlation and the experimental data were 5% and 19.5% in the case of methane and 8% and 34% in the case of iso-octane. However, the dispersion of these values is on the same order as that of the experimental results, namely higher in the case of iso-octane than in the case of methane.

Correlations proposed by other authors [46, 49-51, 58, 61, 62] are summarized in Table 2 with the temperature and pressure range. The first point to note is that there is a great disparity in the constants. A comparison between the present constant values, the correlations proposed in [49, 50] and some experimental values [49-52, 54-56] obtained at P=1, 5, 10 and 15 bars and 300 K<T< 550K is presented in Figures 7.a (P=1, 5 bar) and 7.b (P=10, 15 bar) for

methane/air mixtures. The values given by the present correlation are in good agreement with the experimental data and with the other reported correlations.

Moreover, the present correlation extends the range of pressure and temperature (1 bar < P < 20 bars and 298 K < T < 550 K) compared to the correlation proposed in [49].

Table 2. *Correlations for the laminar burning velocity*

Ref. (CH_4)	S_{l0} **[m/s]**	a_t	a_p	**T_0 (K)**	**Pressure range (bar)**	**Temperature range (K)**
Present	0.34	1.953	-0.398	300	1-20	298-550
[49]	0.36	1.612	-0.374	300	1-10	300-400
[50]	0.375	1.857	-0.435	298	0.75-70	298-550
[51]	0.361	1.5365 +0.1165P	-0.37	298	1-5	298-473
[61]	0.376	1.42	-0.314	298	0.5-10.4	295-454
[62]	0.395	1.58	-0.398	300	0.5-1.5	300-400
Ref. (C_8H_{18})						
Present	0.292	1.892	-0.225	300	1-25	298-450
[46]	0.27	2.26	-0.18	298	1-50	350-700
[58]	0.48	1.01	-0.282	358	1-10	358-450

The values of laminar burning velocity for iso-octane/air mixtures given by the correlations found in [46, 58] and by the present correlation are reported in Figures 8.a (P=1, 5 bar) and 8.b (P=10, 20 bar) and compared with experimental values [52, 58, 59] at P=1, 5, 10 and 20 bars and for 350 K<T< 450K. A good agreement with the other reported correlations and with the experimental data (even though only limited experimental results are available) can also be observed. In this study, under engine conditions, the unburned gas temperature (596K < T < 829K, Table 1) can be higher than the upper limits of the correlation range even when the cumulated heat release is lower than 5% of the total heat release. The low temperature and pressure range limits are lower in the case of iso-octane than in the case of methane due to the higher spark ignition timing advance. Since no experimental results are available at these elevated pressures and temperatures, the present correlations had to be used to extrapolate the laminar burning velocity at these elevated pressures and temperatures. The validity of these correlations is not a major drawback for a qualitative study of $\frac{S_t}{S_{l0}}$ behavior if we assume that the form of Eq.6 does not change at these high temperature conditions (Table 1).

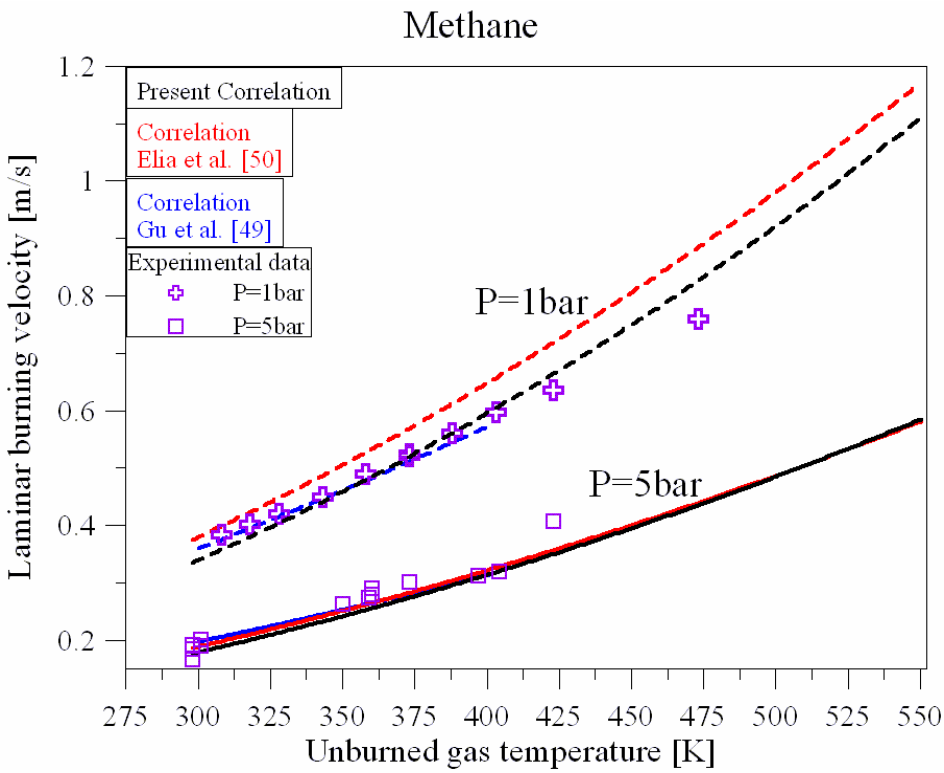

Figure 7.a *Laminar burning velocity versus unburned gas temperature for methane/hydrogen/air mixtures: dashed lines P=1 bar, continuous lines P=5 bar*

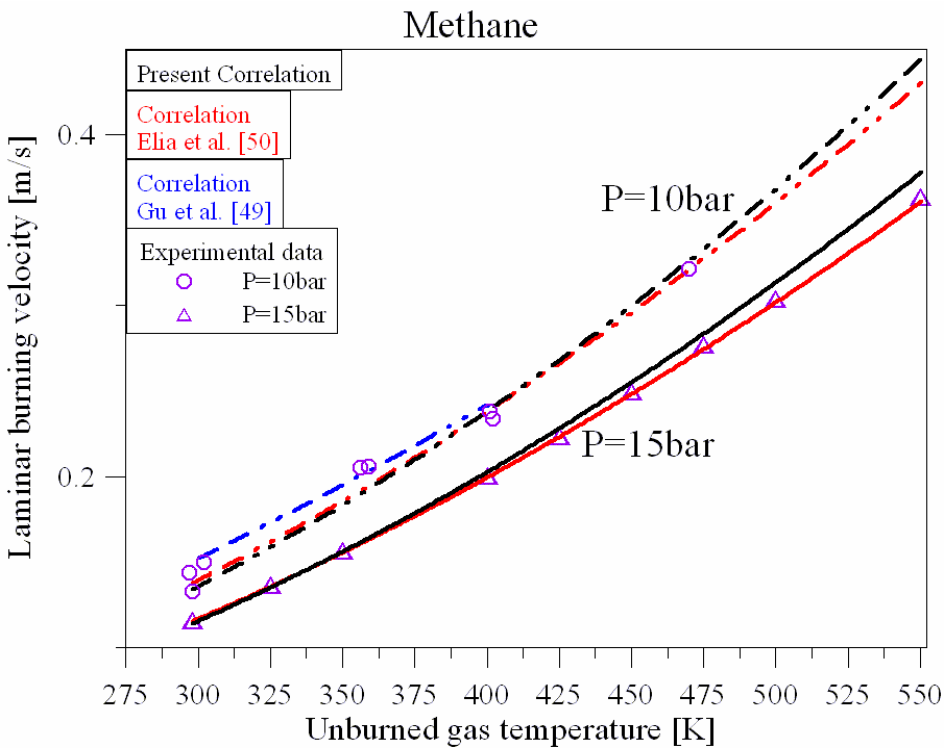

Figure 7.b *Laminar burning velocity versus unburned gas temperature for methane/hydrogen/air mixtures: dashed lines P=10 bar, continuous lines P=15 bar.*

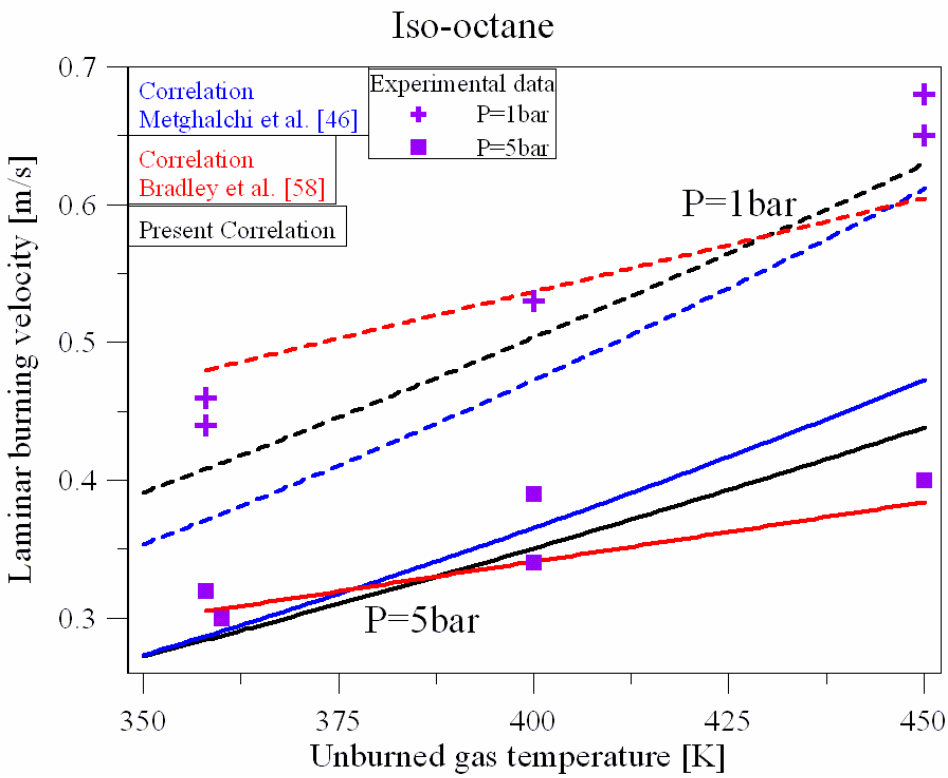

Figure 8.a *Laminar burning velocity versus unburned gas temperature for iso-octane/hydrogen/air mixtures: dashed lines P=1 bar, continuous lines P=5 bar.*

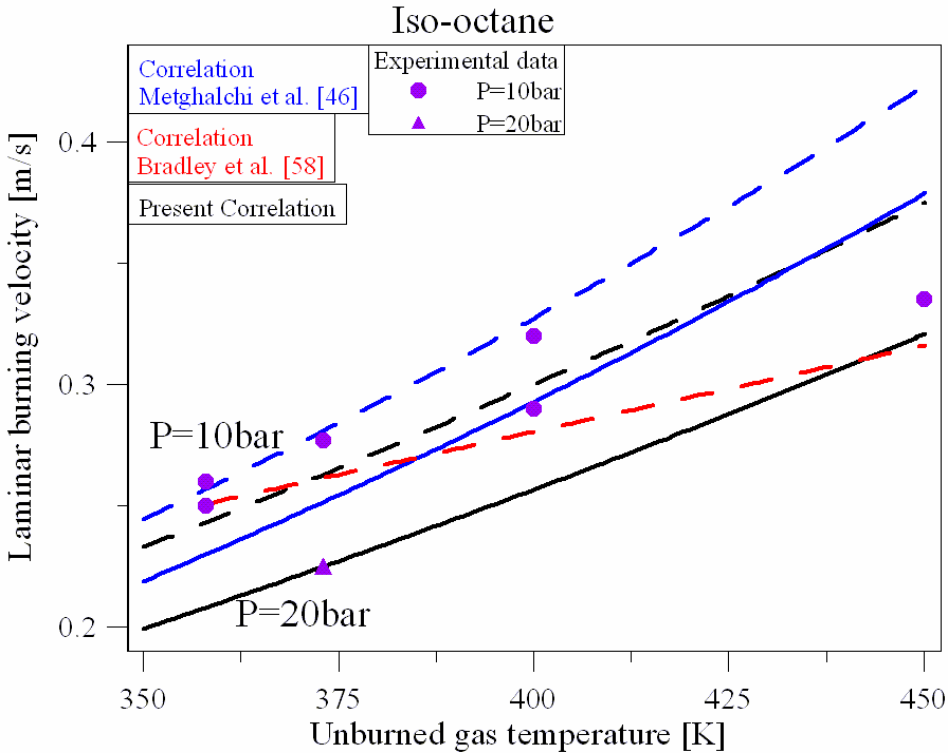

Figure 8.b *Laminar burning velocity versus unburned gas temperature for iso-octane/hydrogen/air mixtures: dashed lines P=10 bar, continuous lines P=20 bar.*

8.4.2 Lewis number formulation

Renou et al. [29] investigated experimentally the effect of curvature on the structure of turbulent freely propagating premixed flames for various Lewis numbers (Le). They found that flame fronts are more distorted for mixtures with a low Le (Le <<1). Large differences in Le values can induce variations in the flame structure and hence in the flame propagation.

Following these observations, the Le for $CH_4/H_2/N_2$/air and $C_8H_{18}/H_2/N_2$/air mixtures were estimated at engine conditions.

Le is typically defined in the case of single fuel/air mixtures as the ratio of thermal diffusivity D_{th} to molecular diffusivity D_{ij} of the deficient reactant [63]:

$$Le = \frac{D_{th}}{D_{ij}} \quad (9)$$

with:

$$D_{th} = \frac{\lambda}{\rho_u \cdot c_p} \quad (10)$$

λ, ρ_u and c_p are thermal conductivity, gas density and specific heat of unburned gas, respectively.

However, this expression (Eq.9) of Le is valid only for single-fuel mixtures. For multi-component fuel mixtures such as methane/hydrogen (or iso-octane/hydrogen), the fuel mixture can be characterized by two Lewis numbers: Le_{CH4} (or Le_{C8H18}) and Le_{H2}.

Another definition of the Lewis number is therefore required for multi-component fuel mixtures. Since all the mixtures investigated were under stoichiometric conditions, we considered that the fuels (methane/hydrogen or iso-octane/hydrogen) are the deficient reactants, as they are present in relatively small amounts compared to the abundant inert gas (nitrogen). Moreover the purpose in the present study is to investigate the effect of hydrogen addition on the Lewis number of the fuel mixture. Thus, in the following, only the Lewis number for bi-fuel mixtures will be provided.

One expression based on heat release weighting for multi-component fuel mixtures was suggested in [64, 65] as:

$$Le_{Bi-fuel} = 1 + \frac{q_1.(Le_1 - 1) + q_2.(Le_2 - 1)}{q} \quad (11)$$

with subscript i=1 or 2 for fuel 1 or fuel 2

q_i: the non-dimensional heat release obtained by using the following expression:

$$q_1 = \frac{x_{m1} \bullet LHV_1}{x_{m1} \bullet LHV_1 + x_{m2} \bullet LHV_2}; \quad q_2 = \frac{x_{m2} \bullet LHV_2}{x_{m1} \bullet LHV_1 + x_{m2} \bullet LHV_2} \quad (12)$$

with x_{mi} and LHV_i : the mass fractions of fuel (1 or 2) in the total fuel mixture and the lower heating value respectively. The bi-Fuel Lewis number at engine conditions was calculated by using equation 11.

8.4.3 Lewis number at engine conditions

The $Le_{Bi-fuel}$ values depend on pressure and temperature conditions.

They were therefore estimated under the present engine conditions (Table 1), in order to investigate the evolution of this parameter as a function of combustion development (up to 5% of the cumulated heat release).

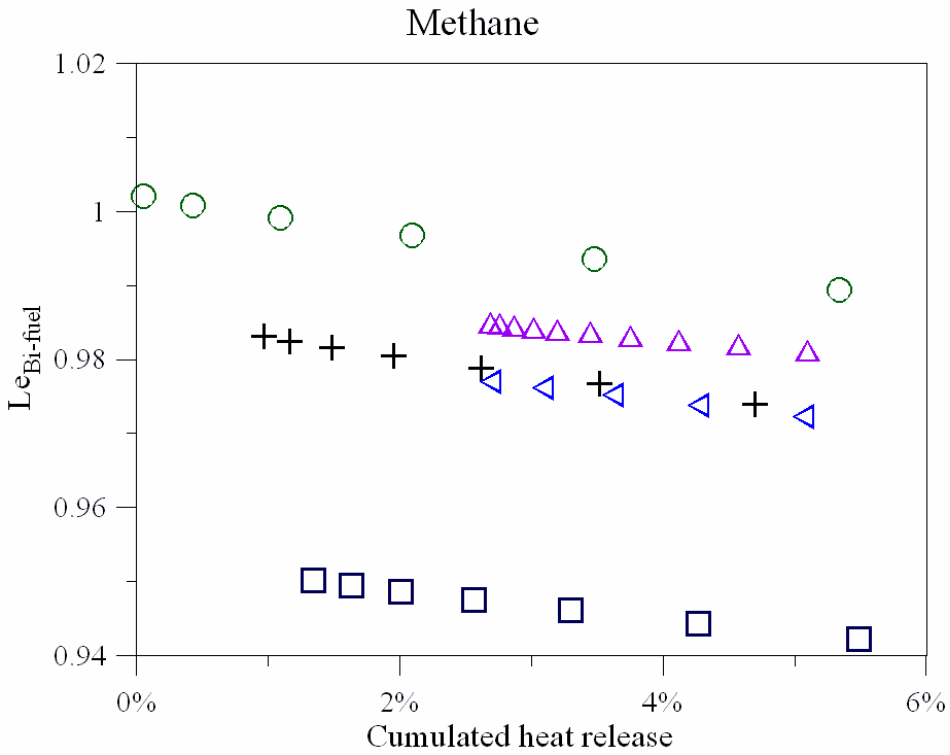

Figure 9. *$Le_{Bi-fuel}$ versus the percentage of cumulated heat release for mixtures with methane (conditions 1-5): 1: + CH_4/Air; 2: △ CH_4/air/20%N_2; 3: ○ CH_4/40%H_2/Air; 4: ◁ CH_4/40%H_2/20%N_2/Air; 5: □ CH_4/60%H_2/20%N_2/Air.*

$Le_{Bi-fuel}$ was then plotted versus the percentage of cumulated heat release in Figure 9 for different methane mixtures (conditions 1-5). It can be observed that these mixtures, for the

different flame development stages investigated, present very similar $Le_{Bi-fuel}$, with a maximum difference of 5.9% between all values. At a given condition, $Le_{Bi-fuel}$ decreases as combustion progresses. This decrease is mainly caused by the increase in unburned gas density due to the dominant effect of pressure rather than temperature, leading to lower values of mixture thermal diffusivity D_{th}. The increase in thermal conductivity values λ with the temperature does not compensate for the variation in ρ_u. Furthermore, the molecular diffusivity of the methane in the nitrogen, $D_{CH4\rightarrow N2}$ is globally decreased with the combustion development due to the dominant effect of pressure with respect to temperature. Despite this decrease in $D_{CH4\rightarrow N2}$ for the pressure and temperature range investigated, the decrease in D_{th} values remains preponderant and leads to lower values of $Le_{Bi-fuel}$. Condition 5 presents the lowest values of $Le_{Bi-fuel}$ due to the high amount of hydrogen (in terms of energy, hydrogen represents 31% of the total) in the fuel mixture.

This leads to a decrease in the $Le_{Bi-fuel}$, since Eq. 11 is based on heat release weighting between $Le_{CH4} \sim 1.2$ and $Le_{H2} \sim 0.37$.

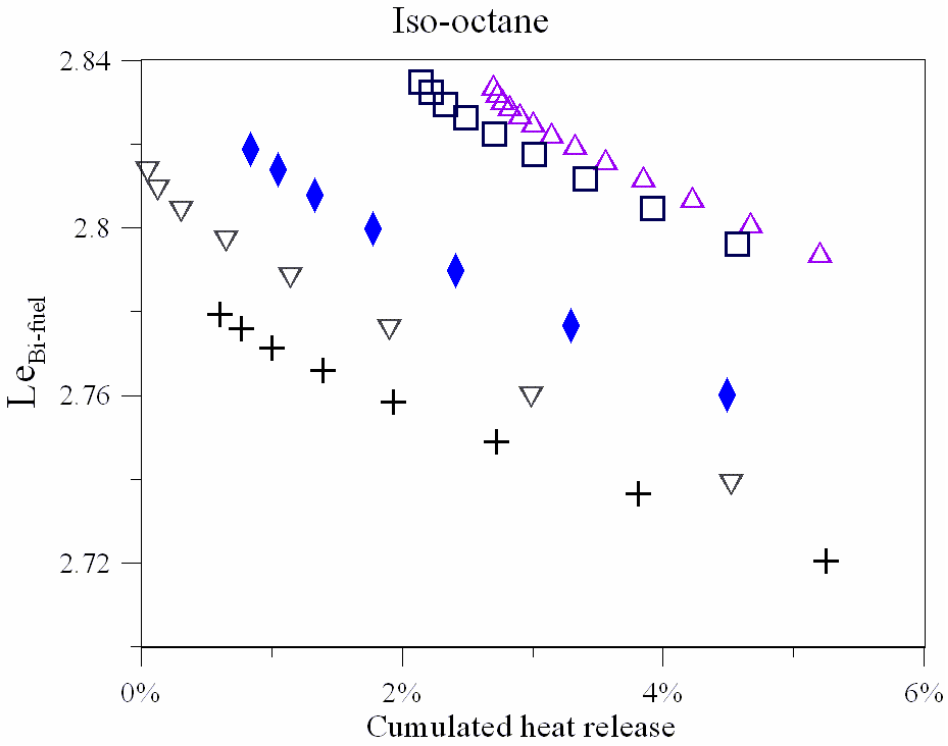

Figure 10. *$Le_{Bi-fuel}$ versus the percentage of cumulated heat release for mixtures with iso-octane (conditions 6-10):*
6: + C_8H_{18}/Air; 7: △ C_8H_{18}/air/20%N_2; 8: ▽ C_8H_{18}/60%H_2/Air;
9: ♦ C_8H_{18}/60%H_2/5%N_2/Air; 10: □ C_8H_{18}/60%H_2/20%N_2/Air.

Similar decrease tendencies in $Le_{Bi-fuel}$ versus the cumulated heat release can be seen for iso-octane cases (conditions 6-10) in Figure 10. A maximum difference of 4.8% in $Le_{Bi-fuel}$ values is observed for all these conditions. Since the amount of hydrogen in the fuel in terms of energy percentage is small (6.7%), the $Le_{Bi-fuel}$ of the mixture is mainly affected by Le_{C8H18}: $Le_{Bi-fuel}$ increases for mixtures with hydrogen substitution or nitrogen dilution due to the increase in Le_{C8H18} values.

The main conclusion that can be drawn from this section is that $Le_{Bi-fuel}$ can be considered constant for all the mixtures investigated here ($Le_{Bi-fuel\ conditions1-5}$ =0.977 ± 3.42 % and $Le_{Bi-fuel\ conditions6-10}$ =2.8 ± 3.46%), implying that the effect of hydrogen substitution or nitrogen addition on the turbulent burning velocity is not linked to a variation in $Le_{Bi-fuel}$ values.

8.5. Turbulent flame characteristics in engine

8.5.1 Local flame curvature

The contour of the flame front was obtained from the flame analysis and the local flame curvature defined as in [66] was deduced :

$$h = \frac{\frac{dx}{ds}\cdot\frac{d^2y}{ds^2} - \frac{dy}{ds}\cdot\frac{d^2x}{ds^2}}{\left[\left(\frac{dx}{ds}\right)^2 + \left(\frac{dy}{ds}\right)^2\right]^{3/2}} \quad (13)$$

with s the curvilinear coordinate.

In this study, the sign convention for curvature yields positive values to regions convex to the unburned gases and negative values to regions convex to the burnt gases. The Probability Density Function (Pdf) of the curvature was then determined at each condition and CAD from the 100 recorded images. An example is given in Figure 11. Pdf values were normalized in order to obtain an area (defined by the Pdf curve) equal to unity.

When the Pdf of curvature was fitted with a normal distribution with $<h>_{pdf}$ the mean and σ the standard deviation, 2σ was ~2.5 mm^{-1} ($\sim\frac{1}{laser\ sheet\ thickness}$) since $<h>_{pdf}$ was ~0 mm.

This implies that, by considering a perfectly normal distribution, 95% of curvature values are in this interval $<h>_{pdf}$ +/- 2σ.

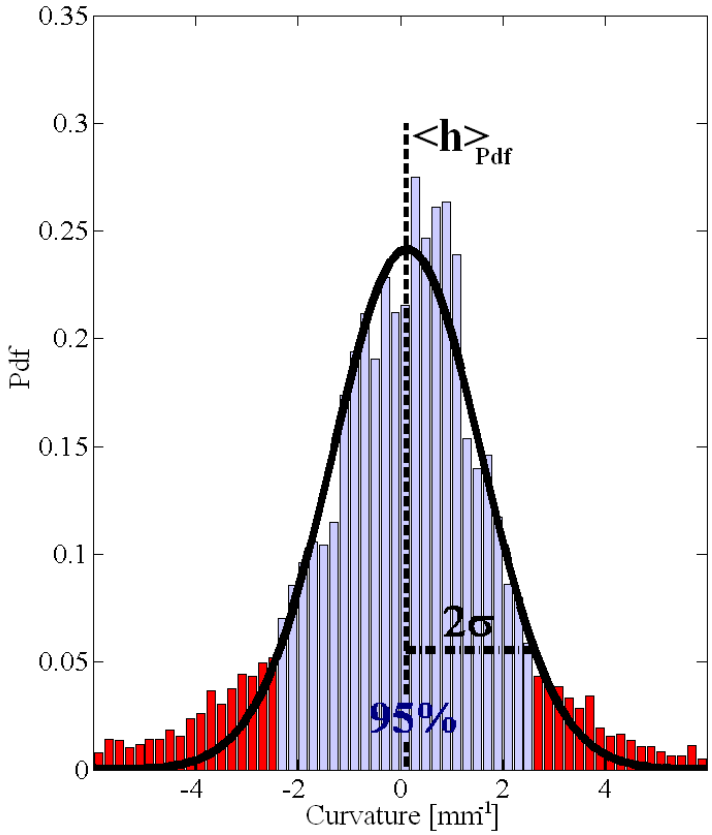

Figure 11. *Pdf of the curvature fitted with a normal distribution.*

The evolution of the mean curvature, $\langle h \rangle_{pdf}$ versus the percentage of the cumulated heat released is shown in Figures 12.a and 12.b for mixtures with methane and iso-octane respectively for all the conditions investigated. All conditions present a similar range of $\langle h \rangle_{pdf}$ values between 0.12 mm^{-1} and 0.33 mm^{-1}. Similar decrease tendencies are also observed in [29, 34]. Dashed lines in Figures 12.a and 12.b correspond to the best linear fit for $\langle h \rangle_{pdf}$ values with the cumulated heat release.

Renou et al. [29] expressed $\langle h \rangle_{pdf}$ as the sum of two terms:

a- the inverse of the laminar flame radius for the same chemical conditions and flame development stages

b- the mean curvature of a similar mono-dimensional turbulent flame front under the same conditions.

They pointed out that the difference in curvature values, for different mixtures and for a fixed development stage (i.e. the same laminar flame radii), is due to the mean curvature of a mono-dimensional turbulent flame, which takes into account turbulence and thermo-diffusive effects. This can explain the similar tendencies obtained in our configuration (Figures 12.a and 12.b), since the turbulence is the same and the Lewis number remains almost constant with hydrogen or nitrogen addition.

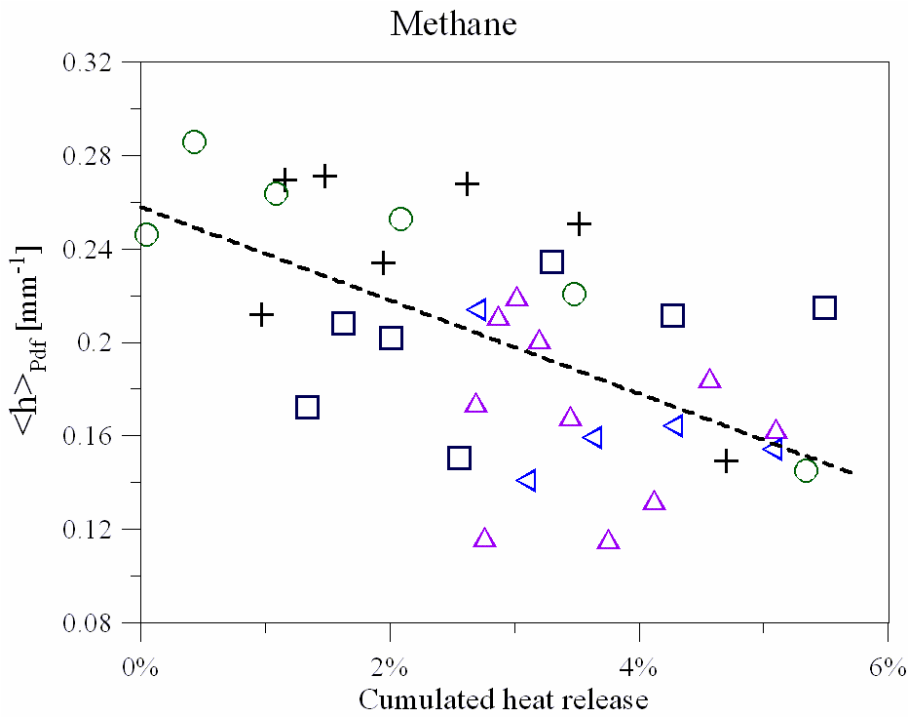

Figure 12.a *Evolution of <h>$_{pdf}$ for methane/hydrogen fuels (conditions 1-5) versus the percentage of the cumulated heat release:*
1: + CH_4/Air; 2: △ CH_4/air/20%N_2; 3: ○ CH_4/40%H_2/Air;
4: ◁ CH_4/40%H_2/20%N_2/Air; 5: □ CH_4/60%H_2/20%N_2/Air.

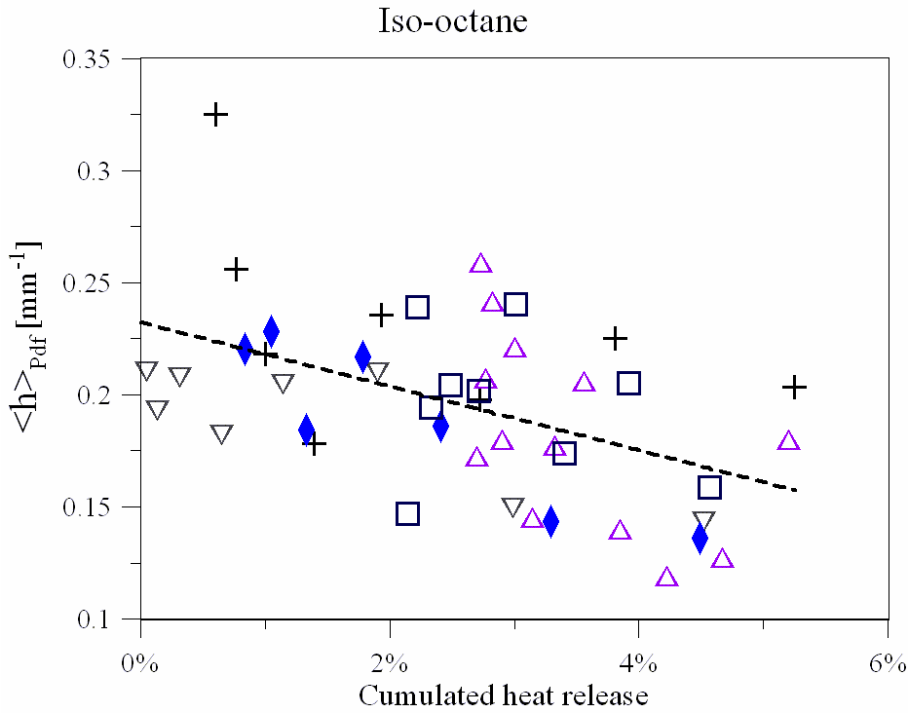

Figure 12.b *Evolution of <h>$_{pdf}$ for iso-octane/hydrogen fuels (conditions 6-10) versus the percentage of the cumulated heat release:*
6: + C_8H_{18}/Air; 7: △ C_8H_{18}/air/20%N_2; 8: ▽ C_8H_{18}/60%H_2/Air;
9: ♦ C_8H_{18}/60%H_2/20%N_2/Air; 10: □ C_8H_{18}/60%H_2/20%N_2/Air.

8.5.2 Turbulent burning velocity

I- Determination of turbulent velocity

To estimate the turbulent burning velocity, the smoothed contour of the flame front was filtered in order to eliminate the different fluctuations [39, 67] as explained in section 8.3.4 concerning image analysis. The local turbulent velocity, S_t, perpendicular to the flame front as illustrated in Figure 13, can be written as:

$$S_t = (\overrightarrow{U_d} - \overrightarrow{U_{gas}}) \cdot \vec{n} \quad (14)$$

where $\overrightarrow{U_d}$ and $\overrightarrow{U_{gas}}$ are the flame front displacement and the fresh gases (just behind the flame front) velocities respectively, and $\vec{n}$ the normal to the flame front.

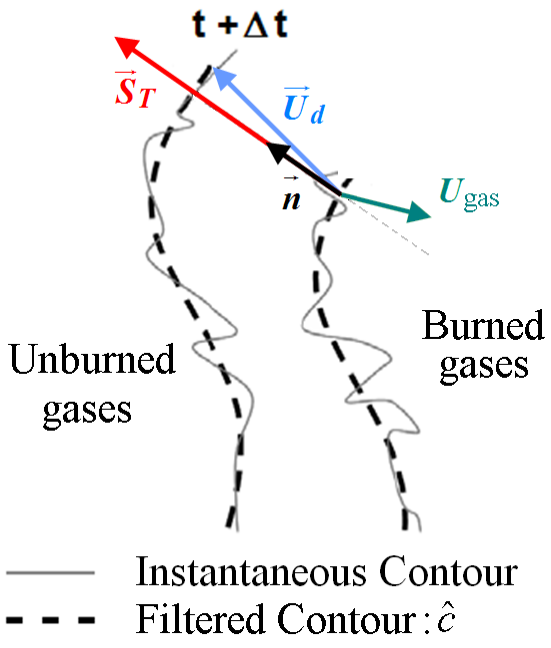

Figure 13. *Local turbulent velocity.*

The local turbulent velocity S_t was experimentally determined thanks to the simultaneous acquisition of aerodynamic fields and instantaneous flame front displacement. The displacement given by the product of flow field velocity (in x and y directions) just behind the flame front and the time interval between two consecutive PIV images (Δt=166.67 µs) was subtracted from this filtered flame contour, $\hat{c}$ to obtain a new contour $\hat{c}_{new}$. Then, from two consecutive contours (the new contour $\hat{c}_{new}$ and the filtered contour $\hat{c}$ of the previous image), the local displacement for all pixels along the contour was evaluated considering a displacement normal to the flame front. The local turbulent velocity was evaluated as the ratio between the local displacement and the time interval Δt.

First, the impact of the filtering process on the turbulent burning speed evaluation was tested. Figure 14 presents the evolution of S_t versus the 'artificial' flame thickness $\Delta\delta_{thick}$ (defined previously). As expected, S_t increases with $\Delta\delta_{thick}$ since the contour length decreases, i.e. the flame surface itself. Moreover, for small values of $\Delta\delta_{thick}$, the application of this methodology to deduce the turbulent velocity is no longer valid since neither of the consecutive flame fronts are homothetic any more due to the strong fluctuations. For high values of $\Delta\delta_{thick}$, S_t tends to an asymptotic value, and the use of a filter induces an additional error on the flame front displacement determination. A value of $\Delta\delta_{thick}$=21 pixels was therefore applied in this study, because it corresponds to the intermediate zone (Figure 14) and is on the same order of magnitude as the integral scale length.

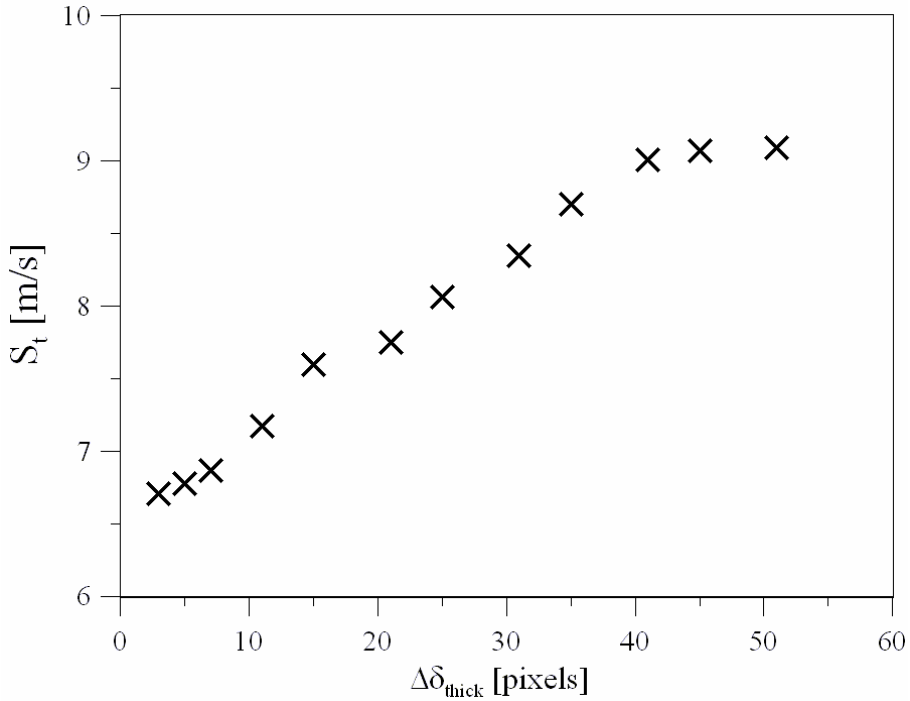

Figure 14. *Example of S_t evolution versus the artificial flame thickness $\Delta\delta_{thick}$.*

II- Turbulent velocity results

The instantaneous turbulent burning velocity was evaluated for all conditions by using Eq.14. For each CAD, the values were first averaged for each image and then averaged for the 100 combustion cycles. The resulting values are plotted as a function of the cumulated heat release in Figure 15 for methane mixtures (conditions 1-5). As expected, the highest values of S_t are obtained when hydrogen is added and without dilution. Case 3 (40% of hydrogen by volume in the fuel mixture, no nitrogen dilution) exhibits values about 21.5 % higher than Case 1 (without hydrogen addition). On the other hand, the lowest values are obtained for diluted mixtures. Case 2 (20% of nitrogen dilution) presents values about 42% lower than Case 1.

The values for Cases 4 and 5 are on the same order as those for Case 1, even if slightly lower values can be seen for Case 4.

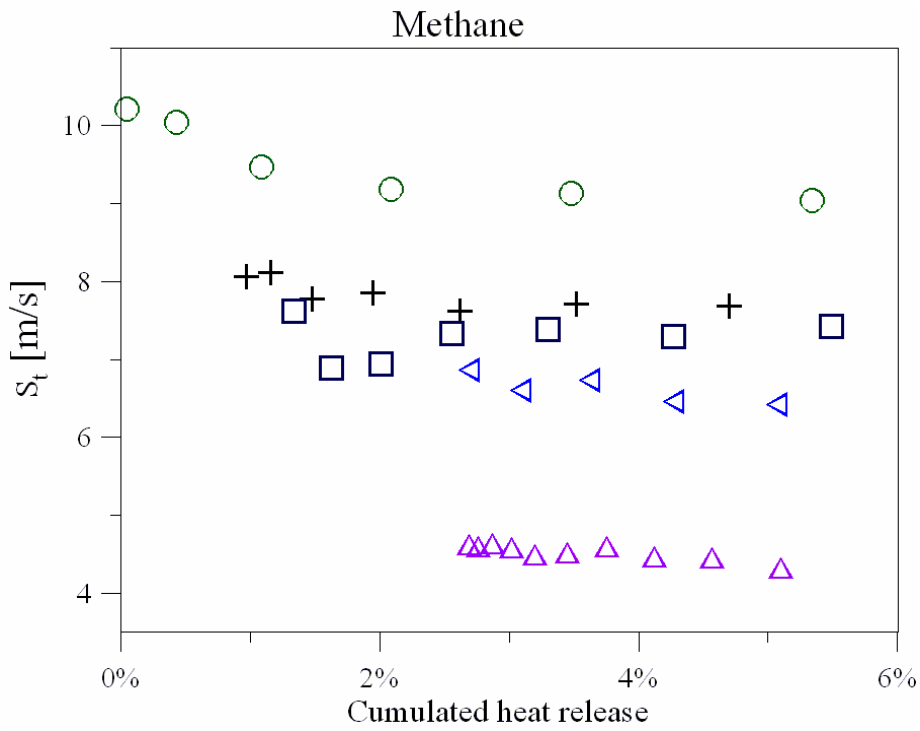

Figure 15. *S_t versus the percentage of cumulated heat release for mixtures with methane (conditions 1-5): 1: CH_4/Air; 2: CH_4/air/20%N_2; 3: CH_4/40%H_2/Air; 4: CH_4/40%H_2/20%N_2/Air; 5: CH_4/60%H_2/20%N_2/Air.*

This behavior as a function of the hydrogen and/or nitrogen contents is in very good agreement with that of the laminar burning velocity values obtained at ambient conditions [47]: 60% of hydrogen substitution is needed to compensate for the effect of 20% of nitrogen dilution in terms of laminar burning velocity. Furthermore, these trends of S_t in this SI engine are also in very good agreement with the conclusions pointed out in our previous study for the same engine conditions but using direct visualization of flame radiation [68], where the initial stages of flame propagation were found to be correlated with the laminar burning velocity values. Figure 16 presents turbulent burning velocities of iso-octane mixtures (conditions 6-10). A nitrogen dilution of 20% (case 7) in volume induced a significant reduction in S_t (about 42%). The case with the highest amount of hydrogen and without nitrogen addition (Case 8) also presents the highest values of S_t. However, the effect of hydrogen is less pronounced in the case of iso-octane than in that of methane: only 5.9% of increase is obtained when 60% of hydrogen is added. This is mainly due to the fact that 60% of hydrogen substitution in volume corresponds respectively to 15.9% and 2.6% in mass for methane and iso-octane. Moreover, at a fixed equivalence ratio, the laminar burning velocity was found to evolve linearly with the mass fraction of hydrogen in the fuel mixture [47, 48] .

As the bi-fuel Le number is quasi-constant for all the conditions investigated, the dominant effect in the evolution of S_t is mainly due to S_l. The values of S_t for Cases 6 and 9 are very close together and linked to very similar values of S_{l0} (0.29m/s and 0.28m/s respectively).

It can also be observed from Figures 15 and 16 that the values of turbulent burning velocity become constant when the heat release reaches 3% of the total heat release. This can be explained by the similar values of laminar burning velocity at these instants since a rise in pressure (reducing effect) counterbalances the effect of a rise in temperature (increasing effect) on the laminar burning velocity (Eq. 6).

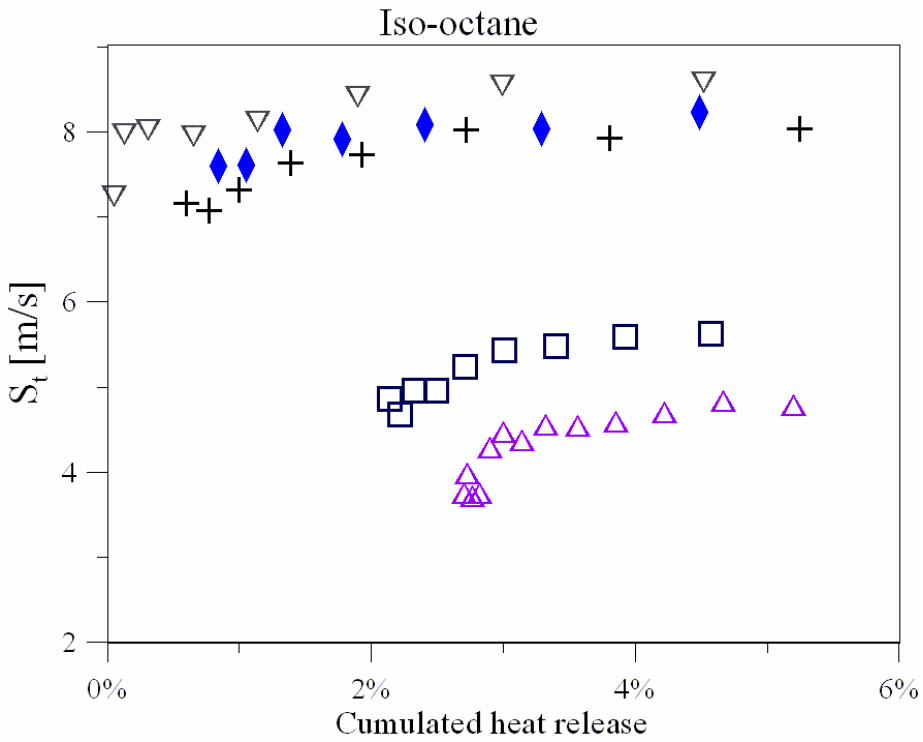

Figure 16. *S_t versus the percentage of cumulated heat release for mixtures with iso-octane (conditions 6-10): 6: + C_8H_{18}/Air; 7: △ C_8H_{18}/air/20%N_2; 8: ▽ C_8H_{18}/60%H_2/Air; 9: ♦ C_8H_{18}/60%H_2/20%N_2/Air; 10: □ C_8H_{18}/60%H_2/20%N_2/Air.*

Many authors have proposed [69-74] expressions to link turbulent burning velocity with laminar burning velocity and turbulent intensity. The ratio S_t / S_l was plotted versus the ratio of the turbulence intensity and the laminar burning velocity (q'/S_l) in Figure 17 for all experimental data, i.e. 81 values, with a constant value of q'. A very good fit was found by using the correlation:

$$S_t / S_l = A \cdot \left(\frac{q'}{S_l} \right)^B \quad (15)$$

with A =9.39 and B =0.4.

The value of coefficient B is very similar to those determined by Kobayashi et al. [71], namely 0.38 for methane/air flames and 0.4 for propane/air flames.

Fairweather et al. [27] determined the turbulent burning velocity of methane/hydrogen mixtures (10%, 20% and 50% hydrogen by volume) but for a wide range of turbulence velocities (0.5m/s-10m/s). They observed that under stoichiometric conditions, the increase in S_t appears to be linked to the increase in the laminar burning velocity due to the addition of hydrogen, but the ratio S_t / S_l did not change with hydrogen addition.

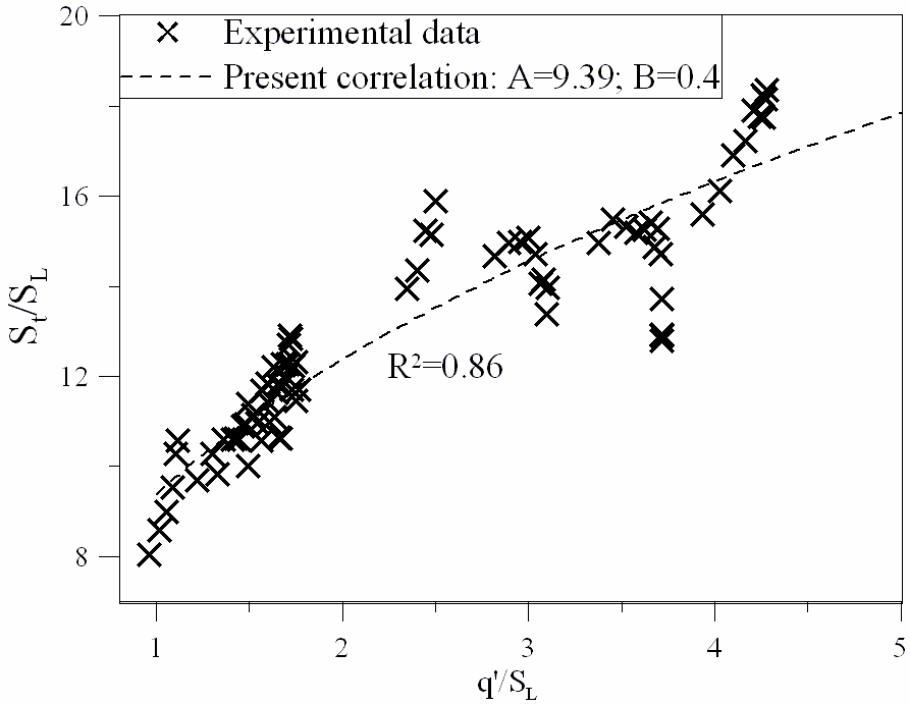

Figure 17. *The ratio S_t / S_l versus the ratio of the turbulence intensity and the laminar burning velocity (q'/S_l) for all experimental data (81 points)*

8.5.3 Comparison of the estimate of ST with a flame growth velocity

In a previous study using a direct flame radiation visualization technique in the same engine [1], a mean equivalent flame radius, $R_{AF,}$ was deduced from the temporal evolution of the projected flame area, A_F:

$$R_{AF} = \left\langle \sqrt{\frac{A_F}{\pi}} \right\rangle \quad (16)$$

A mean flame growth speed S_{AF} can be defined as in [75]:

$$S_{AF} = \frac{\rho_b}{\rho_u} \cdot \frac{dR_{AF}}{dt} \quad (17)$$

The evolution of S_{AF} versus the cumulated heat release for the cases investigated in both studies are plotted in Figures 18 and 19. While this evolution is very similar to that of S_t, plotted in Figures 15 and 16, the quantitative values are lower for S_{AF}: as the flame front was not filtered, this induces higher values of flame surface, leading to lower values of S_{AF} . However, a very good linear correlation is observed (Figure 20) when S_t is plotted versus S_{AF} for all these cases (Cases 1-8 and 10), leading to a linear relationship:

$$S_t = 2.25 S_{AF} - 0.38 \quad (18)$$

The constant, 0.38, represents less than 9% of the minimum value of S_t, which confirms the accuracy of the direct proportionality between S_t and S_{AF}. The coefficient of proportionality is directly linked to the filtering used in the determination of S_t.

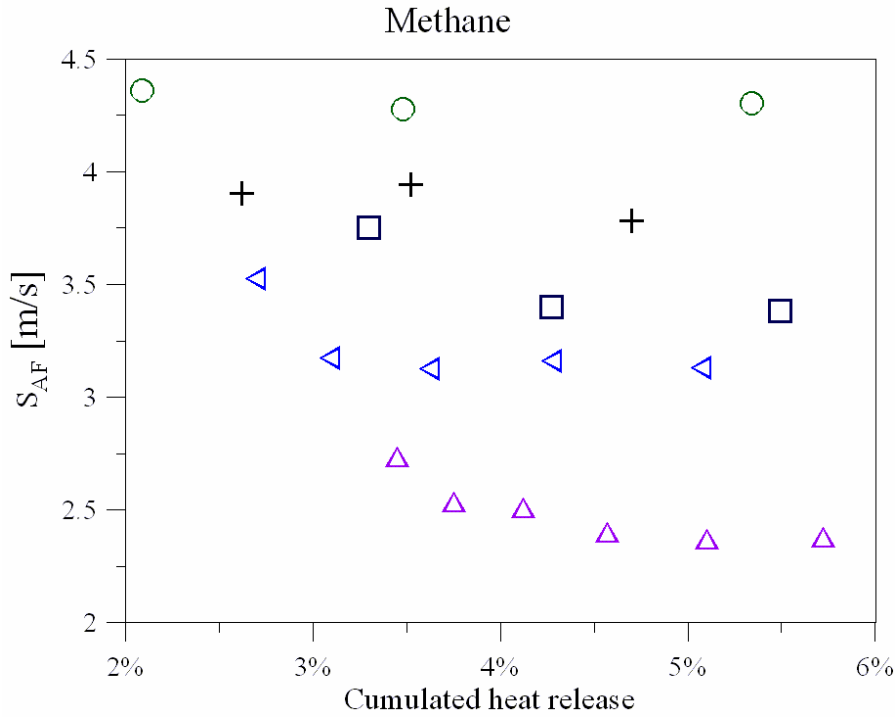

Figure 18. . *Evolution of S_{AF} versus the percentage of cumulated heat release for the mixtures common to this and the previous one [68] for mixtures with methane (conditions 1-5): 1: + CH_4/Air; 2: △ CH_4/air/20%N_2; 3: ○ CH_4/40%H_2/Air; 4: ◁ CH_4/40%H_2/20%N_2/Air; 5: □ CH_4/60%H_2/20%N_2/Air.*

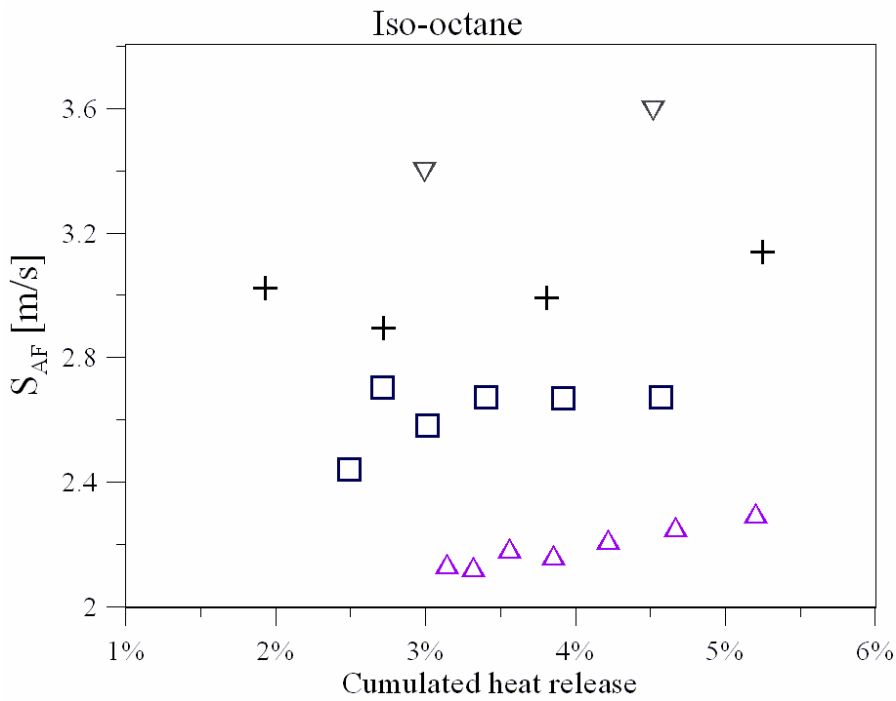

Figure 19. *Evolution of S_{AF} versus the percentage of cumulated heat release for the mixtures common to this study and the previous one [68] for mixtures with iso-octane (conditions 6-8 and 10): 6: + C_8H_{18}/Air; 7: △ C_8H_{18}/air/20%N_2; 8: ▽ C_8H_{18}/60%H_2/Air; 10: □ C_8H_{18}/60%H_2/20%N_2/Air.*

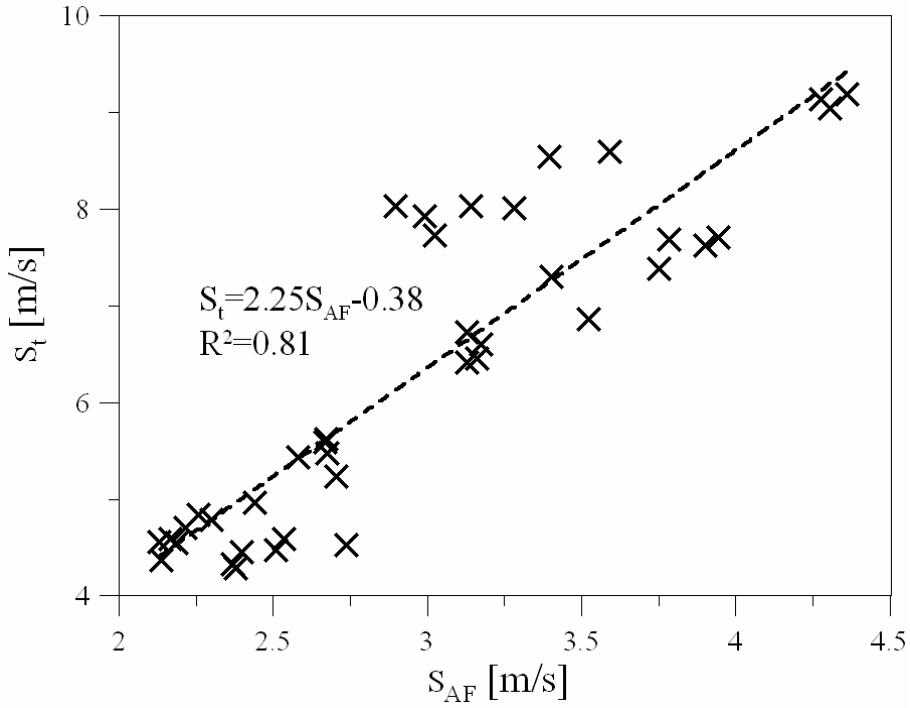

Figure 20. *S_t versus S_{AF} for the conditions common to this study an the previous one [68] (1-8 and 10).*

8.6 Conclusions

The effects of hydrogen substitution with and without nitrogen dilution were experimentally investigated in an optical S.I. engine fuelled with iso-octane or methane as the main fuel under stoichiometric conditions. A new correlation based on data available in the literature is proposed to estimate laminar burning velocities for hydrogen blended fuel mixtures for a wide range of pressure and temperature. The objective was to provide a correlation to estimate the laminar burning velocities at thermodynamic conditions occuring in S.I engines. Turbulent burning velocity was determined by using simultaneously laser tomography imaging and Particle Image Velocimetry (PIV). The values were compared to the mean flame growth speed reported in our previous study by using the direct flame radiation visualization technique [68].

The main conclusions of this work are:

- The increasing effect of hydrogen substitution (by volume) on the turbulent burning velocity was found to be more pronounced in the case of methane than in the case of iso-octane. Moreover this increase was found to be in very good agreement with the laminar burning velocity results.
- The reducing effect of nitrogen dilution on the turbulent velocity is similar for methane and iso-octane: with 20% of nitrogen dilution the turbulent burning velocity decreases by ~42% compared to the fuel/air mixture without dilution.
- A very good correlation between the turbulent burning velocity, the laminar burning velocity, and the turbulence intensity was found. This correlation, having the form: $S_t / S_l = A \cdot \left(\frac{q'}{S_l} \right)^B$ is the same for iso-octane/hydrogen and methane/hydrogen fuels. This confirms that it is the laminar burning velocity, rather than the Lewis number, that has the dominant effect on the turbulent burning velocity for these S.I. engine conditions. The Lewis number was found to be almost constant for all the conditions investigated ($Le_{Bi-fuel\,CH4\_H2}$ =0.977 ± 3.42 % and $Le_{Bi-fuel\,C8H18\_H2}$ =2.8 ± 3.46%).
- The present values of turbulent burning velocity show a similar evolution to the mean flame growth velocity determined in our previous study by using the direct flame radiation visualization technique. Moreover, a linear correlation was observed between the turbulent burning velocity and flame growth speed.
- The excellent agreement observed in the results of these two different experimental techniques leads to the main conclusion of this study: mean flame growth velocity and turbulent burning velocity, at a given turbulence intensity, are defined by the laminar burning velocity of the mixture. The effect of dilution and fuel composition on the

flame development in a spark ignition engine can, therefore, be simply predicted by estimating the laminar burning velocity of the mixture considered.

8.7 References

[1] T. Shinagawa, T. Okumura, S. Furuno, K.-O. Kim, *Effects of Hydrogen Addition to SI Engine on Knock Behavior*, SAE paper, 2004-01-1851 (2004).

[2] J. A. Topinka, M. D. Gerty, J. B. Heywood, J. C. Keck, *Knock Behavior of a Lean-Burn, H2 and CO Enhanced, SI Gasoline Engine Concept*, SAE paper, 2004-01-0975 (2004).

[3] T. Suzuki, Y. Sakurai, *Effect of Hydrogen Rich Gas and Gasoline Mixed Combustion on Spark Ignition Engine*, SAE paper, 2006-01-3379 (2006).

[4] J. Wang, Z. Huang, Y. Fang, B. Liu, K. Zeng, H. Miao, D. Jiang, *Combustion behaviors of a direct-injection engine operating on various fractions of natural gas-hydrogen blends*, International Journal of Hydrogen Energy, 32 (2007), pp. 3555-3564.

[5] T. Thurnheer, P. Soltic, P. Dimopoulos Eggenschwiler, *S.I. engine fuelled with gasoline, methane and methane/hydrogen blends: Heat release and loss analysis*, International Journal of Hydrogen Energy, 34 (2009), pp. 2494-2503.

[6] B. Morrone, A. Unich, *Numerical investigation on the effects of natural gas and hydrogen blends on engine combustion*, International Journal of Hydrogen Energy, 34 (2009), pp. 4626-4634.

[7] N. Apostolescu, R. Chiriac, *A Study of Combustion of Hydrogen-Enriched Gasoline in a Spark Ignition Engine*, SAE paper, 960603 (1996).

[8] N. Kahraman, B. Çeper, S. O. Akansu, K. Aydin, *Investigation of combustion characteristics and emissions in a spark-ignition engine fuelled with natural gas-hydrogen blends*, International Journal of Hydrogen Energy, 34 (2009), pp. 1026-1034.

[9] C. Pana, N. Negurescu, M. G. Popa, A. Cernat, D. Soare, *An Investigation of the Hydrogen Addition Effects to Gasoline Fueled Spark Ignition Engine*, SAE paper, 2007-01-1468 (2007).

[10] M. A.-R. Sadiq Al-Baghdadi, H. A.-K. Shahad Al-Janabi, *Improvement of performance and reduction of pollutant emission of a four stroke spark ignition engine fueled with hydrogen-gasoline fuel mixture*, Energy Conversion and Management, 41 (2000), pp. 77-91.

[11] C. D. Rakopoulos, M. A. Scott, D. C. Kyritsis, E. G. Giakoumis, *Availability analysis of hydrogen/natural gas blends combustion in internal combustion engines*, Energy, 33 (2008), pp. 248-255.

[12] P. Dimopoulos, K. Boulouchos, C. Rechsteiner, R. H. P. Soltic, *Combustion Characteristics of Hydrogen-Natural Gas Mixtures in Passenger Car Engines*, SAE paper, 2007-24-0065 (2007).

[13] T. Alger, J. Gingrich, B. Mangold, *The Effect of Hydrogen Enrichment on EGR Tolerance in Spark Ignited Engines*, SAE paper, 2007-24-0015 (2007).

[14] E. J. Tully, J. B. Heywood, *Lean-Burn Characteristics of a Gasoline Engine Enriched with Hydrogen from a Plasmatron Fuel Reformer*, SAE paper, 2003-01-0630 (2003).

[15] E. Hu, Z. Huang, B. Liu, J. Zheng, X. Gu, B. Huang, *Experimental investigation on performance and emissions of a spark-ignition engine fuelled with natural gas-hydrogen blends combined with EGR*, International Journal of Hydrogen Energy, 34 (2009), pp. 528-539.

[16] E. Hu, Z. Huang, B. Liu, J. Zheng, X. Gu, *Experimental study on combustion characteristics of a spark-ignition engine fueled with natural gas-hydrogen blends combining with EGR*, International Journal of Hydrogen Energy, 34 (2009), pp. 1035-1044.

[17] B. Huang, E. Hu, Z. Huang, J. Zheng, B. Liu, D. Jiang, *Cycle-by-cycle variations in a spark ignition engine fueled with natural gas-hydrogen blends combined with EGR*, International Journal of Hydrogen Energy, 34 (2009), pp. 8405-8414.

[18] A. A. Quader, J. E. Kirwan, M. J. Grieve, *Engine performance and emissions near the dilute limit with hydrogen enrichment using a on-board reforming strategy*, SAE paper, 2003-01-1356 (2003).

[19] T. Allgeier, M. Klenk, T. Landenfeld, E. Conte, K. Boulouchos, J. Czerwinski, *Advanced Emission and Fuel Economy Concept Using Combined Injection of Gasoline and Hydrogen in SI-Engines*, SAE paper, 2004-01-1270 (2004).

[20] I. Saanum, M. Bysveen, P. Tunestål, B. Johansson, *Lean Burn Versus Stoichiometric Operation with EGR and 3-Way Catalyst of an Engine Fueled with Natural Gas and Hydrogen Enriched Natural Gas*, SAE paper, 2007-01-0015 (2007).

[21] R. Herweg, R. R. Maly, *A Fundamental Model for Flame Kernel Formation in S. I. Engines*, SAE paper, 922243 (1992).

[22] E. Conte, K. Boulouchos, *Experimental investigation into the effect of reformer gas addition on flame speed and flame front propagation in premixed, homogeneous charge gasoline engines*, Combustion and Flame, 146 (2006), pp. 329-347.

[23] F. Meier, J. Köhler, W. Stolz, W. H. Bloss, *Cycle-Resolved Hydrogen Flame Speed Measurements with High Speed Schlieren Technique in a Hydrogen Direct Injection SI Engine*, SAE paper, 942036 (1994).

[24] M. F. Rosati, P. G. Aleiferis, *Hydrogen SI and HCCI Combustion in a Direct-Injection Optical Engine*, SAE paper, 2009-01-1921 (2009).

[25] P. G. Aleiferis, A. M. K. P. Taylor, J. H. Whitelaw, K. Ishii,Y. Urata, *Cyclic Variations of Initial Flame Kernel Growth in a Honda VTEC-E Lean-Burn Spark-Ignition Engine*, SAE paper, 2000-01-1207 (2000).

[26] P. G. Aleiferis, A. M. K. P. Taylor, K. Ishii,Y. Urata, *The nature of early flame development in a lean-burn stratified-charge spark-ignition engine*, Combustion and Flame, 136 (2004), pp. 283-302.

[27] M. Fairweather, M. P. Ormsby, C. G. W. Sheppard, R. Woolley, *Turbulent burning rates of methane and methane-hydrogen mixtures*, Combustion and Flame, 156 (2009), pp. 780-790.

[28] G. Woschni, *Universally Applicable Equation for the Instantaneous Heat Transfer Coefficient in the Internal Combustion Engine*, SAE paper, 670931 (1967).

[29] B. Renou, A. Boukhalfa, D. Puechberty, M. Trinité, *Local scalar flame properties of freely propagating premixed turbulent flames at various Lewis numbers*, Combustion and Flame, 123 (2000), pp. 507-521.

[30] B. Lecordier, *Etude de l'interaction de la propagation d'une flamme prémélangée avec le champ aérodynamique, par association de la tomographie laser et de la vélocimétrie par images de particules* PhD Thesis, University of Rouen (1997).

[31] D. L. Reuss, *Cyclic Variability of Large-Scale Turbulent Structures in Directed and Undirected IC Engine Flows*, SAE Technical Paper, 2000-01-0246 (2000).

[32] Y. Li, H. Zhao, Z. Peng, N. Ladommatos, *Tumbling flow analysis in a four-valve spark ignition engine using particle image velocimetry*, International Journal of Engine Research, 3 (2002), pp. 139-155.

[33] F. Foucher, L. Landry, F. Halter, C. Mounaïm-Rouselle, *Turbulent flow fields analysis of a Spark-Ignition engine as function of the boosted pressure*, 14th International Symposium on Laser Applications to Fluid Mechanics (2008).

[34] O. Pajot, *Etude expérimentale de l'influence de l'aérodynamique sur le comportement et la structure du front de flamme dans les conditions d'un moteur à allumage commandé*, *PhD Thesis, University of Orleans, France*, 2000.

[35] W.-C. Choi, Y. G. Guezennec, *Experimental Investigation to Study Convective Mixing, Spatial Uniformity, and Cycle-to-Cycle Variation During the Intake Stroke in an IC Engine*, Journal of Engineering for Gas Turbines and Power, 122 (2000), pp. 493-501.

[36] C. F. a. V. Sick, D. L. Reuss, W. J. A. Dahm, *Turbulence Properties of High and Low Swirl In-Cylinder Flows*, SAE Technical Paper, 2002-01-2841 (2002).

[37] O. Vermorel, S. Richard, O. Colin, C. Angelberger, A. Benkenida, D. Veynante, *Towards the understanding of cyclic variability in a spark ignited engine using multi-cycle LES*, Combustion and Flame, 156 (2009), pp. 1525-1541.

[38] J. B. Heywood, *Internal Combustion Engine Fundamentals*, McGraw-Hill, 1988.

[39] L. Landry, *Etude expérimentale des modes de combustion essence sous forte pression et forte dilution*, PhD Thesis, University of Orleans, France (2009).

[40] F. Foucher, *Etude Expérimentale de l'Interaction Flamme-Paroi: Application au Moteur à Allumage Commandé*, Ph.D. thesis, University of Orléans, France (2002).

[41] D. Linse, C. Hasse, B. Durst, *An experimental and numerical investigation of turbulent flame propagation and flame structure in a turbo-charged direct injection gasoline engine*, Combustion Theory and Modelling, 13: 1 (2009), pp. 167-188.

[42] O. Colin, F. Ducros, D. Veynante, T. Poinsot, *A thickened flame model for large eddy simulations of turbulent premixed combustion*, Physics of Fluids, 12 (2000), pp. 1843-1863.

[43] C. Nottin, R. Knikker, M. Boger, D. Veynante, *Large eddy simulations of an acoustically excited turbulent premixed flame*, Proceedings of the Combustion Institute, 28 (2000), pp. 67-73.

[44] R. Knikker, D. Veynante, C. Meneveau, *A priori testing of a similarity model for large eddysimulations of turbulent premixed combustion*, Proceedings of the Combustion Institute, 29 (2002), pp. 2105-2111.

[45] R. Borghi, D. Escudie, *Assessment of a theoretical model of turbulent combustion by comparison with a simple experiment*, Combustion and Flame, 56 (1984), pp. 149-164.

[46] M. Metghalchi, J. C. Keck, *Burning velocities of mixtures of air with methanol, isooctane, and indolene at high pressure and temperature*, Combustion and Flame, 48 (1982), pp. 191-210.

[47] T. Tahtouh, F. Halter, E. Samson, C. Mounaïm-Rousselle, *Effects of hydrogen addition and nitrogen dilution on the laminar flame characteristics of premixed methane-air flames*, International Journal of Hydrogen Energy, 34 (2009), pp. 8329-8338.

[48] T. Tahtouh, F. Halter, C. Mounaïm-Rousselle, *Laminar premixed flame characteristics of hydrogen blended iso-octane-air-nitrogen mixtures*, International Journal of Hydrogen Energy, doi:10.1016/j.ijhydene.2010.08.148 (2010).

[49] X. J. Gu, M. Z. Haq, M. Lawes, R. Woolley, *Laminar burning velocity and Markstein lengths of methane-air mixtures*, Combustion and Flame, 121 (2000), pp. 41-58.

[50] M. Elia, M. Ulinski, M. Metghalchi, *Laminar Burning Velocity of Methane--Air--Diluent Mixtures*, ASME, 2001, pp. 190-196.

[51] P. Han, M. David Checkel, B. A. Fleck, N. L. Nowicki, *Burning velocity of methane/diluent mixture with reformer gas addition*, Fuel, 86 (2007), pp. 585-596.

[52] C. Mandilas, M. P. Ormsby, C. G. W. Sheppard, R. Woolley, *Effects of hydrogen addition on laminar and turbulent premixed methane and iso-octane-air flames*, Proceedings of the Combustion Institute, 31 (2007), pp. 1443-1450.

[53] M. I. Hassan, K. T. Aung, G. M. Faeth, *Measured and predicted properties of laminar premixed methane/air flames at various pressures*, Combustion and Flame, 115 (1998), pp. 539-550.

[54] F. Halter, C. Chauveau, N. Djebaïli-Chaumeix, I. Gökalp, *Characterization of the effects of pressure and hydrogen concentration on laminar burning velocities of methane-hydrogen-air mixtures*, Proceedings of the Combustion Institute, 30 (2005), pp. 201-208.

[55] G. Rozenchan, D. L. Zhu, C. K. Law, S. D. Tse, *Outward propagation, burning velocities, and chemical effects of methane flames up to 60 ATM*, Proceedings of the Combustion Institute, 29 (2002), pp. 1461-1470.

[56] R. T. E. Hermanns, *Laminar Burning Velocities of Methane-Hydrogen-Air Mixtures*, PhD. Thesis, Eindhoven University of Technology (2007).

[57] Y. Ogami, H. Kobayashi, *Laminar Burning Velocity of Stoichiometric CH4/air Premixed Flames at High-Pressure and High-Temperature*, JSME Internation Journal, 48 (3) (2005), pp. 603-609.

[58] D. Bradley, R. A. Hicks, M. Lawes, C. G. W. Sheppard, R. Woolley, *The Measurement of Laminar Burning Velocities and Markstein Numbers for Iso-octane-Air and Iso-octane-n-Heptane-Air Mixtures at Elevated Temperatures and Pressures in an Explosion Bomb*, Combustion and Flame, 115 (1998), pp. 126-144.

[59] S. Jerzembeck, N. Peters, P. Pepiot-Desjardins, H. Pitsch, *Laminar burning velocities at high pressure for primary reference fuels and gasoline: Experimental and numerical investigation*, Combustion and Flame, 156 (2009), pp. 292-301.

[60] R. J. Johnston, J. T. Farrell, *Laminar burning velocities and Markstein lengths of aromatics at elevated temperature and pressure*, Proceedings of the Combustion Institute, 30 (2005), pp. 217-224.

[61] R. Stone, A. Clarke, P. Beckwith, *Correlations for the Laminar-Burning Velocity of Methane/Diluent/Air Mixtures Obtained in Free-Fall Experiments*, Combustion and Flame, 114 (1998), pp. 546-555.

[62] S. Y. Liao, D. M. Jiang, Q. Cheng, *Determination of laminar burning velocities for natural gas*, Fuel, 83 (2004), pp. 1247-1250.

[63] M. Matalon, B. J. Matkowsky, *Flames as gasdynamic discontinuities*, Journal of Fluid Mechanics Digital Archive, 124 (1982), pp. 239-259.

[64] G. S. Jackson, R. Sai, J. M. Plaia, C. M. Boggs, K. T. Kiger, *Influence of H2 on the response of lean premixed CH4 flames to high strained flows*, Combustion and Flame, 132 (2003), pp. 503-511.

[65] C. K. Law, G. Jomaas, J. K. Bechtold, *Cellular instabilities of expanding hydrogen/propane spherical flames at elevated pressures: theory and experiment*, Proceedings of the Combustion Institute, 30 (2005), pp. 159-167.

[66] F. Mokhtarian, A. Mackworth, *Scale-based description and recognition of plananr curves and two-dimentsional shapes*, IEEE Transactions, 34-43 (1986).

[67] F. Foucher, S. Burnel, C. Mounaïm-Rousselle, *Evaluation of burning rates in the vicinity of the piston in a spark-ignition engine*, Proceedings of the Combustion Institute, 29 (2002), pp. 751-757.

[68] T. Tahtouh, F. Halter, C. MounaÏm-Rousselle, E. Samson, *Experimental Investigation of the Initial Stages of Flame Propagation in a Spark-Ignition Engine: Effects of Fuel, Hydrogen Addition and Nitrogen Dilution*, SAE Technical Paper 2010-01-1451 (2010).

[69] Ö. L. Gülder, *Laminar burning velocities of methanol, ethanol and isooctane-air mixtures*, Symposium (International) on Combustion, 19 (1982), pp. 275-281.

[70] B. Bédat, R. K. Cheng, *Experimental study of premixed flames in intense isotropic turbulence*, Combustion and Flame, 100 (1995), pp. 485-494.

[71] H. Kobayashi, Y. Kawabata, K. Maruta, *Experimental study on general correlation of turbulent burning velocity at high pressure*, Symposium (International) on Combustion, 27 (1998), pp. 941-948.

[72] H. Kobayashi, K. Seyama, H. Hagiwara, Y. Ogami, *Burning velocity correlation of methane/air turbulent premixed flames at high pressure and high temperature*, Proceedings of the Combustion Institute, 30 (2005), pp. 827-834.

[73] Ö. L. Gülder, *Turbulent premixed flame propagation models for different combustion regimes*, Symposium (International) on Combustion, 23 (1990), pp. 743-750.

[74] S. Daniele, P. Jansohn, J. Mantzaras, K. Boulouchos, *Turbulent flame speed for syngas at gas turbine relevant conditions*, Proceedings of the Combustion Institute, In Press, Corrected Proof.

[75] B. Renou, A. Boukhalfa, D. Puechberty, M. Trinité, *Effects of stretch on the local structure of preely propagating premixed low-turbulent flames with various lewis numbers*, Symposium (International) on Combustion, 27 (1998), pp. 841-847.

Conclusions et Perspectives

Ce travail de thèse avait pour but une étude détaillée des effets combinés de l'ajout de l'hydrogène et de la dilution dans un moteur à allumage commandé. En effet, dans les modes de fonctionnement des moteurs actuels, la recirculation des gaz d'échappement (EGR) est souvent utilisée comme stratégie de réduction des monoxydes d'azote à leur source. Or le fonctionnement des moteurs à fort taux de dilution n'est pas si simple que ca, pouvant mener à des instabilités cycle à cycle importantes, voire des ratés d'allumage. L'intérêt de l'ajout de l'hydrogène combiné avec de la dilution réside donc dans l'amélioration de la stabilité de la combustion tout en diminuant la consommation en carburant et les émissions polluantes, spécialement les NO_X.

L'étude bibliographique, présentée en première partie a permis de mettre en évidence le potentiel de cette combinaison (hydrogène et dilution). Toutefois, la plupart de ces études effectuées sont basées sur des approches globales d'analyse de performances et d'émissions polluantes.

Afin d'atteindre nos objectifs, nous avons divisé ce travail en trois parties principales :

I- Analyse des performances et des émissions de polluants sur moteur mono-cylindre à injection indirecte

L'objectif de cette première partie était donc de faire varier séparément plusieurs paramètres : la richesse du mélange, le taux de dilution (dilution ici simulée par le N_2), la fraction d'hydrogène dans le carburant et la pression d'admission, pour une iso-puissance motrice disponible.

Les principaux résultats de cette étude dans le moteur à allumage commandé peuvent se résumer comme suit:

- ✓ Pour des faibles quantités d'hydrogène dans le carburant (<40% en volume), l'ajout de l'hydrogène n'a pas d'effet sur la limite de fonctionnement du moteur en mélange pauvre ni en dilution. Ces limites de fonctionnement sont déduites en utilisant comme critère la variation cycle-à-cycle du travail du moteur (<5%). Cependant l'ajout des quantités d'hydrogène plus importantes permet une extension de ces limites de fonctionnement du moteur.
- ✓ Les émissions HC diminuent quand la quantité d'hydrogène, dans le mélange carburant, augmente. Cette diminution est principalement due, dans le cas des mélanges sans dilution, à l'augmentation du rapport H/C dans le mélange air-carburant.

- ✓ Les émissions de NO_X diminuent avec la dilution à l'azote et l'ajout d'air (dans le cas de mélanges pauvres). Cependant la dilution à l'azote (simulant l'EGR) a plus d'effet sur cette réduction que la dilution à l'air (mélanges pauvres). Finalement, pour tous les cas étudiés, l'ajout d'hydrogène n'affecte pas les émissions NO_X.
- ✓ L'ajout de l'hydrogène entraine une réduction des émissions CO, accentuée dans le cas avec dilution.
- ✓ A iso-conditions, le rendement de combustion s'améliore avec l'ajout de l'hydrogène, ce qui permettrait de compenser sa diminution dans le cas de dilution par l'EGR ou par l'air.
- ✓ L'ajout de l'hydrogène permet l'extension des limites de fonctionnement en dilution et richesse. Il permet donc, pour un travail du moteur fixé, d'atteindre des pressions d'admission plus importantes et donc de réduire les pertes par pompage. Le rendement indiqué du moteur, à une pression d'admission fixe, croit avec l'ajout de l'hydrogène, de la dilution à l'azote et à l'air.

II- Analyse de l'effet de l'hydrogène dans des mélanges air-carburant dilué ou non sur la vitesse de combustion laminaire

Pour réaliser cette étude, une chambre de combustion à volume constant a été utilisée afin d'estimer les vitesses fondamentales de flamme laminaires à partir de la méthodologie basée sur la propagation de flamme sphérique.

Dans un premier temps nous avons comparé trois méthodes différentes de traitement des données (dont une nouvelle) afin de déduire la vitesse de combustion laminaire à taux d'étirement nul et la longueur de Markstein. Ces méthodologies se basent sur la relation linéaire entre l'étirement de flamme et la vitesse de combustion laminaire étirée dans le cas d'une propagation sphérique. Nous avons montré que :

- ✓ La nouvelle méthodologie proposée possède deux avantages principaux par rapport à celles existantes dans la littérature :
    - Lissage des fluctuations générées durant la phase de détermination expérimentale du rayon du front de flamme.
    - Elimination des erreurs causées par la dérivation temporelle du rayon du front de flamme.

Cette nouvelle méthodologie a été utilisée par la suite pour la détermination de la vitesse de combustion laminaire et des longueurs de Markstein des mélanges méthane/hydrogène/nitrogène/air. Nous avons ainsi montré que :

- ✓ La vitesse de combustion laminaire :
  - augmente linéairement avec le pourcentage massique d'hydrogène dans le mélange carburant (méthane/hydrogène).
  - diminue (mains non linéairement) avec le pourcentage volumique de diluant dans le mélange des gaz frais.
- ✓ La longueur de Markstein
  - diminue avec l'augmentation de la quantité d'hydrogène dans le mélange carburant, montrant ainsi l'augmentation de la stabilité de la combustion.
  - augmente avec la dilution, image de l'augmentation de l'instabilité.

Une nouvelle approche non-linéaire, reliant l'étirement et la vitesse de propagation étirée, a été décrite et comparée à l'approche classiquement utilisée linéaire. Cette approche est fondamentale dans le cas de l'utilisation de l'iso-octane comme carburant.

- ✓ Dans certains cas de mélanges pauvres ou fortement dilués, le rapport de la vitesse étirée sur la vitesse non-étirée atteint des valeurs >>1. Or, la validité de l'approche linéaire est basée sur l'hypothèse d'une valeur égale à 1. Cette hypothèse n'est plus donc valable dans ces cas et le calcul de la vitesse de combustion laminaire est donc plus exact par l'approche non-linéaire.
- ✓ Un critère basé sur le rapport entre la longueur de Markstein et le rayon initial a été proposé pour l'utilisation de l'approche non-linéaire plutôt que l'approche linéaire. Des valeurs de ce rapport < à 0.18 impliquent des erreurs liées à l'utilisation de l'approche linéaire < à 5%, ce qui est du même ordre de grandeur que les incertitudes liées à la procédure expérimentale. Pour des valeurs de ce rapport plus grandes (>0.18), il est ainsi préférable d'utiliser l'approche non-linéaire afin de limiter les erreurs induites par l'approche linéaire.

La détermination de la vitesse de combustion et de la longueur de Markstein a été effectuée par la suite en utilisant l'approche non-linéaire. Nous avons ainsi obtenu des conclusions tout à fait similaires au cas du méthane.

Enfin, pour les deux carburants principaux, méthane et iso-octane, des corrélations ont été proposées à partir des nos résultats expérimentaux permettant d'estimer la vitesse fondamentale de combustion laminaire à étirement nul pour des mélanges carburant-hydrogène- air avec ou sans dilution à pression atmosphérique et température ambiante.

III-Analyse de la combustion turbulente dans le moteurs à allumage commandé

Dans cette partie, deux types d'expériences ont été réalisées dans le moteur mono-cylindre à accès optiques: des visualisations directes du rayonnement de flamme et la tomographie de flamme couplée à la mesure de vitesse par PIV à haute cadence dans un moteur à allumage commandé muni d'un accès optique. Les principales conclusions obtenues durant cette étude sont les suivantes :

- ✓ L'effet positif de l'hydrogène sur la vitesse de combustion, c'est-à-dire l'augmentation, est le plus prononcé dans les phases initiales de la combustion, quand le dégagement de chaleur est inférieur à 10% du dégagement de chaleur total. En contre-partie, la dilution a un effet contraire qui s'étend même dans les phases plus avancées de la combustion (50% du dégagement de chaleur total). Cet effet positif de la présence de l'hydrogène devient plus important avec la dilution.

- ✓ 60% d'hydrogène en volume dans le mélange carburant sont nécessaires pour compenser l'effet de 20% de dilution par N_2 dans le moteur, pour maintenir la même durée combustion et le même niveau de variations cycliques. Or cela est en très bon accord avec les résultats obtenus sur la vitesse fondamentale de flamme : dans le cas de 20% de dilution, il faut ajouter 60% d'hydrogène en volume pour maintenir la vitesse de combustion laminaire au même niveau que celle du mélange méthane/air. Par conséquent, une très bonne corrélation entre la phase initiale de combustion et la vitesse de combustion laminaire mesurée sous pression atmosphérique et température ambiante a été obtenue.

- ✓ Les variations cycle-à-cycle diminuent avec l'ajout d'hydrogène et augmentent avec la dilution. En plus, l'effet positif de l'hydrogène sur ces variations est plus important dans le cas des mélanges dilués. Il est aussi plus visible sur les phases avancées de la combustion (50% du dégagement de chaleur total) que dans les phases initiales (10% du dégagement de chaleur total).

- ✓ La détermination du nombre de Lewis a montré que ce dernier est constant pour tous les mélanges étudiés dans nos conditions ($Le_{Bi-fuel\ C8H18\_H2}$=2.8±3.46%, $Le_{Bi-fuel\ CH4\_H2}$ =0.977 ± 3.42 %).

- ✓ L'effet positif de l'hydrogène sur la vitesse de combustion turbulente est plus prononcé dans le cas des mélanges méthane/hydrogène que les mélanges iso-octane/hydrogène, ce qui est en très bon accord avec les évolutions de vitesse de combustion laminaire.

- ✓ L'effet négatif de la dilution sur la vitesse de combustion turbulente est similaire dans le cas des mélanges méthane/hydrogène et iso-octane/hydrogène : 20% de dilution en volume induit une réduction de ~42% de la vitesse de combustion turbulente.

- ✓ En se basant sur nos résultats expérimentaux de vitesses de combustion turbulente, déterminés dans la chambre de combustion d'un moteur à allumage commandé, nous avons proposé une corrélation liant la vitesse de combustion turbulente, la vitesse de propagation laminaire et l'intensité turbulente. Cette corrélation, identique dans le cas méthane/hydrogène et iso-octane/hydrogène, a confirmé le fait que la vitesse de combustion laminaire a un effet prépondérant comparé au nombre de Lewis, sur la vitesse de combustion turbulente dans un moteur à allumage commandé et dans les conditions étudiées.
- ✓ Finalement, les valeurs de vitesse de combustion turbulente corrèlent linéairement avec celles de la vitesse de propagation de flamme obtenues, à l'aide de deux différentes techniques.

Perspectives

Lors de notre étude, nous avons utilisé 2 diagnostics optiques dans un moteur accès optique (la chemiluminescence de la flamme et la tomographie par plan laser du front de flamme couplé à la mesure de vitesse par vélocimétrie par imagerie de particules). La cohérence des résultats obtenus à partir de ces deux types de mesures est très intéressante, puisqu'elle permet de conclure que finalement les informations obtenues à partir de la visualisation de la propagation de flamme dans un moteur caractérisent suffisamment la combustion turbulente qui se propage dans un moteur à allumage commandé et ainsi de prédire des effets relatifs au mélange air-carburant.

De plus, nous avons montré qu'en variant de nombreux paramètres du mélange, pendant la phase initiale de la combustion, si les conditions aérodynamiques sont identiques, le déroulement de la combustion dépend uniquement de la vitesse de combustion laminaire. Cela confirme et affirme l'importance de la vitesse de combustion laminaire, caractéristique principale du mélange air-carburant. Ceci résulte très utile pour des futures études de combustion turbulente dans le domaine des moteurs à combustions internes traitant « des nouveaux carburants » ou bien des nouvelles compositions de gaz frais à l'admission.

Les résultats obtenus sur l'effet de l'hydrogène dans les gaz admis en particulier dans le cas de dilution vont permettre une estimation assez précise du gain au niveau des émissions polluantes et du rendement du moteur dans le cas de l'utilisation de reformer. Il serait donc intéressant d'envisager le couplage de cette étude avec une étude détaillée d'un système de production d'hydrogène 'à bord' pour une évaluation technico-économique assez précise de cette alternative intéressante pour la réduction des émissions polluantes et le développement des moteurs propres.

Toni TAHTOUH

Les effets combinés de l'hydrogène et de la dilution dans un moteur à allumage commandé

Une des solutions pour diminuer les émissions polluantes émises par un moteur à combustion interne est de réinjecter une partie des gaz d'échappement (Exhaust Gas Recirculation, EGR) à l'admission. Cependant, dans le cas d'une dilution du mélange air-carburant trop importante, la combustion est plus instable voire ne pas s'entretenir. L'ajout d'une faible quantité d'hydrogène a le potentiel de contrer cet effet négatif de forte dilution. C'est dans ce contexte que ce travail de thèse est basé sur une étude détaillée des effets combinés de l'ajout de l'hydrogène et de la dilution dans un moteur à allumage commandé alimenté par du méthane ou de l'iso-octane. Dans la première partie de ce travail, le potentiel de l'ajout de l'hydrogène combiné à la dilution, en termes d'émissions polluantes et de rendement global du moteur, est montré. Dans la deuxième partie, afin de mieux comprendre l'effet de l'hydrogène et de la dilution dans un moteur à combustion interne et leurs influences sur les propriétés fondamentales de la combustion, la vitesse de combustion laminaire, paramètre fondamentale, a été déterminée expérimentalement pour des mélanges iso-octane ou méthane avec de l'air contenant différents pourcentages d'hydrogène et de dilution. Des corrélations ont pu ainsi être formulées permettant d'estimer la vitesse fondamentale de combustion laminaire pour ces mélanges. Dans la dernière partie, l'utilisation de deux diagnostics optiques (la chemiluminescence de la flamme et la tomographie par plan laser du front de flamme couplé à la mesure de vitesse par vélocimétrie par imagerie de particules) a permis de quantifier l'effet de l'hydrogène et de la dilution sur la propagation de flamme turbulente dans un moteur à allumage commandé muni d'accès optiques. Nous avons ainsi montré que le la vitesse de combustion laminaire a un effet prépondérant, comparé au nombre de Lewis, sur la vitesse de combustion turbulente dans un moteur à allumage commandé.

Mots clés : Dilution, Hydrogène, Moteur à allumage commandé, Vitesse de combustion laminaire, Vitesse de combustion turbulente.

Combined effects of hydrogen and dilution in a spark ignition engine

Optimization of the intake air-fuel mixture composition is one way to reduce pollutant emissions in Spark-Ignition (SI) engines. This can be achieved by operating with a diluted mixture, i.e by recirculating the exhaust. There are however limitations on the level of dilution that can ensure the smooth running of SI engines since diluting the air-fuel mixture induces an increase in combustion duration and in cyclic variations which impair engine performance. Adding an amount of hydrogen to the fuel can extend the dilution and the lean engine operability limits, which is beneficial in reducing both emission levels and fuel consumption. The objective of this study is to investigate the combined effects of hydrogen addition and nitrogen dilution in an SI engine fuelled with iso-octane or methane. In the first part of this study, we proved that high values of indicated engine efficiency and low values of pollutant emissions can be achieved by combining hydrogen addition and diluted air-fuel mixtures in the case of SI engines. In the second part, we provided experimental values of laminar burning velocity for diluted methane or iso-octane/hydrogen/air mixtures for a better understanding of the hydrogen and dilution effects on the fundamental properties of laminar combustion. New correlations to estimate laminar burning speeds of these mixtures were also presented. In the last part, the effects of hydrogen addition, with and without nitrogen dilution, on the turbulent flame propagation were investigated in an optical SI engine fuelled with iso-octane or methane. This study was done by using two different experimental techniques (direct flame radiation visualization and laser tomography images with Particle Image Velocimetry). The main conclusion is that the laminar burning velocity, rather than the Lewis number, has the dominant effect on the turbulent burning velocity in an SI engine.

Keywords: Dilution, Hydrogen, Spark ignition engine, laminar burning velocity, turbulent burning velocity.

PSA PEUGEOT CITROËN

INSTITUT PRISME
Institut Pluridisciplinaire de Recherche Ingénierie des Systèmes, Mécanique, Énergétique UNIVERSITE D'ORLEANS

Région Centre